Mechanisms Affecting the Metallization of Carbon Fiber Reinforced Polymers through the Cold Spraying of Sn-based Mixed Metal Powders

By Andre Constance John-Peter Liberati

Department of Materials Engineering

McGill University, Montréal

August 2021

A thesis submitted to McGill University in partial fulfilment of the requirements of the degree of Doctor of Philosophy

Abstract

Metallizing polymeric substrates via cold spraying has been viewed as a viable solution for building thick metallic coatings onto these substrates. Notably, cold spraying onto carbon fiber reinforced polymers (CFRP) for the aerospace industry could provide interesting alternatives for light-weighting aircraft, while providing electrical conductivity to a relatively insulating material. Previous studies explored the deposition of tin (Sn) onto CFRP, then improvements in the deposition of Sn were observed following the addition of other metallic powders ("secondary components", SC); this was associated with shot-peening by the SC. This work focuses on studying the role of the SC in the deposition process of Sn onto CFRPs, with the greater objective of better understanding the metallization of CFRP via cold spray.

Feedstock powder Sn was mixed with aluminum (Al) and cold sprayed at low pressure onto an epoxy CFRP to reproduce previous deposition efficiency (DE) trends on a wider range of input gas pressures. The observation of protrusions developing in-lieu of a coating at higher pressures led to the discovery of an indirect deposition phenomenon. Sub-micron Sn particles, absent from the initial feedstock powder also appeared, supporting the occurrence of partial melting of the powder during the spraying process. Computational fluid dynamics (CFD) simulations were conducted to validate the findings and support the described mechanisms.

The effects of SC hardness, then other SC properties (density, morphology and, by extension, impact energy) were considered. Sn was mixed in 90:10 weight ratios with a variety of SC (Al, Al alloys (5083, 6061, 7075), iron (Fe), stainless steel 316L, copper (Cu), titanium (Ti) and Ti6Al4V), then cold sprayed on several substrates: three epoxy CFRPs with different surface finishes and a thermoplastic polyether–ether–ketone (PEEK)-CFRP.

The results with SC Al/Al alloys revealed an ideal SC hardness range, similar to that of the underlying substrate, and this was associated with catalyzing the first-layer deposition phase: this led to the description of an enhanced "crack-filling" mechanism. The results also indicated that shot peening during the build-up phase may not be as relevant a mechanism, as was previously suggested. When considering the full spread of SC properties, the greatest improvements to deposition were achieved with SC hardness on par with the substrate hardness, and with SC impact energies around 2 x 10^{-6} J. These observations provided revised considerations for deposition of single component metallic feedstocks onto CFRP and requirements in terms of particle hardness

and particle size were presented: these conclusions would suggest that developing fully dense Cu or Al coatings on CFRP is possible with smaller powder size distributions.

Finally, the pull off strengths of the coatings were assessed and the importance of the substrate nature, and surface finish, were highlighted. Results in opposition to the pure Sn DE improvement mechanism were obtained: here, SC with low hardness/low impact energy lead to lower pull off strengths, when compared to the pure Sn coatings, while SC with higher hardness (and/or higher impact energies) lead to improved pull off strengths. The electrical conductivity of the coatings was also studied, and results were generally better than those previously reported. These results are believed to be an indication of the extent and quality of the tin particle-particle bonding in the coatings.

Résumé

La métallisation de substrats polymériques par projection à froid a été considérée comme une solution viable pour réaliser des revêtements métalliques épais sur ces substrats. Notamment, la projection à froid sur des polymères renforcés de fibres de carbone (PRFC) pour l'industrie aérospatiale pourrait fournir des alternatives intéressantes pour alléger les avions, en rendant conducteur d'électricité un matériau relativement isolant. Des études ont exploré la déposition d'étain (Sn) sur des PRFC, puis des améliorations de dépôt de Sn ont été observées suite à l'ajout d'autres poudres métalliques (« composés secondaires », CS); ceci a été associé à un effet de bourrage par le CS. Ce travail se concentre sur l'étude du rôle du CS dans le processus de dépôt de Sn sur les PRFC, avec l'objectif plus large de mieux comprendre la métallisation des PRFC par projection à froid.

De la poudre d'aluminium (Al) a été mélangée à Sn et projetée à froid à basse pression sur un PRFC à base d'époxy afin de reproduire des tendances d'efficacité de déposition (ED) précédemment obtenues, sur une gamme plus large de pressions de gaz d'entrée. L'observation de protubérances se développant à la place d'un revêtement à des pressions plus élevées a conduit à la découverte d'un phénomène de dépôt indirect. Des particules de Sn submicroniques, absentes dans la poudre initiale, sont également apparues, soutenant l'existence d'une fusion partielle de la poudre pendant la projection. Des simulations de dynamique des fluides (CFD) ont été réalisées pour valider les résultats et soutenir les mécanismes décrits.

Les effets de la dureté des CS, puis d'autres propriétés des CS (densité, morphologie et, par extension, énergie d'impact) ont été considérés. Sn a été mélangé dans des rapports de masse de 90:10 avec une variété de CS (Al, alliages d'Al (5083, 6061, 7075), fer (Fe), acier inoxydable 316L, cuivre (Cu), titane (Ti) et Ti6Al4V), puis projeté à froid sur plusieurs substrats: trois PRFC à base d'époxy avec différentes finitions de surface et un polyéther-éther-cétone (PEEC)-PRFC thermoplastique.

Les résultats avec les CS d'Al (et alliages associés) ont révélé une plage de dureté idéale du SC, similaire à celle du substrat sous-jacent, et cela a été associée à la catalyse de la phase de dépôt de la première couche: ceci a conduit à la description d'un mécanisme amélioré de "remplissage des fissures". Les résultats ont également indiqué que le bourrage pendant la phase d'accumulation du revêtement n'est peut-être pas aussi pertinent que ce qui était suggéré

auparavant. En considérant l'ensemble des propriétés des CS, les plus grandes améliorations de déposition ont été obtenues avec une dureté de SC proche de la dureté du substrat, et avec des énergies d'impact de SC autour de 2 x 10^{-6} J. Ces observations ont permis de revoir les considérations relatives au dépôt de poudres métalliques avec une seule composante sur les PRFC et des exigences en termes de dureté et de taille des particules ont été présentées: ces conclusions suggèreraient que le développement de revêtements de Cu ou d'Al sur PRFC soit possible avec des distributions de tailles de poudres plus petites.

Enfin, la force de traction des revêtements a été évaluée et l'importance de la nature du substrat, et de la finition de la surface, a été soulignée. Des résultats en opposition avec le mécanisme d'amélioration de l'ED du Sn ont été obtenus: ici, les SC de faible dureté/faible énergie d'impact conduisent à des forces de traction plus faibles, par rapport aux revêtements de Sn pur, tandis que les CS avec une dureté plus élevée (et/ou des énergies d'impact plus élevées) conduisent à des forces de traction améliorées. La conductivité électrique des revêtements a également été étudiée, et les résultats étaient généralement meilleurs que ceux rapportés. Ces résultats pourraient être une indication de l'étendue et de la qualité des liaisons particule-particule de Sn dans les revêtements.

Acknowledgements

As this thesis signs the nearing end of my PhD studies, I stand grateful for the journey that it has been and I would like to thank all those who have supported me professionally and personally throughout the course of my degree, from close or afar. It was more than just a learning experience, it was the adventure of a lifetime, and it would not have been possible without them.

I would first like to express my sincere gratitude to my supervisor, Prof. Stephen Yue, for giving me the opportunity to join his research group and discover the world of thermal/cold spray. His unique and critical perspective on research, as well as his constructive advice have helped me grow my ideas and learn to defend them. Prof. Yue also encouraged learning from the research community at an early stage by taking part in conferences, and there was no greater motivation nor learning experience. Finally, he offered me great autonomy in my work which allowed me to explore many aspects of my project, but also to delve into a variety of activities outside of research that have made my degree even more valuable: I believe there could have been no greater gift.

I would also like to thank Prof. Jun Song for his co-supervision. Though not directly associated with any of the chapters of this manuscript, he provided much support and feedback over the course my degree. These shall continue beyond the scope of this thesis as an extension of work provided here (specifically Chapters 4-5) is currently being explored with Prof. Song, Dr. Rohan Chakrabarty (a postdoctoral fellow of Prof. Song) and Prof. Yue.

Special thanks are due to the collaborators at National Research Council of Canada (NRC) in Boucherville, and notably Dr. Phuong Vo, Dr. Maniya Aghasibeig, Dr. Kintak Raymond Yu, Marco Zeman and Kévin Bricault: my project would not have been possible without their technical expertise, their support, their feedback and their relentlessness in front of sometimes mind-boggling issues that my cold spray conditions would cause.

My thanks also go to the Green Surface Engineering for Advanced Manufacturing (Green-SEAM) Network, directed by Prof. Christian Moreau from Concordia University, and managed by Simon Durham. Joining this national network from its inception was truly an amazing opportunity to see the power of collaboration and understand the intricacies of the research world. It was also a source of fascinating discussions and discoveries with professors, researchers and industrial partners that allowed me to keep a broad mindset while focusing on my project, specifically concerning Life Cycle Assessment and its relevance concerning greener engineering.

In the context of this network, I would also like to thank our partners at Bombardier Aerospace (notably through Mario Simard) and Pratt and Whitney Canada for providing us with the substrates required for our project and the discussions we had.

I am grateful for the funding sources and awards that allowed me to carry out this project, and I would notably like to acknowledge McGill University, the Natural Sciences and Engineering Research Council of Canada (NSERC) (through Green-SEAM) and Hydro-Québec for supporting my studies through the Hydro-Québec Doctoral Fellowship, the Vadasz Doctoral Fellowship, the McGill Engineering Doctoral Award (MEDA), the AeroCREATE program, the Graduate Excellence Fellowship and the Graduate Research Enhancement and Travel (GREAT) Award.

On another note, I would like to address sincere thanks to Prof. Sidney Omelon, Dr. Florence Paray, Prof. Stephen Yue, Prof. Nathaniel Quitoriano, Prof. Jun Song and Prof. Raynald Gauvin, with whom I had the opportunity to work with as a Teaching Assistant or a Grader. There was no greater reward during the long Montreal Winter than guiding students through complex projects or inspiring students Electrical Engineering students to consider Materials Engineering. It was also fascinating to experience and discuss teaching methods, to understand how to transmit a passion or to help students find their own path: these experiences were a gift of their own.

I would also like to thank Dr. Florence Paray for trusting me to help her as a Course Assistant, assuring the transition from in-person to online labs in the midst of a pandemic and day to day operations in the common labs. Special thanks are also due to the organizers of the TRaCE McGill Project, notably Prof. Paul Yachnin, as well as Dr. Marie-Claude Felton and Dr. Chantelle Thauvette, for giving me the opportunity to (T)rack, (R)eport (a)nd (C)onnect, (E)xchange with former PhD students, and thus explore the countless possibilities and stories tied to PhD studies. I would also like to thank Heather Smart and Bamidele Akinrinlola from Precision ADM for the opportunity to explore the industrial applications of cold spray while finishing my thesis.

I would like to extend sincere thanks to the members of the department of Mining and Materials Engineering, namely the support staff with Barbara, Leslie, June, Genny, Heather and Diti, who made all the magic happen behind the scenes, and offered a smile or a chat that would make anyone’s day. From the technical support staff, I would like to thank Dr. Florence Paray, Robert Paquette, Alexandra Djuric and Stéphanie Bessette for their help in the lab.

My sincere gratitude goes to my friends and colleagues in Prof Yue's lab, namely Yang, Panteha, Denzel, Tuhin, Xin, Baoqi, Basel, Meixin, as well as Sriraman and Evelin for their continued support and exchanges. Special thanks are due to Hanqing and Christina for their assistance, motivation and friendship throughout this project. I would also like to extend warm thanks to other members of the department such as Konstantinos, Luis, Rana, Lori, Hyeree, Mark, Ronghao, Aniruddha, Sara, Mahmoud, Will, and many, many others, for fun moments at Thomson House or deep discussions in the lab on how to make the department a better place for all.

On this note, I would like to thank all of those with which I have crossed paths, through various activities or groups who enriched my academic experience greatly, such as the McGill Mining and Materials Graduate Engineering Student Association (MMGESA), MetSoc McGill Chapter, the SALTISE Special Interest Group, GradLife, MIME Time, the Blades of Wood, the Bats of Glass, Stanger Danger, Plan B, the Boston Brewskies or the McGill Cycling Team.

After long lab sessions, it was heartwarming to head to what I called home over the past years, and I am especially thankful to my roommates of the Bloc Marquette, Chloé, Brice, Zoé, Romain, Solène, Jon, Tammie, Camille, Mathilde, Floriane as well as Ronan, Paul, Fabien, Romain, Lauriane, Eva, Pierrot, Thibaut, Perrine, Floriane, Damien, Maëva, Quentin and Paul. They were always there to help me keep my head up high and enjoy my experiences to the fullest. Special thanks go to my good Montreal friends Jérémy, Laura, Valentine, Thibault, Rose, Fawzi, Nicolas, Alex, Xavier, Joachim, Camille, Valentin, Maurine, Naomi and Clémence for their continued moral support. Extra special thanks are due to my girlfriend Pauline, who helps me feel proud of all the small efforts I can put into things and who inspires me to give it my best every day. Finally, extra special thanks also go to my dear friends from Chimie ParisTech, Yacine, Bastien, Yann, Stan, Guilhem, Cyrielle, Natacha, Tomas, Flavien et Marion. Si on me demande si c'était une bonne situation ça thésard, je répondrais qu'il n'y avait pas de bonnes ou de mauvaises situations – il n'y avait que les bons moments avec vous tous !

Finally, I am especially grateful for the endless support of my family: no matter how far apart, I could always count on their love and their motivation. I would especially like to thank my grandparents, Flora and Costanzo, for always teaching us the importance of a job well done, respect and love, as well as my parents, Dana and Bernard, for paving the way for me to write these lines today. My gratitude also extends to my sisterds Daniella and Ariella for all their encouragements.

Per Aspera Ad Astra

"When life leaves us blind

Love, keeps us kind"

Chester Bennington – *The Messenger*

Contribution of Authors

The present thesis is manuscript-based and includes the work completed from September 2017 and August 2021 over the course of the author's Ph.D. at McGill University. This thesis includes two publications, one submitted manuscript and one manuscript ready for submission. The manuscripts are included as Chapters 3, 4, 5 and 6, respectively.

Chapter 3: Andre C. Liberati, Hanqing Che, Phuong Vo, Stephen Yue, "*Observation of an Indirect Deposition Effect while Cold Spraying Sn-Al Mixed Powders onto Carbon Fibre Reinforced Polymers*", J. Therm. Spray Technol. 29 (2020), 134-146.

Chapter 4: Andre C. Liberati, Hanqing Che, Phuong Vo, Stephen Yue, "*Influence of Secondary Component Hardness When Cold Spraying Mixed Metal Powders on Carbon Fiber Reinforced Polymers*", J. Therm. Spray Technol. 30 (2021), 1239-1253.

Chapter 5: Andre C. Liberati, Hanqing Che, Maniya Aghasibeig, Kintak Raymond Yu, Phuong Vo, Stephen Yue, "*On the Importance of Secondary Component Properties for Cold Spray Metallization of Carbon Fiber Reinforced Polymers*", Journal of Thermal Spray Technology (2021): **Invited Paper selected from presentations at the 2021 International Thermal Spray Conference** (Submitted, In Revision)

Chapter 6: Andre C. Liberati, Hanqing Che, Panteha Fallah, Phuong Vo, Stephen Yue, *"Pull-off Testing and Electrical Conductivity of Sn-based Metal Powder Mixtures Cold Sprayed on Carbon Fiber Reinforced Polymers"*. (Submitted)

Andre C. Liberati created and developed the experimental plan, performed all experiments (besides cold spraying) and characterization, performed the CFD simulations of **Chapter 3**, analyzed the various results, established discussion points, and wrote the manuscripts. Cold spraying was performed by the equipment operators at National Research Council of Canada in

Boucherville, Québec. Dr. Hanqing Che helped in the design of the cold spray experiments, provided feedback for all manuscripts, and provided insight for the discussions. Dr. Maniya Aghasibeig and Dr. Kintak Raymond Yu provided the results from National Research Council of Canada's (Boucherville, QC) in-house particle velocity model in **Chapter 5**, as well as feedback for this manuscript. Panteha Fallah provided help for the conductivity measurements conducted in **Chapter 6** and provided feedback for this manuscript. Dr. Phuong Vo from National Research Council of Canada (Boucherville, QC) provided assistance with all cold spray experiments and comments on all manuscripts. Prof. Stephen Yue defined the project, actively supervised the research, provided valuable feedback and insight for the organization of ideas and discussions, and he edited the manuscript.

Table of contents

List of Figures

Permissions from Springer Nature and Elsevier were obtained for all figures in Chapter 2, Chapter 3 and Chapter 4. These permissions are available upon request.

List of Tables

Chapter 1

Introduction

1.1 General Background

Applying metallic coatings or "metallizing" polymeric substrates has received increasing interest in recent decades [1, 2], from food packing to microelectronics [3], to heating elements for possible de-icing applications [4]. More recently, interest has been given to polymers or polymeric composite materials for structural applications as in the aerospace industry: these materials possess high strength-to-weight ratios but low electrical conductivity, so they require lightning strike protection (LSP) measures such as electrically conductive metallic coatings [5-7]. For this purpose, several polymer metallization techniques have been explored, such as vacuum deposition techniques (e.g. physical vapor deposition (PVD) [8] or chemical vapor deposition (CVD) [9]) but these techniques are not suitable for developing thick metal coatings substrate (over 100 μm) on the substrates [10]. Several thermal spray techniques have been explored, such as wire-arc spray [11-14], flame spray [15], plasma spray [16] or air plasma spray [17, 18], but ultimately, cold spray has emerged as one of the most legitimate approaches. Cold spraying is a solid state thermal spray process, where powder particles are accelerated by a supersonic gas jet and form a coating through plastic deformation upon impact with a substrate [19]. Due to its operating conditions (several hundred degrees versus several thousand degrees for other thermal spray techniques [20]), cold spray reduces the risk of oxidation of the metallic powder and heat damage to the substrate [21].

While cold spraying onto metallic substrates is generally efficient and well understood [22-24], cold spraying on polymeric substrates has proven difficult to achieve as a result of substrate erosion from hard particles on substrates with poor erosion resistance [25-28]. In recent years, researchers have encountered some success in metallizing polymeric substrates via cold spray with a variety of metals such as tin [28-31], iron [29], 316L stainless steel [32, 33], AlSi10Mg [33-35], copper [28, 29, 31, 36-38] or aluminum [38]. On the downside, these coatings included issues that related to substrate damage [28, 31], relatively low deposition efficiencies (DEs) (i.e. the ratio of

effectively deposited particles on the substrate versus the amount of sprayed particles) [29, 31, 32, 34], or delamination issues [36-38].

In some of the first studies on cold spray metallization of CFRP, Lupoi and O'Neill [31] followed by Ganesan et al. [26], observed that harder materials like copper would lead to erosion of the substrate, while soft elements such as tin could deposit with some success: this was associated with facilitated deformation of the tin upon impact that favors mechanical anchoring with the substrate [26]. In their studies, Che et al. [28] described the tin deposition mechanism in further detail with the introduction of a "crack-filling" mechanism, where it was hypothesized that thermally softened or partially melted tin particles impact the substrate and, while the harder core of the particle generates microcracks in the surface polymer, the molten part of the tin would be squeezed into these cracks and provide mechanical interlocking with the substrate. They also underlined the importance of differentiating the metallization process into two separate phases : the first-layer deposition phase (metallic powders impact the polymeric substrate) and the build-up phase (metallic powders impact the previously deposited metallic powders) [29].

In parallel, several researchers described enhancement effects relating to the mixing of metal feedstock powders with ceramic powders: improvements were observed in the deposition process (increased DE, decreased porosity), but also in the coating properties (hardness, adhesion strength between coating and substrate) [39-41]. Fernandez and Jodoin [42, 43] recently conducted an extensive study on mixed powder improvement mechanisms and they explained that coating deposition improvements would be associated with surface roughening through generation of asperities and oxide removal by the secondary component (SC), while coating property improvements would be related to generation of oxide clean surfaces and peening of the SC. Che et al. explored the deposition of mixed metal powders by cold spraying tin with SC like zinc and copper [44] and they observed similar improvements that they associated with the shot-peening effect of the SC on the relatively softer tin. The addition of aluminum to feedstock tin powder was recently also recently shown to improve the deposition of tin on CFRP [45], but while the improvement trend for pure tin, mixed tin-zinc and mixed tin-copper were decreasing with pressure [28, 44], mixed tin-aluminum presented an increasing trend, with an undetermined

maximum DE for pure tin. Furthermore, cold spray studies generally discuss deposition behavior in terms of relative hardness of powders and substrates (i.e. “hard on soft materials”) [46, 47], yet they fail to quantify the effect of relative hardness on DE improvement. Since shot-peening depends on the impact energy of the impinging particles and their hardness (to transfer the energy to the underlying material), it appears necessary to elucidate the parameters and mechanisms that influence the deposition of Sn-based mixed metal powders onto CFRP.

1.2 Aims and objectives

The aim of this work is to understand the role of the SC in the improvement mechanism associated with the deposition of tin on CFRP, to provide better understanding of the metallization of CFRP via cold spray and, of course, better coatings. More specifically, tin was cold sprayed with a variety of SCs to understand the influence of the various SC properties on the cold sprayability of Sn on CFRP. This was achieved by various approaches:

- Mixing tin with aluminum to determine the maximum DE of pure tin on CFRP with this mixture and compare it with results obtained with tin-zinc or tin-copper mixtures.
- Mixing tin with aluminum and aluminum alloys (Al5083, Al6061, Al7075) to understand the influence of SC hardness on the deposition of tin on a variety of CFRP substrates.
- Mixing tin with a variety of other metal powders (iron, SS316L, copper, titanium, Ti6Al4V) to study a broader scope of SC properties (namely density, morphology, and by extension, particle impact energy) and assess their impact on deposition of tin on the same CFRP substrates.
- Assessing pull off strength and electrical conductivity of the obtained coatings to correlate SC properties and deposition trends to mechanical properties of deposited tin on CFRP.

1.3 Thesis Layout

This thesis is divided into seven chapters. The current chapter (Chapter 1) introduces the engineering rationale for applying metallic coatings onto polymeric or composite substrates (notably CFRP) as well as the limitations provided by current techniques. Cold spray is introduced as a viable thermal spray solution to metallize these substrates but identifies limitations that need

to be addressed. The use of tin as feedstock powder is described as a first step to cold spray metallization of composite substrates, then the improvement mechanism of mixing tin with other metallic powders is described. From here, a brief description of the objectives and research approach is provided, followed by the outline of the thesis.

Chapter 2 is the literature review, which comprises an overview of the interests for metallizing composite materials, a description of the fundamentals of cold spray, insights associated with the cold spraying of mixed metal powders and, finally, a review of current knowledge when metallizing polymeric substrates through cold spray.

In Chapter 3, tin mixed with aluminum is cold sprayed onto carbon fibre reinforced polymers for a wide range of gas pressures. An unusual coating morphology is observed, and the study of these "coatings" allowed the description of an indirect deposition mechanism. These observations are supported by CFD modeling of the powders in the cold spray gas flow. This chapter provides additional support to previously described deposition mechanisms for tin on CFRP substrates.

In Chapter 4, tin is mixed with aluminum and several aluminum alloy powders (Al5083, Al6061, Al7075) and cold sprayed onto a benchmark steel substrate and on several CFRP substrates (three thermosetting CFRP with different surface finishes and one thermoplastic CFRP). This chapter is focused on the effect of SC hardness, with the objective of understanding the suspected improvement mechanism that was tamping. The various coatings are characterized from top-surface and cross-sectional points of view and profilometric data is acquired to study the variations of roughness across the coatings. A refined deposition mechanism for tin on CFRP is described, and the role of the tamping as an improvement mechanism is discussed.

In Chapter 5, tin is mixed with iron, stainless steel 316L, copper, titanium and Ti6Al4V, then sprayed onto the same substrates. The diversity of SC chosen here allows a broader approach to SC properties to be taken. The effect on Sn deposition on CFRP of SC hardness, density,

morphology, particle size, and, by extension, impact energy, were studied. SC hardness and impact energy are determined to have the most influence on the deposition of tin on CFRP. The results also provide revised considerations for deposition of single component metallic feedstock powders onto CFRP regarding requirements of particle hardness and particle size.

In Chapter 6, the adhesion strengths of the various coatings are measured and the peeled coatings and substrates are characterized. The importance of the substrate nature, and surface finish, are noted, and the adhesion strengths are related to the SCs. Results indicate an opposite trend compared to those observed for the deposition improvement of tin on CFRP. The electrical conductivity of the coatings was also studied and, while results do not indicate specific trends, better values were obtained than those previously reported suggesting approaches towards improved bonding in tin coatings.

In Chapter 7, the findings made in the previous chapters are regrouped in a global discussion, relating to discoveries on the deposition of tin on to CFRP, the role of the SC in the deposition process and in the pull off strengths of the coatings, the role of the substrates in the pull off strengths, as well as a potential opening for cold spraying of other metallic powders onto CFRP. Conclusions are made based on the work provided in this thesis, followed by a description of the contribution to original knowledge and suggestions of future work.

Chapter 2

Literature Review

2.1 Interest in metallizing CFRP

Applying metallic coatings or "metallizing" polymeric substrates has received increasing interest in recent decades [1, 2, 48], from food packing to microelectronics [3], to creating heating elements for possible de-icing applications [4]. The aerospace industry has typically shown great interest in replacing metallic structures by CFRP materials given their light-weighting potential for aircraft [49], as portrayed by the Boeing 787 Dreamliner that is composed of over 50% in weight in composites (80% in volume) [50, 51]. There is still further potential for these materials as manufacturers may look towards replacing external metallic structures by CFRP (such as fuselage) [52].

Aircraft are struck by lightning on average once per year [53] so they naturally require forms of lightning strike protection (LSP) to dissipate thermal and mechanical energy (direct effects) [54], electromagnetic fields and sharp rises in structural voltage (indirect effects) [55]. Aircraft made of metallic materials possess a natural shielding to electromagnetic fields ("Faraday cage" effect) but polymer-based materials have lower operational temperatures, electrical and thermal conductivities than their metallic counterparts: typically, the carbons fibers and epoxy resins that compose an epoxy-based carbon fibre reinforced polymer (CFRP) are respectively 1 000 and 1 000 000 more electrically resistive than aluminum [56]. As a result, most LSP methodologies look to provide a conductive layer on the composite structure [5, 7, 57], usually through a metal mesh or expanded foil over the composite outer structure [58]. However, lightning strikes can still cause damage to these structures either by delamination between layers [54] or by burning of the composite material (resin, fiber or mesh materials) [59], and repairs generally require replacement of the area.

Other techniques of metallization have been explored as alternatives but these have struggled to provide compelling results: metallizing glass or carbon fibers via electroless plating, chemical vapor deposition (CVD) or physical vapor deposition (PVD) has been studied [5, 7-9] and provided more electrically conductive substrates [60], but these LSP strategies were less efficient and repair was more complex than with the metal mesh solution. Moreover, these do not develop thick metal coatings (over 100 µm) [10]. Finally, thermal spray approaches have been considered such as wire-arc spray [11-14, 61, 62], flame spray [15], plasma spray [16, 62], air plasma spray [17, 18] or pulsed-gas dynamic spraying [63] but these techniques require high levels of thermal energy that could lead to the accumulation of residual stresses [64], oxidation of the metallic powder as well as heat damage to the substrate [21]. On the other hand, cold spray emerged as one of the most legitimate approaches, as it provides better potential to limit these negative effects due to its operating conditions (several hundred degrees versus several thousand degrees for other thermal spray techniques [20]). This allows for better conductivity of the deposited metallic particles while maintaining the structural properties of the composite. Repairability of substrates damaged by lightning strikes would also be far less problematic as cold spray has become a mature repair method for damaged parts [65, 66].

2.2 Introduction to the cold spray process

Cold spraying is a solid state thermal spray process, where powder particles are accelerated by a supersonic gas jet and form a coating through plastic deformation upon impact with a substrate [19]. The discovery of this process is usually attributed to Dr. Anatolii N. Papyrin at the Institute of Theoretical and Applied Mechanics of the Siberian Branch of the Russian Academy of Sciences in Novosibirsk, Russia, in the early 1980s [67]. The discovery was quite fortuitous as it was made while studying models subjected to a supersonic two-phase flow (gas + solid particles) in a wind tunnel [67], and it has been designated by a variety of names such as cold gas-dynamic spray, kinetic spray, supersonic particle deposition or metal powder application (MPA) [68]. Since its discovery, it has become a mature coating and repair technique [66, 69, 70], with the possibility of spraying pure metals, alloys, composites or even polymeric powders.

2.2.1 Process overview

Cold spray is a high-rate material deposition process in which a gas is heated and accelerated through a converging-diverging ("De Laval") to supersonic velocities [71]. Powders are then inserted in the gas flow and also accelerated. Depending on the conditions chosen for the inlet gas processing, these velocities can be varied from 300 to 1500m/s for high pressure cold spray systems (HPCS, max pressure ~9 MPa), or 300 to 550 m/s for low pressure cold spray systems (LPCS, max pressure ~1 MPa) [72, 73]. A schematic of both HPCS and LPCS is presented in Fig. 2-1 [23]. Of notable difference, the HPCS a compressed gas is split into two streams (one as propulsive gas, the other as powder carrier gas) and they are mixed before entering the "De Laval" nozzle, while the LPCS generally uses a portable air compressor and the powder injection point is at the nozzle divergent section where the local gas pressure is sufficiently low to allow the

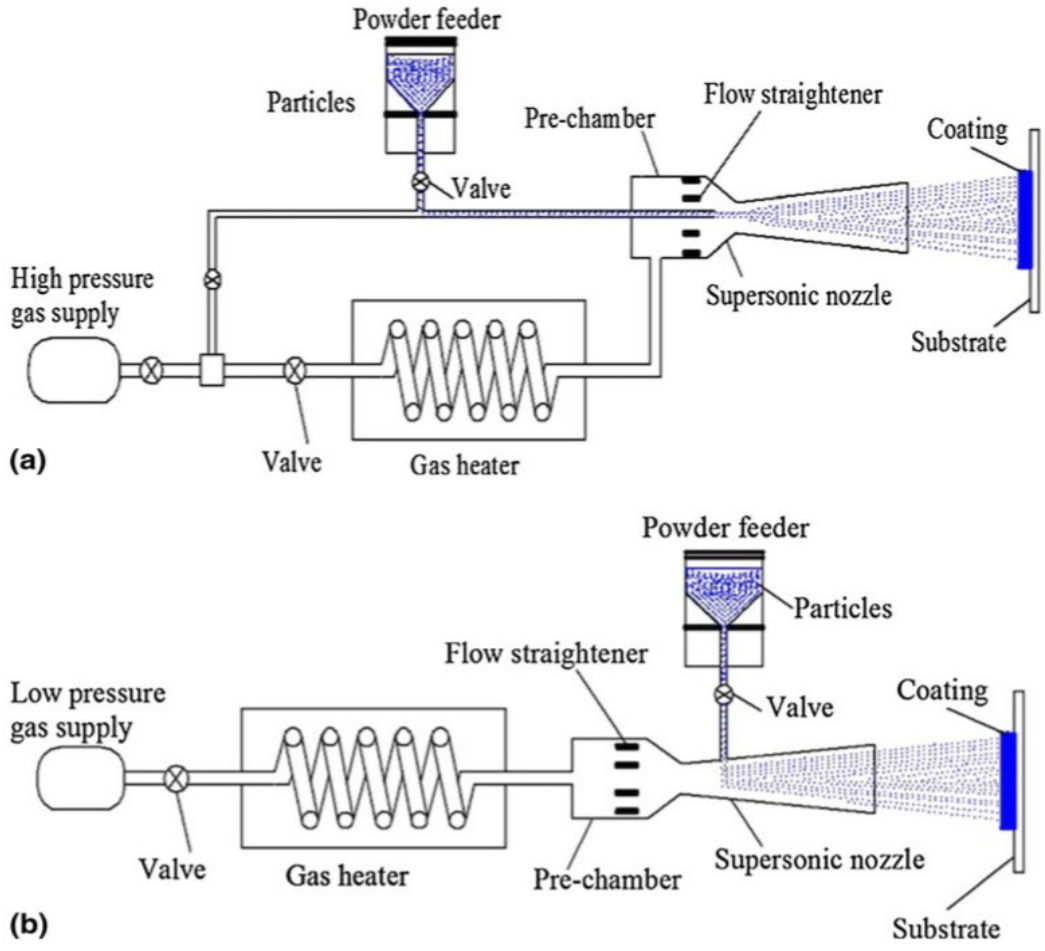

Fig. 2-1: *Schematic representation of (a) HPCS process and (b) LPCS process [23]*

release of powders from the powder feeder system at the atmospheric [72, 74]. These differences also make cold spray systems more flexible and much cheaper in both equipment and processing costs than high pressure cold spray systems, and they can be portable making them particularly suitable for the restoration of damaged components [72, 75]. However, the particle velocity of LPCS is lower than that of HPCS, so only a limited range of powders are sprayable with LPCS (e.g. Cu and Al) [72]. Therefore, in most cases, "cold spray" refers to HPCS and "low pressure cold spray" must be specified [72].

If the solid particles travel at a sufficiently high velocity, known as the critical velocity, they will deform plastically upon impact and bond with the substrate or the previously deposited particles substrate [76-79]. Deposition efficiencies (DEs), i.e. the ratio of powder material adhering to the substrate compared to the amount of sprayed powder, above 95% have been reported (for Cu [80] and for Ti [81]), high deposition rates are achievable (up to 14 kg/h for various metals [82]) and dense coatings, up to several centimeters in thickness have been obtained [83]. Since the cold spray process leads to coatings with low porosity and negligible oxidation of the powders, coatings of high thermal and electrical conductivity can be obtained (with Cu [84]), as well as coatings with high corrosion resistance (with Al [85], Ta [86]). Finally, the cold sprayed coatings generally exhibit high hardness compared to the bulk material because of the high levels of plastic deformation underwent by the feedstock powder [80]. It is also possible to obtain enhanced fatigue properties, and this was associated with compressive residual stresses and excellent coating bonding [87, 88].

Since the cold spray process uses high-speed impact and solid-state deposition, it has many advantages compared to other thermal spray techniques where particles are melted. These being less accumulation of residual stresses [64], less oxidation of the metallic powder in the coatings [89], no forming of undesirable phases [90] as well as less heat damage to the substrate [21]. Furthermore, the spray plume is relatively small as compared to other thermal spray processes [73], so overspray is reduced and masking is not as necessary as it is for other spray processes [90, 91]. This could be particularly advantageous for the electronics industry to manufacture customized circuits with a high degree of precision [92]. Another practical feature of cold spray is

the possibility to deposit particles on substrates of dissimilar materials [89], such as metals on ceramics [92-99], metal matrix composites (MMC) on metals [39, 41, 43, 99-110] or metals on polymers [26, 29, 31, 64, 111-113]. However, while metal/metal cold spray mechanisms are fairly well understood [22-24] with well-described bonding mechanisms and deposition conditions, additional work is still required to expand the technology to other systems.

The cold spray process may seem simple, but a wide range of parameters need to be optimized to generate high quality coatings. For a given powder feedstock, processing parameters can be modified such as the input gas pressure, gas temperature, gas type, standoff distance, gun traverse speed and feed rate. While the traverse speed and feed rate influence the coating deposition, most studies focus on optimizing gas temperatures, gas pressures or gas type, as they directly influence the particle impact velocity [71, 74, 114-117]. Notably, gas with low molecular weights are generally preferred (air, nitrogen or helium [81]) to facilitate gas acceleration, with helium offering the highest velocities. Nevertheless, given the high costs associated with helium, it is used only for specific materials combinations [77]. The spray gun nozzle is also a subject of many studies to optimize the gas acceleration, and the geometry and materials of this nozzle can be modified [118-121]. On the materials side, highly considered factors are the critical velocity (which depends on the material's intrinsic properties), powder morphology (which affects the acceleration capacity of the powder and thus its velocity) [122, 123], as well as the substrate material, morphology, geometry and preparation [124, 125]. Particle size distributions can range from 1 to 100 μm [123, 126, 127], but sizes between 15 and 50 μm are preferred. Large powders are generally avoided as they are more difficult to accelerate (lower velocity) and therefore generate coatings with more porosity [126]. Smaller particles are also not desired as they are greatly affected by the shockwave occurring as the supersonic gas flow adjusts to perturbations around the substrate [128]: given the smaller mass of small particles, this shockwave, or "bow shock", has been shown to reduce the particle velocity [129]. Finally, single component powders are generally used but studies have shown that mixing a second (ceramic or metallic) powder could improve the sprayability of the matrix powder while decreasing the porosity of the coatings and improving the mechanical properties of the coating [39-43, 130-133]. A table of typical cold pray parameters and some references related to their impact on the cold spray process are summarized in Table 2-1.

Table 2-1: *Typical cold spray process parameters with studies related to their impact on cold spray*

Section of the apparatus	Variables	Typical parameters
Gas	Gas type	Helium, Nitrogen, Air [81, 85, 134]
	Gas pressure	0.3 MPa to 8 MPa
	Gas temperature	Room temperature to 1000°C
Operation	Gun travel speed	10 to 1000 mm/s
	Stand-off distance	20 to 100 mm
	Step size	0.5 to 1 mm
Nozzle	Nozzle type	Metal, glass, ceramic, polymer, etc.
	Nozzle geometry	[119, 121, 127, 135]
	Powder injection mode	Upstream, downstream [119, 135]
Feeder	Powder composition	Pure or mixed powders [39, 133], pure metals or alloys [136]
	Powder morphology	Spherical or irregular (dendritic, angular, etc.) [122, 123]
	Powder preheating temperature	None to 800°C [137, 138]
	Powder size	1 µm to 100 µm [123, 126, 127]
	Feeding rate	10 to 50 g/min
	Feeding mode (mixed powder)	Single or dual feeder
Sample	Preparation	Degreasing, grit blasting, laser blasting, "cold" blasting (with the spray material) [27, 139, 140]
	Preheating	None to several hundred °C [125]

2.2.2 Bonding mechanisms

Many studies over the past 20 years have tried to explain and model the bonding process of cold spraying metallic particles onto metal substrates [137, 139, 141, 142], but the exact bonding mechanisms are considered to still not be clearly understood [90, 91, 143]. Two main mechanisms

have been described, mechanical interlocking and metallurgical bonding, and they are associated with deformation of particle/substrate and particle/particle pairs upon impact [68] (with strain rates up to 10^9 s^{-1} [144-146]). Mechanical interlocking is a non-chemical phenomenon occurring when particles are physically trapped in the substrate surface topology [147-149], while metallurgical bonding involves atomic bonds that are usually stronger than interlocking (mechanical) bonds [149].

Mechanical interlocking can be understood as the self-interlocking effects between two rough surfaces, which can be generated by sandblasting the substrate (grit-blasting) or using irregular powder morphologies [150]. This phenomenon can also be obtained when particles are cold sprayed on to a relatively softer substrate, such as copper on aluminum (Fig. 2-2 a) [139], in which case the soft material is extruded and envelopes the hard particle. Champagne et al. [151] described another phenomenon called "interface mixing" where the impact of copper on relatively softer aluminum substrate generates forced mixing and the formation of interfacial waves, vortices and roll-ups (Fig. 2-2 b): this would be facilitated by lower hardness substrates and higher density coating materials. A way of increasing mechanical interlocking is by increasing the process gas temperature and pressure: this leads to higher velocities of impinging particles and therefore, more plastic deformation. This allows the particles to embed deeper into the substrate, which in turn

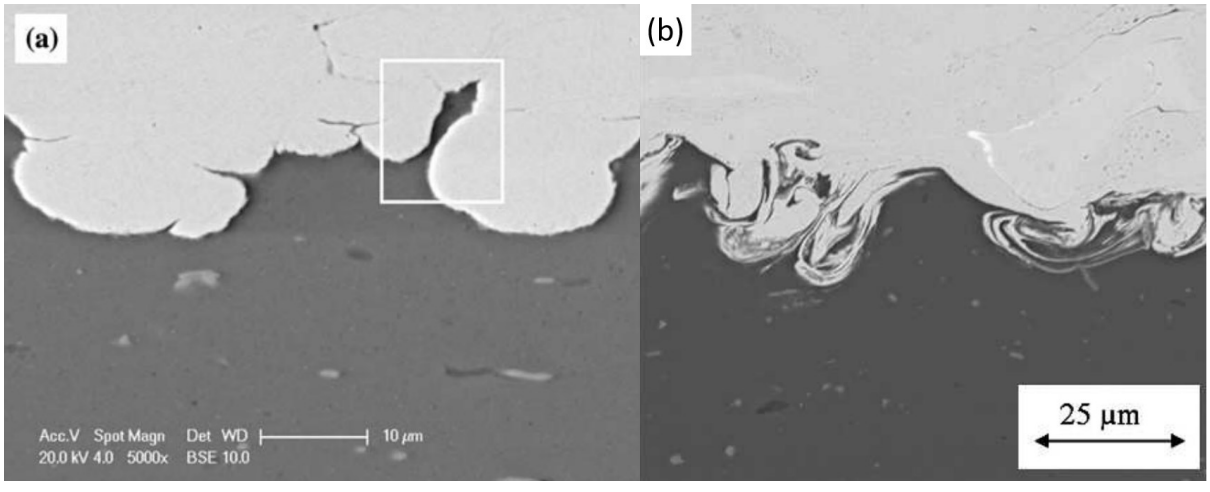

Fig. 2-2: *(a) High magnification image of copper coating on ground and annealed aluminum substrate showing aluminum extruded in between copper particles [139]*
(b) EDS image of a copper coating on aluminum showing interfacial waves and vortices [151]

reinforces the mechanical interlocking at the interface and produces superior bond strength [23]. When coatings with non metals (e.g. metal powders on polymeric substrates [26]), the mechanical interlocking mechanism is the only adhesion mechanism at the coating/substrate interface.

For metallurgical bonding to occur, it is widely accepted that the native oxide of the powders must be removed [152] but the precise mechanism is still unclear. Adiabatic shear instability is process that occurs as a result of severe plastic deformation, where the plastic strain energy is dissipated as heat and leads to severe plastic flow of the material and to a degree of material jetting [153] [154]. Adiabatic shear instability has often been described as the main mechanism for oxide layer breakup/removal [99, 137, 141, 144, 153, 155-157], and for allowing two clean/fresh metallic surfaces to contact at the atomic level [68]. Some researchers have argued that metallurgical bonding in cold spray is not related to the occurrence of adiabatic shear instability [158, 159], most recently with the works of Hassani-Gangaraj et al. [160] who consider that jetting would rather be caused by release of hydrodynamic pressure; this has lead to some interesting debates over the generation of jetting in cold spray and the mechanisms involved [160-162]. Typically, Assadi et al. matched experimental critical velocities to a numerical Johnson-Cook model, and by varying particle velocities, they hypothesized that the localization of plastic strain and thermal softening effects upon particle impact would lead to temperature increases at the interface [141]. As a result, the particle would lose its shear strength as the temperature locally approaches the melting point, and the interfaces would behave like viscous fluids and undergo excessive plastic deformation to form metal jets [141]. This is illustrated in Fig. 2-3, where copper impacting copper above its critical velocity (570m/s) lead to jetting [141]. Here, jetting is described as a consequence of adiabatic shear instability, and not a criterion per se for bonding to occur

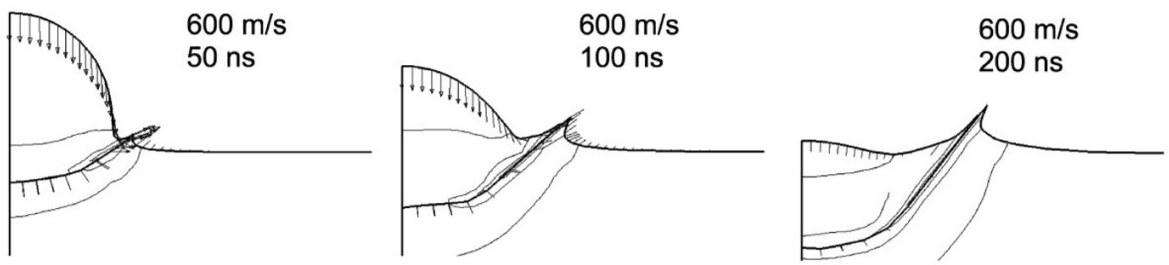

Fig. 2-3: *Simulation results of a Cu particle impacting a Cu substrate at 600 m/s [141] (adapted)*

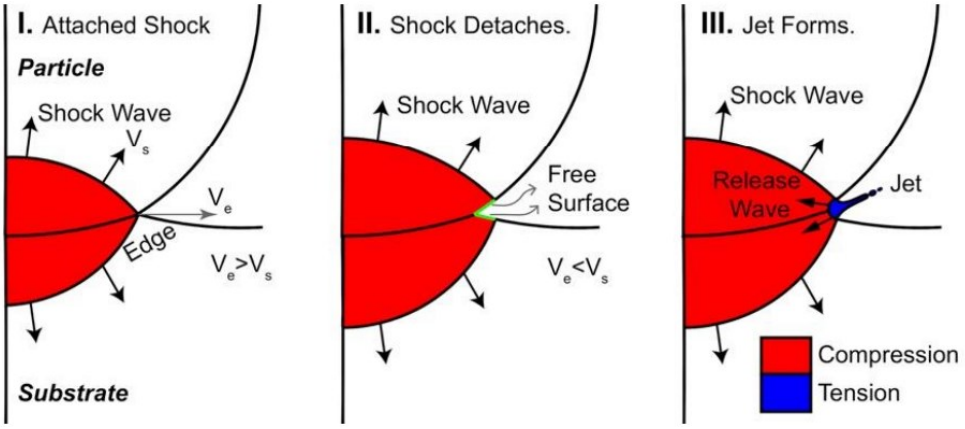

Fig. 2-4: *Schematic representation of jetting in cold spray: Stage I. Impact induces a shock wave. Stage II. Shock detaches form the leading edge. Stage III. Jet forms on the basis of pressure releases. [160]*

[141]. On the other hand, Hassani-Gangaraj et al. [160] recently argued that adiabatic shear bands (perceived as evidence of adiabatic shear instability formation) are not commonly observed at cold sprayed interfaces, and, when removing the materials thermal softening capacity from numerical modelling, they still observed jetting [163]. As a result, they proposed a shock pressure release mechanism and considered that jetting is formed due to the interaction of strong pressure waves with the free surface at the particle edges (Fig. 2-4), and that this can cause hydrodynamic plasticity that effects bonding [160].

Over the past decades, other studies have attempted to model and better understand the deformation process of impinging particles onto a substrate, or the minimum amount of energy required to plastically deform a particle to obtain bonding [164-166]. Others like Kang et al. [167] or Li et al. [168] studied the effect of oxidation on feedstock powder and they showed that as the oxide thickness increased, the oxide would accumulate at the interface and obstruct the adhesion between the particle and the substrate. Meanwhile, other studies have been led to delimit when bonding will occur or if rebounding will take place instead [169], to determine the impact of the substrate on the bonding process [25] and to understand how the sharp local increase of temperature at the contact point, brought to light by local melting, can impact bonding of the impinging particle [136, 170]. Nevertheless, regardless of the differences in approaching bonding,

all studies agree that the impacting particles require a minimum velocity to adhere to the substrate: the “critical velocity” [149].

2.2.3 Critical velocity and window of deposition

Adhesion of impinging particles does not occur until a critical particle velocity has been exceeded so that deformation (adiabatic shear instability, or other) may occur. This critical velocity is specific to the particle material (plastic deformation characteristics) and temperature at the moment of impact [171]. Particles below the critical velocity will abrade and peen the substrate, while particles above the critical velocity may deposit and coating formation can occur [172]. From this, a direct correlation between DE and particle velocity can generally be described for a given material and substrate, as shown in Fig. 2-5. A wide range of studies have aimed to determine critical velocities for various powder/substrate combinations, both by means of experimental data or numerical simulations [123, 136, 141, 173, 174]. Schmidt et al. [144] offered one of the first semi-empirical equations to predict the critical velocity of a powder depending on its properties, and the equation mainly depended on the tensile strength of the powder material, temperature of the particle at impact, melting point of the powder and density of the particle. From this semi-empirical model, critical velocities of 25 µm particles of different materials were calculated, as shown in Fig. 2-6. On this figure, the dark area represents the range of uncertainty with respect to the range of available materials data [144]. It can be noticed that materials with relatively low

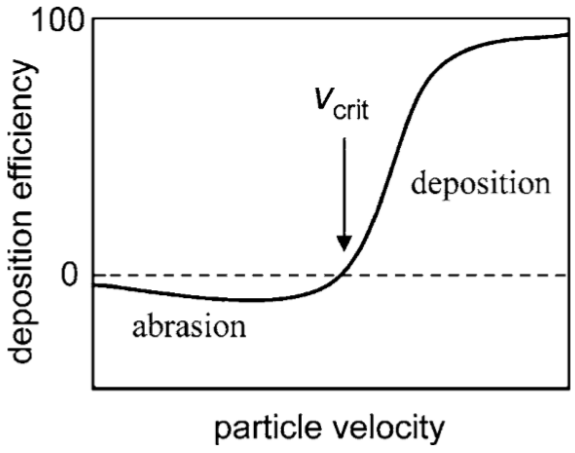

Fig. 2-5: *Schematic of the deposition efficiency as a function of the particle velocity [172]*

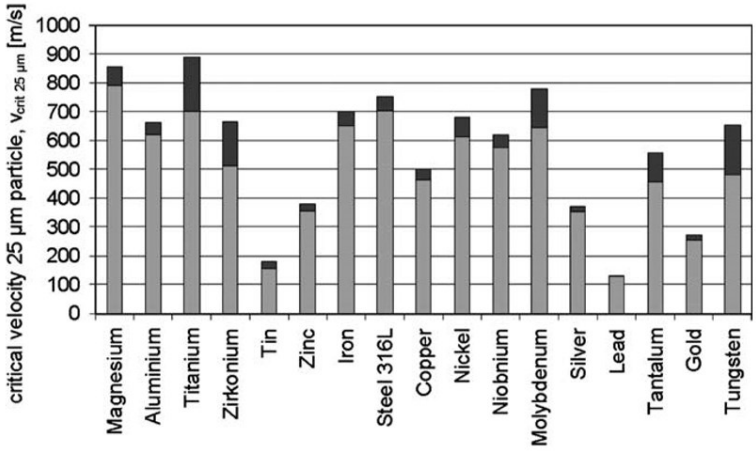

Fig. 2-6: *Critical impact velocity for a 25 µm particle calculated for different materials [144]*

melting points (e.g. tin, lead, zinc) or ductile materials/materials more resistant to oxidation (e.g. gold, silver) require relatively lower critical velocities, whereas materials that are naturally passivated by a dense layer of oxide (e.g. magnesium, aluminum, titanium) usually require relatively higher velocities. As materials are more oxidized, their critical velocity was also shown to increase: this was related to higher levels of deformation being required to break up and remove the oxide layer, as well as dissipation of the particle's energy into oxide removal as opposed to plastic deformation and bonding [167, 168].

Schmidt et al. [144] modified the empirical factors of their equation and also described the existence of the erosive velocity limit, above which a particle will not deposit on the substrate[144]. The erosive velocities were typically two to three times higher than the critical velocity for most materials [142]. They then coined the principle of a so-called deposition window where the critical velocity designates the lower boundary for deposition to take place and where the upper boundary is designated by the erosion limit. For velocities outside of the deposition window, no deposition will occur and a varying degree of erosion may be obtained. Particle impact temperature also plays an important role when determining cold sprayability, as shown in Fig. 2-7 [144]: as the particle impact temperature increases, the velocity limits decrease – this could be related to the decreasing strength of the material with temperature. As the material gets softer, the

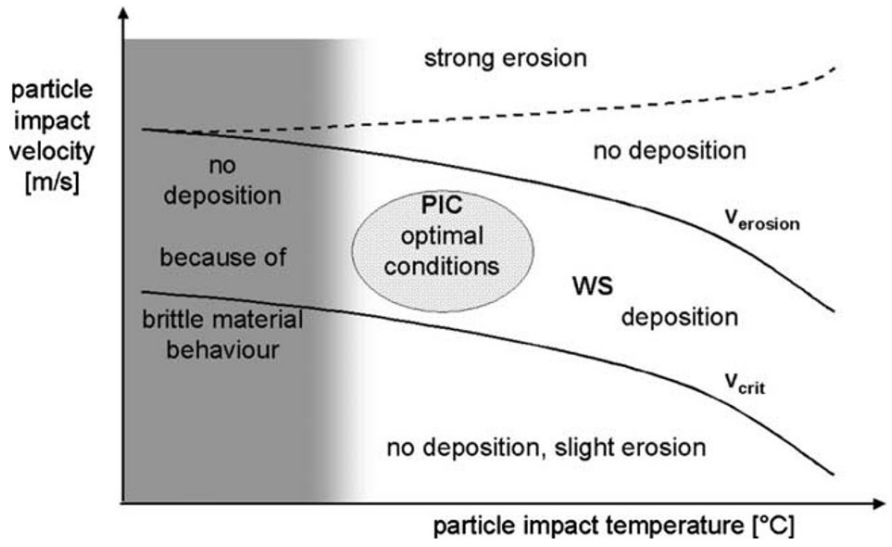

Fig. 2-7: *Schematic of the particle velocity as a function of particle temperature with the window of sprayability (WS) and the regime of particle impact conditions (PIC) [144]*

erosion limit also decreases – but as previously mentioned, this designates the point after which deposition no longer occurs, so for a soft material (e.g. above the erosive limit, on the right side of Fig. 2-7) no deposition would occur at higher velocities, while harder materials would quickly lead to erosion after the erosion limit. This window of deposition illustrates that there is a set of limited parameters that allow deposition of coatings onto substrates, and it serves as the first step to exploration of coating property optimization. Notice must be taken that this window will vary depending on the particle parameters (e.g. size, density, melting point) but it can also strongly depend on other parameters (e.g. morphology, substrate nature, substrate pre-treatment).

Over the following years, this semi-empirical model was further developed and extended into a simplified model depending on η, the ratio of the particle velocity versus the particle's critical velocity, or the "coating quality parameter" [74]. In this paper, the deposition window is established for values of η between 1 and 2, and η in the vicinity of 1.5 is considered to be a benchmark for cold spraying of high strength coatings process [74]. Parameter maps are developed with respect to particle size, gas temperature and gas pressure, and this allows for a complete predictive model matching material deposition with operating conditions [74]. Pérez-Andrade et al. [175] used this model to optimize deposition and coating properties with Inconel 718: with increasing η between 1.12 and 1.34, they did not observe a specific change in DE (as they were already in the deposition window), but they observed decreased porosity, improved electrical conductivity and increased residual stresses. These results may be expectable as higher "coating quality parameter" translates to "higher particle velocity", but the value of η at which these coating improvements stop occurring is unclear. In recent work, Hassani-Gangaraj et al. [163, 176, 177] suggested a new technique to measure the critical velocity of metal powder/substrate pairs. With this technique, a laser excitation pulse is focused onto a launching pad assembly from which single metallic particles are launched toward a target sample by ablation of a gold layer and rapid expansion of an elastomeric polyurea film [163]. The particle approach and impact on the target are observed in real time using a high-frame-rate camera and a synchronized quasi-continuous wave laser imaging pulse for illumination [163]. The data are then considered from the perspective of the coefficient of restitution (ratio between the rebound velocity and the impact velocity), as shown in Fig. 2-8: particles that have a coefficient of restitution equal to zero have adhered to the substrate, which allows the determination of the critical velocity with good precision [163].

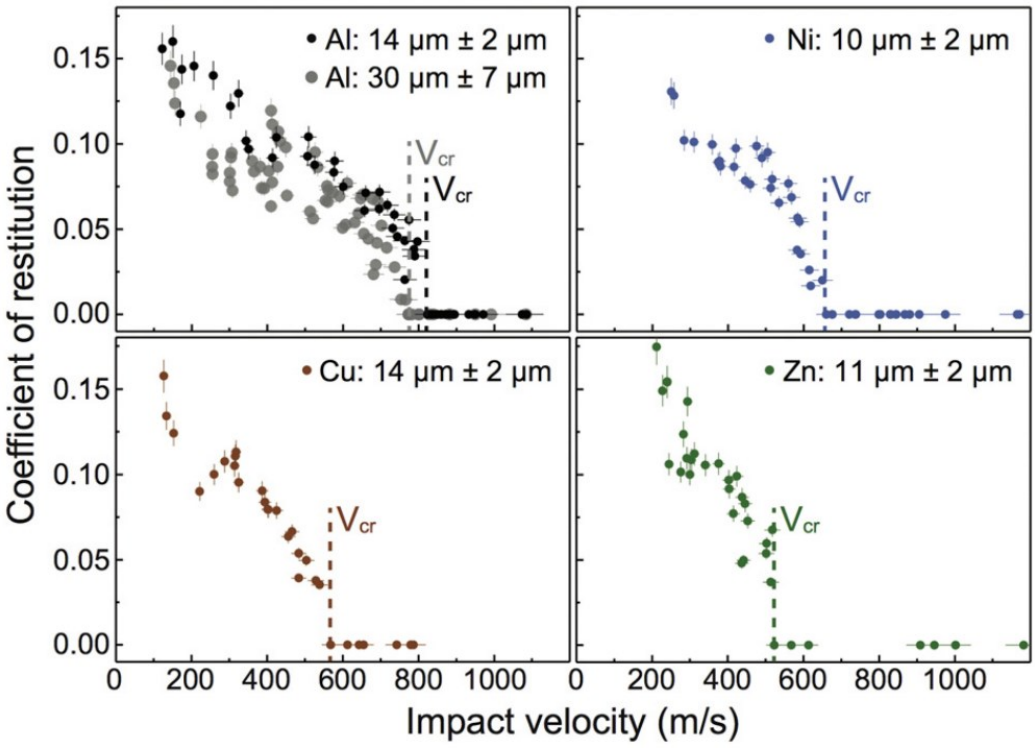

Fig. 2-8: *Coefficient of restitution for Al, Ni, Cu, and Zn.*
The coefficient of restitution is equal to zero above the critical velocity [163].

2.3 Elements of cold sprayed coating evaluation

2.3.1 Deposition

One of the first levels of evaluation of cold sprayed coatings is through measurement of the deposition efficiency (DE): it is defined as the ratio of weight of adhered particles to the total weight of sprayed particles [46]. In practice, it is calculated as the weight gain divided by the product of the calibrated mass feed rate and the spray time on the substrate [114]: this method of determination does not take into account variation of the weight of the substrate material that may be removed as it is considered minimal in front of the deposited coating [114]. As shown in Fig. 2-5, it is typically assumed that, once the particle exceeds the critical velocity, DE will greatly increase, with reported values that can be above 95% (e.g. for Cu [80] and for Ti [81]). For a given powder feedstock, DE is a function of particle velocity, and it is generally possible to increase DE by increasing cold spray process parameters (namely gas temperature and pressure). However, as previously mentioned, the DE increases quickly once the critical velocity is exceeded, so the only expected differences thereafter would be concerning coating properties and their optimization.

Deposition is a two-step process, as presented in Fig. 2-9. The first is the deposition of the powder particles onto the substrate (first-layer deposition phase), and second, the deposition of particles onto the previously deposited layer with reinforcement of bonding and reduction of voids (build-up phase) [178]. It was suggested that the first layer of coating involves substrate surface cratering (i.e. roughening) and activation of the surface by removing surface contamination [80]. This stage is critical as it establishes the bonding of the coating with the substrate, and it is sensitive to the preparation level and the properties of the surface material [91]. Grit-blasting or other surface preparation methods are typically assumed to be another means of improving the first layer deposition [179]. During the build-up phase, particles impact previously deposited layers, leading to deposition as well as reduction of voids and densification through a shot-peening (tamping) mechanism [178]. Both deposition stages occur in the same pass and current DE measurements cannot separate the two phenomena, rendering difficult the quantitative prediction of the DE of a

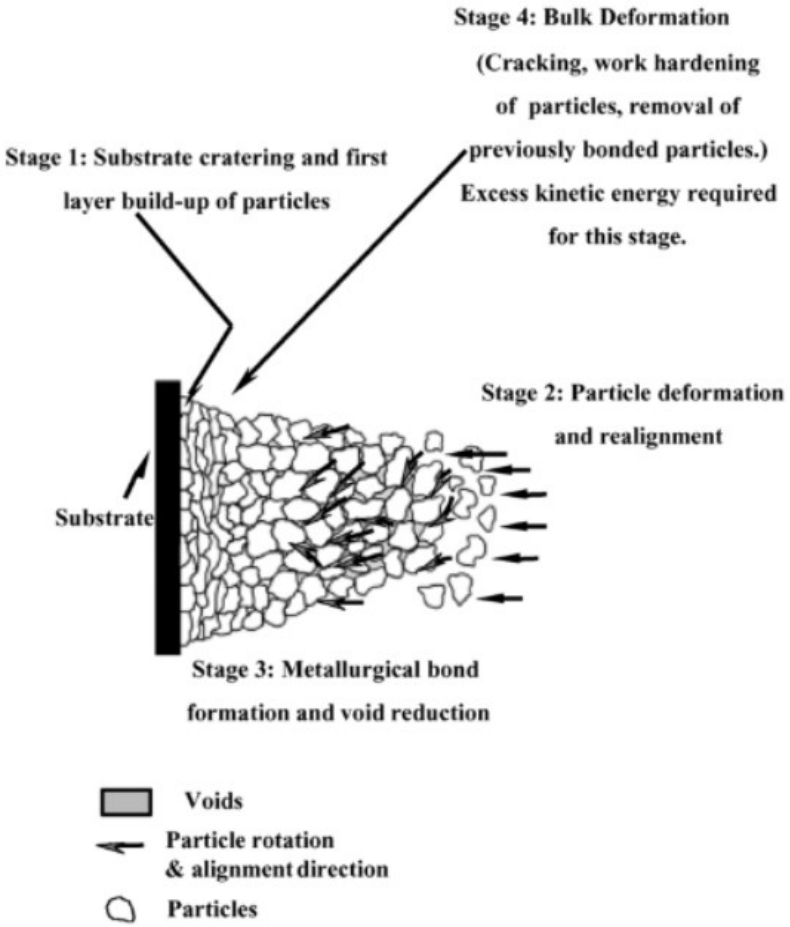

Fig. 2-9: *Stages of coating formation in the kinetic spray process [178]*

powder on a given substrate [150]: for thick coatings, this may not be an issue, but for thin films (thickness several times the particle size, ~50 to 200µm) it could be quite relevant. As with the critical velocity, some researchers have attempted to model the DE of particles on substrate: notably, Meng et al. recently correlated the DE with an effective deformation rate, R_{EQ}, from finite element simulations on single particle deposition [46, 180]. This deformation rate was calculated as the average slope of the squared average equivalent plastic strain ($\overline{PEEQ}^2$) over all particle elements [180].

Another, more empirical, methodology for determining single particle deposition and deformation behaviour is to perform impact tests (or "splat tests") [27, 95, 131, 176, 181-184]. To conduct this test, gun traverse speed is generally set to high values (e.g. around 1000mm/s) and the feed ratio is set as low as possible so that only a small amount of powders are deposited per unit area [169]. With this approach, the DE is associated with the bond ratio, i.e. the ratio of bonded particles (splats) to the total impacting particles (splats + craters) in a given area, as illustrated in Fig. 2-10 a [169]. Fukumoto et al. [185] took a slightly different approach and considered the ratio of particles exhibiting jetting to the total particles deposited over the chosen area: they reported consistent results when compared with the DE. In their work, Wu et al. [169] related the bond ratio of a cold sprayed particle to the competition between adhesion energy and rebound energy of this particle, as shown in Fig. 2-10 b. While adhesion energy was defined as the energy for detaching

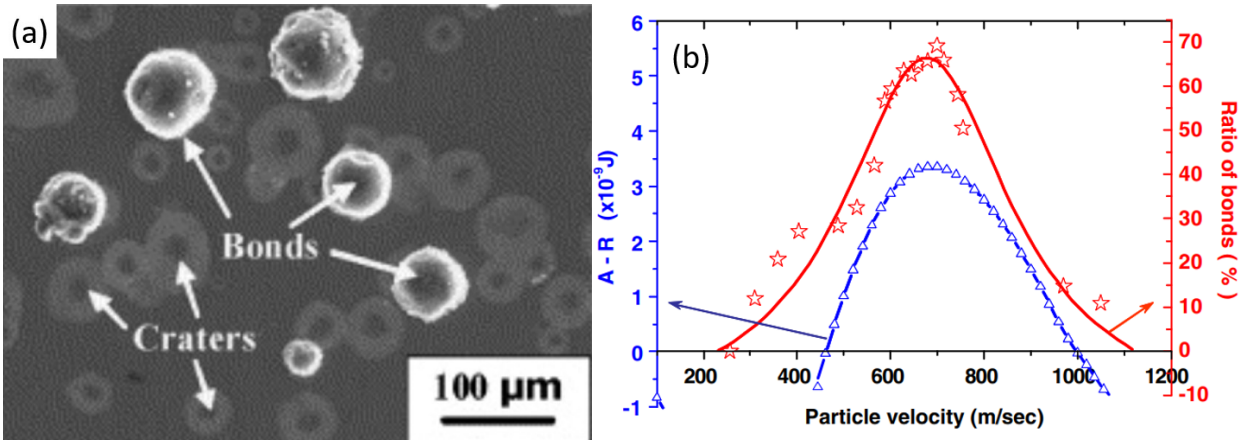

Fig. 2-10: *(a) SEM micrographs showing craters and bonded splats, after single particle impact testing, (b) Comparison of the ratio of bonds to "adhesion energy–rebound energy" for the impact of 25 µm Al–Si feedstock onto the mild steel substrate [169] (adapted)*

the bonded particle from the substrate, the rebound energy was defined as the energy required for bouncing the particle from the substrate, upon elastic recovery of the particle [169]. This work provided the framework for predicting particle deposition behaviors onto substrates and was notably a reference point for the model described by Meng et al. [180].

2.3.2 Porosity

Another metric for evaluating cold sprayed coatings is to consider the percentage of porosity in the coatings. This is generally measured on cross-section optical microscope and scanning electron microscope images with some contrast mechanism, but these can be sensitive to sample preparation, and sub-micron pores cannot be reliably measured [80]. Other techniques such as mercury intrusion porosimetry (MIP) [186], X-ray computed microtomography (CMT) [187] or ultra-sound [188], were summarized by Ang and Berndt [189]. Cold spray is appreciated for its capacity to produce coatings with low porosity and negligible powder oxidation (when compared to other thermal spray techniques), which allows it to provide coatings with high thermal and electrical conductivity (e.g. with Cu [84]), as well as coatings with high corrosion resistance (e.g. with Al [85], Ta[86]). Nevertheless, while some materials such as copper, nickel and aluminum may lead to fully dense coatings, others can show much higher porosity, for example titanium generally shows porosity up to 20% [80, 190, 191]. To reduce the level of porosity, processing conditions (e.g. gas temperature and pressure) are generally increased to increase particle velocity and thus increase the deformation of the particles at initial impact as well as increase the peening of particles on previously compacted particles [80]. Higher particle velocity could lead to nozzle clogging though and, in the same study, Song et al. [192] suggested that preheating the powder to soften it would be a more practical solution to increasing plastic deformation. Another option would be to use helium as a processing gas to accelerate the particles to higher velocities: this was reported to provide coatings with porosity as low as 0.5% [81]. More recently, Aydin et al. mixed titanium powders with Ti6Al4V powders to decrease the levels of porosity in the coatings [130]. Interestingly though, recent studies on the effect of porosity would indicate that Ti6Al4V coatings with higher levels of porosity would actually display better wear behaviour, given their potential to entrap debris [193], therefore depending on the desired coating properties, various coating morphologies could be sought.

2.3.3 Mechanical properties

The structural integrity of deposits is of utmost importance for the various fields looking to use the cold spray process, such as the defense, aerospace and automotive industries, which have integrated cold spray as a repair process [194, 195]. Given the high requirements imposed by these industries, HPCS has garnered more interest than LPCS due to higher velocities, greater particle deformation, and ultimately better coatings [23].

As with bulk materials, microhardness testing is a useful means to assessing the uniformity of basic strength properties. Given the high amount of plastic deformation upon particle impact, and therefore work hardening, the hardness of the coatings will be higher than the substrate (if coating and substrate are the same material) [23]. While this could be expected, some studies have pointed out that the hardness can be higher or on par with the substrate in the interface region (before the substrate) which is suspected to be a resultant of larger plastic strain, shot-peening of underlying powders and smaller grain sizes [196]. The effect of powder property effects are still uncertain though as Zahiri et al. [197] reported that decreasing particle sizes led to increasing microhardness when cold spraying titanium, while Cinca et al. [198], followed by Marrocco et al. [190], found the opposite trend.

Given the "coating" nature of cold spray deposits, adhesion strength of coating to substrate is naturally a property of interest for industrial applications. These are typically determined by conducting adhesion tests or pull-off tests, according to ASTM C633 [199]: the sprayed area is glued to a respective counter-body of the same size and the assembly is then pulled in tension to failure, resulting in adhesive failure of the coating [39] or cohesive failure [200]. Since the bond strength may be stronger than the adhesive strength of the glue (around 70 MPa), some researchers have profited from cold spray's potential to build thick coatings to make bulk samples, that were then machined as tensile samples [201]. With this approach, it is possible to measure higher adhesion strengths, typically above 200 MPa [202]. In parallel, Chromik et al. [203] devised a method for assessing single particle adhesion termed "modified ball bond shear test": this test was shown to provide adhesion strengths on par with those reported in the literature for titanium sprayed with nitrogen [115].

Adhesion strength is intimately related to most cold spray metrics as higher particle velocity has been associated with greater particle deformation and increased bonding with the substrate [185, 190, 201, 202, 204, 205]. As a result, higher adhesion strength is generally obtained with increased gas temperature and pressure [204] or by using a process gas with lower molecular weight such as helium [116, 206]. Another important aspect to consider is the nature of the substrate as softer substrates seem to lead to better adhesion strengths [201, 206]: this could be associated with better mechanical interlocking as the embedding potential of a relatively harder powder is greater [139]. Finally, these improvements provide some limitations: Sharma et al. [140] observed that thicker deposits will generally lead to lower adhesion strength, as a result of higher residual stresses. These authors also observed that different surface preparation methods, such as grit-blasting, could improve adhesion strength [140], while Marrocco et al. [190] observed that adhesion was poorer on grit-blasted surfaces than on polished or ground surfaces, so the effect of surface pre-treatment is still unclear.

With its low process temperature, cold spray is a prime candidate for generating conductive coatings compared to other thermal spray techniques [76, 207]: with relatively lower temperatures, deposits with low oxide content, low porosity and low thermal stresses can be obtained, therefore providing higher electrical conductivity, as shown by the black bars in Fig. 2-11 [206]. Improving

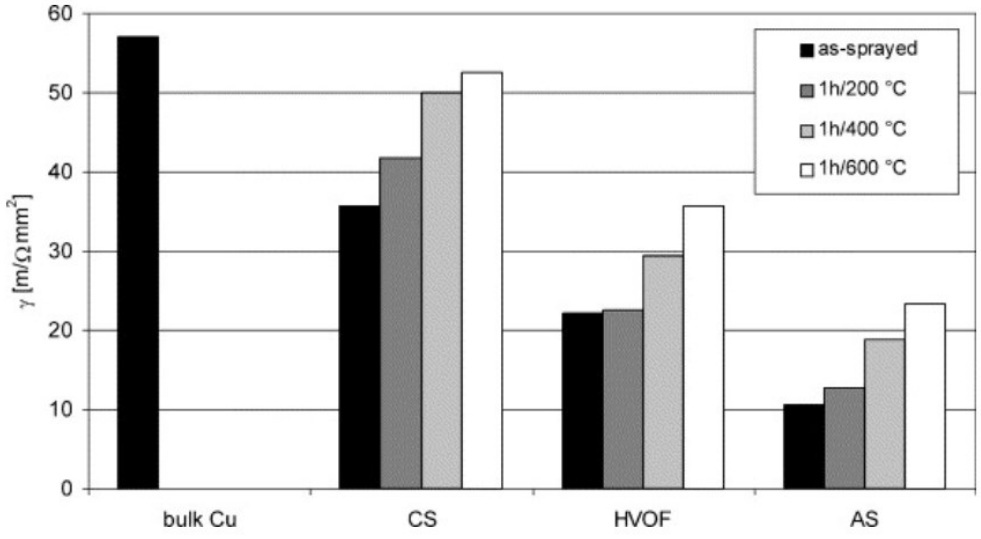

Fig. 2-11: *Conductivity of Cu deposits processed by cold spray (CS), high velocity oxy-fuel (HVOF), and wire-arc spraying (AS) in the as-deposited state and after different annealing conditions. Annealed bulk Cu serves as reference material. [206]*

electrical conductivity is generally associated with higher levels of deformation between particles (i.e. lower porosity) and improvement of bonding quality [208], such that the process conditions that improve particle velocity positively influence conductivity [209, 210]. As-deposited coatings are reported to have conductivities between 30 and 60% the conductivity of bulk copper [210].

Cold sprayed particles undergo severe plastic deformation upon impact to generate bonding with the substrate and so deposits display similar properties to work hardened materials. As with bulk materials, heat treatments can be performed to reduce the residual stresses and initiate recrystallization. As could be typically expected, microhardness of the coatings has been reported to decrease to near-bulk values as a result of annealing [211]. Some reports of increasing microhardness were nevertheless reported, such as in [212], and this was attributed to further consolidation and densification of the deposits through closure of pores, inter-splat boundaries and cracks in the microstructure [23]. Regarding other properties, Stoltenhoff et al. [206] observed an increase of both electrical conductivity and (Fig. 2-11) and bond strength (Fig. 2-12) by annealing cold sprayed copper deposits on various substrates. After annealing, electrical conductivities of cold sprayed copper coatings were reported to reach values above 90% the conductivity of bulk copper [206, 207]. Similar property recoveries were noticed for the ductility of annealed cold sprayed Al7075 coatings [213].

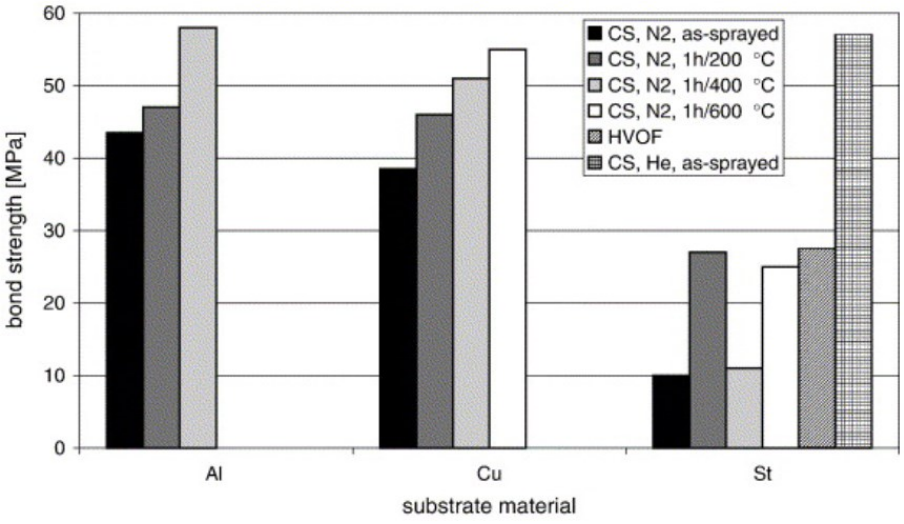

Fig. 2-12: *Bond strength of cold sprayed copper coatings on various substrate materials (Al: aluminum, Cu: copper, St: low carbon steel); as-sprayed and annealed states [206]*

2.4 Cold spray of mixed metal powders

With a demand for highly specialized coatings using brittle materials (e.g. ceramics, MMCs), innovations have had to be made and depositing these materials through co-deposition, i.e. spraying a hard-to-deposit material with a more ductile metal, has received some interest in recent years [99]. Mixing powders is the most common approach as it is fairly straightforward and simpler to implement than the use of composite powders (e.g. mechanically milled) or cladded powders that are not commercially available and that do not provide any flexibility for composition variations [90]. Mixing powders has included a variety of metals mixed with non-metallic, but also metallic, secondary components (SCs).

In the first case, metal powders have often been mixed with small amounts of alumina powder to improve feedstock cold sprayability (generally 10-30 wt.% [150]). Shkodkin et al. [214] reported an "activating" behavior of ceramic particles by showing that aluminum-alumina and copper-alumina mixtures gave positive DEs at significantly lower spraying pressure and temperature in comparison with the deposition of pure metallic powders (Fig. 2-13). Several other researchers noticed similar improvements in DE and adhesion properties when mixing metallic and ceramic powders (generally copper/aluminum with alumina or silicon carbide) [39-43, 90]. The improvements were related to a peening effect of the hard alumina powder that could either

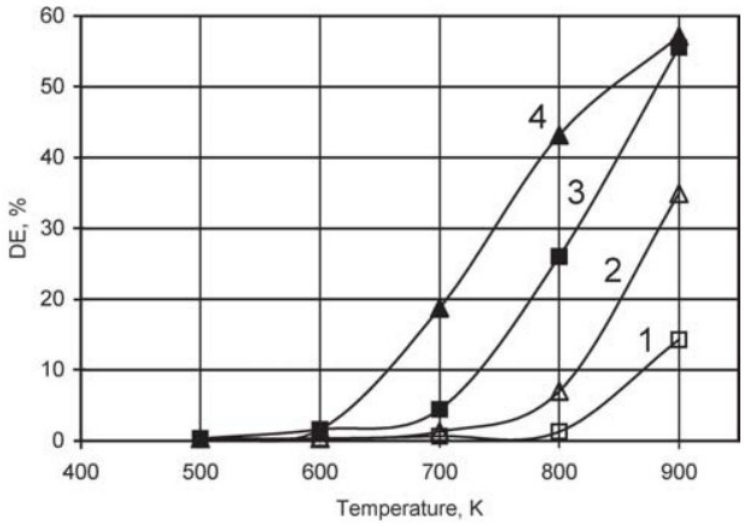

Fig. 2-13: *(1) and (2) Deposition efficiencies of aluminum and (3) and (4) mixed aluminum-ceramic powders at different air stagnation temperatures and velocities (1) and (3) 130 to 180 m/s and (2) and (4) 200 to 250 m/s [214]*

generate surface roughening or surface cleaning (i.e. removal of the substrate oxide layer by the ceramic, thus leaving an activated area for the metal) [90]. Process improvements were also noted as the hard particles keep the nozzle clean and further eliminate the nozzle clogging [40]. Other improvements that were noticed were the reduction in coating porosity and improved bond strength due to shot peening by the relatively harder ceramic powders on the deposited metal layers, while asperities were observed between the metal and ceramic powders, leading to believe that bonding between these particles were weak [39]. Fernandez and Jodoin reported on the effect of alumina content and morphology in aluminum coatings [42, 43]: a maximum overall DE was obtained at 30 wt.% of alumina, whereas only 12% was obtained with pure aluminum. They also observed that angular alumina lead to consistent increases of partial aluminum deposition with some alumina retention (associated with mechanical interlocking), while the use of spherical alumina was associated with the greatest increases of adhesion strength due to better peening effects [43].

Some studies on mixing metallic powders were carried out and provided similar observations, such as enabling/enhancing deposition of tin on composite materials [44]: tin was mixed with 10 wt.% of copper or zinc and notably improved DEs were observed, while further increases of copper content (30 wt.%, 50 wt.%) resulted in decreasing DEs as well as lower electrical conductivities. Spencer et al. [215] took another approach and mixed “fine”/”coarse” stainless steel 316L powders and observed they provided similar coating density and corrosion resistance then the single component “fine” powder, without the processing difficulties of fine particles such as inconsistent powder feeding or nozzle fouling [215]. Perry et al. [216] went a step further and looked into the potential recycling of powder by recovering cold sprayed aluminum powder (“reclaimed”, i.e. work hardened) and spraying it with as-received spherical aluminum: the addition of reclaimed powder to as-received only ended in minor decreases of DE. Some researchers took profit from the benefits provided by the SC and developed an in-situ shot peening mechanism with stainless steel particles (200-300 μm) [132, 217, 218]. Finally, Chu et al. [131, 219-221] extensively studied the deposition behavior of iron mixed with stainless steel 316L: they noticed that the rule of mixture was not respected when varying the proportion of the SC, and explained the variation in DEs through the bond ratios between the various metal/metal couples involved in the system [131]. Sova et al. [47] proposed a simple mathematical model to interpret the DE of mixed powders, and it was verified by cold spraying of a copper-316L-tribaloy T700,

but this model does not account for potential particle-particle interactions, substrate effects, surface/coating roughening, nor does it clarify the difference between “hard” and “soft” particles. Ultimately, this shows the difficulty of modelling DE of mixed metal powders, as it is not as simple as correlating the independent deposition effects for each single component powder.

2.5 Metallization of polymeric substrates through cold spray

2.5.1.1 Key polymer properties

Polymers can be regrouped into three main groups that depend on their thermal processing behavior: thermoplastics (e.g. acrylonitrile butadiene styrene (ABS), polyvinyl chloride (PVC), polyether ether ketone (PEEK), polystyrene, etc.), thermosets (e.g. epoxy, Bakelite, polyimide, etc.) and elastomers (e.g. natural rubbers) [222]. Thermoplastics consist of long molecular polymeric chains held together by inter-molecular bonds with relatively weak forces. This enables thermoplastics to be softened and melted when heated, then to be remolded or reformed upon cooling . On the other hand, thermosets cannot melt as they are based on complex tridimensional cross-linking bonds (covalent bonds) that break when heated. Therefore, while thermoplastics can be heated and reformed, thermosets can only be heated and formed once [223]. Another relatable property is that thermosets tend to be harder, stiffer, and more brittle than thermoplastics.

When cold spraying solid particles onto polymers and polymer matrix composites, it is important to acknowledge the difference in material properties as polymers possess poor erosion resistance, generally two or three orders of magnitude less that that of metallic materials [224]. Typically, thermosets exhibit brittle erosive behavior while thermoplastics usually show ductile erosive behavior [225]. A summary of various erosion mechanisms has been provided by Stachowiak and Batchelor [226], as shown in Fig. 2-14. Some of these behaviors, such as abrasion (Fig. 2-14 a), plastic deformation (Fig. 2-14 c, left) and melting (Fig. 2-14 d), could be relevant for thermoplastic substrates, while surface fatigue/cracking (Fig. 2-14 b) and erosion (Fig. 2-14 c, right) would be more relevant for thermosetting substrates. The macroscopic erosion of Fig. 2-14 e could occur for both substrates, depending on chosen spray conditions. These behaviors are highly impacted by particle velocity [224], as well as the hardness of the material and the powder

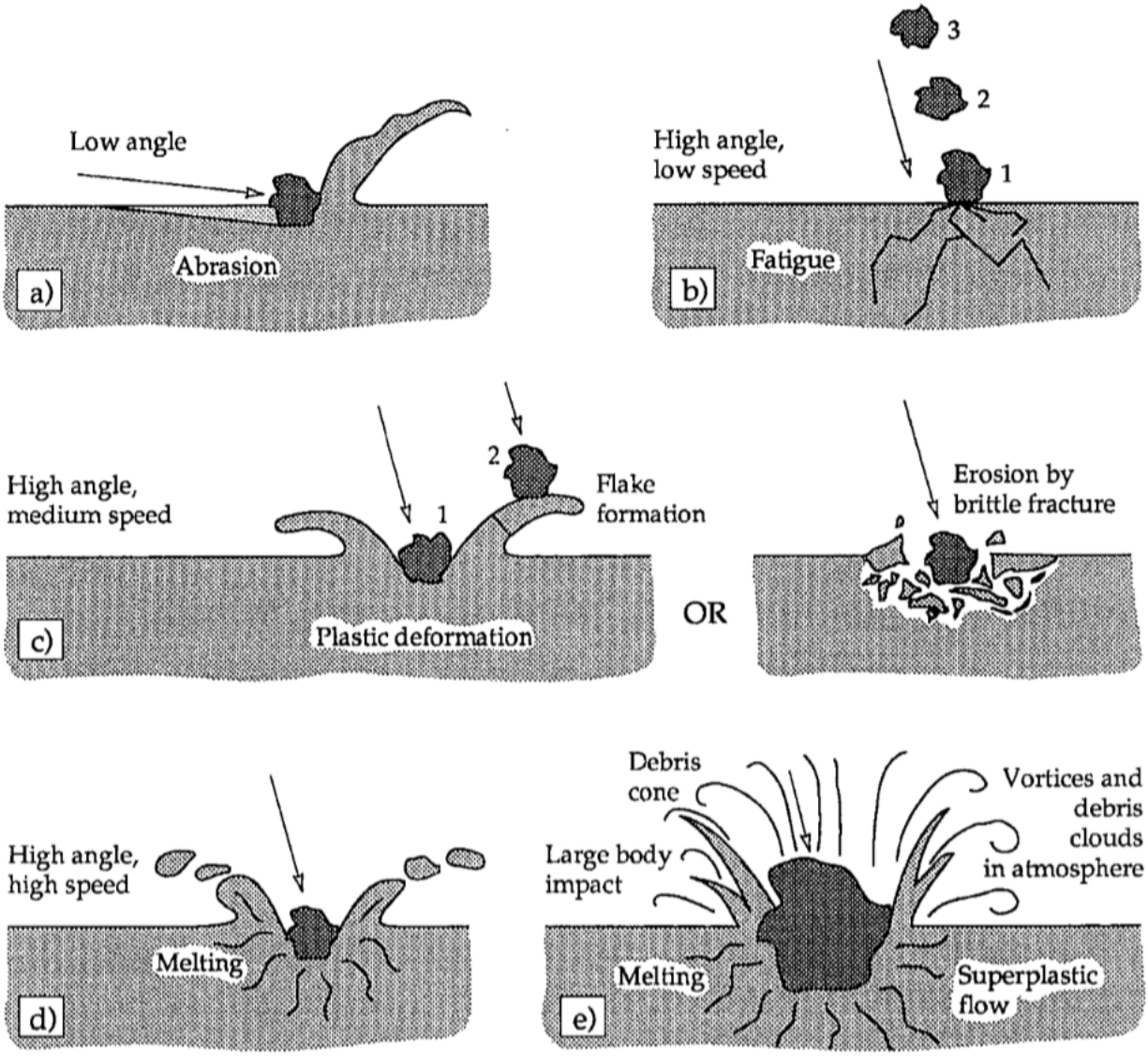

Fig. 2-14: *Possible mechanisms of solid particle erosion: (a) abrasion at low impact angles, (b) surface fatigue during low speed, high impingement angle impact, (c) brittle fracture or multiple plastic deformation during medium speed, large impingement angle impact, (d) surface melting at high impact speeds, (e) macroscopic erosion with secondary effects [226] (adapted)*

size (larger and harder particles are usually associated with higher erosion rates) [227]. There have also been reports of higher erosion rates with at higher temperatures than at room temperature [228]. Therefore, while cold spraying on metallic substrates is generally not an issue (large window of deposition), deposition on polymeric substrates is limited by erosion (narrow or possibly inexistent window of deposition) [29].

2.5.1.2 Cold spraying on polymers and polymer matrix composites

The first reports of cold spraying onto polymeric materials were published around 15 years ago by Zhang et al. [25]: they attempted to cold spray aluminum powders onto various types of substrates (namely ABS), but very little deposition was observed, and this was mostly attributed to the lack of metallic bonding between the aluminum particles and the polymer substrate. Shortly after, Sturgeon et al. [64] successfully cold sprayed aluminum on carbon fibre reinforced PEEK substrates with helium gas at 300°C and 20 bar, while previous cold spraying of aluminum and silver on carbon fibre reinforced epoxy substrates was unsuccessful. Lupoi and O'Neill [31] then tried cold spraying copper, tin and aluminum powders on various thermoplastics (Polycarbonate/ABS, polyamide-6, polypropylene and polystyrene) and on a glass-fibre composite material. Deposition of aluminum was unsuccessful (no deposition or erosion) and cold spraying of copper led to erosion, while cold spraying of tin led to successful deposition, as shown on Fig. 2-15. Ganesan et al. [26, 111] cold sprayed tin and copper (spherical and dendritic) onto PVC

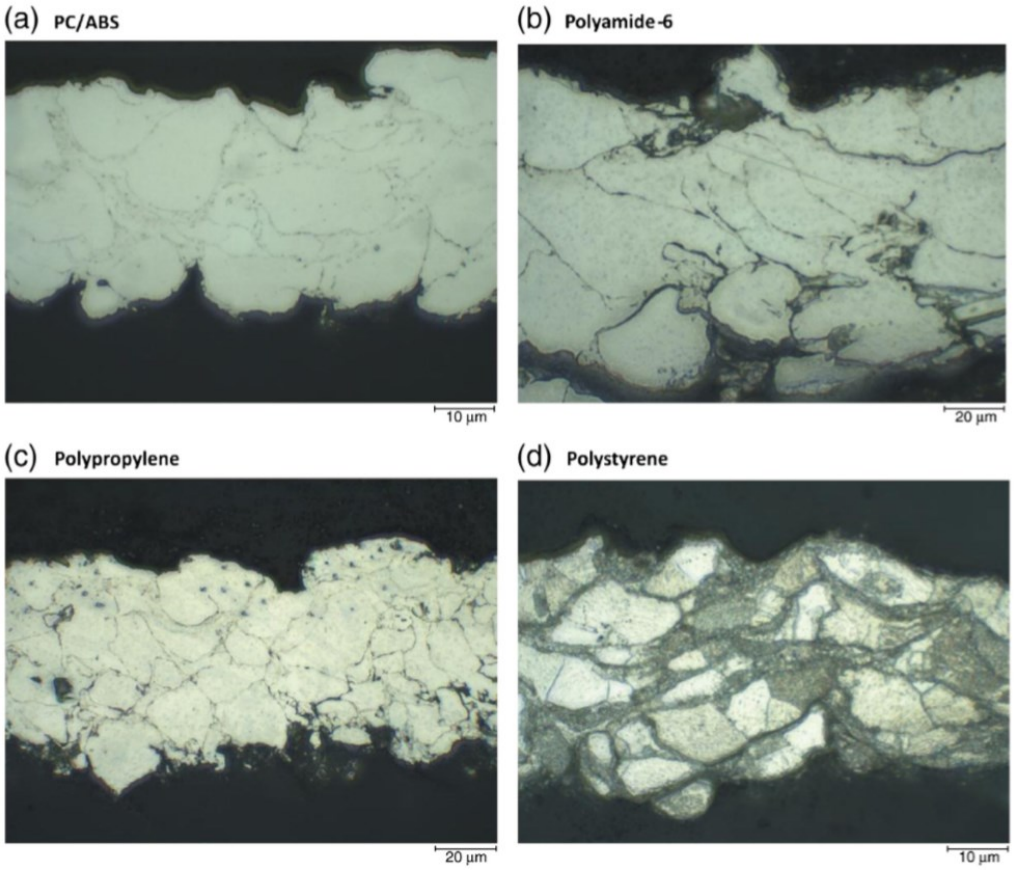

Fig. 2-15: *Cross-sectional micrographs of tin coatings on various polymer substrates [31]*

substrates and they showed that tin gave better DEs than both copper powders, most likely due to lower yield strength of the tin leading to better mechanical interlocking. In the following years, much importance was given to the metallization of polymers through cold spraying, with extensive reviews conducted by Gonzalez et al. [1], and more recently, by Parmar et al. [229] regrouping the major works in the field. Of notice, they highlighted numerous reports of successful cold spraying of copper on PEEK [29, 36-38, 113, 230, 231]. Thermoplastics being heat-deformable and ductile materials, they can be viewed as more prone to cold spray. Other studies, many quite recent, showed some success in cold spraying a variety of metals onto a variety of substrates, such as aluminum (or Al-based alloys) [33-35, 38], tin [28-31], iron [29], 316L stainless steel [32, 33], copper [31, 36-38, 232], or titanium [233]; on the substrate side focus was mainly turned towards thermoplastics such as nylon 6 [234, 235], polyamide 6 [232, 236] or polycarbonates [237]. On the downside, these coatings included issues that related to substrate damage [28, 31], relatively low DEs [29, 31, 32, 34] and delamination issues [36-38].

When working with thermosetting substrates, deposition was more difficult due to their relative brittleness. Affi et al. [21] could not cold spray aluminum on carbon fibre reinforced epoxy composites with satisfying results as coarse powders (~15µm) would erode the substrate and finer powders (~3µm) would produce easily peeled-off coatings. When a plasma-sprayed aluminum interlayer was sprayed on the surface before cold spraying, it was possible to obtain a thick aluminum coating [21]. With a pulse gas dynamic spray system, Robitaille et al. [63] could not successfully deposit zinc powders onto carbon/epoxy composites (erosion of the substrates), but deposition was possible with good adhesion strength when the substrate surface was co-cured with a thin layer of copper particles. Ganesan et al. [26] went further and studied the difference of deposition mechanism between thermoplastic and thermosetting substrates. They found that the particles did not undergo any plastic deformation due to the soft nature of the polymers and that, while deposition was possible on thermoplastics (seemingly through mechanical interlocking), only localized fracture was observable on thermosetting substrates hence an absence of retention. Another of their studies also proved the importance of surface treatment as a means to improve adhesion strength [27] which correlates well with previous successful depositions on thermosetting composites [21, 63]. This has lead to several studies looking at deposition methods involving

surface texturing [238], deposition of interlayers before cold spraying [239] or cold spraying mixtures of metal and polymer to gradually build towards a metallic layer [38].

Che et al. [28] attempted to coat carbon fibre reinforced epoxy composites with tin, copper and aluminum powders at various conditions of gas pressure and temperature: only deposition of tin was successful with the low pressure system. As a result, a "crack filling" mechanism was suggested to explain the deposition of the tin on the thermosetting composite substrate, as shown in Fig. 2-16. In this mechanism, the tin powders are softened/partially melted as the gas temperature is greater than the melting temperature of tin (around 300°C vs 232°C) then as they impact the surface, the still-solid core of the particle will generate cracks on the brittle epoxy surface that the softened tin can fill, thus not only filling cracks and limiting erosion, but also achieving mechanical anchorage [28]. As a means to improve the conductivity of these tin coatings, these tin powders were then mixed with copper or zinc powders: the conductivity was improved as compared to cold sprayed tin and the DE was greatly improved [44]. A tamping/peening effect from the harder SCs was suggested to cause this improvement, just as with

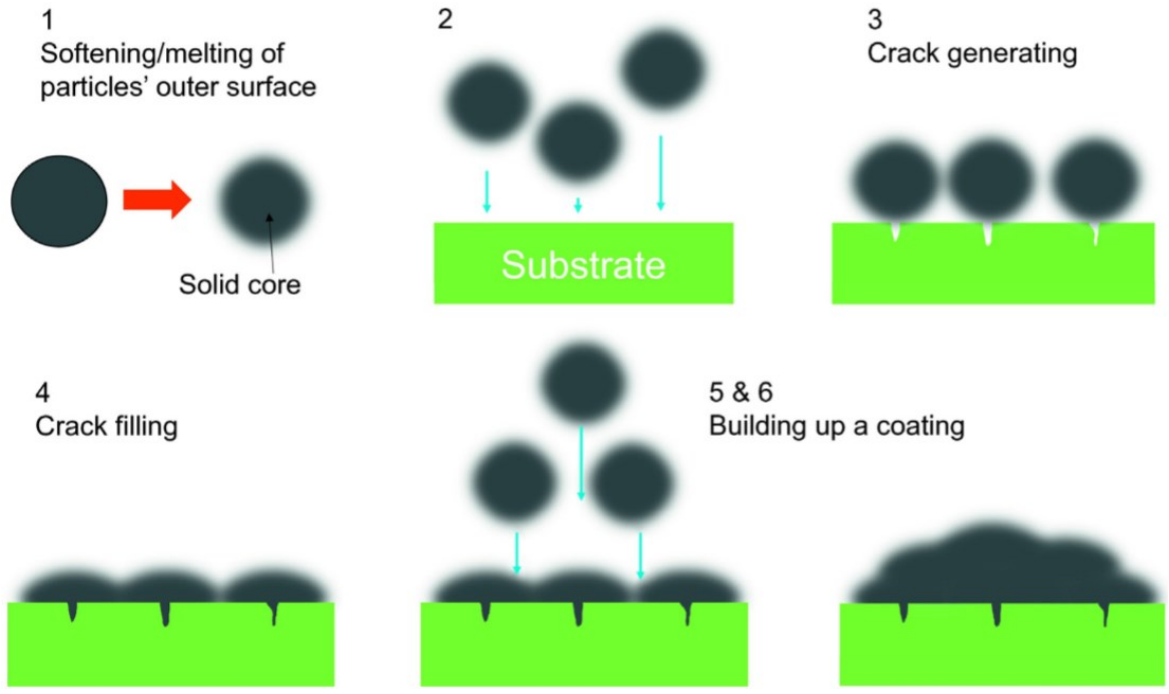

Fig. 2-16: *Schematic of the crack filling mechanism [28]*

the addition of ceramic powders in other studies [39, 130]. The addition of aluminum to feedstock tin powder was shown to also improve the DE of a pure tin coating, yet the degree of improvement brought by the aluminum was noticeably smaller than that of copper or zinc (maximum DE of 15% for pure tin and 20% with 90% Sn – 10% Al, versus 44% with an addition of 10% Zn or Cu) [240].

While some studies have been conducted to understand the metallization of CFRP substrates, with either single component metallic powders or powder mixtures, few studies offer a comprehensive understanding of the mechanisms involved in the deposition of metals onto CFRP. Typically, while it was observed that the addition of a SC could improve the DE of Sn on CFRP [44] and that the metallization of polymers required differentiating deposition into first-layer and build-up phases [29], the role of the SC was never associated with the different deposition phases, and therefore never considered in depth. Furthermore, a relation between SC properties and Sn DE improvement was never clearly established. Finally, only a limited amount of mechanical testing data is available for cold sprayed coatings on CFRP, and there again, it is difficult to establish how the SC may affect the adhesion of the coating to the substrate. This thesis is a continuation of the study on DE improvement brought by the SC, and more notably, this study aims to provide better understanding of SC properties on the cold spraying of tin onto CFRP, and a mechanistic description of the role of the SC. Ultimately, it is hoped that these results can provide better understanding of the cold spraying of single component metallic particles onto CFRP.

Chapter 3

Observation of an Indirect Deposition Effect while Cold Spraying Sn-Al Mixed Powders onto Carbon Fibre Reinforced Polymers

3.1 Rationale

To expand on the findings of the literature review of cold sprayed tin powder with other secondary components (Al, Cu, Zn), this chapter first aimed to understand how the addition of Al as a secondary component brought a change in DE trend, as compared to the addition of Cu and Zn. A Sn-Al powder mixture was sprayed onto epoxy-CFRP substrates for a wider range of gas pressures than previous studies.

This chapter has been published as:

Andre C. Liberati, Hanqing Che, Phuong Vo, Stephen Yue, "*Observation of an Indirect Deposition Effect while Cold Spraying Sn-Al Mixed Powders onto Carbon Fibre Reinforced Polymers*", J. Therm. Spray Technol. 29 (2020), 134-146. (Reproduction permissions obtained from Springer Nature)

3.2 Abstract

Single component tin coatings have successfully been cold sprayed onto carbon fibre reinforced polymers (CFRPs) in previous studies at McGill University. Coatings with mixed metal powders were also sprayed to improve the deposition efficiency and coating conductivity. Results indicated a noticeable improvement in deposition efficiency (DE) related to the addition of a secondary metallic powder (aluminum, copper and zinc); this study is focused on the effect of aluminum. Following cold spray of various Sn/Al mixtures over a wide range of gas pressures, unusual coating morphologies were observed. The study of these morphologies leads to the description of two distinct deposition phases depending on the spray pressure: a direct deposition

effect and an indirect deposition effect. The presence of submicron particles also supports the occurrence of a powder melting phenomenon during the process. Numerical simulations were conducted to support the description of these phenomena.

3.3 Introduction

CFRPs are poor electrical conductors – the carbon fibres are approximately 1,000 times more resistive than aluminum to current flow and epoxy resins are 1,000,000 more resistive [56] – so they are prone to damage from lightning strikes that aircraft endure once per year on average [53]. To improve their conductivity while maintaining low densities, "metallizing" or applying metallic coatings to composites such as CFRPs has received increasing interest, but these coatings still suffer from poor quality (porosity, adherence [241], conductivity [6], etc.). "Metallization" can be achieved through a series of approaches, such as lay-up molding [147] or arc spray [11], but cold spray appears as a legitimate alternative [21, 28, 29, 31, 64] since it uses relatively low temperatures (several hundred versus several thousand degrees for other techniques), thus limiting the risk of oxidation of the metallic powder particles and the heat damage of the substrate [21].

Coating on this substrate through cold spray has been tried and mixed results have been obtained regarding the erosion of the soft substrate due to the higher hardness of most metallic powders [25, 27, 28]. Nonetheless, some researchers have encountered success in depositing tin particles on polymeric substrates [28, 29, 31] all while recording relatively low deposition efficiencies (DE) (i.e. the ratio of effectively deposited particles on the substrate versus the amount of sprayed particles). This was associated with a "crack filling" mechanism described by Che et al. [28], where thermally softened or partially melted tin particles were suspected to impact the substrate, and while the harder core of the particle would generate micro-cracks in the CFRP substrate, the softer outer-core would immediately fill the cracks and provide mechanical interlocking with the substrate. This was supported by microstructural observations and by using process temperatures of 280°C or 300°C, quite largely above the melting point of tin (232°C) [28]. The seemingly small increase in temperature (from 280°C to 300°C) seemed to enable the "crack filling" mechanism, as deposition was almost inexistent at 280°C yet took place at 300°C.

In parallel, several researchers have proven that the deposition of a coating on a substrate can be enhanced by mixing ceramic powders in the feedstock powder, which will produce a shot-peening effect on the relatively softer feedstock powder and produce better coatings [39-41]. Che et al. [44] observed a similar improvement of the coating deposition process when mixing metallic powders (zinc or copper) with tin powders. This improvement was associated with the tamping effect of the secondary component on the relatively softer tin. In a previous study [45], the addition of aluminum to feedstock tin powder was shown to also improve the DE of a pure tin coating, but while the DE trend for tin, mixed tin-zinc and tin-copper powders seemed quite clear (decreasing for the chosen pressure values [28, 44]), mixed tin-aluminum powders presented an increasing DE trend; however, only few spray parameters were tested, so a maximum DE value for tin-aluminum mixed powders was not located.

In this present study, mixed tin-aluminum powder was cold sprayed on CFRP and mild steel substrates over a wide range of carrier gas pressures to corroborate and expand on the results of [45]. Tin-aluminum mixed powder with a 90:10 weight ratio was cold sprayed onto a thermosetting epoxy CFRP substrate at various process conditions with a low-pressure cold spray system. Microanalysis of the coatings was then performed and the deposition mechanism of the mixed powders on CFRPs is discussed, namely for higher pressures where an unusual coating morphology was observed. The DE was also measured and a discussion on the variation of the DE is proposed. Given the absence of references supporting such a coating morphology, a simple 3D model was established based on the parameters chosen in recent computational fluid dynamics (CFD) models, destined to optimize cold spray parameters [119, 121, 127, 135, 242]. The purpose of this model was to simulate the flow of particles in the cold spray process and study the metrics of the powders (namely trajectory, velocity and temperature) as they impinge the substrate surface, and therefore support the mechanisms advanced to explain the observed coating structures.

3.4 Experimental Methods

The feedstock materials used in this work are listed in Table 3-1. The particle sizes of the feedstock powders were measured with a laser scattering particle size analyzer (LA-920,

HORIBA, Japan) and their distribution is presented in Fig. 3-1. The tin powder was relatively spherical and had a broad monomodal and non-symmetrical distribution, whereas the aluminum powder, which was also spherical, had a more continuous size distribution with a higher average particle size. The average Vickers hardness of the feedstock powders was measured by mounting the powders and by using a Clark CM-100AT Microhardness Tester (Sun-Tec, Novi, USA) for a penetration time of 15 s under a load of 10 gf: the hardness of the aluminum powder was more than double that of the tin powder. Both powders were of commercial purity. The scanning electron microscope (SEM) images of the single component powders are presented in Fig. 3-2. The powders were mixed in a metallic can without additional media (e.g. milling balls) with a double movement powder mixer for 1h. No significant morphological changes or hardening were noticed in the mixed powder when compared with the starting powders : the absence of morphological changes was verified through SEM imagery of the mixed powders and the hardness of the mixed powders was measured as per the hardness for the initial feedstock powders.

Table 3-1: *Properties of the feedstock powders used in this work.*

Powder	Morphology	Supplier	D_{avg}	Hardness
Al	Spherical	Valimet	25 µm	27 HV
Sn	Relatively Spherical	CenterLine, SST	17 µm	11 HV

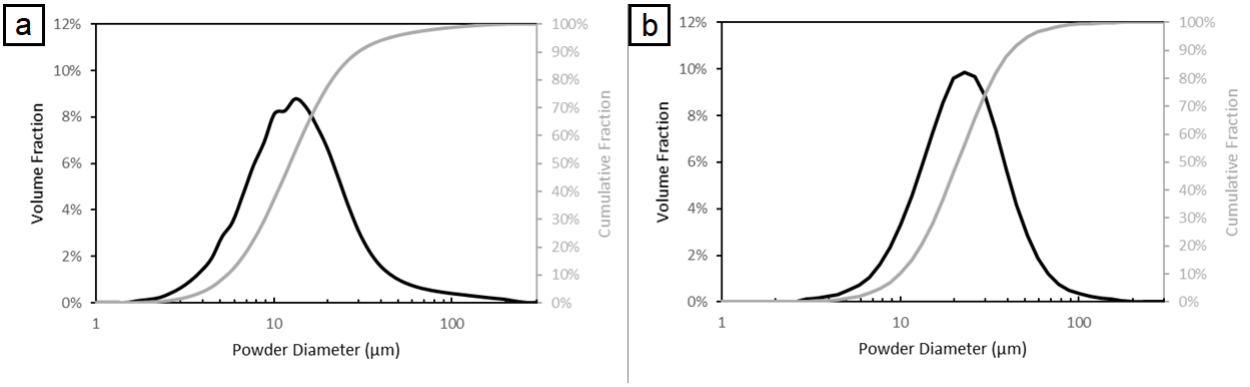

Fig. 3-1: *Powder size distribution (a) of the tin powder and (b) of the aluminum powder.*

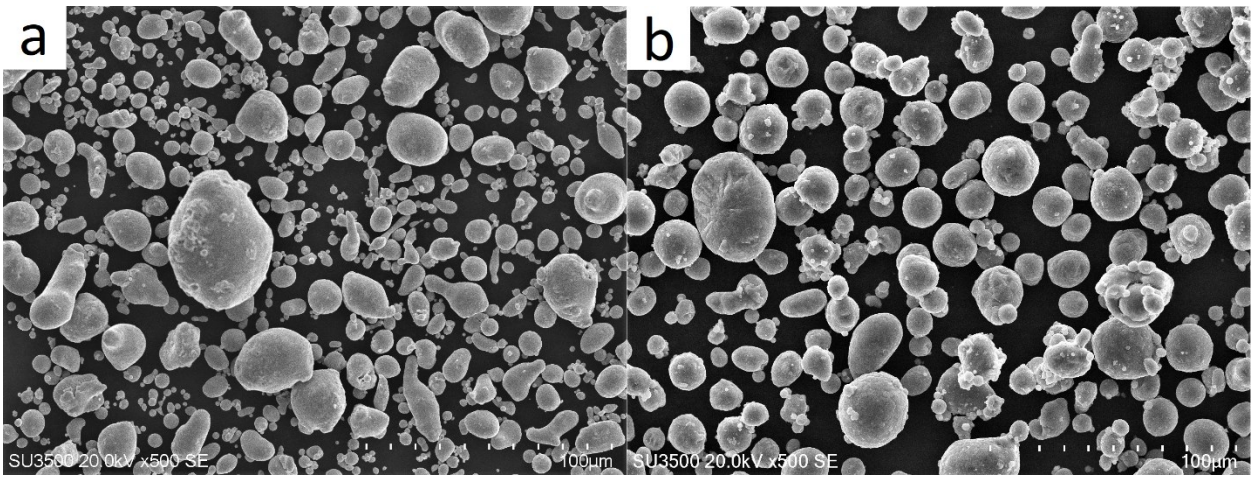

Fig. 3-2: *SEM images of the feedstock powders: (a) Sn, (b) Al.*

The substrates used in this work were CFRPs provided by Bombardier Aerospace (Montreal, Canada) and 1020 mild steel plates. The steel substrates were used as a benchmark to compare the spraying of powders on CFRPs to a typical metal-metal cold spraying situation. The CFRP material used here consists of a thermosetting epoxy matrix with continuous carbon fibre reinforcements. The CFRP-panels were made of four plies of epoxy/carbon fibre prepreg ([0/90]2s) and have a coating finish used by the manufacturer. Sheet sections of dimensions 7 x 3 cm were used as substrates during the cold spray campaigns. The substrates were degreased with acetone and the mild steel plates were grit-blasted with 24 grit alumina before cold spraying. The CFRP substrates were not grit-blasted as it would result in the erosion of the substrate.

The cold spraying was performed at the McGill-NRC cold spray facility at National Research Council Canada in Boucherville. The cold spraying was performed at low pressure with a commercially available CenterLine SST system (Supersonic Spray Technologies, CenterLine Windsor Limited, Canada). This choice enabled the use of the so-called “downstream injection” mode, where the particles were injected in the main gas stream after the throat of the nozzle. The risk of clogging the nozzle when using metals with low melting points, such as tin, was thus reduced. The primary cold spray parameters are listed in Table 3-2. These parameters were chosen based on previously successful cold spray campaigns with tin [28, 44], and a wider range of carrier

Table 3-2: *Principal cold spray parameters.*

Powder	Carrier Gas Temperature °C	Gas Pressure psi (MPa)
Sn-10Al	300	50 (0.34), 55 (0.38), 60 (0.41), 70 (0.48), 80 (0.55), 100 (0.69), 120 (0.83), 150 (1.03)
	320	50 (0.34), 60 (0.41), 80 (0.55), 100 (0.69), 120 (0.83), 150 (1.03)

gas pressures was chosen expand on the results of [45] and determine a maximum DE value for the deposition of mixed tin-aluminum powders. The carrier gas was nitrogen, the stand-off distance was 18 mm and the gun travel speed was 25 mm/s. The powder feeder rate was set to 1 revolution per minute (RPM), which gave a measured feeding rate of 11.5 g/min. Only one pass was sprayed for each set of conditions, with a step size of 1 mm (18 steps), so that the average DE from a large area, together with a study focused on the DE trend, would be meaningful.

Deposition efficiency was measured as the mass gain of the substrate divided by the total mass of feedstock powder fed during the time the gun was over the substrate. After the cold spray process, the samples were observed from a top-surface view then prepared as metallographic samples and characterized with a Hitachi SU3500 Scanning Electron Microscope. The cross-sectional samples were cut and observed parallel to the gun spraying direction. A 3D-Optical Surface Profiler (ZYGO, Connecticut, USA) was also used to measure the surface roughness and support large-scale microstructural observations. On each sample, twelve areas of 3 x 3 mm were analyzed to determine the average surface roughness. The main measurements were carried out around the root mean square roughness Sq and the root mean square gradient of the surface Sdq as they provide insight into the topography of the surfaces regarding not only height but also gradient [243, 244]. More specifically, these parameters offer more detailed information on the surface conditions as compared to the average surface roughness (Sa) as Sq includes Sa and the standard deviation of the roughness as per the definition of the root mean square, and Sdq is affected both by texture amplitude and spacing, therefore Sdq can provide information on the slopes which comprise the surface in the case of coatings with similar values of Sa [243].

ANSYS Fluent (v19.3.0) was used to carry out CFD simulations, based on simulations previously made in the cold spray field [119, 121, 127, 135, 242], and process parameters were chosen to be as close as possible to the system parameters used in this study. The following is a list of the modules and parameters chosen in the software – further understanding on them can be acquired from the Fluent User's Guide [245]. The nitrogen carrier gas was set to be an ideal gas and a steady-state solution for the gas flow was calculated with a density-based solver [119, 121]. Flows were modelled in 3D to account for the downstream lateral injection that the Centerline SST system offers and that simpler 2D-axisymettrical models cannot account for. The structured mesh was developed with approximately 111 000 elements with refinement around the key elements of the system (nozzle throat, powder injection nozzle, nozzle exit, "substrate" wall) to better account for thermodynamic property changes associated with gas expansion. The final mesh can be observed in Fig. 3-3. The Navier-Stokes equations for mass, momentum and energy of the gas flow were solved for a steady state in their Reynolds-averaged form and, consequently, extended by a standard k-ε turbulence model with standard wall functions [121]. Two-way coupling systems with advanced turbulence models can be implemented to provide more accurate simulations [242] but given the dilution of the powder in the gas flow (solid phase volume fraction <10%), it can be assumed that particle-particle and particle-gas interactions are negligible [119, 127] and a Lagrangian (one-way coupling) solution is sufficient to study particles in the flow. The Discrete Phase Model algorithm can be assumed to be accurate [119] and a face normal injection of 20-µm tin powders in the gas flow was implemented at the powder injection point. To account for particle dispersion associated with turbulence effects, the Stochastic-Tracking type model is activated and the Discrete Random Walk model is used to predict the fluctuating components of the total particle

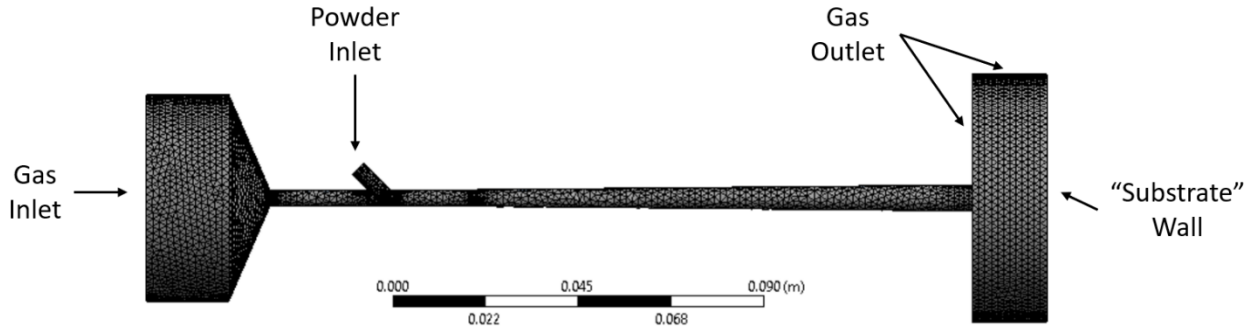

Fig. 3-3: *Illustration of the 3D computational grid.*

velocity and effects on its trajectory [119, 245]. Finally, boundary conditions are set as indicated on Fig. 3-3 : the gas inlet is defined as a pressure inlet with two sets of conditions (320°C/60psi and 320°C/150psi), the powder inlet is defined as a pressure inlet with a pressure of 14.5psi (=0.1MPa) to 43.5psi (=0.3MPa) to assist the injection of powder in the system and avoid potential expulsion of powders before their injection during calculation, the gas outlet is defined as an atmospheric pressure outlet located far enough from the nozzle exit to avoid unrealistic settings [119] and the nozzle wall was set as an adiabatic no-slip boundary. The substrate is defined as a wall and interactions with it are neglected: particles are supposed to rebound on the substrate without energetic loses.

3.5 Results

Fig. 3-4 shows the DE of the mixed powder Sn-10Al on different substrates at 300°C and 320°C as a function of the gas pressure. Coating deposition on steel was achieved for all conditions, while deposition on CFRP was irregular in some cases, namely higher pressures. While the DE on steel provides one maximum for both spray temperatures (around 70 psi), the DE on CFRP seems to provide a local maximum (around 70 psi) then a plateau regime with increasing pressure. Note that previous spraying of single component aluminum on CFRPs generated no deposition because of erosion, whereas pure tin generated a coating with a maximum DE of 20% [28].

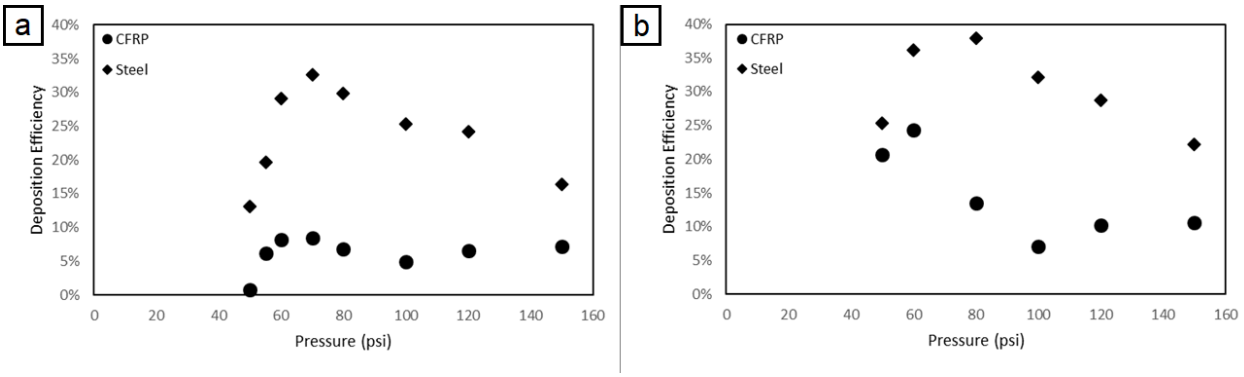

Fig. 3-4: *Deposition efficiency of Sn-10Al mixed powders sprayed on different substrates (a) at 300°C and (b) at 320°C.*

The retention rates of aluminum in the CFRP coatings were measured in the cross-section for several coating conditions (60 psi at 300°C and 60, 80 and 100 psi at 320°C). These rates were estimated by measuring the relative areas of tin and aluminum in SEM BSE-COMP images using an image analysis method. From these retention rates, the DE of each pure element in the coating can be calculated with the following expressions:

$$DE_{Al} = \frac{r_{Al} * DE}{0.1}$$

$$DE_{Sn} = \frac{(1 - r_{Al}) * DE}{0.9}$$

where DE, DE_{Al} and DE_{Sn} are respectively the overall DE of the coating, pure Al and pure Sn and r_{Al} is the weight fraction of Al in the coating. Coating thickness was also measured with these cross-sectional micrographs. The results are listed in Table 3-3. The retention rates in the coating are very low compared to the initial 10% of aluminum in the powder mix. For the coatings at 60 psi, variations are observed in the overall DE, the DE of pure tin and the thickness of the coating while the retention rates of aluminum remain close to 0%. With increasing pressure at 320°C, the overall DE, the DE of pure tin and the coating thickness decrease while the retention rate of aluminum increases. Nevertheless, the effective DE of pure aluminum remains relatively low (under 20% of the initial aluminum input). The cross-sectional micrographs of the mixed powder coatings sprayed for these conditions are presented in Fig. 3-5. These coatings are relatively dense

Table 3-3: *Retention rates of aluminum measured at the cross-sections of the CFRP substrates and calculated deposition efficiencies for aluminum and tin in the coating.*

Temperature	Pressure	Volume fraction of Al	Weight fraction of Al	Deposition Efficiency (%)			Coating thickness
(°C)	(psi)	(%)	(%)	Overall	Al	Sn	(µm)
300	60	0.7	0.2	8	~0	9	90
320	60	0.7	0.3	24	1	27	290
320	80	1.9	0.7	13	1	15	150
320	100	7.6	3.0	6	2	7	70

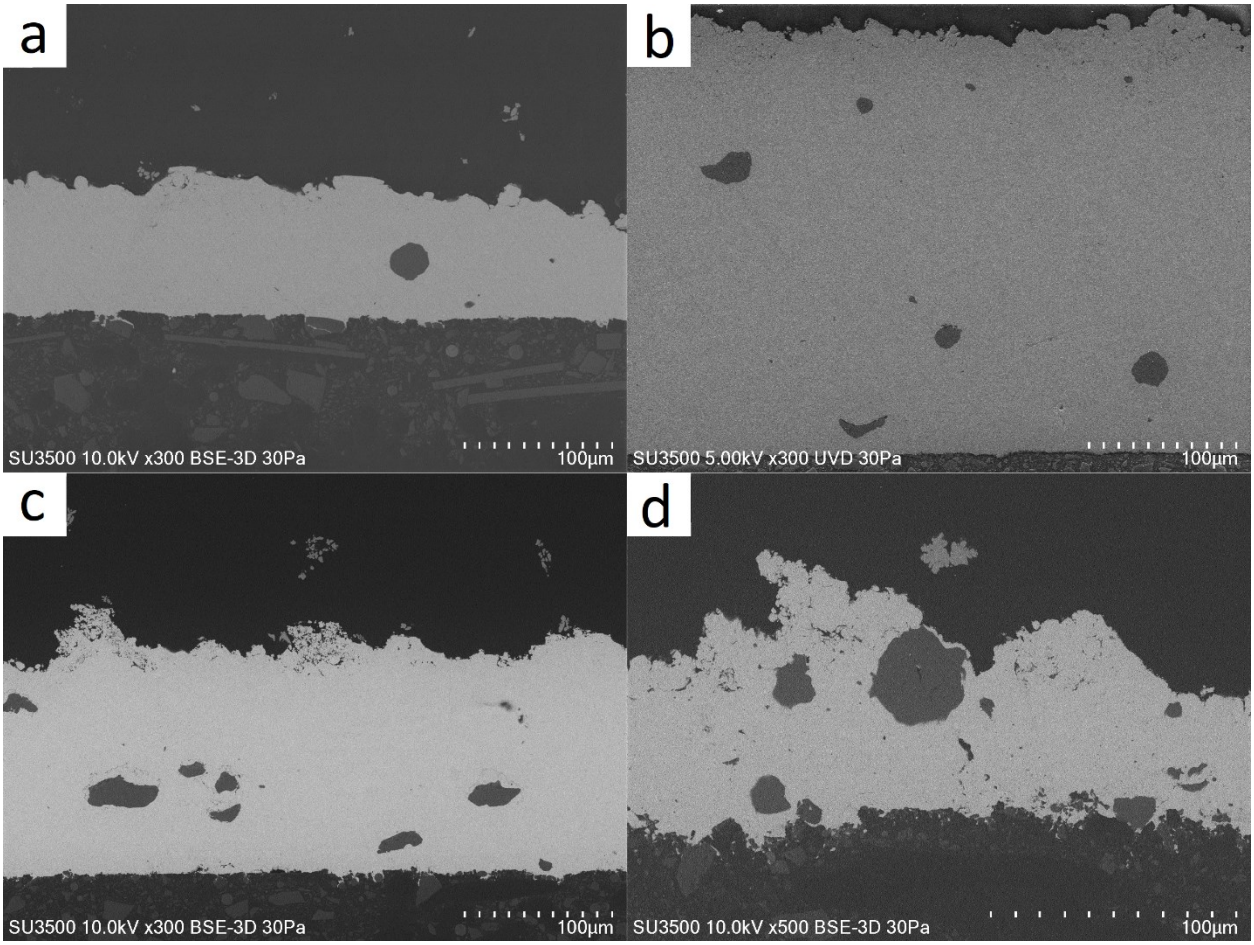

Fig. 3-5: *SEM images of the cross-sectional microstructures for the Sn-10Al coatings at similar magnifications: (a) 300°C and 60 psi, (b) 320°C and 60 psi, (c) 320°C and 80 psi, (d) 320°C and 100 psi.*

with small defects mainly localized around the aluminum particles and only a small number of aluminum particles are noticeable in the coatings, which exemplifies the low retention rates of aluminum. More noticeably, the number of aluminum particles barely increases with increasing pressure at 320°C, while the thickness of the coatings decreases (from 290 to 70 µm) as does the overall DE (from 24% to 6%) and the DE of pure tin (from 27% to 7%). Therefore, there does not seem to be an obvious relation between aluminum retention and overall DE. The area around the top surface seems to indicate more roughness with higher pressures as can be seen in Fig. 3-5 d.

The latter phenomenon can be better visualized with low-magnification top-surface images of the coatings as seen in Fig. 3-6. This figure shows an evolution of the coating with increasing pressure while cold spraying at 300°C. For pressures below 60 psi (Fig. 3-6 a), a relatively uniform and even surface is obtained. For pressures around 80psi (Fig. 3-6 b), small agglomerations of powder can be observed and finally, for relatively higher pressures (Fig. 3-6 c-d), larger dendrite-like protrusions are observable. On another note, the carbon fibre matrix is apparent for very high pressures, as indicated by the white arrow in Fig. 3-6 d, revealing erosion of the CFRP. The previously described protrusions at higher pressures are also clearly visible to the naked eye as shown in Fig. 3-7. These protrusions have the same direction as the spray gun as it descends on the CFRP substrate, but they are not noticed on any of the steel substrates. Fig. 3-7 also reveals a strong difference in deposition throughout the substrate depending on the considered area: in the

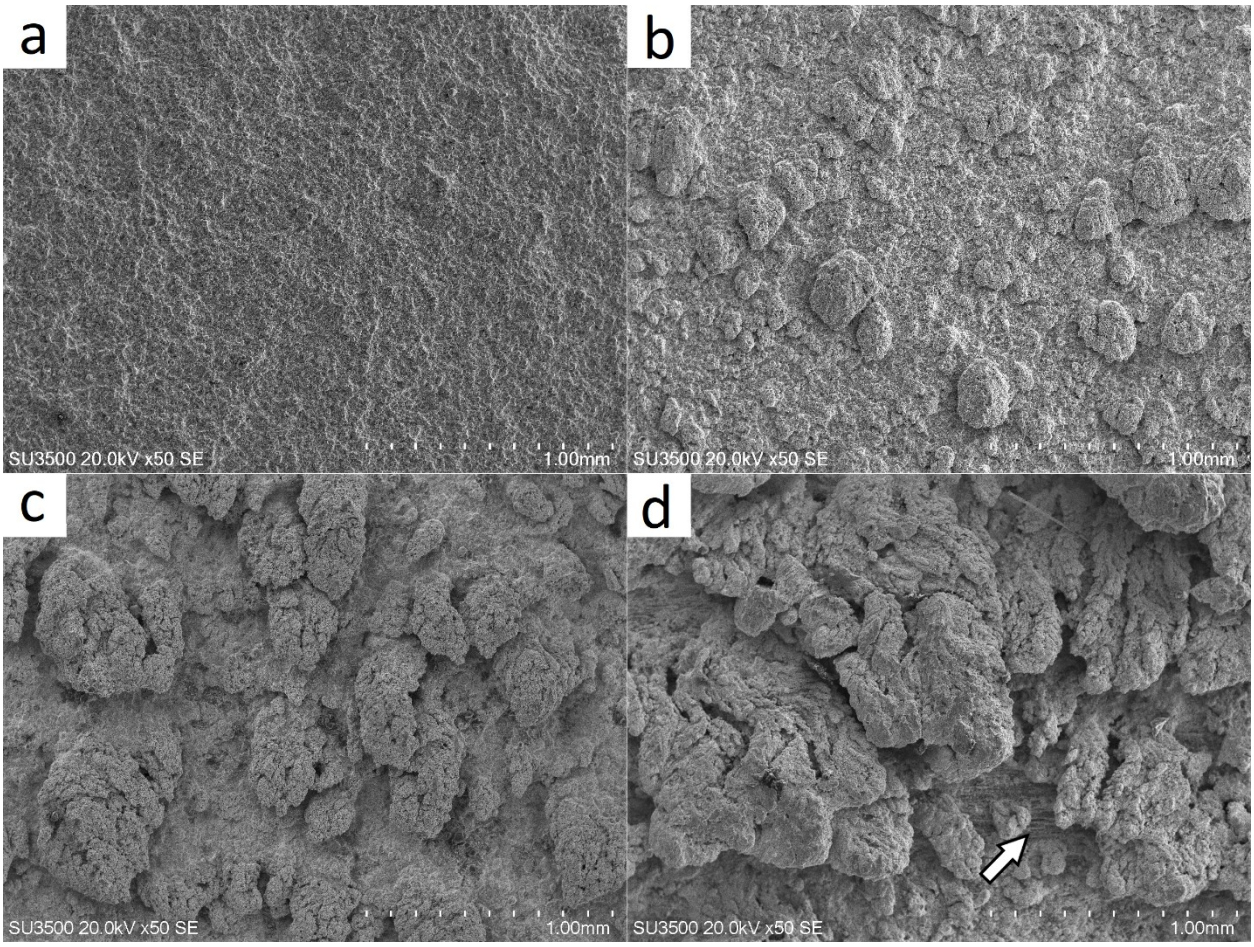

Fig. 3-6: *Low magnification SEM top surface images of the Sn-10Al coatings sprayed on the CFRP substrates at 300°C for various pressures: (a) 60 psi, (b) 80 psi, (c) 100 psi, (d) 150 psi.*

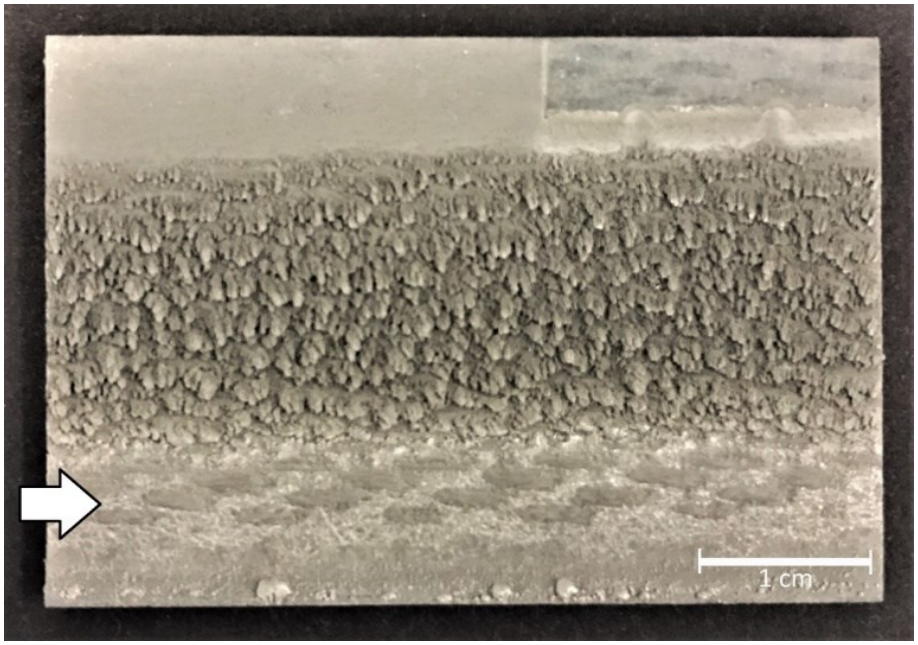

Fig. 3-7: *Image of the Sn-10Al coating on a CFRP substrate at 300°C and 150psi. The white arrow corresponds to the last sprayed step in the raster scan.*

vicinity of the last spray step, there is no coating on the substrate (the carbon fibre matrix is visible) whereas in previously sprayed areas there are the previously discussed protrusions. Below the last spray step, some powder agglomerates can also be noticed. This behavior is representative of all higher pressure cold sprayed CFRP substrates (above 100psi). The coatings at 320°C follow the same structural evolution with increasing pressure. Aluminum retention in the top surface is quite negligible.

Height profiles of areas similar to the low-magnification microstructures presented in Fig. 3-6, are presented in Fig. 3-8, to support the macro- and microscopic observations. For lower pressures (Fig. 3-8 a), the surface roughness is low (Sa < 20µm), the maximum height of the areal surface remains within 100-200µm (several times the diameter of the feedstock powder) and the craters generated by impinging powders on the substrate are visible. For higher pressures (Fig. 3-8 b), surface roughness is higher (Sa >100µm), the maximum height of the areal surface is above 500µm and the previously discussed protrusions appear clearly. For the CFRP coatings at 320°C similar observations are made, whereas for steel substrates, the height profiles are fairly similar to

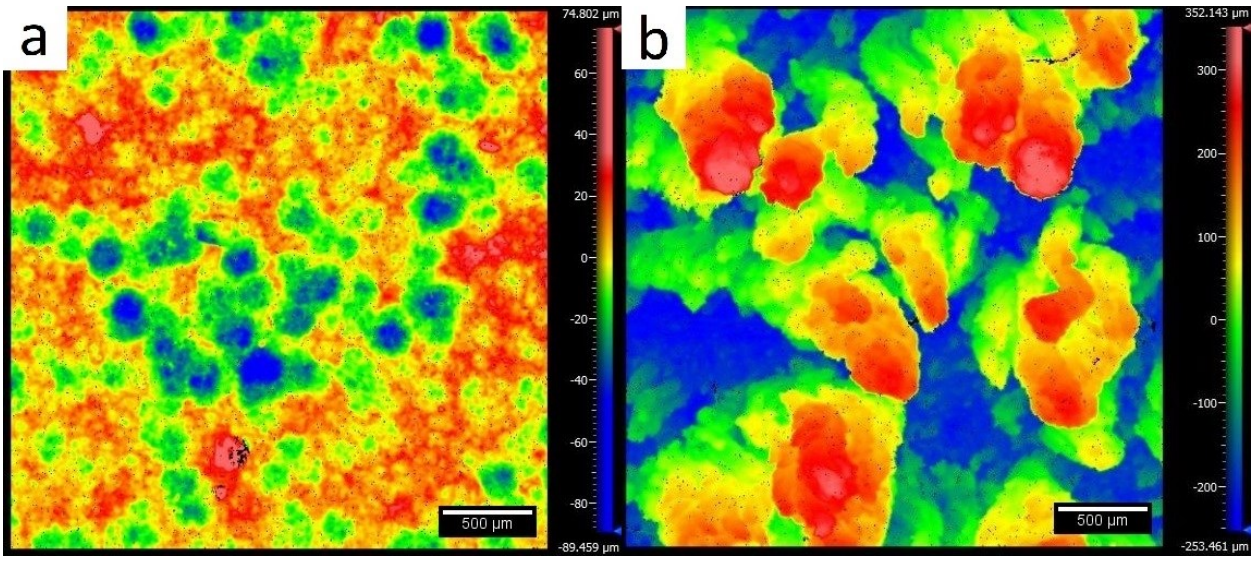

Fig. 3-8: *Height profiles of the coatings sprayed onto the CFRP substrate at 300°C: (a) 55 psi, (b) 150 psi. Note the difference in height scale.*

the case of lower pressure CFRP height profiles (Fig. 3-8 a). The graph presenting Sq as a function of pressure is presented in Fig. 3-9: Sdq presents the same evolution as Sq. These graphs reveal low roughness values of for both substrates at pressures below 70 psi, and at higher pressures, the roughness values remain low for the steel substrate while an increase is observed for the CFRP substrates.

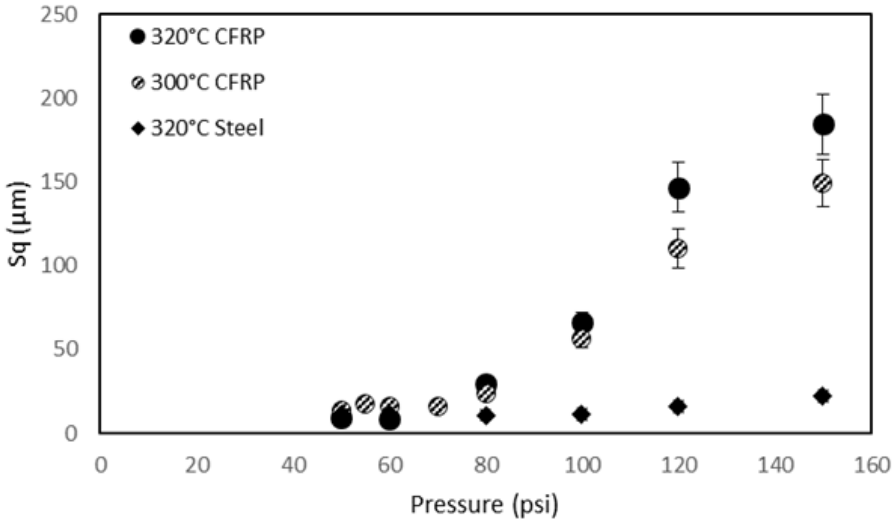

Fig. 3-9: *Root mean square roughness of the surface as a function of gas pressure.*

With higher magnification SEM images of the CFRP coatings at 300°C, tin powders can easily be observed for lower pressures . These particles show minimal deformation and sizes ranging from 10 to 20 µm which is relatively similar to the initial feedstock powder (Fig. 3-2 a). For higher pressures, these particles become less and less discernable. Some larger particles may be observed with intermediate pressures but generally only particles around 5-10 µm are observed on the top surface. With higher pressures (over 100psi), small satellites are observed throughout the top surface and cover the few powders that can be seen. At 150psi, these satellites almost completely cover the top surface. Again, the coatings at 320°C follow the same structural evolution with increasing pressure. Higher magnification images of the high-pressure coatings reveal that the small satellites are small tin particles generally smaller than 1 µm, as seen in Fig. 3-10. As opposed to the feedstock powder (Fig. 3-2 a), these particles are spherical and are not representative of the powder distribution results. It is important to note that the detection limit of the Horiba LA-920 is 0.02 µm and in the particle size distribution of the feedstock tin powder, no powders smaller than 1.5 µm are detected.

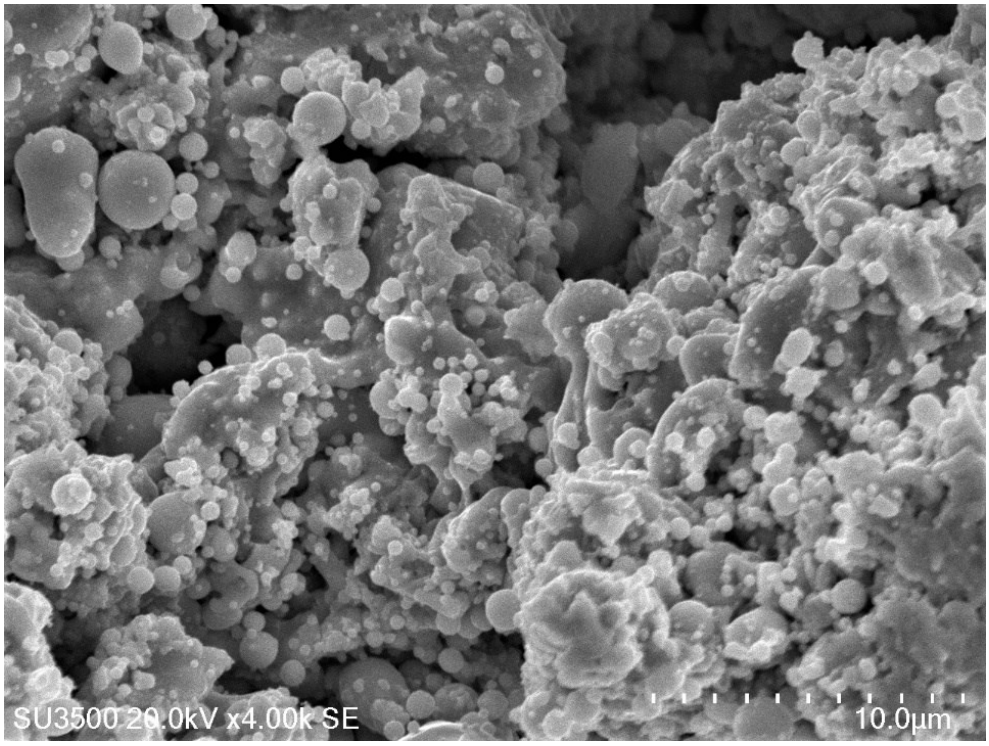

Fig. 3-10: *High magnification SE top surface image of the Sn-10Al coatings sprayed on the CFRP substrates at 320°C and 100 psi.*

3.6 Discussion

The content of aluminum in the studied coatings is far lower than the initial aluminum input, as noted when studying the retention rates and resulting DE of aluminum in Table 3-3. An increasing fraction of aluminum was noticeable in the coatings at 320°C, but the DE of aluminum hardly increased and only the tin content in each coating noticeably evolved, which suggests that the evolution of the overall DE is related to the actual deposition of tin and not the aluminum. Therefore, there seems to be no relation between the cold spray conditions and aluminum retention here as already noted by Liberati et al. [45]. A thorough study of the steel cross-sections would be interesting to compare the retention of aluminum in the steel coatings.

The maximum DE value of pure tin at 300°C (15%) in previous work [28] is higher than that of Sn-10Al at 300°C (8%) measured in this work, while Al was expected to help increase the maximum DE as in [45] (obtained maximum DE of 20%). This increase was nevertheless observed at 320°C, where the maximum of Sn-10Al is 25%. Furthermore, the DE of Sn-10Al at 300°C and 320°C follow a similar trend with increasing pressure as the DE of pure tin on CFRP from [9], but they do not follow the same increasing trend observed in [45]. Therefore, the current results do not allow us to corroborate the results from [45] as initially intended. These differences could be related to process fluctuations between studies. Further experiments comparing pure tin and mixed metal powders such as tin-aluminum should be conducted to determine the effect of the secondary component with better comparability.

On another note, certain trends seem to stand out when comparing the DE results of this study with the obtained macro- and microstructures. For lower pressures (below 60 psi), the obtained coatings seem to be quite uniform with relatively higher DE and dense, uniform coatings (Fig. 3-6 a, Fig. 3-8 a). For intermediate pressures (70-80psi), the coatings tend to be thinner with lower DE and the appearance of small agglomerates on the top surface. For higher pressures (above 100 psi), DE slightly increases then plateaus, but deposition is very inconsistent: two areas clearly stand out from a macroscopic point of view with an area presenting dendrite-like protrusions that follow the same direction as the gun displacement (Fig. 3-6 d, Fig. 3-8 b) and another area, directly below the last spray step, that presents very poor deposition and exposure of the carbon fibres

(indicative of a non-negligible amount of substrate erosion). The acquired roughness data (Fig. 3-9) supports this microstructural evolution and shows that with increasing pressure, coatings on the CFRP present increasing roughness and gradients that are significant of steeper peaks and can be related to the appearance of the high-pressure protrusions. Furthermore, observation of the CFRP coating cross-sections (Fig. 3-5) indicates that increasing carrier gas pressure leads to a decreasing coating thickness. Cross-sections of higher-pressure coatings (120, 150 psi) were not observed but, given the top-surface micrographs of the coatings at 150 psi that reveal the carbon fibre matrix, it can be suggested that the average coating thickness would be minimal and only protrusions would provide a measurable thickness – not an actual coating. Therefore, there seems to be no direct deposition of powders for higher pressures, so the existence of deposited powders under the form of protrusions at these pressures would indicate that an indirect powder deposition phenomenon (or redeposition phenomenon) must be predominant. Nevertheless, given the seemingly uninteresting properties that would be obtained with such coatings, available literature on this matter is quite sparse.

With regards to coating formation on CFRP substrates, the DE curves could then be separated into two curves as shown in Fig. 3-11 a: deposition on the CFRP would take place for pressures below 80 psi (thick line), then the redeposition effect would be observed for higher pressures (dashed line). This can be supported by the roughness results (Fig. 3-11 b) where low pressure results present a near-constant value (thick line), whereas higher pressure results present

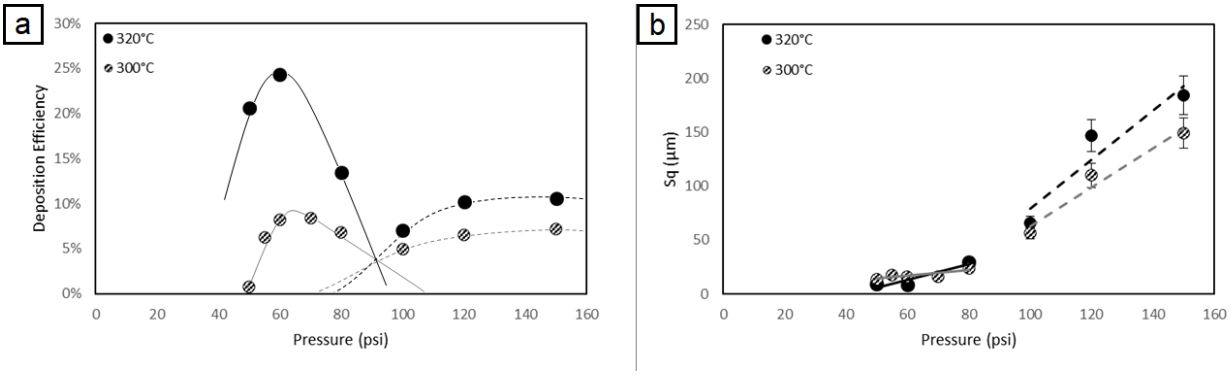

Fig. 3-11: *Different deposition behavior of Sn-10Al mixed powder sprayed on CFRP at 300°C and 320°C: a) Deposition efficiency, b) Root mean square roughness of the surface. The continuous line would represent the deposition curve, while the dashed line would represent the redeposition curve.*

an increasing trend (dashed line). The existence of two different behaviors for the deposition of Sn-10Al on the CFRP substrates could then be explained by these two different phenomena. The absence of an observable redeposition effect on the steel substrates (i.e. no protrusions) would then explain the different behavior for the DE curves or roughness curves of both substrates as described respectively for Fig. 3-4 and Fig. 3-9.

Based on the observations made for the top-surface views of the CFRP coatings, it is possible to explore potential mechanisms for the redeposition process. Intermediate pressures reveal small agglomerates on the top surface (Fig. 3-6 b) that seem to be either larger powders or accumulations of smaller powders. At higher pressures, sprayed powders do not directly adhere to the substrate (no coating during the last step of the spray gun, as seen in Fig. 3-7) but they adhere to the previous sprayed steps and give agglomerations or protrusions of particles. For these intermediate and higher pressures, powder velocities must be close to the erosion velocity (upper limit of the deposition window as described by Schmidt et al. [144]) for there to be erosion. This leads to the suggestion that either deposition of a small fraction of powders may be observed in the periphery of the main spray area (with velocities being below the erosion velocity) or a redeposition of the powders with velocities above the erosion velocity takes places. As pressure increases, this redeposition effect would be predominant as there is more erosion, i.e. more powders would be above the erosion velocity. These powders could rebound from the substrate while remaining in the gas flow, then be accelerated anew to a velocity in the deposition window, hence leading to a possible redeposition of the powders. A schematic representation of this mechanism is presented in Fig. 3-12 a. This phenomenon could explain the deposition of powders or agglomerates of powders as described in Fig. 3-6 b but does not explain the development of protrusions that seem to grow as the pressure increases. For this phenomenon, a possible sweeping effect could simultaneously be at cause (Fig. 3-12 b): as the powders impact the substrate, they could be swept laterally by the gas flow (instead of rebounding into the flow), gradually losing velocity and “re-entering” the deposition window to effectively adhere to the deposited agglomerates. This agrees with the idea that the protrusions are oriented in the same direction as the gun displacement direction, since powders swept upwards from the last spray step to a previous

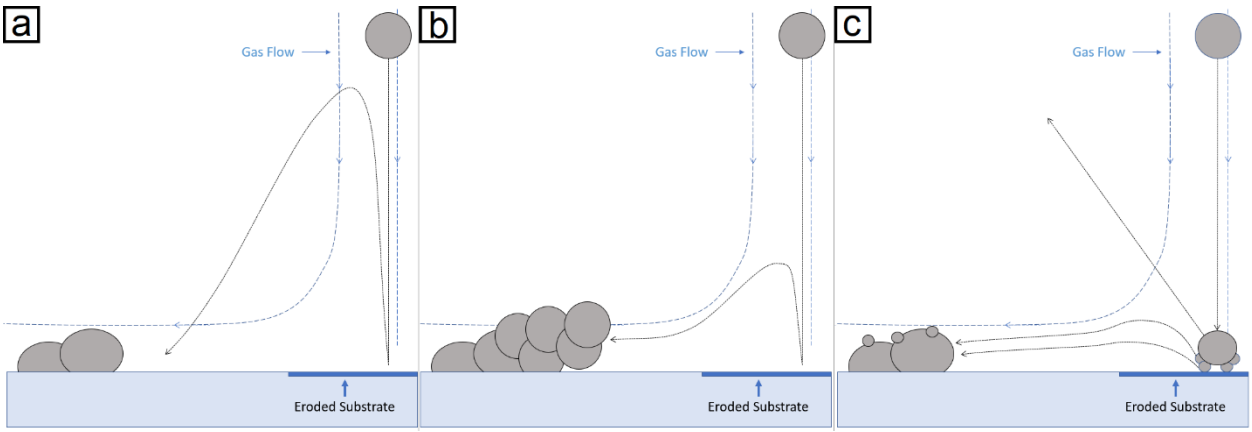

Fig. 3-12: *Schematic representation of potential indirect deposition mechanisms: a) Redeposition of rebounding powders, b) Deposition of laterally swept powders, c) Splashing of partially melted Sn powders.*

spray step would build up on the agglomerates and so the protrusions would build towards the last spray step.

By comparing the DE results on steel and CFRP, the work of Che et al. [29] differentiating the deposition of the first layer of powder on a substrate and the build-up of subsequent layers provides support for these mechanisms. A schematic description of the corresponding deposition windows is proposed in Fig. 3-13. In this figure, the deposition window of Sn on CFRP is as proposed in [29] for polymers while the deposition window of tin on steel shows a larger window for the first layer build-up, as tin is a softer material than steel and therefore will not erode steel, but might erode tin. For deposition of tin on steel, the critical deposition step is the tin-on-tin build-up step as it has the smallest deposition window, which can explain why the DE on steel will increase to a maximum then decrease with higher pressures as tin erodes tin. On the other hand, for deposition of tin on CFRP, the critical deposition step is the tin on CFRP first layer which is quickly exposed to erosion for intermediate pressures as shown by the decreasing DE trend. The observed DE plateau at higher pressures and suggested indirect deposition effect are then only possible from a velocity point of view if high velocity powders rebound on the surface of the substrate and return towards the substrate at a velocity in the deposition window of tin on CFRP, as described in Fig. 3-13.

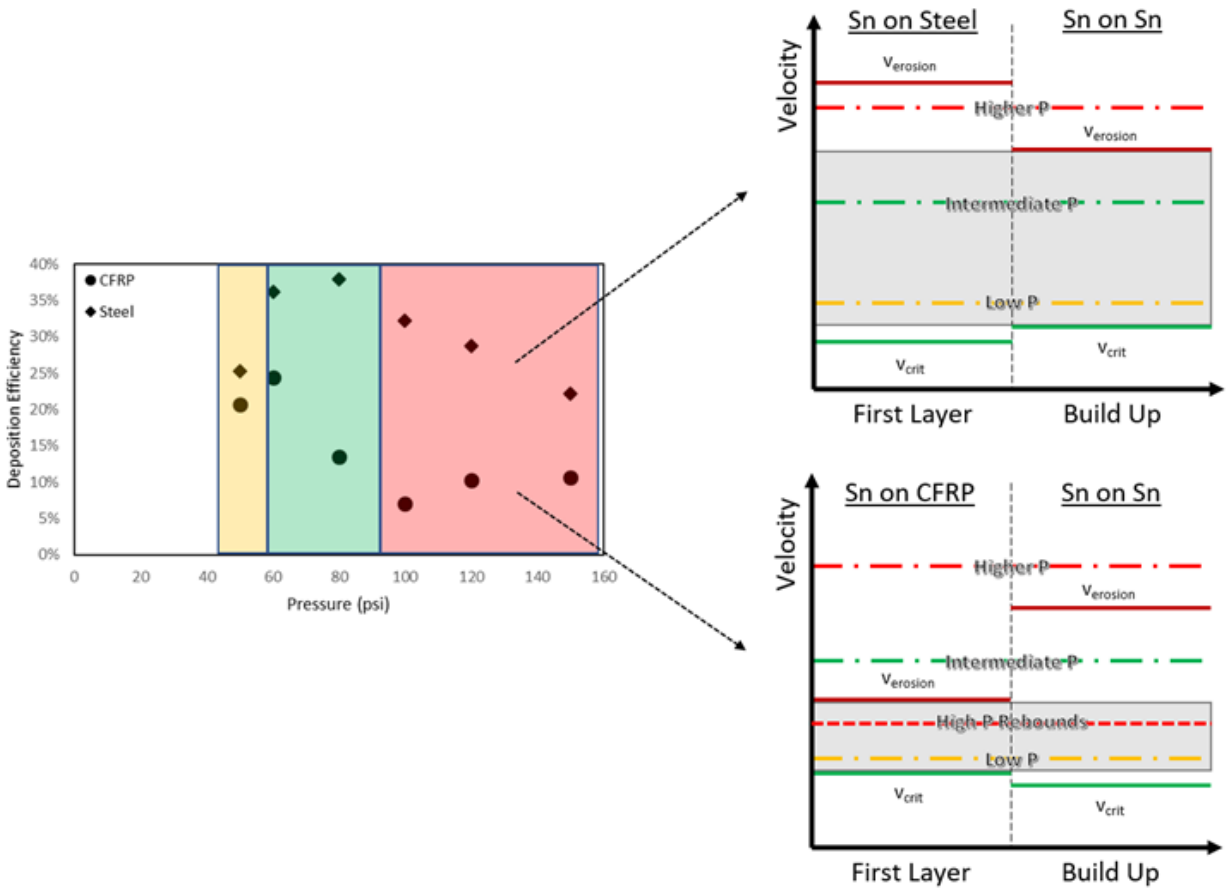

Fig. 3-13: *Schematic diagrams showing the window of deposition for depositing the first layer and coating build-up when cold spraying Sn-10Al on steel or CFRP (right) versus the observed DE trends for both substrates at 320°C (left).*

Another possible idea would be related to a splashing phenomenon occurring with partially melted tin powders. The idea of partially melted tin has already been explained by Che et al. [28] as part of the "crack filling" mechanism that makes tin deposition on CFRPs possible and could explain part of the redeposition process. Additionally, the impact of the partially melted tin powder on the CFRP could generate a splashing effect of the molten particle's outer surface, as described in Fig. 3-12 c. The resulting droplets could then be swept by the gas flow and be deposited on the agglomerates. Proof of this phenomenon could be seen in the large number of tin particles smaller than 1 µm in higher pressure coatings as seen in Fig. 3-10 : these particles were not observed in the initial particle size distribution data nor in the SEM images of the powder (Fig. 3-2 a), whereas they seem quite abundant throughout the top surface of the high pressure coatings. Molten tin tracks and tin satellites of sizes below 1 µm were already observed in [45], but these elements could have appeared upon impact of tin on previously deposited tin powders and not indicate any

melting of the tin powders in the gas flow. A study oriented on cold spraying tin powders with a better controlled size distribution (i.e. minimal content of powder below 5 μm) can be envisioned to determine the precise origin of these particles and their potential correlation with a melting phenomenon.

In the absence of significant references to support this discussion on indirect deposition effects in cold spray, CFD simulations were carried out to model the gas flow and powder metrics during the cold spray process to provide additional support to the described phenomena. Interestingly, when plotting the temperature of the propulsion gas throughout the nozzle at low pressure (60psi), , the temperature of the gas reaches high temperatures of around 575K (300°C) after the throat of the nozzle, while it is usually expected that the expansion of the gas after the throat will lead to a sharp decrease in gas temperature. This can be associated with the short stand-off distance (18mm) and lower velocities at 60psi that can lead to a degree of stagnation and heating of the gas, whereas at high pressure (150psi), the gas velocity is higher and the heating of the gas in the nozzle is less remarkable, with temperatures around 500K (230°C).

The key metrics that regulate the discussed mechanisms are:

- particle trajectory (for rebounding to be possible),
- particle velocity (to comprehend the balance between deposition and erosion),
- particle temperature (for a melting phenomenon to be possible).

In both simulations, over 150 particles impact the surface, and 15% present two or more rebounds on the surface before exiting the gas outlet. An example of a particle rebounding on the substrate is presented in Fig. 3-14. The simulation results reveal that the particles impinge the substrate at lower velocities as the number of rebounds increases. Note should be taken that the substrate offers a reflective boundary condition in the Discrete Phase Model so there are no energetic loses of particles as they impinge the substrate, so in reality these rebound velocities would be smaller than the results of the simulation. The powder velocity upon impact with the substrate is presented in Fig. 3-15. At lower pressure, the main velocity peak is around 175m/s, which is in the range of

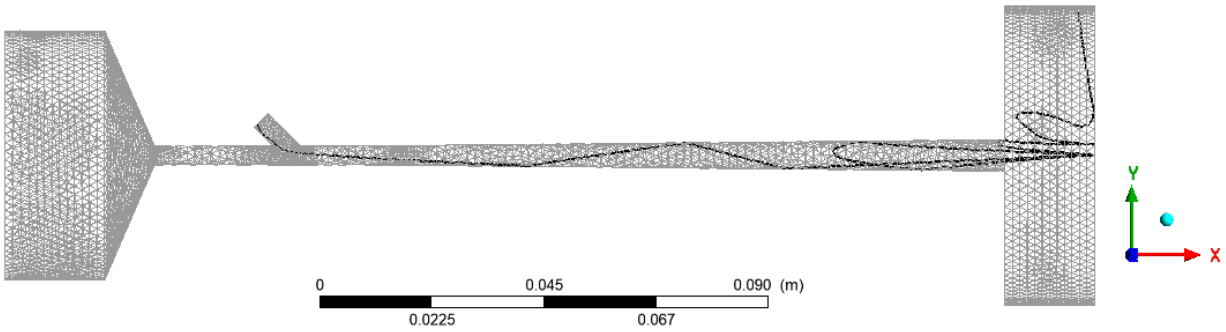

Fig. 3-14: *Particle track of a powder rebounding multiple times on the substrate then being swept out of the gas flow.*

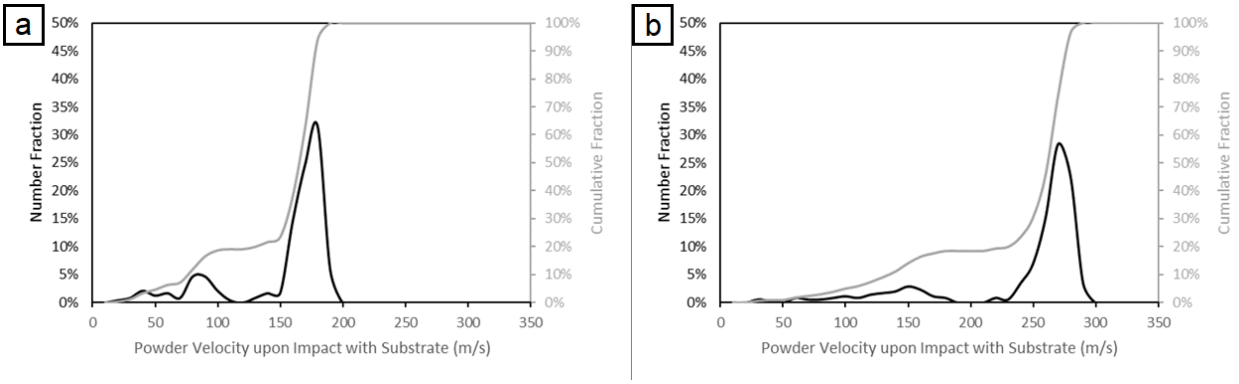

Fig. 3-15: *Powder velocity upon impact with the substrate with initial settings of (a) 320°C/60psi and (b) 320°C/150psi at the gas inlet.*

critical velocities given by Schmidt et al. [144] for tin on tin deposition (for 25µm particles) and is coherent with an acceptable build-up of tin on tin, in the case of steel. Rebounding powders would have velocities of 100m/s and therefore simply rebound from the surface. For higher pressures, the main velocity peak is around 270m/s, which is slightly below the predicted erosion velocity of tin on tin (300-350m/s) [144]. This could explain the decreasing DE of steel at higher pressures, as the DE would be regulated by the tin-on-tin build-up, while the erosion of CFRP by these high velocity powders would be quite clear. On the other hand, 9% of the impinging powders rebound twice on the substrate and the velocity of their second rebound ranges from 110 to 180m/s which leaves potential for the previously discussed indirect deposition mechanisms in Fig. 3-12 and Fig. 3-13. It should again be stressed that the reflective boundary conditions used in this simulation do not account for deformation of the particles as they impinge the substrate (i.e. no energy loss), especially around the critical velocity – so it should be noted that this discussion point

is mostly, if not entirely, qualitative. When considering the temperatures of the powders upon impact with the substrate, this simulation shows that higher initial inlet pressure would lead to particles having lower temperatures than at lower inlet pressures (505K for 150psi, against 550K for 60psi). Note should be taken that the melting point of tin is 232°C (505K). Therefore, a non-negligible amount of melting would be present in both situations, but to quantitatively assert of this melting would be erroneous as the simulation presents some question as to accounting for the phase transformation from solid to liquid (latent heat) and the presence of oxides in the powder which makes melting at the particle surface more complex to consider. With regards to the observed powder morphologies in Fig. 3-10, melting could then be considered as a cause for existence for sub-micron powders at higher pressures, but a more detailed simulation would be required to address the uncertainty these results present.

This simulation therefore provides qualitative support towards the microstructural observations and associated trends for the coating DEs on CFRP or on steel. Nevertheless, this model could be improved by implementing more complete functions that better describe the gas flow in the nozzle (realizable k-e turbulence model instead of standard model [127], refining the near-wall region to capture the boundary layer flow more appropriately [121, 135] or using the "high-Mach-number" drag law rather than the spherical drag law [119]). Other angles of improvement would include using an actual particle size distribution (e.g. Roslin-Rammler distribution) or a particle size of 25µm for better comparability with the works of Schmidt et al. [144]. Finally, implementing user-defined functions on the substrate and on the particles to account for physical interactions between particle and substrate, but also phase transformation in the particles, would offer a strong improvement to the model, as would leaning towards a model that would account for splashing of molten particles impacting the substrate.

As previously noted, the presence of aluminum in the top surface of the CFRP coatings is negligible, and as the initial gas pressure increases, retention of aluminum becomes highly unlikely as aluminum does not deposit on CFRP [28] and the indirect deposition process would not lead to any redeposition as the first-layer and build-up layer deposition windows of Al on CFRP would be dissociated, like for Cu on CFRP [29]. Given the discussion on indirect deposition of tin, it

strongly appears as if the role of aluminum in the observed indirect deposition process is negligible. Nevertheless, the aluminum powder can contribute to the erosion of the substrate directly under the spray gun. When considering the substrates that were used, it would seem plausible to extend the mechanisms from CFRP substrates to polymer substrates in general as the reasonings rest on the deposition window explanations of Che et al. [29] for tin on several polymers (PEEK, ABS, PEI and epoxy CFRP).

3.7 Conclusion

Mixed Sn-Al powders were cold sprayed onto CFRP and mild steel substrates with a CenterLine low-pressure cold spray system. Corroborating the results of [45] over a wider range of gas pressures was difficult as the DE trends observed in the present study were different. The addition of aluminum led to better DE than with pure tin at a higher temperature than previously observed, but retention rates of aluminum remained relatively low with the coatings being mainly composed of tin, as previously noted. Spraying at higher pressures led to noticing unusual surface structures on the CFRP substrates and a redeposition phenomenon was described. Even though of no actual interest with regards to substrate coating, the microstructure of the observed protrusions reveals the existence of submicron tin particles seemingly inexistent in the initial feedstock powder. These particles could be proof of a melting phenomenon described in previous studies and will be studied in future works. 3D numerical simulations were conducted and provide support to the different mechanisms that would explain the topical microstructures observed when considering effects related to velocity, but the model requires improvement to draw conclusions with regards to potential melting effects.

3.8 Acknowledgment

The authors wish to acknowledge the financial support of the Natural Sciences and Engineering Research Council of Canada (NSERC) through the Green-SEAM strategic network and the McGill Engineering Doctoral Award (MEDA). The industrial partner, Bombardier Aerospace, is gratefully acknowledged. Mr. Marco Zeman from National Research Council Canada, Boucherville, is acknowledged for his contribution to the cold spray experiments.

Chapter 4

Influence of Secondary Component Hardness When Cold Spraying Mixed Metal Powders on Carbon Fiber Reinforced Polymers

4.1 Rationale

From the previous chapter, the cold spraying of Sn-Al powder mixtures revealed a different trend than what had previously been discovered, but provided additional elements reinforcing what was known of tin deposition mechanisms onto CFRP, namely for the "crack-filling" mechanism and the split window of deposition (between the "first-layer" and "build-up" phase) [246]. It was decided to further explore the correlation between the secondary component (SC) and the improvement of the tin deposition on CFRP, suspected to be associated with tamping. Tamping is a process where particles strike the substrate (or deposited powders) with a certain force to generate plastic deformation, and so tamping correlates with the impact energy of the particle as well as its capacity to deform (i.e. its hardness). This chapter aimed to understand how the SC hardness affected the deposition of tin on CFRP. These SCs were Al and several Al alloy (Al5083, Al6061, Al7075) and had similar densities, but different hardnesses, which allowed a study focused on the SC hardness.

This chapter has been published as :

Andre C. Liberati, Hanqing Che, Phuong Vo, Stephen Yue, "*Influence of Secondary Component Hardness When Cold Spraying Mixed Metal Powders on Carbon Fiber Reinforced Polymers*", J. Therm. Spray Technol. 30 (2021), 1239-1253. (Reproduction permissions obtained from Springer Nature)

4.2Abstract

In previous studies at McGill University, tin has successfully been cold sprayed onto carbon fiber reinforced polymers (CFRPs) and, with the idea of improving the coating conductivity, other metal powders (aluminum, copper and zinc) were added to tin and also sprayed. Results indicated that addition of any of the aforementioned secondary components (SCs) provided a noticeable increase in deposition efficiency (DE); it was hypothesized that a tamping mechanism might explain the improvement. In this study, aluminum and several aluminum alloys (5083, 6061, 7075) were mixed with tin powders to understand how the hardness of secondary components with similar densities may affect the deposition of tin on CFRPs. The top-surface and cross-section of the coatings were examined, and DE and coating thicknesses were measured. Profilometric data was acquired on some coating top surfaces, as well as directly on some substrates after coatings peeled off. Mixing tin with other metallic powders is discussed and a refined "crack filling" mechanism related to SC hardness is explored as an improvement mechanism in the cold spraying of mixed powders on CFRPs.

4.3 Introduction

Applying metallic coatings onto (i.e. "metallizing") carbon fiber reinforced polymers has received a lot of interest in recent years [1], as it would provide an efficient light-weight replacement for aluminum in aerospace materials, all while maintaining electrical properties that are currently difficult to implement in these composites [5]. Different means of metallization have been considered through a variety of approaches, such as layup molding [147] or arc spray [11-13], but cold spray appears to be one of the most legitimate alternatives since it uses relatively low temperatures (several hundred degrees, versus several thousand degrees for other thermal spray techniques), thus limiting the risk of oxidation of the metallic powders and heat damage to the substrate [21].

Although cold spraying onto a metallic substrate is generally quite efficient, cold spraying metal powders onto polymer composite materials has provided mixed results as a consequence of substrate erosion from hard particles on a substrate with poor erosion resistance [25-28]. In recent years, some success in depositing metallic particles on polymeric substrates has been achieved [28,

29, 31, 36-38, 231, 232, 247, 248], but issues were observed that generally included substrate damage [28, 31, 231], relatively low deposition efficiencies (DEs) (i.e. the ratio of effectively deposited particles on the substrate versus the amount of sprayed particles) [29, 31, 232, 247, 248] or delamination issues [36-38]. Initially, Ganesan et al. suggested that soft powders such as tin could deform upon impact, favoring mechanical anchoring and therefore deposition, while harder particles such as copper could not [26]. The adhesion mechanism was associated with ‘‘crack filling’’ described by Che et al. [28], where it was hypothesized that thermally softened or partially melted tin particles impacted the substrate and, while the harder core of the particle would generate microcracks in the CFRP substrate, the softer outer core would immediately fill the cracks and provide mechanical interlocking with the substrate.

Previously, several researchers have proven that mixing ceramic powders in metal feedstock powder can enhance the deposition process, by producing a shot peening effect on the relatively softer feedstock powder [39-41, 217]. Most recently, Fernandez and Jodoin [42, 43] advanced potential mechanisms leading to coating deposition improvement (surface roughening by the secondary component (SC) through generation of asperities and oxide removal) and coating property improvement (generation of oxide clean surfaces and peening of the SC). A similar observation was made by Che et al. [44] when mixing metallic powders (zinc or copper) with tin powders, and this improvement was associated with the tamping effect of the SC on the relatively softer tin. In a previous study, the addition of aluminum to feedstock tin powder was shown to also improve the DE of a pure tin coating, yet the degree of improvement brought by the aluminum was noticeably smaller than that of copper or zinc (maximum DE of 15% for pure tin and 20% with 90% Sn – 10% Al, versus 44% with an addition of 10% Zn or Cu) [240]. These studies generally discuss deposition behavior as relating to relative hardness of powders and substrates (i.e. “hard on soft materials”) [46, 47], yet most fail to quantify the effect of relative hardness on DE improvement. This preliminary study aims to bring elements to assessing the impact of SC hardness on deposition efficiency improvement and expand the understanding of how the SC can lead to such improvements.

In this study, tin mixed with pure aluminum and a variety of aluminum alloys (Al5083, Al6061, Al7075) are cold sprayed on CFRP and mild steel substrates to study the effect of SC hardness on the deposition of pure tin, while maintaining similar particle densities (therefore, differences relating to particle energy would mostly depend on particle size/velocity). The use of different substrates enables the investigation of how different CFRP materials and surface conditions influence deposition. Tin and tin-aluminum mixed powders with 90:10 weight ratio are cold sprayed with a low-pressure cold spray system, onto thermosetting epoxy-CFRP substrates with varying surface finishes, a thermoplastic Polyether-Ether-Ketone (PEEK)-CFRP and mild steel substrates. Microanalysis of the coatings is then performed, and the DE is measured to evaluate the effect of the secondary component hardness on the deposition process.

4.4 Experimental Methods

The feedstock materials used in this work are listed in Table 4-1. The tin powder was relatively spherical and the pure aluminum and aluminum alloy powders (Al5083, Al6061, Al7075) were spherical with a higher average particle size. The average Vickers hardness of the feedstock powders was measured by mounting the powders and by using a Clark CM-100AT Microhardness Tester (Sun-Tec, Novi, USA) for a penetration time of 15 s under a load of 10 gf on 10 well-spaced areas: The hardness of the aluminum powder was more than triple that of the tin powder, whereas the hardness of the aluminum alloy powders was 9 to 17 times higher. The scanning electron microscope (SEM) images of the single-component powders are presented

Table 4-1: *Properties of the feedstock powders used in this work*

Powder	Supplier	D_{10}	D_{50}	D_{90}	D_{avg}	Hardness
Sn	CenterLine, SST	6 µm	12 µm	20 µm	11 µm	7 ± 1 $HV_{0.01}$
Al	Valimet	15 µm	23 µm	39 µm	24 µm	24 ± 2 $HV_{0.01}$
Al5083	Valimet	8 µm	17 µm	39 µm	20 µm	66 ± 11 $HV_{0.01}$
Al6061	Valimet	10 µm	23 µm	45 µm	24 µm	72 ± 8 $HV_{0.01}$
Al7075	Valimet	9 µm	20 µm	39 µm	21 µm	118 ± 23 $HV_{0.01}$

alongside the powder size distributions of each powder in Fig. 4-1. The particle sizes of the feedstock powders were measured with a laser scattering particle size analyzer (LA920, HORIBA,

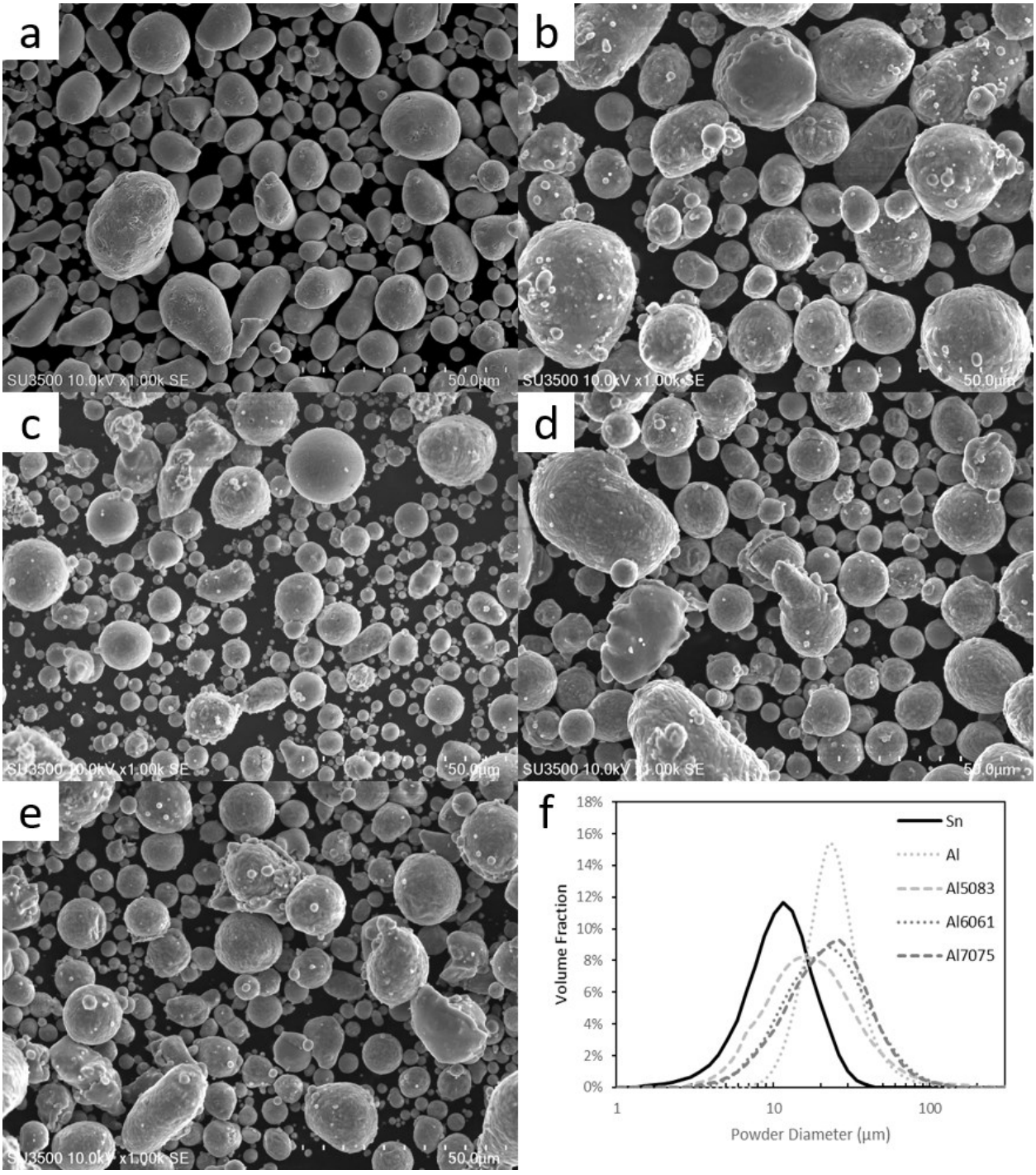

Fig. 4-1: *SEM images of the feedstock powders: (a) Sn, (b) Al, (c) Al5083, (d) Al6061, (e) Al7075. (f) particle size distribution of the feedstock powders*

Japan). Powder mixtures with 90%wt tin and 10%wt of the secondary component were made. The powders were mixed for 1h in a metal can without additional media (e.g., milling balls) with a double movement powder mixer. No significant morphological changes or hardening was noticed in the mixed powder when compared with the starting powders: The absence of morphological changes was verified through SEM of the mixed powders, and the hardness of the mixed powders was measured as per the hardness for the initial feedstock powders.

The substrates used in this work were epoxy-CFRPs provided by Bombardier Aerospace (Montreal, Canada), Polyether-Ether-Ketone (PEEK)-CFRPs provided by TenCate (Netherlands) and 1020 mild steel plates. The CFRP substrates are presented in Fig. 4-2. The steel substrates were used as a benchmark to compare the spraying of powders on CFRPs to a typical metal–metal cold spraying situation. The epoxy-CFRPs (abbreviated as e-CFRP) used here consist of a

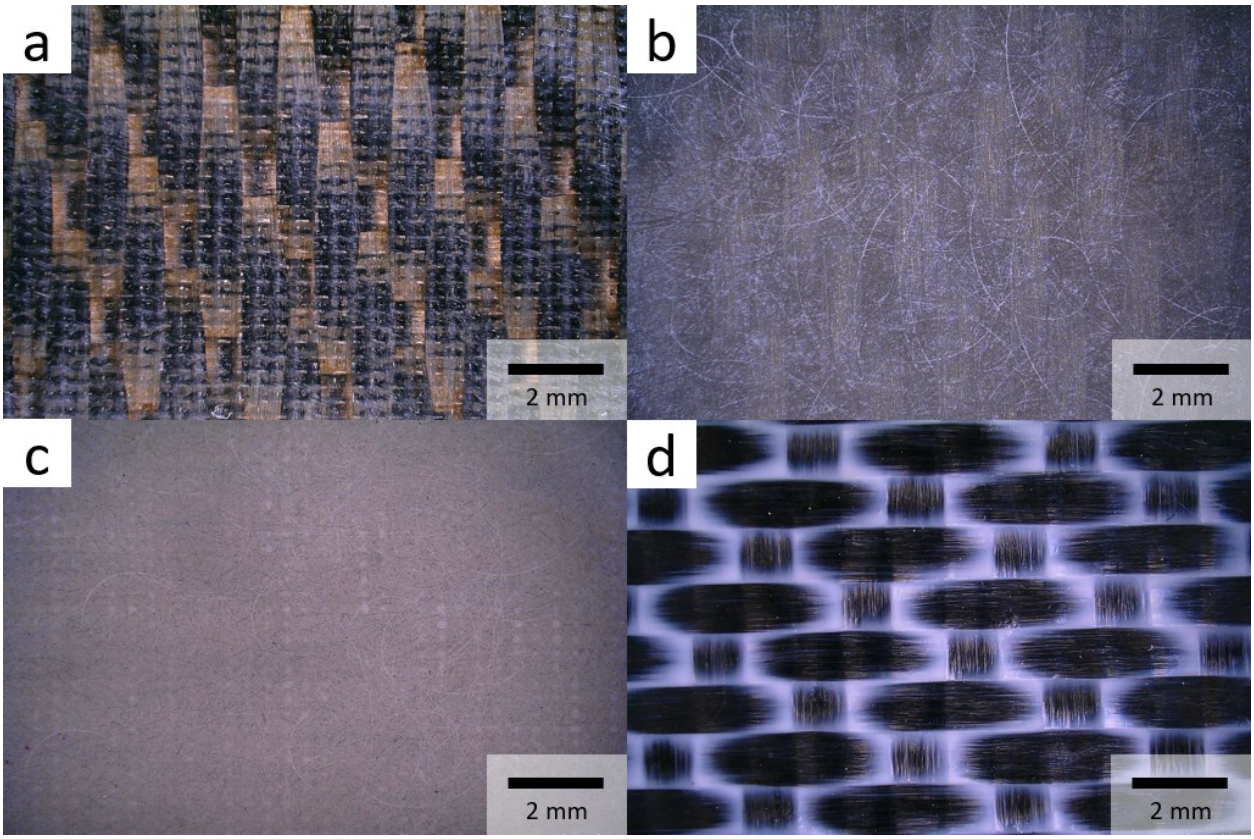

Fig. 4-2: *Keyence Digital Microscope image of the CFRP substrates:*
(a) bare e-CFRP, (b) putty e-CFRP, (c) surface film e-CFRP, (d) PEEK-CFRP

thermosetting epoxy matrix with continuous carbon fiber reinforcements. The e-CFRP panels were made of four plies of epoxy/carbon fiber prepreg ([0/90]2s) and have various coating finishes used by the manufacturer: a bare finish (Fig. 4-2 a), a putty finish (Fig. 4-2 b) and a surface film finish (that could be described as a fine-squared mesh finish on the substrate) (Fig. 4-2 c). The hardness of these substrates was measured as per the powders, and the values were respectively 39±8 HV0.01 for the bare finish e-CFRP, 51±15 HV0.01 for the putty finish e-CFRP and 40±13 HV0.01 for the surface film finish e-CFRP. The PEEK-CFRP used here consists of a thermoplastic polyether-ether-ketone matrix with continuous carbon fiber reinforcements (Fig. 4-2 d). These panels were made of five plies of PEEK/carbon fiber ([(0,90)2/(0,90)3R]). The hardness of this substrate was differentiated between areas showing superficially pure PEEK areas, and superficially predominant carbon fiber areas. The respective hardness values for each area are 26±3 HV0.01 and 63±22 $HV_{0.01}$. Sheet sections of dimensions 7 x 7 cm were used as substrates during the cold spray campaigns, with thickness of 1.7 mm for the CFRP substrates and 3mm for the steel substrates. The substrates were degreased with ethanol, and the mild steel plates were grit-blasted with 24 grit alumina before cold spraying. The CFRP substrates were not grit-blasted as it would result in the erosion of the substrate.

The cold spraying was performed at the McGill-NRC cold spray facility at National Research Council Canada in Boucherville. The cold spraying was performed at low pressure with a commercially available CenterLine SST SSM-P3300 system (Supersonic Spray Technologies, CenterLine Windsor Limited, Canada) and a #440-00125 standard straight, hydroformed, round, stainless-steel nozzle. This choice enabled the use of the so-called ‘‘downstream injection’’ mode, where the particles are injected in the main gas stream after the throat of the nozzle. The risk of clogging the nozzle when using metals with low melting points, such as tin, is thus reduced. The primary cold spray parameters are listed in Table 4-2. These parameters were chosen based on previously successful cold spray campaigns with tin [28, 44, 240] and at the selected conditions, melting was observed in previous work [28, 44, 246]. A comparison between cold spraying pure tin and the powder mixtures with secondary components of varying hardness was thus possible, on a variety of CFRP substrates. The carrier gas was nitrogen, the standoff distance was 18 mm, the step size was 1 mm with 38 steps, and the gun travel speed was 25 mm/s. The powder feeder

Table 4-2: *Principal cold spray parameters*

Powder	- Sn - Sn-10Al - Sn-10Al5083 - Sn-10Al6061 - Sn-10Al7075
Substrate	- Steel - e-CFRP: • bare • putty • surface film - PEEK-CFRP
Carrier Gas Temperature (°C)	- 310
Gas Pressure (psi/MPa)	- 60/0.41 (all substrates)

rate was set to 1 revolution per minute (RPM), which gave a measured feeding rate between 10.0 and 13.5 g/min, measured every three sprays to accurately assess the variation. The substrates were pre-heated by operating a single pass, without powder injection, at the given conditions (Table 4-2). Then, only one pass was sprayed for each set of conditions, so that the average DE from a large area, together with a study focused on the DE trend, would be meaningful. All the substrates were aligned and sprayed at the same time for one condition, so that any external variation (e.g. feeding, temperature effects) may be neglected.

Deposition efficiency was measured as the mass gain of the substrate divided by the total mass of feedstock powder fed during the time the gun was over the substrate. After the cold spray process, the samples were observed from a top surface view, then prepared as metallographic samples and characterized with a Keyence (Japan) digital microscope and a Hitachi (Japan) SU3500 scanning electron microscope. The cross-sectional samples were cut (Delta Abrasimet, Buehler, Illinois, USA) and observed parallel to the spraying direction. The coating thickness was measured using an image analysis method on a cross-section of each sample, studied under a Keyence digital microscope, and the hardness of the tin in the coatings was measured to assess any

changes during the coating process. These cross-sections measured between 1.0 and 2.5cm. The method consisted in applying a threshold filter to isolate the relatively brighter metallic coating from the substrate, then taking the average thickness from 20 different areas. The retention rates of the SC were also estimated, by measuring the relative areas of tin and aluminum in SEM BSE-COMP images using an image analysis method, then converting the obtained volume fractions into weight fractions. From these weight fractions, the relative DE of each coating element could be determined as described in [246].

A 3D optical surface profiler (ZYGO, Connecticut, USA) was also used to measure the surface roughness and support large-scale microstructural observations. Magnifications of 5x, 20x and 50x were chosen, corresponding to areas of 1661x1661 µm, 429x429 µm and 167x167 µm, respectively. The lateral resolution of the objectives used is below 2 µm. In the case of coating height profiles, ten areas were analyzed to determine the average surface roughness. The main measurements were taken around the roughness Sa, the peak-to-valley height Sz, and the root mean square gradient of the surface Sdq as they provide insight into the topography of the surfaces regarding not only height but also gradient [243, 244]. More specifically, Sdq is affected both by texture amplitude and spacing; therefore, Sdq can provide information on the slopes which comprise the surface in the case of coatings with similar values of Sa [243].

4.5 Results

4.5.1 Cold sprayed coating conditions

Fig. 4-3 shows some typical top-surface views of the observed coating structures. Deposition on steel was achieved for all conditions (Fig. 4-3 a), while deposition on CFRP provided mixed results with many coatings being poor or irregular. These poor coatings are generally characterized by uneven build-up on the surface of the substrate, with some areas being effectively coated, while others are not, with no detectable trend (Fig. 4-3 b). ‘Irregular coatings’ are coatings where the powders deposited to build a partially complete coating (Fig. 4-3 c) or a coating with visible variation in coating thickness. Fig. 4-3 d presents a typically expected “good quality” coating on CFRP.

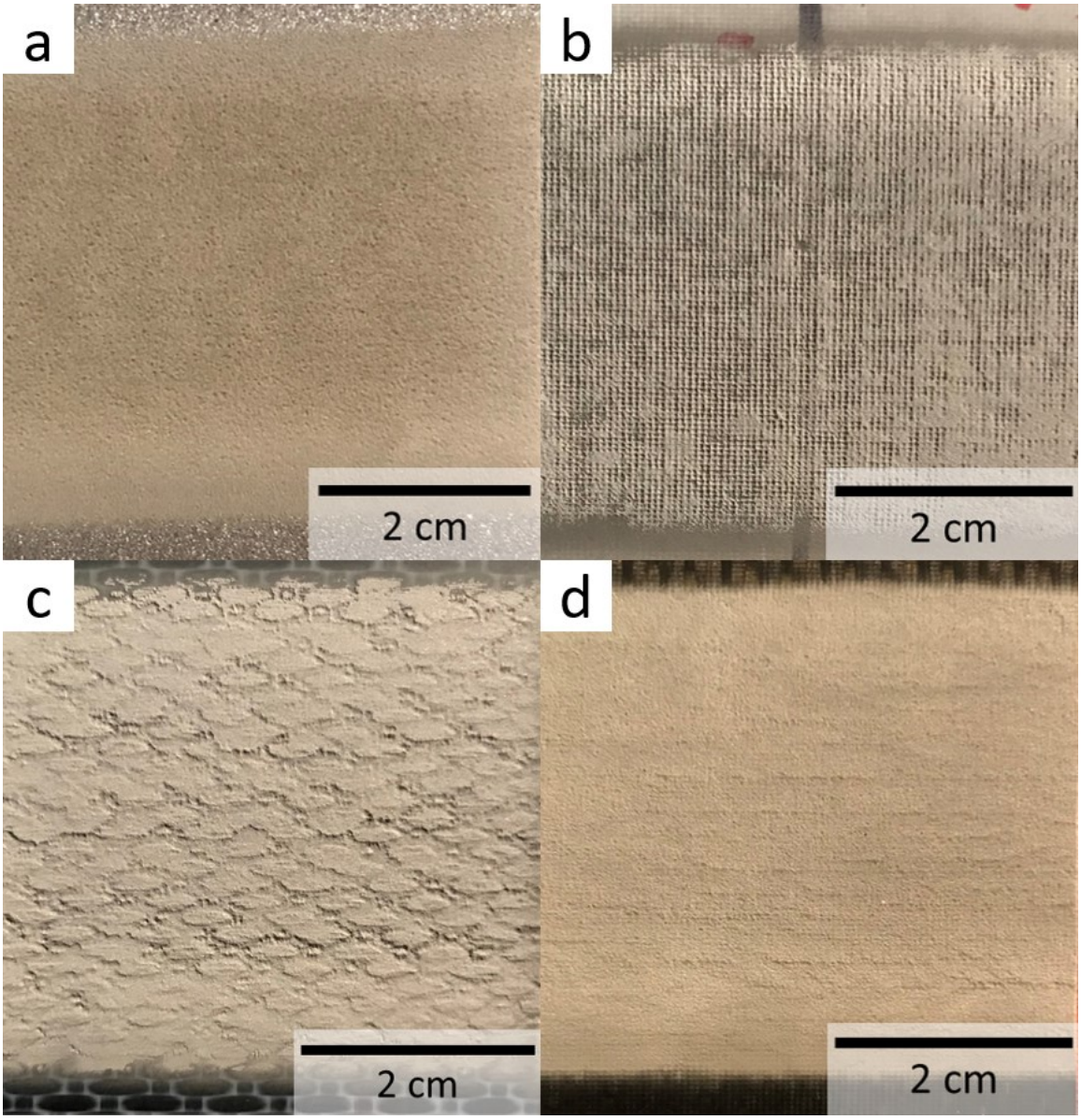

Fig. 4-3: *Top surface images of various coatings: (a) Sn on Steel, (b) Sn on surface film e-CFRP, (c) Sn-10Al on PEEK-CFRP, (d) Sn-10Al5083 on bare e-CFRP*

The tin coating on the bare e-CFRP was successfully deposited, whereas the other pure tin coatings were relatively poor or irregular. The powder mixtures with Al and Al5083 provided relatively uniform coatings on the bare e-CFRP and PEEK-CFRP, but most peeled off when cutting the samples. It is uncertain if the peeling was due to poor bonding and/or operational damage from the cutting (e.g. friction). These powders also provided relatively irregular coatings on the putty and surface film e-CFRPs. The powder mixtures with Al6061 and Al7075 provided

relatively uniform coatings on all the CFRP substrates, but peeling was observed for the bare e-CFRP, the putty e-CFRP and the PEEK-CFRP. These coating conditions are summarized in Table 4-3. Above these variations, it was observed that the Sn-Al5083 powder mixture provided coatings with a visible waviness and longitudinal streaks, similar to the surface structure of Fig. 4-3 d.

4.5.2 Deposition efficiency, secondary component retention and thickness variation

Fig. 4-4 shows the DE of single component tin and of the different powder mixtures on the various substrates. With regard to deposition on steel, no specific trend with the powder mixtures is noticeable when compared with the DE of pure tin. On the bare and putty e-CFRP, the addition of a secondary component (SC) helps moderately improve the DE of pure tin; the most noticeable improvement is brought by the addition of Al5083 (increase of DE from 17% to 27% on the bare e-CFRP, and from 14% to 22% on the putty e-CFRP). On the surface film e-CFRP and PEEK-CFRP, larger improvements of DE are observed as compared to single component tin; the DE of the powder mixtures are between 21% and 26%, up from 11-12% for pure tin. Here again, the addition of Al5083 yields the highest increases.

The retention rates of Al/Al alloy SC were measured in the cross section for all sprayed coating conditions. An example of these cross sections is presented in Fig. 4-5. For all coatings, it was found that SC retention was always below 1% (as compared to the initial 10% addition of SC) which corresponded to an effective SC DE below 1.5%. This is in line with previous studies where the retention rate of Al in Sn-Al coatings sprayed on CFRPs was also low [240, 246]. This also

Table 4-3: *Deposited coating condition on the various substrates. Italics (i.e. "good") indicates peeling upon cutting.*

Powder	**Sn**	**Sn-Al**	**Sn-Al5083**	**Sn-Al6061**	**Sn-Al7075**
Steel	Good	Good	Good	Good	Good
Bare e-CFRP	Good	*Good*	Good	*Good*	*Good*
Putty e-CFRP	Irregular	*Irregular*	Irregular	*Good*	*Irregular*
Surface Film e-CFRP	Poor	Irregular	Irregular	Good	Good
PEEK-CFRP	Poor	*Irregular*	*Irregular*	*Good*	*Good*

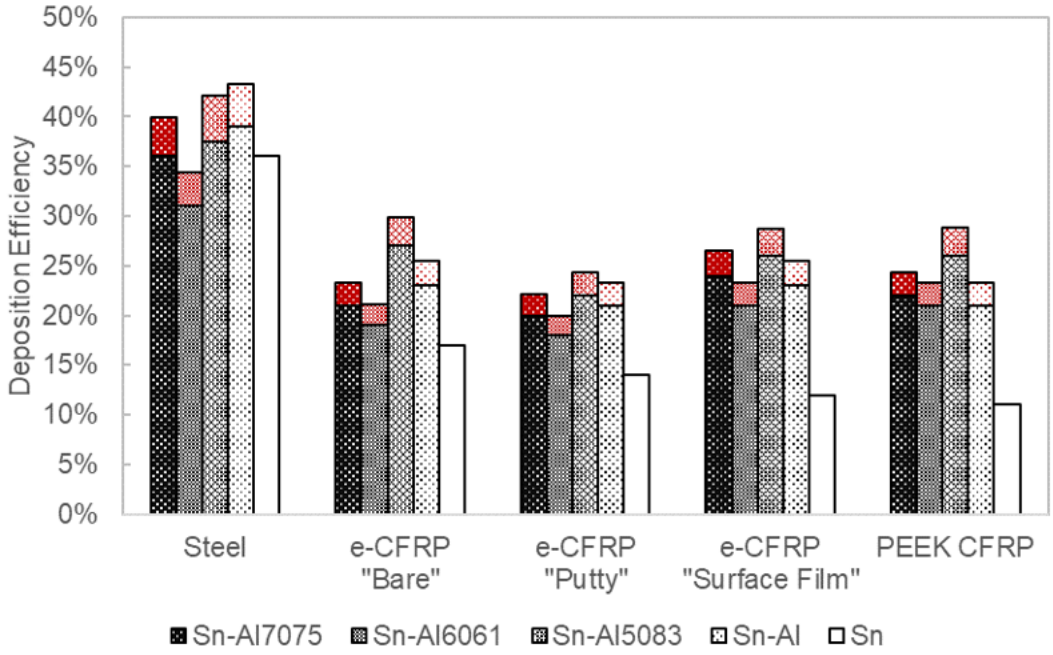

Fig. 4-4: *Deposition efficiency of the different powder mixtures sprayed on several substrates. The red columns designate the calculated DE of pure tin on the various substrates, which was found to be higher than the overall DE*

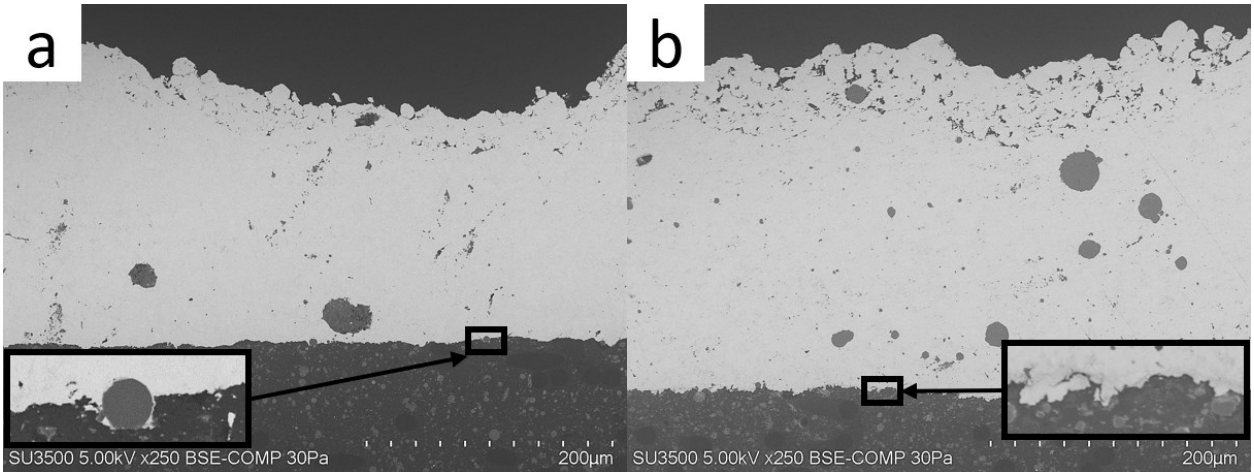

Fig. 4-5: *SEM-BSE images of the cross-sectional microstructures for the (a) Sn-10Al and (b) Sn-10Al5083 coatings on the surface film e-CFRP. Particles with darker contrast in the coatings are Al/Al alloy particles. The inserts show the detail of the coating/CFRP interfaces*

means that the effective DE of tin in the mixed coatings is always higher than the obtained DE values, and this is shown by the red columns of Fig. 4-4: effective DE of tin is 2% to 5% higher than the values of overall DE. For instance, the addition of a SC while spraying on the surface film

e-CFRP and PEEK-CFRP actually leads to a pure Sn DE between 23% and 29%, up from 11-12% with single component pure tin. The cross-sections of Fig. 4-5 also reveal the detail of the coating/CFRP interfaces and some inclusion of particles at the interface can be noted (Al particle in Fig. 4-5 a, Sn particles more deeply embedded in Fig. 4-5 b).

To understand the variation in deposited coating quality in comparison to the DE, the thickness of each coating was measured and is presented in Fig. 4-6. The average variation corresponds to the standard deviation of the thickness and is an indicator of the uniformity of the coating. It can be noted that the thickness of the tin coatings is relatively low (<200µm on CFRP) when compared with the coatings produced by the other powder mixtures. In most cases (PEEK-CFRP, putty and surface film e-CFRP), the tin coating is poor, and the mixtures enable a better deposition that would explain this increase in thickness. The addition of Al does not notably increase the thickness of the coatings, except in the case of PEEK-CFRP. On the other hand, Sn-Al5083 provides the highest average values of coating thickness (300-350µm). The aforementioned irregularity of coatings with Al5083 is also noticeable with higher average

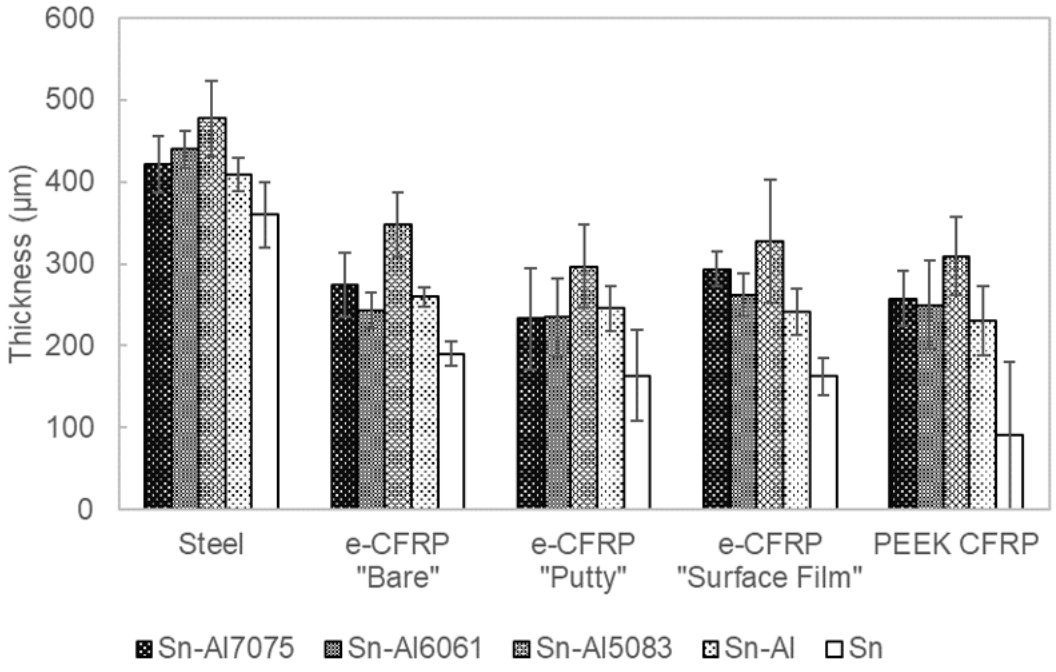

Fig. 4-6: *Thickness of the coatings on the various substrates*

variations around these high values (>40µm). When adding Al6061 or Al7075 to Sn, coatings with similar thickness to coatings obtained with Al are obtained on all substrates. The coating thickness follows a similar trend as the DE on the CFRP coatings, but interestingly enough this is true regardless of the deposited coating condition, i.e. even on irregular coatings (Fig. 4-3 c), the average thickness follows the trend of the DE. The hardness of the tin in the coatings was also measured and found to be between 12±1 $HV_{0.01}$ and 14±1 $HV_{0.01}$, indicating that the average hardness of tin in the coatings was about double the hardness of the pure tin feedstock powders; this was true regardless of the presence of SC in the feedstock powder.

4.5.3 Top surface observation, coating and substrate roughness analysis

The peeled coatings of PEEK-CFRP were observed under a Keyence digital microscope as this substrate presented peeling for all powder mixtures. It would seem that there is no major surface erosion on the substrate after removal of the coating, as can be seen when comparing Fig. 4-7 a and Fig. 4-2 d. The backing of the coatings (Fig. 4-7 b) reveals the pattern of the underlying substrate, and only the carbon fiber structure is visible. Macroscopic observations of the peeled coatings of bare and putty e-CFRP show similar details. When observing the carbon fiber area of a PEEK-CFRP at a higher magnification (Fig. 4-8), it is possible to assess the effect of spraying on the substrate more thoroughly. PEEK-CFRP under the SEM is presented before spraying in Fig. 4-8 a. On this figure, the linear carbon fiber structure seems to stand out. After spraying and peeling of the coating, the substrate is quite different, and a non-negligible amount of residual

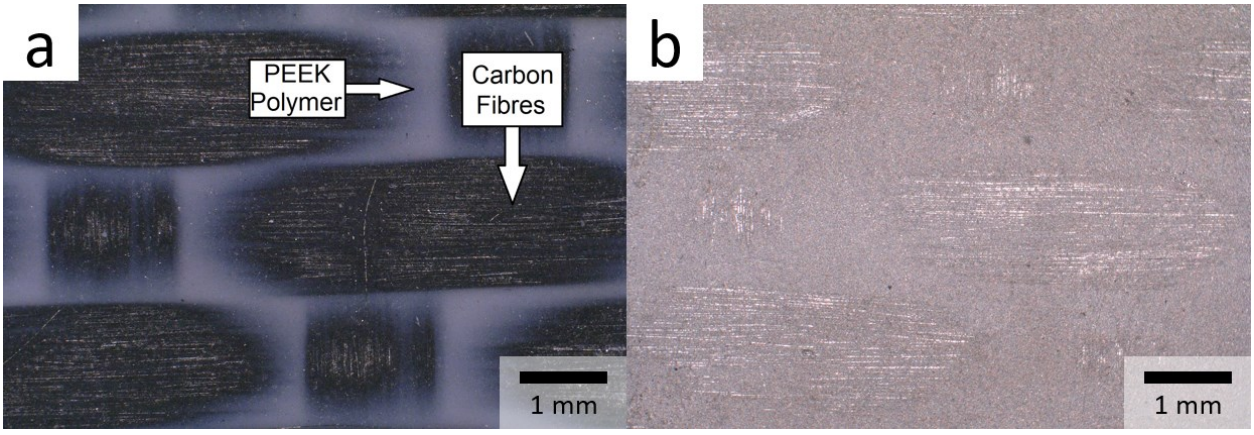

Fig. 4-7: *Keyence Digital Microscope image of a peeled Sn-10Al5083 coating, sprayed on PEEK-CFRP: (a) surface of the substrate after removal of the coating and (b) back of the coating*

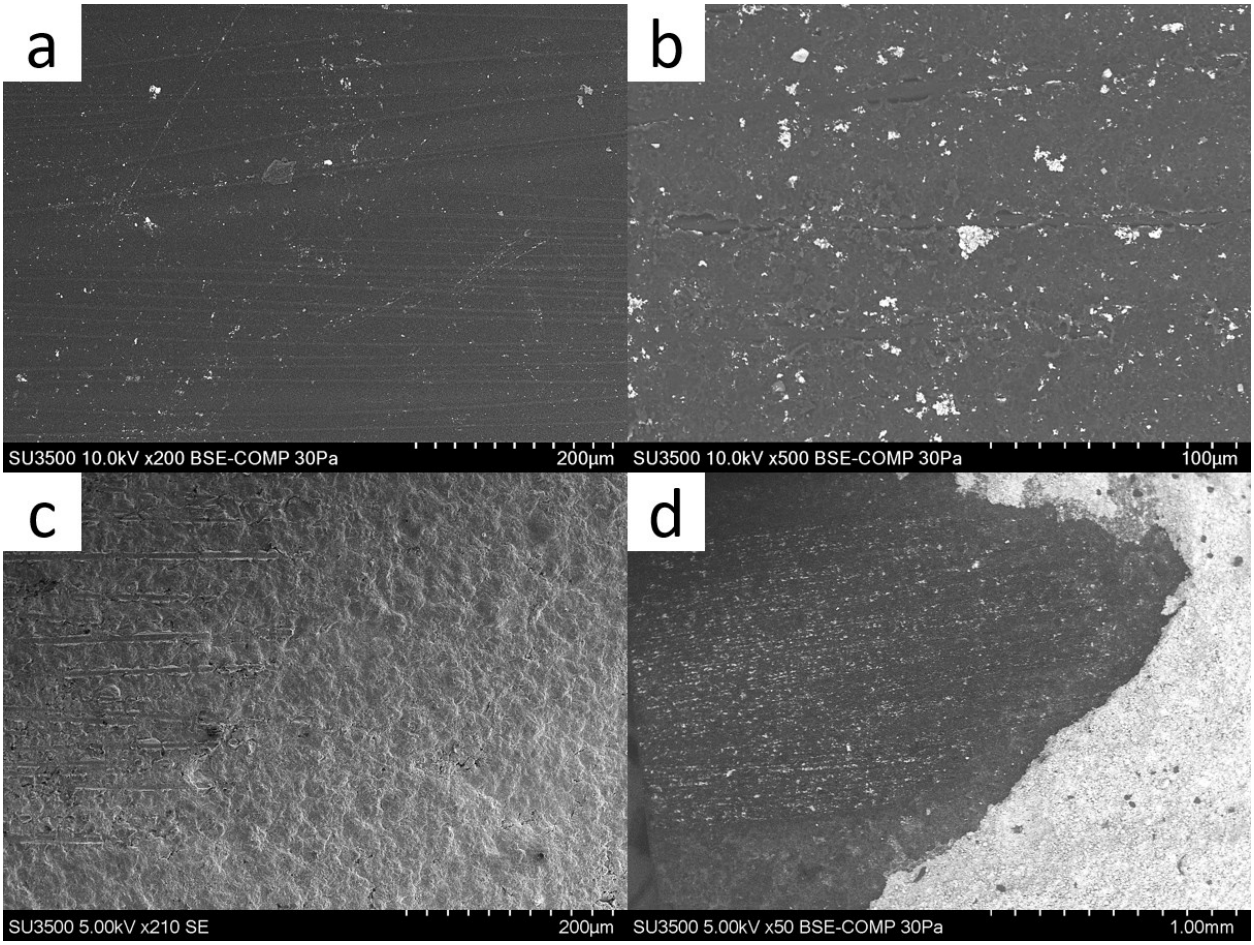

Fig. 4-8: *SEM-BSE images of the PEEK-CFRP (a) before spraying and (b) after spraying and peeling of an Sn-10Al5083 coating. (c) is the backside of a peeled Sn-Al coating, recovered after peeling. (d) is the substrate at low magnification, in an area where a Sn coating partially peeled*

powder seems to remain on the substrate as can be noted by the bright features on Fig. 4-8 b. There seems also to be some damage of the substrate that reveals linear structures that could be associated with the carbon fibers. When focusing on the backing of the coatings (Fig. 4-8 c), two areas stand out as noted for Fig. 4-7 b: an area with a linear structure, relatable to an underlying carbon fiber structure, with seemingly strongly deformed powders, and an area where the powders conserve the structure of a typical cold sprayed coating, as observed in Fig. 6 a of [246]. When observing the overall substrate (i.e. at a lower magnification) in the vicinity of a peeled coating (Fig. 4-8 d), it appears that the carbon fiber area retains metallic particles while the area between the coating and the carbon fiber area, i.e. the PEEK-polymer area observed in Fig. 4-7 a, seems relatively devoid of particles: this area only presents some observable roughness.

Height profiles of these areas, obtained with a 3D optical surface profiler, are presented in Fig. 4-9. Before coating (Fig. 4-9 a), the surface roughness is low (Sa < 2 µm) and the peak-to-valley height (Sz) is 10 µm. The corresponding image clearly reveals a pattern depicting that of the carbon fibers with gradual evolutions of height throughout the image. After cold spray and

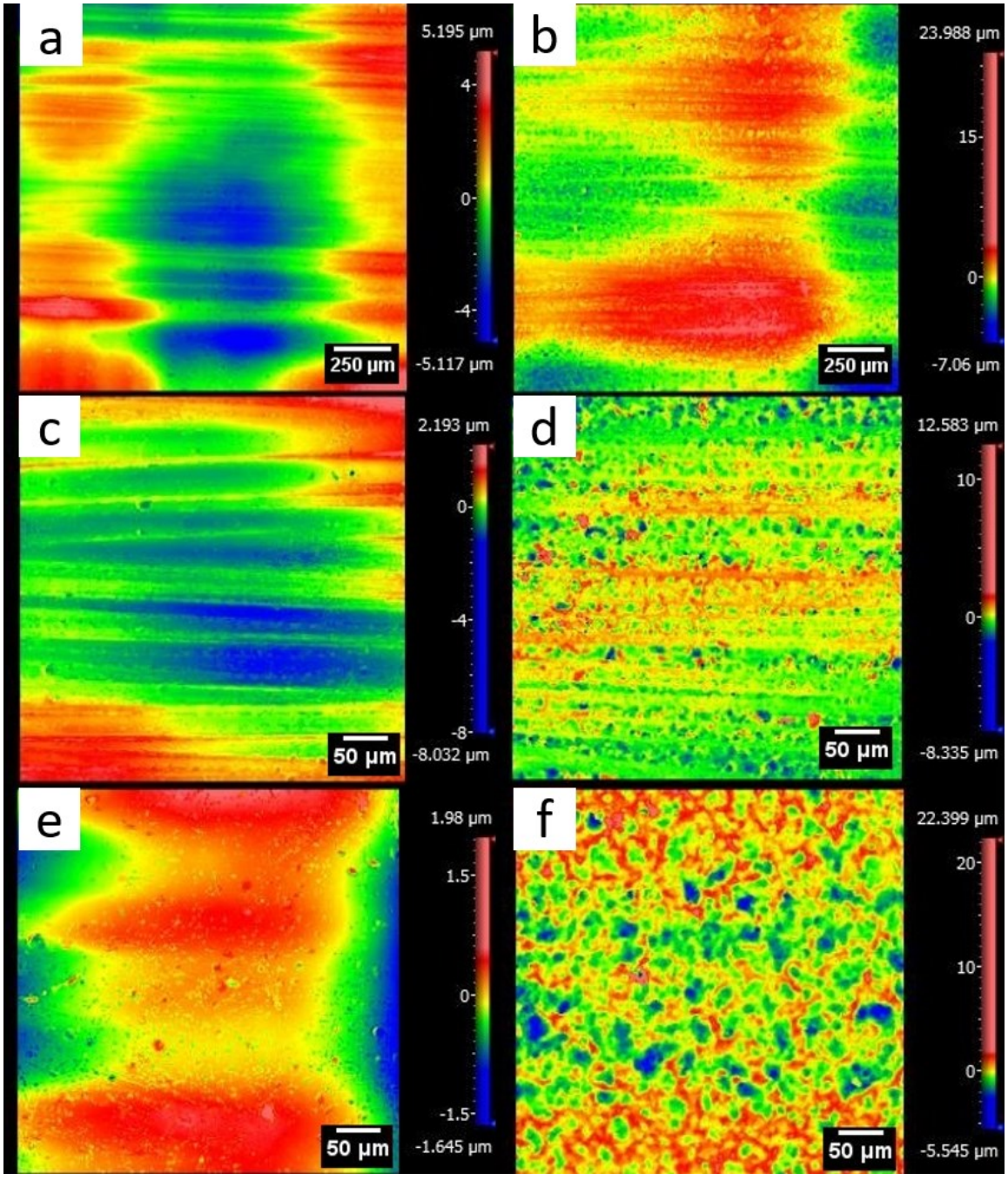

Fig. 4-9: *Height profiles of an Sn-10Al7075 coating on PEEK-CFRP substrate: (a) before and (b) after peeling at 5x; superficial carbon fiber area (c) before and (d) after peeling 20x; superficial polymer area (e) before and (f) after peeling at 20x*

removal of the peeled coating (Fig. 4-9 b), the substrate surface roughness remains low and the peak-to-valley height is increased to around 30 μm, which is several times the average particle size of the tin in this study. The corresponding image reveals the aforementioned carbon fiber structure, but a slightly less continuous and more speckled height distribution also seems to stand out. At greater magnifications, it is possible to differentiate the height profiles of areas with superficial carbon fibers (Fig. 4-9 c-d) from those with superficial polymer (Fig. 4-9 e-f). As noted for lower magnifications, the roughness of these profiles is low, before and after removal of the peeled coating (< 1 μm), and again there is a noticeable increase of the peak-to-valley height : from 10 μm (Fig. 4-9 c) to 20 μm (Fig. 4-9 d) for the superficial carbon fiber area, and from 4 μm (Fig. 4-9 e) to 28 μm (Fig. 4-9 f) for the superficial polymer area. After peeling of the coating, the carbon fiber area (Fig. 4-9 d) still reveals a pattern similar to that of the raw substrate (Fig. 4-9 c), albeit with a more noticeably speckled height profile. After removal of the coating, the initially flat superficial polymer area (Fig. 4-9 e) presents a heterogeneous height profile (Fig. 4-9 f), similar to that observed for other cold sprayed coatings (Fig. 8 a of [246]).

With regard to deposited coatings, the top surface strongly resembled that of a typically cold sprayed coating, as seen in Fig. 6a of [246]. To assess the surface condition of the coatings and any variability due to varying powder mixtures, height profiles of the tin and tin-aluminum (alloy) coatings on the bare e-CFRP were also obtained at various magnifications (5x, 20x, 50x). This substrate was studied as it provided generally good coatings (Table 4-3), in such that the deposited coatings are comparable and any surface roughness differences would be solely associable with the variation of powder mixtures. It was observed that each powder mixture produced coatings with similar roughness information (standard deviation generally around 5%), as shown in Table 4-4. For other substrates, more variability in roughness values is naturally observed as the coating is of variable quality, i.e. comparing the effect of the powder mixtures on the roughness after coating is not meaningful. All the corresponding height profile images strongly resembled that of Fig. 4-8 f in this study, and previously observed height profiles (Fig. 8 a of [246]).

Table 4-4: *Average roughness values associated with the various powder mixtures sprayed onto the bare e-CFRP, at different magnifications*

Parameter	Magnification	Average Value	Std Deviation	Std. Dev. (%)
Sa (µm)	5x	9	0.6	6%
	20x	7	0.4	5%
	50x	6	0.1	1%
Sz (µm)	5x	92	9	10%
	20x	65	4	6%
	50x	45	2	4%
Sdq (µm/mm)	5x	805	29	4%
	20x	1473	77	5%
	50x	2173	107	5%

4.6 Discussion

4.6.1 Improvement of DE by the addition of a SC

As previously noted [44, 240], adding a secondary component to tin powder improves the deposition of tin on CFRP (Fig. 4-4) and, in this study, it has been observed on a variety of CFRP substrates. As observed elsewhere [246], the coating thickness (Fig. 4-6) follows a similar trend as the DE, but interestingly enough, this occurs regardless of the quality of the deposited coating and notably, irregular coatings with preferential deposition areas (Fig. 4-3 c) follow the same trend as good coatings, particularly in the case of the PEEK-CFRP. This could be an indication that the SC acts as a catalyst to generating the improvement of the deposition process, i.e. the presence of the SC suffices to generate better deposition, regardless of the coating being complete or not.

The powder mixture that provided the most successful results appears to be Sn with Al5083. With this SC, the coatings with both the highest DEs (Fig. 4-4) and overall thickness (Fig. 4-6) were obtained, as well as coatings that did not peel from the e-CFRP substrates (Table 4-3). The other SC provided coatings of similar DE (Fig. 4-4) and thickness (Fig. 4-6), but with more variable quality (Table 4-3): addition of Al or Al7075 to Sn led to mostly irregular coatings that led to peeling, while the addition of Al6061 led to good coatings albeit with peeling. Therefore, when considering the results provided by this study within the reference of SC hardness, certain

trends would appear to emerge: while the adhesion of the coatings may be questionable, the addition of Al5083, and to a lesser extent Al6061, led to developing better coatings in this study. These powders have a hardness roughly 9-10 times greater than that of pure tin, while Al and Al7075 had a hardness respectively 3 or 17 times greater than that of tin. This could be an indication of an optimal choice of SC particle hardness relative to the main component, to improve the deposition of tin: too soft and an improvement is observable with an increased DE but a sometimes questionable coating quality; too hard and the quality may eventually decrease, which could be related to more erosion of the coating and/or the substrate during deposition. The comparison of this hypothesis with previous studies seems to hold as Che et al. observed that SC with higher hardness values (Zn, Cu – 33-55 HV0.01) led to higher DE values of tin on a CFRP substrate (44%) [44], as compared to the addition of softer (27 HV0.01) Al powders (20%) [240]. Nevertheless, the difference in hardness was less notable in this study and the non-sphericity of the Zn and Cu powders could have a non-negligible effect on the improvement of the deposition process.

4.6.2 Deposition of pure tin onto CFRP

In this study, it appeared that build-up of coatings could be preferential around surface areas where the carbon fibers were apparent, as can be seen on the irregular coatings (Fig. 4-3 c). The back of the peeled coatings (Fig. 4-7 b) were imprinted with the carbon fiber structure of the composite substrate, with higher magnification observation showing strongly deformed tin powders (Fig. 4-8 c). Particles are occasionally retained in the substrate after peeling of the substrate, as can be seen when comparing Fig. 4-8 a and Fig. 4-8 b. Nevertheless, this seems to be localized in the carbon fiber area, as the superficial polymeric area seems to retain relatively less particles (Fig. 4-8 d), and the back of the peeled coating show little deformation of the powders in these areas. Therefore, these observations seem to reveal that the coating development is actually initiated around the carbon fiber area and that the development in the PEEK area would be secondary and/or an after-effect of the coating developing in the carbon fiber area. It can be hypothesized that bonding would also be strongly associated with these observations, but this is not studied here.

Che et al. initially explained the deposition of tin on CFRP through a “crack-filling” mechanism [28]. In this mechanism, thermally softened or partially melted tin particles would impact the substrate and, while the harder core of the particle would generate microcracks in the CFRP substrate, the softer outer core would immediately fill the cracks and provide mechanical interlocking with the substrate. They further continued by exploring the idea of a multi-phase deposition process, where deposition is differentiated between a first-layer build-up phase, followed by an ensuing coating build-up phase [29]. In the light of the first study [28], and of the current observations (Fig. 4-7, Fig. 4-8), it would seem that the generation and filling of micro-cracks would be most likely localized around the superficial carbon fiber area, and not the superficially pure polymeric substrate. Proof of the presence of micro-cracks being preferential in this area could be seen while observing Fig. 8b as the deposition of a coating that has peeled seems to reveal the underlying carbon fibers to some extent. The morphology of the tin particles in the corresponding troves (Fig. 4-8 c) are highly deformed and could be indicators of the “crack-filling” mechanism, whereas the particles in the second area of this figure seem to show deformation comparable to the top surface of a coating (as seen in Fig. 6a of [246]). The particles retained at the substrate interface present the same profile as particles present at the top surface after cold spraying, which would suggest that the particles at the interface undergo relatively little deformation compared to those in the carbon fibre area, which in turn suggests little potential for mechanical interlocking. The height profiles presenting the substrate before and after removal of the sprayed coating (Fig. 4-9) reveal no obvious change in coating roughness that could be attributed to microcracking as observed in Fig. 4-8 b, such as a change from a relatively flat surface to a narrow valley-like feature. Nevertheless, the cold spray process seems to generate some amount of roughness throughout the substrate with a notable increase of peak-to-valley height Sz, from 10 μm (Fig. 4-9 a) to 30 μm (Fig. 4-9 b), which is several times the average Sn particle size. More surprisingly, in the specific superficial areas of the substrate (carbon fiber and polymer), this increase seems to exist as well, as Sz increases from 10 μm (Fig. 4-9 c) to 20 μm (Fig. 4-9 d) for the superficial carbon fiber area, and from 4 μm (Fig. 4-9 e) to 28 μm (Fig. 4-9 f) for the superficial polymer area. This increase is accompanied by a discontinuous and more speckled height distribution, which can be viewed as the effect of particles impacting the surface and/or being retained on the surface. In the case of the carbon fiber area, it has already been established that localized damage and some retention of metallic particles takes place (Fig. 4-8 b), but in the case

of the superficial polymer area, little to no particles are retained, which would indicate that the increase of roughness is effectively related to the tamping of the substrate by the particles (which would explain the speckled aspect of Fig. 4-9 f), but that this tamping does not permit any crack-generation and/or filling.

Following the previous observations, the deposition mechanism of pure tin can be assumed to start with a first layer build-up occurring preferentially around the superficial carbon fibers of the CFRP, accordingly to what has been observed in Fig. 4-7 and Fig. 4-8. Tin has relatively lower hardness (7 HV0.01 in the solid state, likely lower in case of thermal softening) than the substrates on which it is impinging (between 26 and 63 HV0.01), therefore micro-cracking of the surface could be considered as minimal, and bonding of tin to the CFRP substrate would be fairly limited. Since the interfacial adhesion strength between fibers and resin matrix is considered to be one of the weakest points of fiber reinforced materials when considering erosion [224, 249] and that the impinging particles nevertheless generate roughening of the surface as observed through Fig. 4-9 f, it could be hypothesized that the repeated impacting of tin on the carbon fiber area could generate some superficial debonding of the carbon fiber and the resin, which would, in turn, facilitate some mechanical interlocking of tin in this area, and not in the PEEK-CFRP area, as discussed in the previous paragraph. Therefore, during the build-up phase, the coating can be supposed to develop from the deposits on the superficial carbon fibers and extend towards superficial polymer areas, effectively establishing a coating on the substrate with the greatest extent being a "good" coating (Fig. 4-3 d), but with the possibility of "irregular"/uncomplete coatings (Fig. 4-3 c).

4.6.3 Potential improvement mechanism associated with SCs in the case of cold spraying CFRPs

Building on the mechanism advanced for the deposition of tin on CFRP, the SC could have a beneficial effect during the first-layer build-up phase: the relatively harder SC (24 to 118 HV0.01) would have a stronger likelihood of generating superficial cracking than the Sn powders (7 HV0.01 or lower), as higher hardness would lead to greater transfer of the SC powder's kinetic energy to the substrate (hardness ranging from 39 to 63 HV0.01 on average). This is illustrated by the insert of Fig. 4-5 a, showing an Al particle embedded at the coating/CFRP interface, generating localized roughness. The resulting effect would then be increased deposition and, potentially,

mechanical interlocking of particles, as can be observed from the insert of Fig. 4-5 b. All SC generate some degree of improvement in the deposition process as previously mentioned (Fig. 4-4, Fig. 4-6, Table 4-3), therefore they should all generate a certain amount of superficial roughening on the substrates. Nevertheless, Al having the lowest hardness of the SC (24 HV0.01), it could be suggested that a limited degree of roughening occurs, while Al7075 would more strongly deform the substrate, to the potential extent of erosion, or disrupt the first-layer deposition of tin with its higher hardness (118 HV0.01). In between, Al5083 (66 HV0.01) and, to a lesser extent Al6061 (72 HV0.01), seem to have the best improvements in deposition. Their hardnesses match, or are slightly higher, than those of the CFRP substrates. Thus it may be that the balance between surface roughening and substrate damage is optimal, so that deposition may occur without compromising the coating that is being deposited. The repeated impacting of harder powders could also lead to a greater amount of carbon fiber/polymer delamination than pure tin. These combined effects could then allow facilitated mechanical interlocking of the tin powders with the CFRP substrate, along the lines of the "crack-filling" mechanism [28], and thus facilitate the first layer build-up phase.

During the build-up phase, the SC could offer two major roles: generation of asperities within the metal coating (i.e. increased surface roughness), as seen in [42, 43], and consolidation of the pre-deposited powders through a shot-peening mechanisms or tamping, mentioned in [44, 240]. Nevertheless, several results here contradict the influence of these mechanisms in the case of deposition of tin on CFRP. Firstly, when comparing the height profiles of complete coatings with all five powder mixtures (Table 4-4) on a good coating, similar average roughness values (Sa), peak-to-valley heights (Sz) and especially root mean square gradient of the surface (Sdq) are observed for all coatings, which would suggest that the various Sn-Al (alloy) mixtures do not generate any particular surface roughness that would lead to improvement. As previously mentioned, Sdq is affected both by texture amplitude and spacing, so Sdq could provide information on the slopes which comprise the surface in the case of coatings with similar values of Sa [243], but there does not seem to be a notable difference here. Furthermore, when comparing the obtained coatings on steel (Fig. 4-4), no notable difference in DE stands out between pure tin and the powder mixtures. This suggests that in the case of a deposition scenario generating maximum tin DE (limited only by the DE of tin on tin, as discussed in [246]), the secondary component does not bring any notable improvement to the deposition of tin. Finally, the hardness

of the tin in the cold sprayed coatings is about double that of the initial feedstock tin powder (13±2 HV0.01), regardless of the sprayed powder or powder mixture. Thus, a certain amount of hardening of the tin occurs during the cold spray process, but the SC does not generate a noticeable increase that would be an indication of tamping as a potential improvement mechanism. Since the surface condition after coating (i.e. roughness), optimal DE and tin hardness in the coating are seemingly similar with or without SC, the initial hypothesis that shot peening would be a cause for deposition improvement is questionable. Generation of oxide clean surfaces during the build-up could also be a possibility as discussed in [42, 43], but this was not studied here.

The previous discussion on an optimal hardness value would still be coherent, not from the perspective of generating shot-peening improvement effects as noted elsewhere [44], but more from the perspective of generating sufficient superficial roughening of the CFRP during the first-layer build-up. This would also support the idea of the SC acting as a catalyst for tin deposition on CFRP, as it shows that the presence of the SC initiates and allows better coating deposition, wherein lies the actual improvement of the process, and not necessarily a better coating build-up. Thus the results indicate the existence of this optimal value, more experiments need to be performed to obtain a precise numerical value. Nevertheless, it would appear from these current results that an SC hardness on par with the substrate hardness approaches this optimal SC hardness value.

It should be considered that this discussion mainly concerns the development of the metallic coating and does not necessarily reflect the adhesion of the coating to the substrate. It is possible that the generation of superficial roughening of the CFRP by the SC, and the ensuing improved mechanical interlocking of the first-layer suggested with the “crack-filling” mechanism, would lead to increased adhesion of the coating to the substrate. It was explained here that the SC that would generate the best superficial roughening would also generate the best DE/coating thickness, so this would presume that improved superficial roughening by the SC would generate improved adhesion and also improved DE/thickness. Nevertheless, in a recent paper by Rokni et al. [231], it was found that coatings with higher DEs and thicknesses could have lower adhesion strengths. Therefore, even though it is acknowledgeable that the adhesion would naturally depend

on the coating process (first layer then build up), the actual effect of the SC on the adhesion can only be determined through thorough physical testing (e.g. pull-off tests), and will be the scope of a follow-up study where more systematic analysis will be performed.

4.6.4 Considerations regarding the powders and substrates in this study

While studying the current results, certain other observations were made that indicate that SC hardness is not the sole factor of influence to be considered. Firstly, with all other SC properties being similar (similar size (Fig. 4-1 f), density, morphology), different hardness values led to comparable coating DE and thickness values (Fig. 4-4 and Fig. 4-6), but varying coating qualities, as shown by the comparison of adding Al6061 and Al7075 to tin (Table 4-3): Al6061 led to the deposition of good quality coatings whereas Al7075 led to an irregular coating (putty e-CFRP). Furthermore, all coatings on bare e-CFRP, putty e-CFRP and PEEK-CFRP peeled for these powders. On the other hand, when comparing Al5083 and Al6061, the main SC property differences are observed around the particle size, with all else being equal, and differing results were obtained: adding Al5083 to tin provided the coatings with the highest DE (Fig. 4-4), thickness (Fig. 4-6) and overall quality with no peeling (Table 4-3). Al5083 has a size distribution with smaller particles than Al6061 (6µm less), so it can be thought that a smaller SC could provide better DE results, but with the SC Al, Al6061 and Al7075, no specific trend of DEs appears when considering particle size. This absence of a clear trend suggests that SC hardness is still the main factor in deposition improvement, but the observed results show that the variability in powder properties (particle size distribution, particle morphology, material density) and mixture ratios can complement the influence of SC hardness, and it is possible that a combination of these properties may yield optimal deposition of Sn onto CFRP. For instance, it was reported elsewhere that SC with non-spherical morphologies were shown to greatly increase the DE of tin on a CFRP substrate (44%) [44]. These powders had hardness values similar to the ones considered here and, given that powders with irregular morphologies are known to travel at faster velocities [123], these would have increased kinetic energy and could, as a result, have increased potential for crack generation on the substrate, via asperity/roughness generation on the coating, as well as erosion. A broader study focusing on various SC properties will be the scope a follow-up study, to elucidate how these properties affect deposition.

Furthermore, no specific attention is given to comparing the different substrate types and their respective properties (thermosetting epoxy polymer vs thermoplastic PEEK polymer) nor to the different surface finishes in this study. The DE for tin and the powder mixtures are similar (Fig. 4-4) between the substrates, so there seems to be no notable difference with regard to powder deposition, even though the surface finishes of each substrate are fairly different, i.e. the carbon fiber areas may be closer to the substrate surface in some substrates like the PEEK-CFRP. Nevertheless, from the perspective of coating bonding, the CFRP substrate and surface finish seems to have a non-negligible effect, as seen in Table 4-3 and Fig. 4-6: most notably, the surface film e-CFRP shows no coating peeling while PEEK-CFRP always shows peeling regardless of the powder mixture, which suggests that other phenomena should be considered for coating bonding. Measurements of the bonding strength of these coatings should be carried out to effectively assess the mechanical properties of these coatings.

Finally, the suggested "crack-filling" mechanism and observed carbon fibers potentially present at the surface (Fig. 4-8 b) could suggest potential bonding of the metallic tin directly with the carbon fiber. This could be a source of galvanic corrosion, slightly less troublesome than it could be with aluminum, but an issue nevertheless (difference in electrostatic potential of 0.26eV with Sn, as compared to 0.8eV with Al), and so further investigation into this phenomenon should be considered in future studies.

4.7 Conclusion

Tin and tin-aluminum (alloy) mixed powders with 90:10 weight ratio were cold sprayed with a CenterLine low-pressure cold spray system, onto thermosetting epoxy-CFRP substrates with varying surface finishes, a thermoplastic PEEK-CFRP and mild steel substrates. The addition of aluminum generally provided better coating of the substrates than single component tin, and the addition of Al5083 and Al6061 provided the coatings with the greatest thickness, DE and/or overall uniformity. These improvements reveal a certain trend when considering relative hardness values, as Al5053 and Al6061 have intermediate hardness values when compared to Al or Al7075, and similar hardness when compared to the substrates they impinge. Initial observations reveal

that bonding on CFRPs could be limited to interaction between the metal powders and the carbon fibers of the substrate. This hypothesis is supported by previous studies, and a mechanism explaining how the SC contributes to improving the deposition process in the case of cold spraying CFRPs was advanced. Future investigations will look to assess coating properties more precisely and relate the powder mixtures to potential variations in bonding strength.

4.8 Acknowledgments

The authors wish to acknowledge the financial support of the Natural Sciences and Engineering Research Council of Canada (NSERC) through the Green-SEAM strategic network and the McGill Engineering Doctoral Award (MEDA). The industrial partners, Bombardier Aerospace and Tencate (through Pratt and Whitney Canada) are gratefully acknowledged. Mr. Kévin Bricault from National Research Council Canada, Boucherville, is acknowledged for his contribution to the cold spray experiments.

Chapter 5

On the Importance of Secondary Component Properties for Cold Spray Metallization of Carbon Fiber Reinforced Polymers

5.1 Rationale

In the previous chapter, cold spraying of tin on to CFRP was observed to be preferential in superficial carbon fiber areas, where the tin could more easily mechanically interlock with the substrate. The role of the secondary component (SC) was described as a catalyst for the first layer deposition of tin on the substrate, and results seemed to indicate that shot peening of the coating by the SC, during the build up phase, may not be as relevant as initially suspected. However, the potential for crack generation by the SC during the build up phase not only depends on the SC hardness (i.e. resistance to plastic deformation), but also on the kinetic energy with which this particle impacts the substrate. Therefore, particle mass (i.e. density, size) and velocity (morphology, size) may also have an importance. In this chapter, tin was mixed with several copper (spherical and irregular), iron, SS316L, titanium (spherical and angular), and Ti6Al4V powders, and cold sprayed onto various CFRP substrates. The study was first focused on individual SC properties, and ultimately a comparison was made between pure tin deposition efficiency improvement, SC hardness and SC impact energy.

This chapter is an invited paper selected from presentations at the 2021 International Thermal Spray Conference, and has been submitted to the Journal of Thermal Spray Technology as :

Andre C. Liberati, Hanqing Che, Maniya Aghasibeig, Kintak Raymond Yu, Phuong Vo, Stephen Yue, "*On the Importance of Secondary Component Properties for Cold Spray Metallization of Carbon Fiber Reinforced Polymers*", Journal of Thermal Spray Technology (2021) (Submitted, In Revision)

5.2 Abstract

In previous studies at McGill University, tin was successfully cold sprayed onto carbon fiber reinforced polymers (CFRPs). A "crack-filling" mechanism was described as the deposition mechanism that allowed deposition of tin onto the CFRP. Improving the coating conductivity for lightning strike protection (LSP) purposes was explored by adding other metal powders (aluminum, copper, zinc) to tin and cold spraying on the CFRP. At the same time, it was noticed that the addition of this secondary component (SC) provided an increase in deposition efficiency (DE); tamping was initially hypothesized to explain this improvement, thus prompting a study solely on the effect of SC hardness. However, it is recognized that other powder characteristics may also be influencing the DE. Thus, in this study, SCs with a wider variety of particle sizes, morphologies, densities and hardness values were mixed with tin and sprayed on CFRPs. The effect of SC properties on tin deposition is discussed and, while SC particle size, morphology and density individually do not notably influence the DE, the impact energy of the SC does. This opens a discussion on optimal parameters for deposition of metals on CFRP, based on results and observations from the literature.

5.3 Introduction

"Metallizing" or applying metallic coatings onto polymeric substrates has received increasing interest in recent decades [1], being used extensively for applications from food packaging [3] to generating heating elements for potential de-icing applications [4]. In recent years, interest has been given to polymers and polymeric composites for structural applications as they possess high strength-to-weight ratios, but low electrical conductivity has limited their use in some fields such as the aerospace industry [1, 5]. As a result, different technologies for polymer metallization have been studied. Vacuum deposition techniques, such as physical vapor deposition (PVD) [8] or chemical vapor deposition (CVD) [9] have provided potential pathways to metallization of polymers but they are not suitable to fabricate thick metal coatings (over 100 μm) [10]. Other techniques have been considered such as layup molding [147], wire-arc spray [11-14], flame spray [15], plasma spray [16] or air plasma spray [17, 18], but cold spray has appeared as one of the most legitimate approaches as it uses relatively low temperatures (several hundred

degrees versus several thousand degrees for other thermal spray techniques), thus limiting the risk of oxidation of the metallic powder and heat damage to the substrate [21].

Cold spraying metal feedstock onto a metallic substrate is generally efficient, while cold spraying metal powders onto polymeric substrates has provided mixed results as a consequence of substrate erosion from the impact of hard particles on a substrate with poor erosion resistance [25-28]. In recent years, some success has been obtained in depositing metallic layers on polymeric substrates with a variety of metals, e.g. tin [28-31], iron [29], 316L stainless steel [32, 33], AlSi10Mg [33-35], copper [28, 29, 31, 36-38] or aluminum [38]. On the other hand, generally reported issues include substrate damage [28, 31], low deposition efficiencies (DEs) (i.e. the ratio of the weight of the effectively deposited particles to sprayed particles onto the substrate) [29, 31-34], or delamination issues [21, 36-38].

Lupoi and O'Neill [31] explored the deposition of various metals on polymeric substrates and established an impact energy criterion that would regulate deposition versus erosion of the substrate by the metallic powder. Affi et al. [21] sprayed micron-sized aluminum directly onto a CFRP substrate, to respect this energetic criterion, but faced debonding of the cold sprayed coating. Shortly afterwards, Ganesan et al. [26] suggested that soft powders such as tin had the possibility to deform upon impact favoring mechanical anchoring, while harder particles such as copper could not. Che et al. [28] introduced a ''crack filling'' mechanism, where it was hypothesized that thermally softened or partially melted tin particles impacted the substrate and, while the harder core of the particle would generate microcracks in the CFRP substrate, the softer outer core would immediately fill the cracks and provide mechanical interlocking with the substrate. Considering the overall deposition process, Che et al. [29] also advanced the importance of differentiating the process into two separate steps: the first-layer deposition phase (occurring between the metal powder and the substrate) and the build-up phase (occurring between the metal powder and previously deposited metal powders).

In parallel, several researchers proved that mixing ceramic powders in metal feedstock powder may enhance the deposition process, by producing a shot peening effect on the relatively softer feedstock powder [39-41]. This effect has been used to establish an in-situ shot peening cold spray deposition process, that improves deposition and coating properties through the addition of large stainless steel particles (200-300 μm) [132, 217, 218]. Recently, Fernandez and Jodoin [42, 43] advanced potential mechanisms explaining the coating deposition improvement (surface roughening by the secondary component (SC) through generation of asperities and oxide removal), as well as the coating property improvement (generation of oxide clean surfaces and peening by the SC). Che et al. [44] made similar observations related to coating deposition improvement when mixing metallic powders (zinc or copper) with tin powders, and this improvement was associated with the shot-peening effect of the SC on the relatively softer tin.

Nevertheless, in a more recent study [250], evidence appeared that other factors than shot-peening may play a role. When comparing the DE of pure tin to tin powders mixed with aluminum or aluminum alloy powders on a steel substrate (ideal deposition scenario of a soft metal on a relatively harder metal), no notable improvements were brought by the use of the aluminum/aluminum alloy SCs [250]. Height profiles of the coatings were acquired, and the addition of the SC did not noticeably modify the roughness of the surface. This would imply that surface roughening may not apply during the build-up phase, and so the observed improvement of the DE of tin on the CFRP would not occur in the build-up phase, but necessarily during the first-layer deposition phase [250]. The study suggested that an ideal SC hardness was one of the main causes for deposition improvement, and that this improvement would be most noticeable when the SC hardness was close to the hardness of the substrate: the nature of the improvement would then originate from the potential of the SC to generate cracks that the impinging tin could fill [250], and so the quicker the substrate surface would be activated, the quicker the build-up phase could begin.

However, comparisons between powders can be quite difficult as powders possess a variety of properties ranging from the material (density and hardness) to the characteristics of the powder itself (morphology and particle size distribution). Should the improvement be associated to crack

generation by the SC at the substrate surface, a certain amount of kinetic energy would need to be transferred to the surface for this to occur. Properties related to particle energy would be associated to particle mass (i.e. density, size) and velocity (morphology, size), while the transfer of this energy would depend on the hardness (i.e. resistance to plastic deformation) of the powder. Furthermore, retention of the SC also seems to be quite correlated with the morphology of the particles [26, 44]. Therefore, in tandem with the results offered by the previous study [250], this study aims to assess the relative effects of the SC properties and how they lead to the improvement of the DE of tin on CFRP substrates.

In this study, tin mixed with a variety of SC are cold sprayed on CFRP and mild steel substrates to study the effect of SC properties on the deposition of pure tin. The choice of SC was based on a factorial-design-like approach, to cover an array of SC properties (hardness, density, morphology, median particle size): the choice of these SCs is described in further detail in the Experimental Methods section. The coatings are sprayed on a variety of different substrates to investigate how different CFRP materials and surface conditions may influence deposition. Tin and tin-SC mixed powders with 90:10 weight ratio are cold sprayed with a low-pressure cold spray system, onto thermosetting epoxy-CFRP substrates with varying surface finishes, a thermoplastic Polyether-Ether-Ketone (PEEK)-CFRP and mild steel substrates. Microanalysis and micro-hardness measurements of the coatings are then performed, and the velocity of the particles is estimated via a CFD model. Finally, the DE is measured to evaluate the effect of the SC properties on the deposition process.

5.4 Experimental Methods

5.4.1 Feedstock materials

The feedstock materials used in this work cover a variety of material and powder properties. The SCs were generally chosen as a pure metal with a corresponding alloy to have a variation of hardness with a similar density to the main component, similarly to the choice of Al and Al alloys in the previous study [250]. Given previous observations around SC addition to cold spraying of tin onto CFRP substrates [44, 240], relations to particle density, hardness and morphology were considered most important to control, while particle size was a variable to be

followed. As each commercial powder had a specific combination of these four properties, it was quite difficult to select a powder with a given property without varying the others, and hence, a factorial-design-like approach was employed. In this type of design, several variables of a process are chosen and scaled using the Taylor expansion approximation [251]. The scaling sets the low-value of a variable to -1 and the high-value to +1. This facilitates a comparison of the variable effects, especially across different ranges. Morphology is relatively difficult to quantify, so it was treated as a discrete variable with the low-level being "Spherical" while the high-level was "Irregular" (i.e. angular, dendritic, or any other non-spherical morphology).

A variety of cold sprayed powders from past studies at McGill University [44, 123, 131, 219] was considered to offer a meaningful spread for each property. As such, copper powders from studies by Che et al. [28, 44], iron and stainless steel 316L powders from studies by Chu et al. [131, 219] and titanium/Ti6Al4V powders from studies by Wong et al. [123] were selected. Aluminium/aluminium alloy powders from previous work [250] and the results provided by these SC were considered for comparison, but these SC were not sprayed in mixtures with Sn in this work. The ranges of considered properties were thus between 2.66 and 8.96 $g.cm^{-3}$ for density, 7 and 340 $HV_{0.01}$ for hardness, and 12 and 37 μm for median particle size (D_{50}). Average impact energy was determined to be between 1.32 x 10^{-6} J and 7.30 x 10^{-6} J. The characterization of the powder hardness, particle size and average impact energy is described in the following sections. The scaled properties of the SC powders considered in this study are listed in Fig. 5-1. The Al/Al alloy powders offer relatively low values for all properties (lower left quadrant), whereas the copper powders allow the study of higher density, size and morphology values. The Ti/Ti6Al4V powders give higher hardness values, density below the middle-level, and offer a variety of sizes/morphologies. Finally, the iron/stainless steel 316L powders complete the variable spread with intermediate hardness values, density above the middle level, and a variety of sizes/morphologies. As such, the choice of powders should offer a reasonable representation of the SC properties versus the deposition of tin onto CFRP substrates.

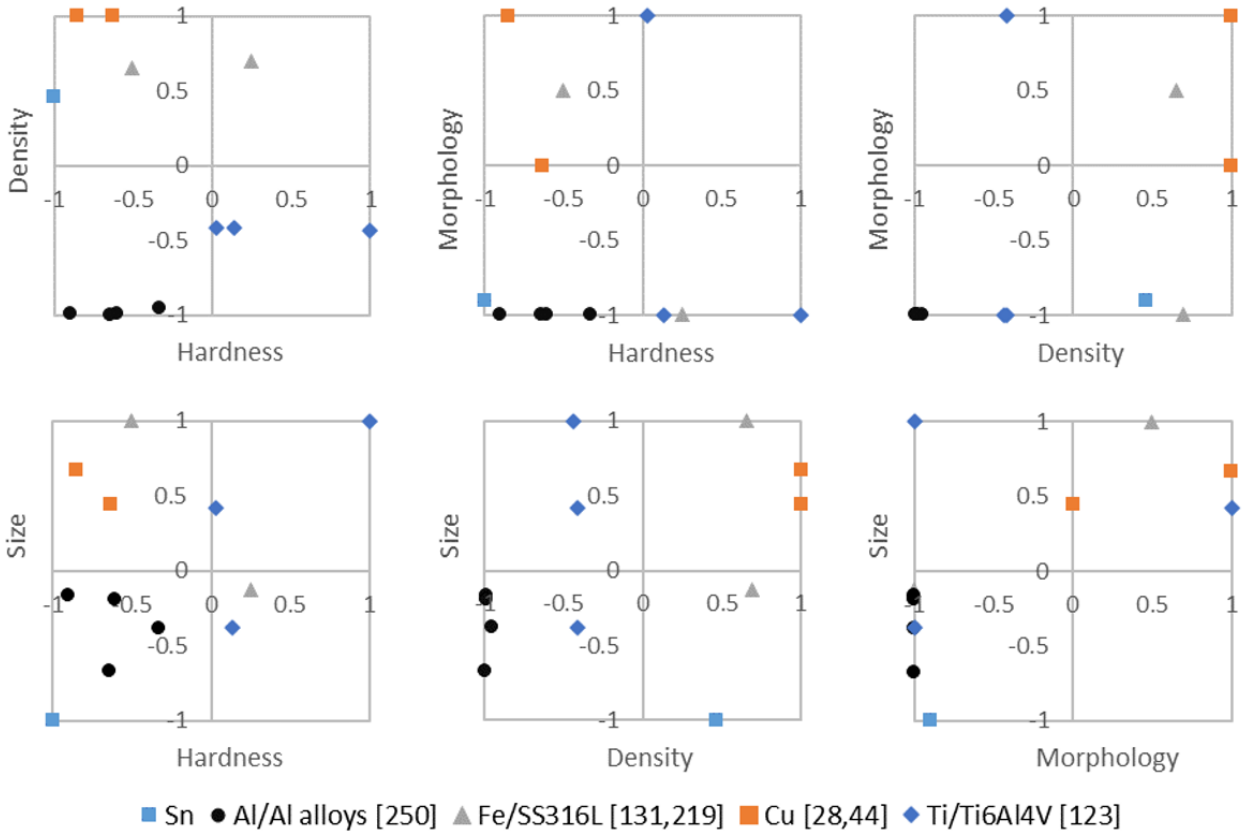

Fig. 5-1: *Comparison of scaled SC properties. The spread of data points shows the complimentary of the various SC in this study.*

Powder mixtures with 90 wt.% tin and 10 wt.% of the SC were prepared by mixing for 1h in a metal can without additional media (e.g., milling balls) using a double movement powder mixer. No significant morphological changes or hardening was noticed in the mixed powder when compared with the starting powders. The absence of morphological changes was verified through scanning electron microscope (SEM) of the mixed powders. Note should be taken that for each SC, the 10 wt.% weight fractions could represent a different volume fraction (based on density) or a different fraction of particles present in the mixture (based on molar mass). For instance, 10 wt.% of Al in Sn represents 33 mol.% or 23 vol.% of Al, while 10 wt.%. of Cu in Sn represents 17 mol.% or 8 vol.% of Cu, meaning that there are twice as many or thrice the volume of Al particles participating in the impinging of the substrate and the coating, as compared to Cu particles [45]. Although not studied here, these metrics could have an impact on the crack-generation on the CFRP or on the deposition of tin.

5.4.2 Powder characterization

The various properties for each powder are listed in Table 5-1. The particle sizes of the feedstock powders were measured with a wet laser diffraction particle size analyzer (FlowSync, Microtrac, PA, USA). The tin powder had a spheroidal morphology and a relatively lower median particle size of 13 µm compared to the other powders, which had a median particle size between 20 and 37 µm. The SEM images of the single-component powders are presented in Fig. 5-2. In Fig. 5-2 a, a broad distribution of particle sizes can be observed for tin, whereas the other powders (Fig. 5-2 b-h) seem to have more homogeneous distributions. This is confirmed by the particle size distributions of the various powders, presented in Fig. 5-3, where tin presents a broad, almost bi-modal size distribution compared to fairly mono-modal distributions of the other powders. The two copper powders had different morphologies with a mixed spherical/irregular powder (Cu, Fig. 5-2 b) being complemented by an irregular copper powder (Cu-IR, Fig. 5-2 c). The iron had a mixed morphology, with mostly irregular particles (Fig. 5-2 d), while the stainless steel 316L powder was spherical (Fig. 5-2 e). Finally, titanium powders in the form of both a spherical (Ti-SP, Fig. 5-2 f) and an irregular, angular powder (Ti-AG, Fig. 5-2 g) were complemented by a spherical Ti6Al4V powder (Fig. 5-2 h)

Table 5-1: *Properties of the feedstock powders used in this work.*

Powder	**Morphology**	**Supplier**	**D_{50}** (µm)	**Hardness** ($HV_{0.01}$)	**Density** ($g.cm^{-3}$)
Sn	Spheroidal	CenterLine	13	8±1	7.29
Cu	Mixed	Giken	30	68±7	8.96
Cu-IR	Dendritic	CenterLine	33	32±4	8.96
Fe	Mixed/IR	Goodfellow	37	89±14	7.87
SS316L	Spherical	Sandvik	23	215±26	8.00
Ti-SP	Spherical	Raymor (AP&C)	20	196±22	4.50
Ti-AG	Angular	Cerac	30	178±34	4.50
Ti6Al4V	Spherical	Raymor (AP&C)	37	340±14	4.43

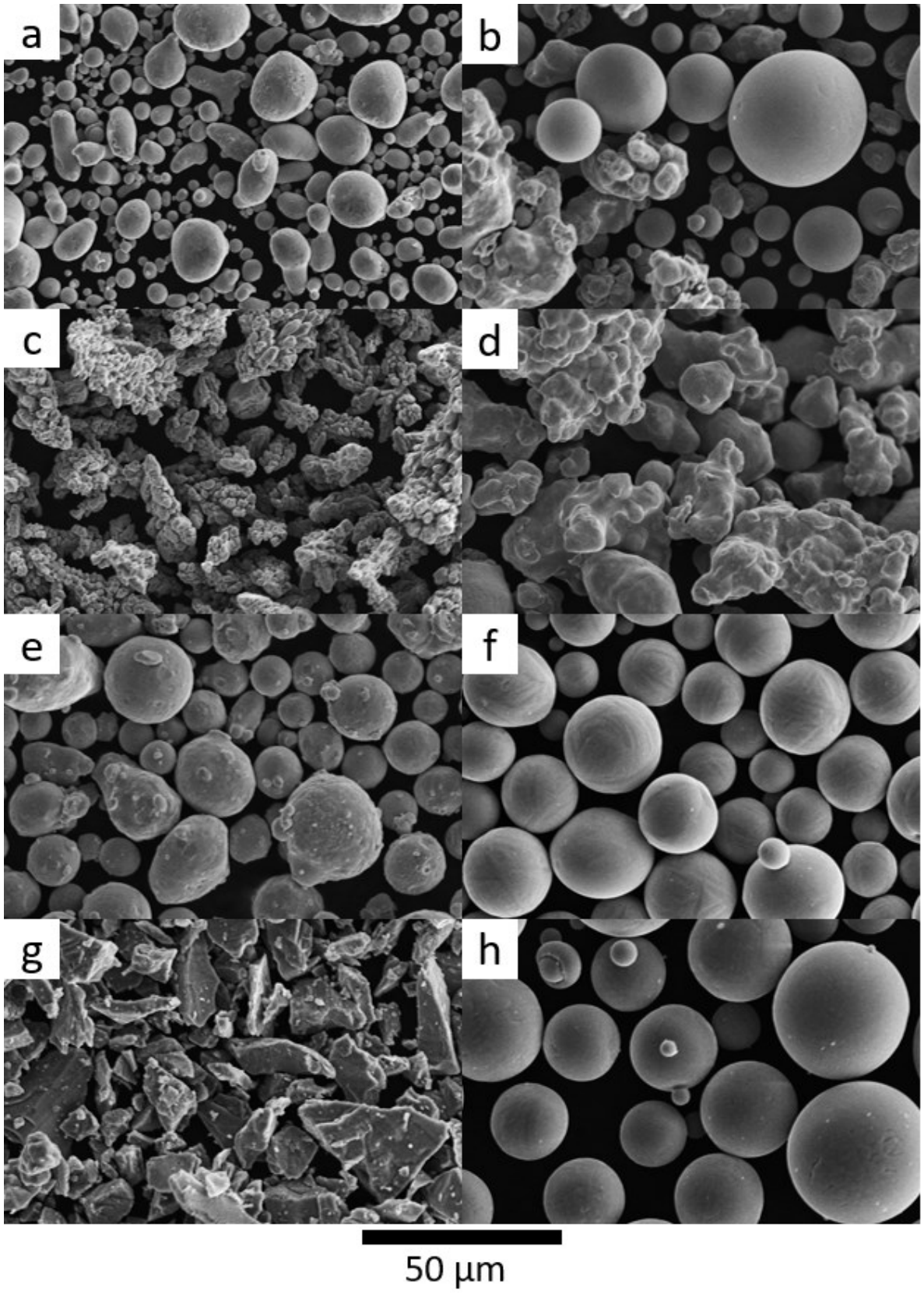

Fig. 5-2: *SEM images of the feedstock powders: (a) Sn, (b) Cu, (c) Cu-IR, (d) Fe, (e) SS316L, (f) Ti-SP, (g) Ti-AG, (h) Ti6Al4V.*

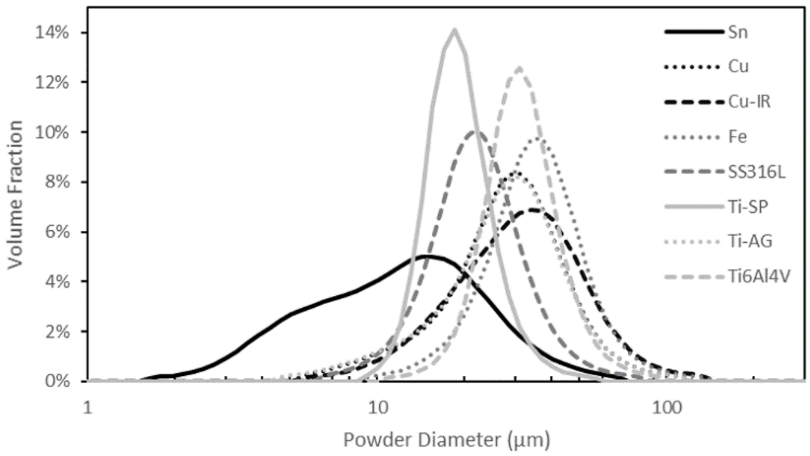

Fig. 5-3: *Particle size distribution of the feedstock powders.*

The average Vickers hardness of the feedstock powders was measured by mounting the powders, grinding to a metallographic finish and using a Clark CM-100AT Microhardness Tester (Sun-Tec, Novi, USA) for a penetration time of 15 s under a load of 10 gf on 10 well-spaced areas. The error given for the hardness values corresponds to the standard deviation of the measurements. Tin had the overall lowest hardness (8±1 $HV_{0.01}$), while copper and iron had hardness values of 32-89 $HV_{0.01}$. The stainless steel 316L, titanium and Ti6Al4V powders had hardnesses that were greater than those previously studied with values reaching 340 $HV_{0.01}$ for Ti6Al4V. By comparison, the hardness values of copper and iron were on par with the aluminum and aluminum alloy powders from previous work [250].

5.4.3 Kinetic energy estimations

The particle velocity from its injection location up to its impact on the substrate is determined accordingly in two steps: first, complete 2D axisymmetric compressible flow simulations of the nozzle were carried out using SU2, then followed by particle tracking simulations using the one-way coupled Particle CFD module of CSAM Digital Solutions, a software developed within the Cold Spray Additive Manufacturing (CSAM) industrial R&D group led by the National Research Council of Canada [252]. The numerical simulation takes into account the complex shock substrate interaction and the influence of the bow shock on the particle trajectory. This model allows the calculation of the particle velocity for each cut of the particle size distribution of the feedstock powders and it considers all particles to be spherical.

The kinetic energy of a particle can be estimated through Eq. 1:

$$\textbf{Eq. 1} \quad E_{C_{1\,particle}} = \frac{1}{2} m v_{part}^2 = \frac{1}{2} \text{ x } \rho_{part} \text{ x } \frac{4}{3} \pi r_{part}^3 \text{ x } v_p^2$$

where $E_{C,1particle}$ is the kinetic energy of a particle, m is the mass of the particle, v_p is the particle velocity upon impact with the substrate, ρ_{part} is the density of the SC, and r_{part} is the particle radius. For the purpose of the estimations conducted in this paper, all particles are assumed to be spherical.

Powders are described by a distribution of sizes (cuts on the particle size distribution), so the average particle energy is considered in this study, and calculated through Eq. 2:

$$\textbf{Eq. 2} \quad E_C = \sum_i (f_{i*} E_{C_{1\,particle}}(r_i)) = \frac{1}{2} \text{ x } \rho_{part} \text{ x } \frac{4}{3} \pi \sum_i (f_i r_i^3 v_i^2)$$

where E_C is the average particle energy, r_i is the radius of a particle of a cut (range) noted i, f_i is the fraction of particles in the cut i, and v_i is the velocity of the particles in the cut i. The average particle impact energies are regrouped in Fig. 5-4. As with the choice of SC properties, it can be

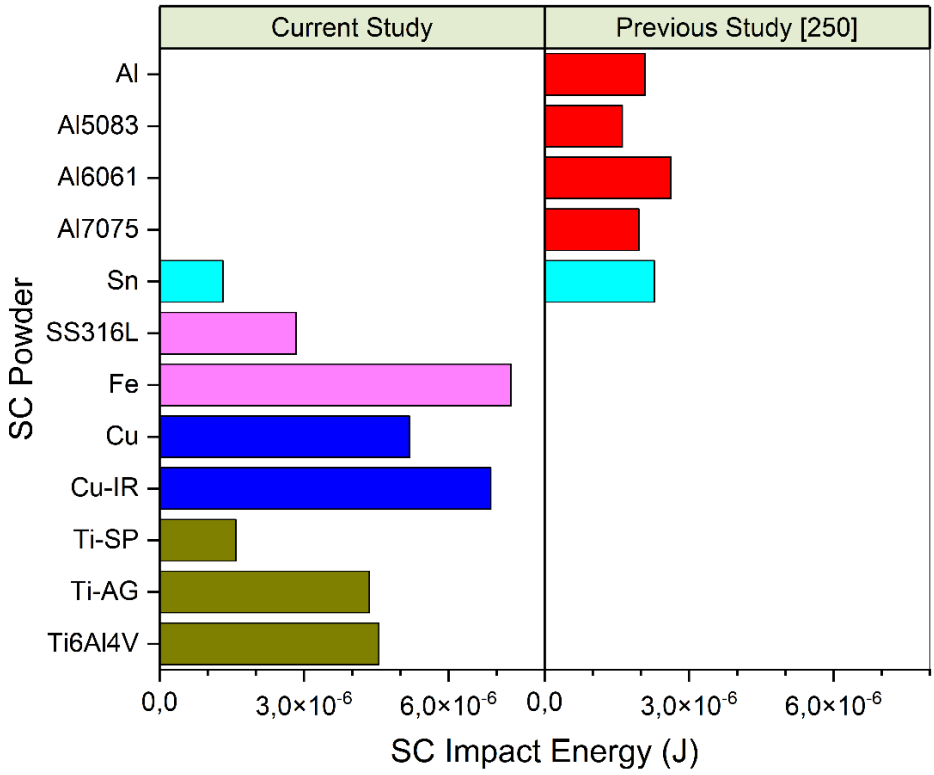

Fig. 5-4: *Kinetic energy of the various powders of this study and of the Al/Al alloy powders used in [250]. Bar color is based on SC density.*

seen that a wide spread of particle impact energies is also obtained. With values between 1 x 10^{-6} J and 8 x 10^{-6} J, it appears that the impact energy of the SC particles from this study are higher than the energy of the Al/Al-alloy particles from [250] (1 x 10^{-6} J to 3 x 10^{-6} J). The tin in this study has a lower average impact energy compared than the tin from the previous study (1.32 x 10^{-6} J compared to 2.28 x 10^{-6} J): this is due to the tin from the previous study having a small fraction of large powders (above 70 µm) that the tin in this work does not have. It is also important to note that the average particle velocity for particles of irregular morphology (Cu-IR, Ti-AG, Fe) may be higher, due to higher drag coefficients [123, 253], such that their kinetic energy may also be higher.

5.4.4 Substrates

The substrates used in this work were epoxy-CFRPs provided by Bombardier Aerospace (Montreal, Canada), Polyether-Ether-Ketone (PEEK)-CFRPs provided by TenCate (Netherlands) and commercially available 1020 mild steel plates. The CFRP substrates are presented in the previous work [250]. The steel substrates were used as a benchmark to compare the spraying of powders on CFRPs to a typical metal–metal cold spraying situation. The epoxy-CFRPs (abbreviated as e-CFRP) used here consists of a thermosetting epoxy matrix with continuous carbon fiber reinforcements. The e-CFRP panels were made of four plies of epoxy/carbon fiber prepreg ([0/90]2s) and have various coating finishes prepared by the manufacturer: a bare finish, a putty finish, and a surface film finish (that could be described as a fine-squared mesh finish on the substrate). The bare finish e-CFRP is the as-manufactured substrate, the putty e-CFRP includes a surface finished with a pinhole filler and surfacer to produce defect-free surfaces and the surface film e-CFRP includes a neat epoxy resin film with an embedded veil, normally a mat, on the top surface, to help handling the resin film. The hardness of these substrates was measured as per the powders, and the values are 39±8 $HV_{0.01}$ for the bare e-CFRP, 51±15 $HV_{0.01}$ for the putty e-CFRP and 40±13 $HV_{0.01}$ for the surface film e-CFRP. The PEEK-CFRP used here consists of a thermoplastic polyether-ether-ketone matrix with continuous carbon fiber reinforcements. These panels were made of five plies of PEEK/carbon fiber ([(0,90)2/(0,90)3R]). The hardness of this substrate was differentiated between areas showing superficially pure PEEK, and superficially predominant carbon fibers. The respective hardness values for each area are 26±3 $HV_{0.01}$ and 63±22 $HV_{0.01}$. Sheet sections of dimensions 7 x 7 cm were used as substrates during the cold spray

campaigns. The substrates were degreased with ethanol, and the mild steel plates were grit-blasted with 24 grit alumina before cold spraying. The CFRP substrates were not grit-blasted as it would result in the erosion of the substrate.

5.4.5 Cold spray conditions

The cold spraying was performed at the McGill-NRC cold spray facility at National Research Council of Canada in Boucherville, using a low pressure commercially available CenterLine SST SSM-P3300 system (Supersonic Spray Technologies, CenterLine Windsor Limited, Canada). The primary cold spray parameters are listed in Table 5-2. These parameters were chosen based on previously successful cold spray campaigns with tin [28, 44, 246, 250] and at the selected conditions, melting was observed in previous work [28, 44, 246]. A comparison between cold spraying pure tin and the powder mixtures with SCs of varying properties was thus possible, on a variety of CFRP substrates. The carrier gas was nitrogen, the standoff distance was 18 mm, the step size was 1 mm with 38 steps, and the gun travel speed was 25 mm/s. The powder

Table 5-2: *Principal cold spray parameters.*

Powder	- Sn - Sn-10Cu - Sn-10Cu-IR - Sn-10Fe - Sn-10SS316L - Sn-10Ti-SP - Sn-10Ti-AG - Sn-10Ti6Al4V

Substrate	- Steel
	- e-CFRP:
	  • bare
	  • putty
	  • surface film
	- PEEK-CFRP

Carrier Gas Temperature (°C)	- 310
Gas Pressure (psi/MPa)	- 60/0.41 (all substrates)

feed rate was set to 1 revolution per minute (RPM), which gave a measured feeding rate between 10.1 and 16.9 g/min, measured every three sprays to accurately assess the variation. The substrates were pre-heated by operating a single pass without powder feeding, at the given conditions (Table 5-2), then, only one pass was sprayed for each set of conditions. With this procedure, the acquired results would be meaningful as the average DE from a large spray area is acquired, and the study is focused on trends rather than absolute values. All the substrates were aligned and sprayed at the same time for one condition, so that any external variation (e.g. feeding, temperature effects) may be neglected.

5.4.6 Result analysis

After the cold spray process, the samples were observed from a top surface view, then prepared as metallographic samples and characterized with a Hitachi (Japan) SU3500 scanning electron microscope. The cross-sectional samples were cut (Delta Abrasimet, Buehler, Illinois, USA) and observed parallel to the spraying direction. The hardness of the tin in these samples was also measured. The SC retention rates (i.e. weight fractions of SC in the coatings) were estimated, by measuring the relative areas of tin and SC in 10 different SEM BSE-COMP images using an image analysis method, then converting the obtained volume fractions into weight fractions with Eq. 3.

$$\textbf{Eq. 3} \quad r_{SC} = \%_{wt_{SC}} = \frac{1}{1+\frac{\rho_{Sn}\left(1-\%_{V_{SC}}\right)}{\rho_{SC} \quad \%_{V_{SC}}}}$$

where r_{SC} is the retention rate of the SC, $\%_{wt}$ is the weight fraction, $\%_V$ is the volume fraction, and ρ_{Sn} and ρ_{SC} are respectively the densities of tin and of the SC.

Deposition efficiency was measured as the mass gain of the substrate divided by the total mass of feedstock powder fed during the time the gun was over the substrate. The relative DE of each coating element could be determined from the weight fractions determined with Eq. 3, as described in [246]. The expressions are recalled in Eq. 4 and Eq. 5.

$$\textbf{Eq. 4} \quad DE_{SC} = \frac{r_{SC} \times DE}{0.1}$$

$$\textbf{Eq. 5} \quad DE_{Sn} = \frac{(1-r_{SC}) \times DE}{0.9}$$

where DE, DE_{SC} and DE_{Sn} are respectively the overall DE of the coating, pure SC and pure Sn.

5.5 Results

The top surface views of the samples showed continuous coatings for most mixtures and substrates, and no peeling was observed, unlike in the previous study [250]. Looking into more detail, deposition seemed uniform on all steel, bare e-CFRP and surface film e-CFRP (Fig. 5-5 a), while deposition on putty e-CFRP and PEEK-CFRP presented more irregularity (visible waviness on the surface and/or visible areas of underlying carbon fibers) (Fig. 5-5 b). Only one set of conditions provided a discontinuous surface coating (Sn-10Ti6Al4V on PEEK-CFRP) (Fig. 5-5 c).

The hardness of the tin in the coatings was measured and found to be between 12 ± 1 $HV_{0.01}$ and 14 ± 1 $HV_{0.01}$, which means that the average hardness of tin in the coatings was 50-75% higher than the hardness of the pure tin feedstock powders. This was true regardless of the presence of SC in the feedstock powder, and regardless the choice of this SC. Despite the fact that tin particles may have experienced melting, this would then indicate that there is still some work hardening effect, which is, however, not promoted by the addition of hard SC particles.

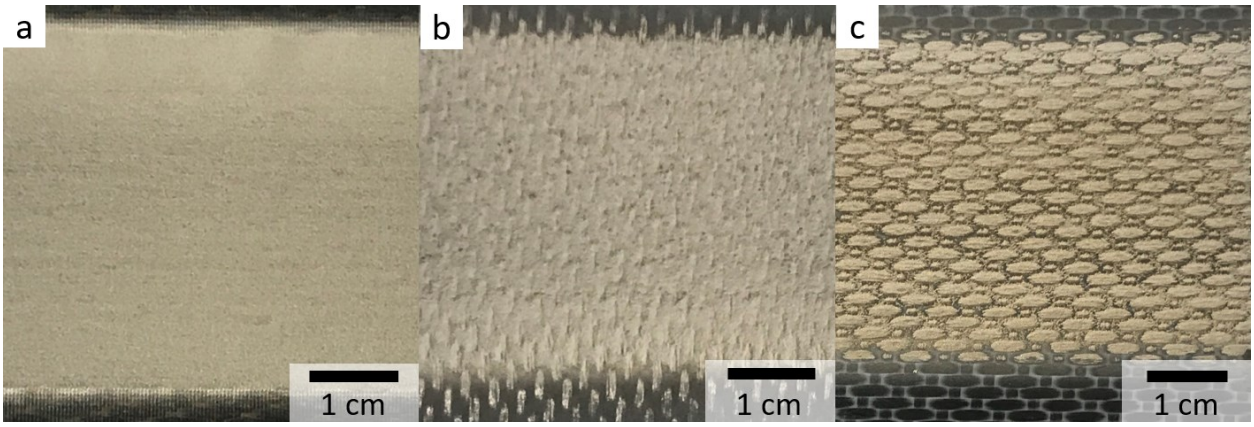

Fig. 5-5: *Top surface images of various coatings: (a) Sn-10Fe on bare e-CFRP, (b) Sn-10SS316L on putty e-CFRP, (c) Sn-10Ti6Al4V on PEEK-CFRP.*

The retention rates of the SC are presented in Table 5-3 with typical micrographs of corresponding coating cross sections presented in Fig. 5-6.

Table 5-3: *Retention rates of the SC measured at the cross sections of the coatings on various substrates, and calculated deposition efficiencies for the SC and tin in the coatings.*

Powder	Substrate	SC Weight fraction (%)	Deposition Efficiency (%)		
			Overall	SC	Sn
Sn	Bare e-CFRP	-	21	-	21
	Putty e-CFRP	-	21	-	21
	Surface Film e-CFRP	-	22	-	22
	PEEK-CFRP	-	20	-	20
	Steel	-	41	-	41
Sn-10Cu	Bare e-CFRP	1	23	3	25
	Putty e-CFRP	1	23	2	25
	Surface Film e-CFRP	2	22	4	24
	PEEK-CFRP	2	20	4	22
	Steel	≈0	40	2	44
Sn-10Cu-IR	Bare e-CFRP	20	23	46	20
	Putty e-CFRP	20	20	40	17
	Surface Film e-CFRP	25	23	57	19
	PEEK-CFRP	17	21	37	19
	Steel	17	42	71	39
Sn-10Fe	Bare e-CFRP	5	18	9	19
	Putty e-CFRP	3	15	4	16
	Surface Film e-CFRP	5	19	10	20
	PEEK-CFRP	3	17	5	18
	Steel	3	37	10	40
Sn-10SS316L	Bare e-CFRP	2	16	3	17
	Putty e-CFRP	2	12	2	13
	Surface Film e-CFRP	3	17	5	18
	PEEK-CFRP	2	16	3	17
	Steel	1	37	3	41
Sn-10Ti-SP	Bare e-CFRP	≈0	18	≈0	20
	Putty e-CFRP	≈0	17	≈0	19
	Surface Film e-CFRP	≈0	19	≈0	21
	PEEK-CFRP	≈0	13	≈0	14
	Steel	≈0	38	≈0	42

Table 5-3 (continued): *Retention rates of the SC measured at the cross sections of the coatings on various substrates, and calculated deposition efficiencies for the SC and tin in the coatings.*

Powder	Substrate	SC Weight fraction (%)	Deposition Efficiency (%)		
			Overall	SC	Sn
Sn-10Ti-AG	Bare e-CFRP	3	17	6	18
	Putty e-CFRP	4	14	5	15
	Surface Film e-CFRP	4	19	7	20
	PEEK-CFRP	4	15	6	16
	Steel	2	37	8	40
Sn-10Ti6Al4V	Bare e-CFRP	≈0	16	≈0	18
	Putty e-CFRP	≈0	15	≈0	17
	Surface Film e-CFRP	≈0	17	≈0	19
	PEEK-CFRP	≈0	11	≈0	12
	Steel	≈0	38	≈0	42

SC retention varies greatly: Ti-SP and Ti6Al4V had retention rates close to 0% while retention rates of 3-5% were observed for SC Fe, and even 17-25% for Cu-IR. This range for Cu-IR is well beyond the 10% in the initial feedstock powder and resulted in SC DE values between 37 and 71% (Table 5-3). This result would suggest that Cu-IR is accumulating in the coating at the expense of Sn (as seen in Fig. 5-6 c), i.e. Cu-IR retention would increase as the Sn retention decreases.

Pure Sn has a DE of 20-22% on the CFRP substrates (Table 5-3). Mixtures with SC Fe, SS316L and Ti/Ti6Al4V all generate overall DE values that are relatively lower than the DE of single component Sn powder (11-19%), with the lowest values being generally obtained on the putty e-CFRP or the PEEK-CFRP. By establishing the SC DE from the retention rates with Eq. 3, it is possible to determine the effective pure Sn DE for each coating [246]. Even with the improvements brought by the addition of the SC for the Sn DE compared to the overall DE, the effective Sn DE in these coatings only reaches the average DE of single component tin coatings in one occurrence (Sn-10Ti-SP sprayed onto surface film e-CFRP). SC Cu, on the other hand, lead to slight improvements of the effective Sn DE as compared to pure Sn coatings on CFRP (from 20-22% to 22-25%), while SC Cu-IR provided coatings with a comparable overall DE (20-23%), but an effective Sn DE below that of the pure Sn coatings (from 20-22%, to 17-20%).

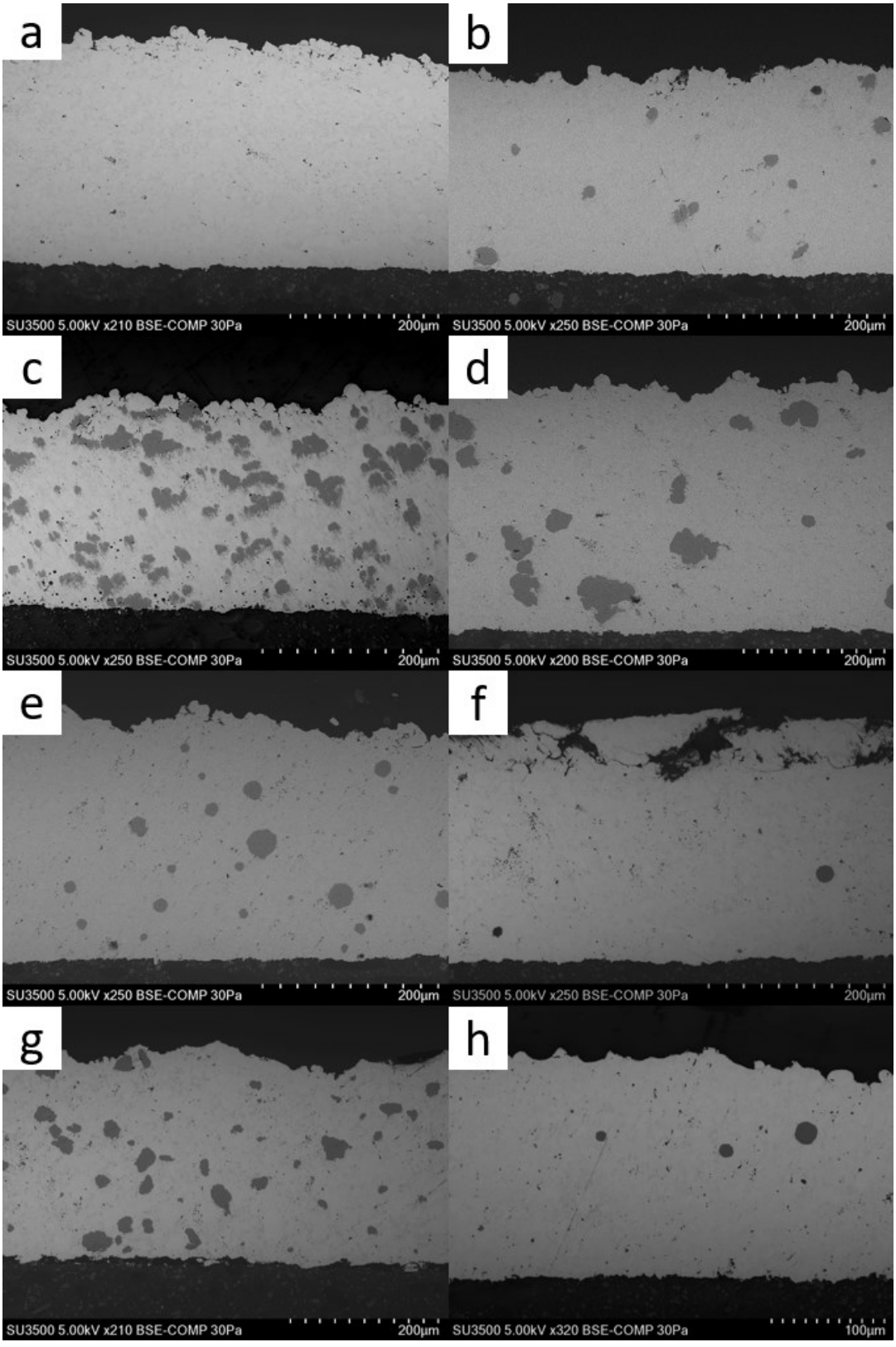

Fig. 5-6: *SEM-BSE images of the cross-sectional microstructures for various coatings on the surface film e-CFRP: (a) Sn, (b) Sn-10Cu, (c) Sn-10Cu-IR, (d) Sn-10Fe, (e) Sn-10SS316L, (f) Sn-10Ti-SP, (g) Sn-10Ti-AG, (h) Sn-10Ti6Al4V. Particles with darker contrast in the coatings are the SC particles (Sn having the highest atomic number).*

Similar observations can be noted on the steel substrates, where the pure Sn coating has a DE of 41%, while the SC Fe, SS316L and Ti/Ti6Al4V provide overall DE values that are slightly lower (37-38%). The improvement brought by these SC allow the effective Sn DE to be around 40-42%, which is more on par with the pure Sn coatings on steel, in contrast to what was observed on the CFRP substrates. Again, SC Cu provides a slight improvement of the Sn DE (44%, up from 41%), while SC Cu-IR, although showing a similar overall DE of 42%, results in a lower effective Sn DE of 39%.

Therefore, it appears that most of the SC of this study generate a decrease of pure Sn DE on the CFRP substrates (Fe, SS316L, Cu-IR, Ti-SP, Ti-AG, Ti6Al4V), while SC Cu generates a slight increase of the pure Sn DE. These comparisons of overall DE and pure Sn DE may not provide notable differences in absolute value (one may consider the values are rather similar in front of measurement errors imposed by powder fluctuations), but certain trends do seem to appear nevertheless, which can provide some value. Furthermore, the retention rates of these SC vary greatly with some particles showing close to no retention versus others that are highly retained. These results could be a combination of factors and will therefore be discussed comparatively to the SC properties, to establish potential trends between pure Sn DE and SC choice.

5.6 Discussion

5.6.1 On the effect of individual SC properties

As shown above, the SC of this study only rarely improve the DE of pure Sn on CFRP, and retention rates were observed to vary from 0% to 25%. On the other hand, in previous work, Sn was mixed with Al or Al alloys and cold sprayed at the same conditions: improvements of pure Sn DE were quite strong (from 11-17% to a range of 18-27% with the SC Al/Al alloy), and it was observed that SC retention was below 1%, compared to the initial 10% in the feedstock powder [250]. Given spraying conditions and substrates were the same, this naturally leads to exploring the different SC properties that could explain the varying effects on both SC retention and DE of tin. The effects of each SC property are summarized in Table 5-4: this table takes into account results obtained in this work and in previous work [250].

Table 5-4: *Effect of each SC property on overall DE, DE of pure tin and SC DE. An empty area indicates "no direct correlation".*

SC Property	Value/Trend	Overall DE	Pure tin DE	SC DE
Hardness	Low (~ hardness of substrate)	Greatly increased (Al, Al alloy) Slight increase (Cu, Cu-IR) Slight decrease (Cu-IR, Fe)	Greatly increased (Al, Al alloy) Slight increase (Cu) Slight decrease (Cu-IR, Fe)	///
	High	Decreased	Decreased	///
Morphology	Spherical	///	Slight increase	Low
	Irregular	///	Slight decrease	High
Density	Increasing	///	///	(Increase?)
Median Size (D_{50})	Any	///	///	///

5.6.1.1 SC Hardness

Cu and Cu-IR offer a hardness value within the range of the substrate hardness (i.e. 25-65 $HV_{0.01}$), while Fe, SS316L, Ti, Ti-AG and Ti6Al4V have hardness values that are greater than 80 HV. As previously discussed, overall DE of the coatings with each of the latter SC group is slightly lower than the DE of a pure tin coating, while SC Cu/Cu-IR offer a slight increase as compared to pure tin. Most noticeably, SC SS316L and Ti6Al4V present the highest SC hardness values (215 and 340 HV, respectively), but also the lowest overall DE values on CFRP (11-17% vs 20-22% for pure Sn coatings): Sn-10Ti6Al4V on PEEK-CFRP is also a rare "poor" coating in this study (Fig. 5-5 c), suggesting that relatively harder particles have detrimental effects on the deposition process. Typically, these negative effects could be explained by the erosion of previously deposited Sn particles by the harder SCs, and this will be discussed further in the second section of the discussion. The current results also seem to support the previous study where the existence of an optimal SC hardness value for pure Sn DE was suggested for powder hardnesses in the range of the substrate hardness [250].

5.6.1.2 SC Morphology

The more spherical powders of this study (Ti-SP, Ti6Al4V, Cu, SS316L), as well as the Al/Al alloys from [250], resulted in very low retention values (below 3%) and as an effect, these coatings presented SC DE values below 5%. The powders with more irregular morphologies (Fe, Ti-AG, Cu-IR) offered the greatest retention values, with Cu-IR offering the highest values (17-25%). These results support the works of Che et al. [44] where they suggested that use of irregular SC morphologies leads towards more SC retention as there is more mechanical interlocking compared to spherical morphologies. Since irregular powders have higher drag coefficients, they could also have higher velocities than their spherical counterparts [123, 253], which could also explain the higher rate of embedding.

While irregular SCs seem to lead to an increased retention of the SC, spherical SCs seem to lead to greater improvements in Sn DE: as previously mentioned, both copper SCs generate a slight increase in overall DE on CFRP as compared to the pure Sn coatings, but Cu-IR results in lower effective pure Sn DE than in the pure Sn coatings, while Cu leads to an overall improvement. This could be related to peening of tin by the spherical SC during deposition, while the irregular SC seems to take the place of the tin in the coating through increased embedding.

5.6.1.3 SC density

When considering SC density, it is more difficult to establish a clear trend regarding overall DE and pure Sn DE. Al/Al alloys provided the greatest improvements in overall DE and Sn DE [250] and these SC were the low-level density of this study (~2.7 $g.cm^{-3}$). SC Cu led to similar improvements, albeit of smaller amplitude (from 20-22% to 22-25%): Cu has a density of 8.96 $g.cm^{-3}$, which would be the high-level of the study that is being conducted. On the other hand, Ti and Fe, as well as their corresponding alloys, have densities respectively of 4.5 $g.cm^{-3}$ and 7.9 $g.cm^{-3}$, and their use as SC has generated a decrease in overall DE and DE of pure Sn on CFRP. The density of Sn is 7.27 $g.cm^{-3}$, therefore indicating that SC with densities higher or lower than Sn, could either have a positive or negative effect on the DE: this would clearly indicate that any direct correlation of DE with density is not possible.

On another note, the higher retention rates of SC Fe, Ti-AG, Cu-IR seem to follow the density of the SCs: in increasing order of density, Ti has a retention of 2-4% (SC DE of 5-8%), while Fe has a retention of 3-5% (SC DE of 4-10%), and finally Cu has a density of 8.96 $g.cm^{-3}$ and a retention of 17-25%, (SC DE of 37-71%). This observation would correlate well with the idea that higher density results in higher kinetic energy, and therefore higher penetration and mechanical restraint in a relatively softer Sn matrix. However, this observation could also be explained by the different morphologies of these powders (dendritic powders having more surface area than angular powders), rendering the mechanical restraint easier to initiate for dendritic powders, as discussed in [44].

5.6.1.4 SC particle size

From the sole stand point of the SC D_{50}, it seems that the SC Al/Al alloy of the previous study had generally smaller particle size distributions (D_{50} between 16 and 22 µm) [250] while the SCs of this study had relatively larger particle size distributions (D_{50} between 20 and 37 µm), so it could have been assumed that the improvements brought by SC Al and its corresponding alloys could be associated with a more ideal, smaller particle size distribution. Nevertheless, Ti-SP has a median size of 20 µm and a density relatively close to that of Al as compared to Sn, and while Al brings improvements in overall DE and effective DE of pure Sn, Ti-SP does not.

This finally leads to approaching the results from the perspective of the kinetic energy of the impinging powders, and therefore correlating the effects of particle size, density and particle velocity (which is impacted by morphology [123, 253]) to estimate the energy of each SC upon impact on the substrate, but also on Sn particles once they have been deposited.

5.6.2 On the effect of SC kinetic energy

The effect of the SC on the pure Sn DE is shown in Fig. 5-7 as a function of the SC hardness and of the SC impact energy. In contrast to the study of each individual property, clearer trends are apparent.

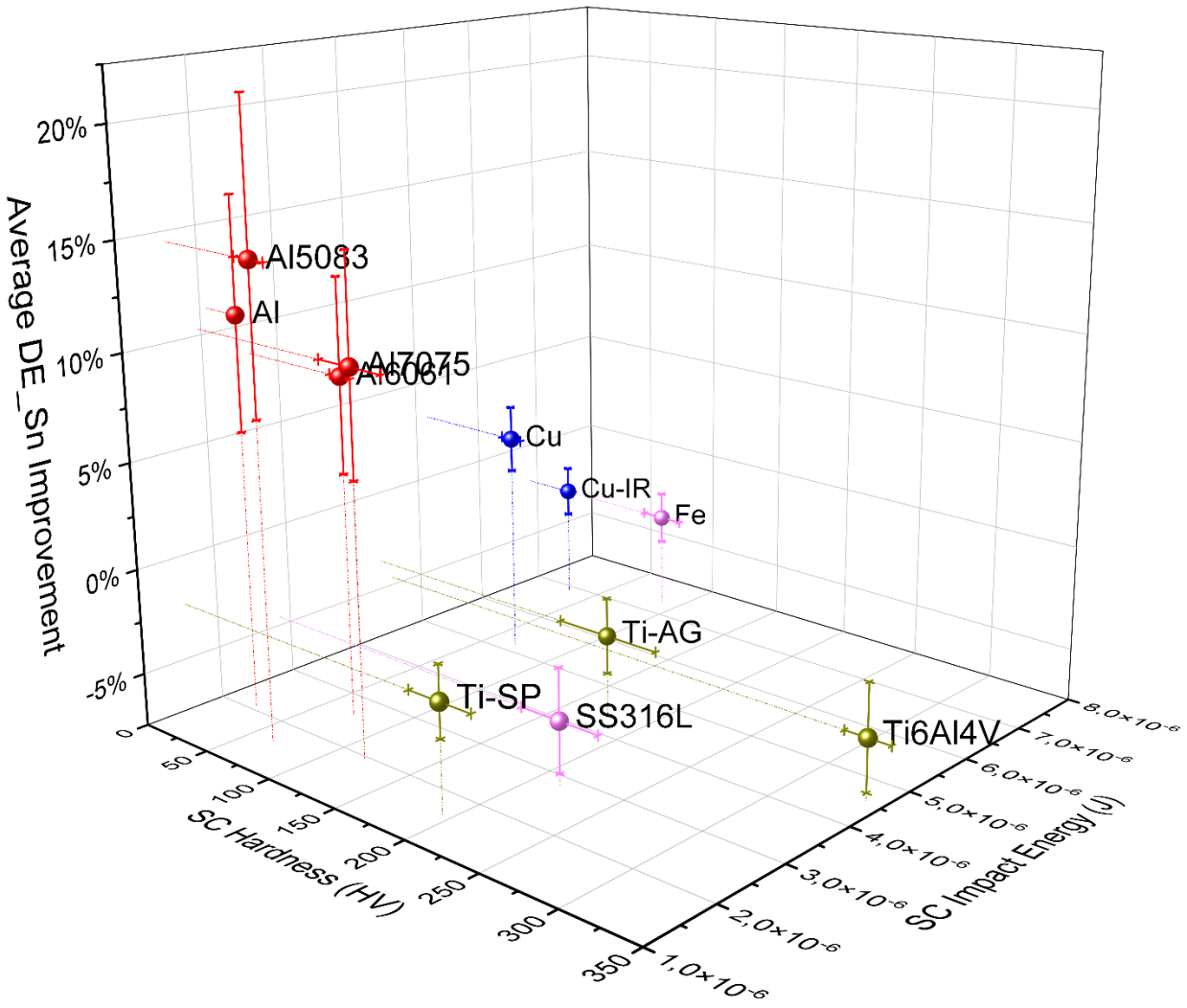

Fig. 5-7: *Average pure Sn DE improvement for the various SCs, represented as a function of the SC hardness and impact energy. Sphere color is based on SC density.*

Low hardness SC impacting the substrate at low impact energy, such as Al or Al alloys, lead to notably positive improvements of Sn DE on CFRP (+9-15%), while SC with higher impact energies, such as Cu and Fe, lead to more neutral effects on the Sn DE : Cu has a slightly positive effect (+3%), and Cu-IR/Fe, with the highest impact energies of this study, have more of a negative effect (-3%). This evolution of Sn DE with low hardness and increasing impact energy seems to evolve with a linear trend and it seems that, below 6 x 10^{-6} J, the SC improves the Sn DE as compared to the cold spraying of pure Sn, while higher impact energies lead to a decrease of Sn DE. Schmidt et al. [144] calculated the erosion velocity of Sn as being equal to around 350m/s for a 25 µm particle, and by using Eq. 1, this corresponds to an impact energy of 3.6 x 10^{-6} J. The

particle tracking simulation allows the calculation of the particle impact velocity for each cut of the measured particle size distribution, which, in turn, allows a particle kinetic energy distribution to be established. Table 5-5 presents the proportion of each feedstock powder below or above the erosion energy of Sn (3.6 x 10^{-6}J); it can be seen that Cu-IR and Fe have a higher-than-average proportion of particles with an erosive effect (54% and 68%, respectively), while Cu has fewer particles that could exhibit an erosive behavior (46%).

It is also important to notice that Cu-IR and Fe have irregular morphologies. Wong et al. [123] provided results that showed that irregular titanium had an average velocity 15% higher than the velocity of the spherical powder with a similar average particle size. Therefore, by factoring in such a difference, it can be suggested that as high as 66% of Cu-IR and 82% of Fe could exhibit an erosive behaviour, thus further explaining the decrease in Sn DE obtained as a result of their use as SC. The obtained energy of 6 x 10^{-6} J for relative neutral effect on Sn DE at low hardness (as compared to the calculated erosive energy of 3.6 x 10^{-6} J) could be a trade-off between the

Table 5-5: *Proportion of particles below or above the erosion energy of Sn, calculated from the information provided by [144] with Eq. 2.*

Reference	Powder	Particles with Impact Energy below 3.6 x 10^{-6}J (%)	Particles with Impact Energy above 3.6 x 10^{-6}J (Erosive Behavior on Sn) (%)
Current Study	Sn	92	8
	Cu	54	46
	Cu-IR	46	54
	Fe	32	68
	SS316L	81	19
	Ti-SP	96	4
	Ti-AG	63	37
	Ti6Al4V	56	44
Previous Study [250]	Sn	89	11
	Al	85	15
	Al5083	88	12
	Al6061	79	21
	Al7075	86	14

proportion of erosive SC, and the fact that 90 wt.% of the sprayed powder is pure Sn that can deposit on CFRP. Therefore, it is possible that the erosive effect of the SC only appears at higher impact energies.

In any case, the previous low-hardness observations would suggest that the SC can provide improved deposition when the SC hardness is on par with that of the substrate (as advanced in the previous study [250], and supported in this work) and when SC impact energy is low or on par with that of the Sn feedstock powder. Furthermore, with low SC hardness and higher SC impact energy, the benefits of the enhanced "crack-filling" mechanism [250] would be lost to increasing erosive behavior of the SC.

Another trend that appears from Fig. 5-7 is that higher hardness SC, such as Ti, SS316L and Ti6Al4V, consistently lead to a decrease of Sn DE as compared to the DE of pure tin, regardless of their impact energy (from 1.6 x 10^{-6}J with Ti-SP to 4.6 x 10^{-6}J with Ti6Al4V). The decrease of Sn DE also occurs regardless the low erosive behavior of some of these powders, such as Ti-SP which only has 4% of powders with an energy above 3.6 x 10^{-6}J (Table 5-5). This may seem controversial as it could be expected that a combination of low kinetic energy and gradually increasing particle hardness would lead to a gradual appearance of erosion through peening or limited degrees of erosion from non-eroding powders, while these results would suggest rapid appearance of erosion (from +10% with Al7075 at 118$HV_{0.01}$, to -3% with Ti-AG at 178$HV_{0.01}$). A possible explanation is that the range of powder size distributions considered in this study is not small enough to obtain sufficiently low impact energies that could offset higher hardness values, and thus avoid erosion.

Based on these observations, it would seem that deposition of tin is most improved when a SC is added with a hardness similar to the substrate and an impact energy on par or lower than the Sn powder. This combination of hardness and low impact energy could be the required elements to enhance the "crack-filling" mechanism and provide better first-layer Sn deposition without eroding the coating – in contrast to what is observed here with Cu or Fe, which erode the coating. This also reinforces the importance of considering the impact energy of powders when

discussing the cold spraying of metallic particles onto CFRP, as initially mentioned by Lupoi et O'Neill [31]: in this work, they defined a deposition window for impact energies below 2 x 10^{-6} J.

5.6.3 Ramifications of SC findings for the deposition of single component powders onto CFRP

Metallization of CFRP via cold spray has been studied under various considerations over the past decade and it has proven to be relatively difficult to achieve given a variety of limitations. These limitations mainly concern most metals being too hard to deform and deposit without eroding the CFRP, which can also be viewed as the difficulty of achieving the critical velocity of the metallic powders without eroding the substrate [28, 31, 36]. By considering the deposition of tin mixed with other metallic powders (i.e. SC), some insight into these limitations has been provided and they may be refined.

The previous study [250] revealed that an optimal SC hardness value seems to exist to enhance the "crack-filling" mechanism, and permit better deposition of Sn on CFRP. The current study supports this idea that powder hardness is a key factor in cold spraying CFRP, as notably higher hardness SCs lead to decreased pure Sn deposition (first section of the Discussion).The improved initiation of the "crack-filling" mechanism by the SC applies well to the deposition of Sn, as single component Sn is too soft to generate sufficient cracks on its own, but the mechanism could be valid for any other single component metal susceptible of 1) generating its own cracks (i.e. hardness on par with the substrate hardness, according to [250]) and 2) deforming to fill the cracks (i.e. a metal in the range of its critical velocity). Therefore, single component powder candidates for deposition on CFRP would be materials such as Sn, Pb, Al, Cu and Zn powders (or associated alloys with similar hardness levels). These results would also explain the difficulty to cold spray coatings with harder materials such as steel on CFRP, as observed elsewhere [32, 33].

Annealing harder alloys to spray them as softer materials could be an alternative. Based on the description of the "crack-filling" by Che et al. [28], thermal softening could lead to better filling of the micro-cracks through facilitated flow of material. Of course, directly lowering the hardness of the particles in the spray process, by increasing the temperature, is another solution. In previous studies at McGill University, the cold spraying of tin at temperatures above the melting point of

tin (300-320°C vs 232°C) led to some degree of melting [28, 44, 246], and while this was never proven to be a requirement for the "crack-filling" mechanism, it could be a metric indicating that sufficient thermal softening has been reached. Therefore, warm spraying [20] or high velocity air-fuel (HVAF) [254] could be interesting alternatives to be considered for improved sprayability of other metals such as Cu or Al on CFRP, and should be the focus of another study. Exploring this path may have the effect of diminishing some advantages of cold spray (i.e. heat damage and powder oxidation may increase), but these effects would still be relatively lower than other thermal spray techniques such as high velocity oxygen-fuel (HVOF) or plasma spray which use temperature of several thousand degrees [21].

This study also highlights the importance of the impact energy of the SC, for a hardness similar to that of the substrate. The role of SC impact energy in affecting the DE of pure Sn is also highlighted, as lower SC impact energies are suspected of allowing better activation of the CFRP, which in turn allows the "crack-filling" mechanism to occur (second section of the Discussion). In their study, Lupoi and O'Neill [31] had already mentioned the preference for using powders with lower impact energies to obtain deposition on CFRP, and by considering the existence of an ideal SC impact energy range, it could be suggested that this may apply to a single component powder as well (which would then act as its own SC). Therefore, the results from the current work can reinforce the kinetic energy limit that Lupoi et O'Neill described, around 2 x 10^{-6} J [31].

This value of energy was presented as an average for several polymeric substrates [31], so it is important to note that the nature of the substrate could affect this value. Typically, it may be lower for CFRP, given the weaker nature of the interfacial adhesion strength between fibers and resin matrix [224, 249], versus that of a bulk polymeric substrate. Furthermore, this criterion will probably vary depending on the deformation characteristics of the particles: with tin in this study, some thermal softening has been previously reported [28, 44, 246], so the energy value could be higher. In any case, tin was deposited with an impact energy around 2 x 10^{-6} J, and the highest DEs were observed with SC Al and Al alloys that had impact energies between 1 x 10^{-6} and 3 x 10^{-6} J (i.e. when the criterion was respected). Therefore, regardless the variation, the order of magnitude of the energy criterion described by Lupoi and O'Neill [31] seems valid.

5.7 Additional Implications

The results and discussion provided in this study focus on SC property effects on the deposition of Sn onto CFRP and allowed some insight into requirements for deposition of single component materials onto CFRP. Beyond these suggested requirements, the standard requirements for cold spray apply and would need to be achieved, notably around the critical velocity of the powders (to fulfil the "build-up" phase). This section aims at addressing this specific factor based on the conclusions from this work as well as results provided by the literature.

Most models that define the critical velocity do not clearly account for the variability of the substrate that the metal is impinging, as they generally study same metal powder/substrate pairs [74, 144], so it is difficult to define a critical velocity required for metal deposition onto CFRP. Nevertheless, by taking the critical velocity of metals on metals and the maximal advisable impact energy for polymeric substrates [31], it is possible to establish a relation between the velocity of the particle and a desirable particle size to obtain deformation of the powder, and therefore deposition. Morphology can vary to affect the velocity of the powders in flight and density is immutable to the material considered, so only the diameter of the powder could be reasonably modified.

From Eq. 1, $E_c = \frac{1}{2}$ x ρ x $\frac{4}{3}\pi r_p^3$ x v_{crit}^2, or $E_c = \frac{1}{2}$ x $\frac{4}{3}\pi \frac{d_p^3}{8}$ x ρ x v_{crit}^2, we can obtain Eq. 6:

$$\textbf{Eq. 6} \quad \boldsymbol{d_p = \sqrt[3]{\frac{12 \text{ x } E_c}{\pi \text{ x } \rho \text{ x } v_{crit}^2}}}$$

where d_p is the diameter of the particle and v_{crit} is its critical velocity. The critical velocity varies as a function of the particle size, but given recent empirical results [163], it seems that the critical velocity of several materials (Al, Ni, Cu, Zn) only varies by 10-30m/s for particle sizes ranging from 14 to 30 µm. Therefore, a first order assumption would be to assume that the critical velocity varies slightly for a varying particle size, and so the critical velocity is considered as a constant. By taking $E_c = 2 * 10^{-6} J$ as a kinetic energy limit for deposition [31], theoretical particle size limitations can be calculated, as presented in Table 5-6.

This table shows the difficulty to spray most powders on CFRP as most particles would need to be relatively small (below 15 µm, while cold spray uses powders generally between 5 and 50 µm). This could provide some level of difficulty to address as smaller powders are generally not desired: they are presumed to be greatly affected by the bow shock that appears in the gas flow, which leads them to being slower than would be expected [128, 129]. The results from Table 5-6 also shows that Sn is relatively easier to spray with a more flexible particle size. Also, the varying critical velocity between references has a limited effect on the indicated diameters, as can be seen with copper (50 m/s difference between both references, and only 1um limit differences for the maximum powder diameter for deposition), which supports the assumption that the variation of critical velocity with particle size that should be accounted for can be deemed minimal in front of the overall limitation on particle sizes.

Table 5-6: *Theoretical maximal powder diameters for deposition on CFRP with a maximal kinetic energy of* $E_c = 2 * 10^{-6} J$*, based on critical velocities from the literature [144, 163].*

Hardness close to CFRP hardness	Powder	Density	Critical velocity (for particles around 25 µm)	Maximum Powder Diameter for Deposition
		g/cm3	m/s	µm
Yes	Sn	7.29	180 [144]	32
	Pb	11.35	130 [144]	34
	Cu	8.96	553 [163]	14
			500 [144]	15
	Al	2.70	800 [163]	16
			660 [144]	19
	Zn	7.10	520 [163]	16
			380 [144]	20
No	Fe	7.87	700 [144]	14
	SS316L	8.00	750 [144]	13
	Ti	4.50	800 [144]	12

Results in the literature support smaller particle sizes for deposition, as shown in the works of Gillet et al. [36], where differently sized Cu powders were cold sprayed onto CFRP substrates. The fine powder of their work led to the deposition of Cu onto the CFRP, with indicated impact energies of $3.9.10^{-7}$ J, whereas the medium and large powders had impact energies of 10 or 100 times greater, which led to cratering and erosive behavior [36]. The works of Affi et al. [21] explored the cold spraying of small Al particles (15 μm) on a CFRP substrate, but this only resulted in erosion of the substrate: no indication of particle velocity was recorded here, so it is possible that energy (i.e. velocity) of the particles was too high for deposition, or the proportion of powders above the maximum powder size (Table 5-6) was too large. In a second experiment of the same study, they also sprayed smaller Al particles (3 μm) to account for the energetic limitation advanced by Lupoi and O'Neill [31], and were able to obtain thin coatings [21].

It should be noted that this discussion only considers deposition and does not address the condition of the coatings (the deposited coatings were not optimal as porosity persisted [36] or peeling occurred [21]), nor does it address other improvement techniques such as interlayer deposition [21] or spraying in multiple steps [36]. Typically, in the second part of their work, Gillet et al. [36] sprayed fine powders after having sprayed the medium or large powders and obtained growing coatings, which may be due to roughening provided by the medium or large powders.

The initial observation that no peeling occurred while cutting the samples from this study may indicate a difference in mechanical properties of these coatings as compared to those of the coatings with SC Al/Al alloy in [250]; therefore a follow-up study on coating properties will be considered to fully assess the effect the SC properties on the coating properties such as adhesion strength, and not only on the deposition as was the case here.

5.8 Conclusions

Tin was mixed in 90:10 weight ratio with various secondary components that covered a wider spread of hardness, density, morphology and median sizes than previous studies concerning cold spray of mixed powders on to CFRPs. These mixtures were cold sprayed with a CenterLine

low-pressure cold spray system, onto thermosetting epoxy-CFRP substrates with varying surface finishes, a thermoplastic PEEK-CFRP and mild steel substrates. The secondary components of this study offered varying degrees of improvement as compared to what had previously been observed, and the effect of secondary component properties on the overall deposition efficiency, and effective deposition efficiencies of pure tin and of the secondary component, were discussed:

- The results confirm the ideal hardness range that was identified in the previous study with secondary component Al and Al alloys, and that would be within the hardness range of the substrates.
- Morphology of the secondary component was confirmed to have a significant role in the retention of the secondary component in the coating, and while spherical morphologies generally lead to increased overall deposition, more irregular morphologies would often lead to a decrease.
- The SC density, morphology and median particle size do not seem to reveal a specific trend on their own, but the SC impact energy seems to be a key factor in the improvement of Sn deposition on CFRP. Most notably, while SC with low hardness and low impact energy seem to provide the greatest improvement for pure Sn deposition, SC with higher impact energy lead to erosion, and SC with higher hardness lead to decreased pure Sn DE.

Based on this study and on previous work, it was possible to provide insight into the key conditions for deposition of Sn on CFRP with mixed powders. Furthermore, by extending the observations on SC to single component powders, limitations on powder hardness and impact energy were discussed for deposition of metals onto CFRP: these conditions seem to rest on smaller particle sizes for particles with higher critical velocities. The properties of such directly deposited coatings may not be ideal, and future work will focus on studying adhesion of the mixed-powder coatings, versus the deposition of these powders.

5.9 Acknowledgments

The authors wish to acknowledge the financial support of the Natural Sciences and Engineering Research Council of Canada (NSERC) through the Green-SEAM strategic network and the McGill Engineering Doctoral Award (MEDA). The industrial partners, Bombardier

Aerospace and Tencate (through Pratt and Whitney Canada) are gratefully acknowledged. Mr. Kévin Bricault from National Research Council Canada, Boucherville, is acknowledged for his contribution to the cold spray experiments.

Chapter 6

Pull-off Testing and Electrical Conductivity of Sn-based Metal Powder Mixtures Cold Sprayed on Carbon Fiber Reinforced Polymers

6.1 Rationale

The previous chapters focused on deposition of tin on to CFRP, and the effect of the secondary component (SC) in the deposition process, it appeared that the SC hardness and impact energies were metrics of interest for improving the deposition of tin. While deposition is required to obtain coatings on substrates, it is also important to study the properties of these coatings, as it may better assist in understanding the adhesion of the metallic coatings to the polymeric substrates. Furthermore, these properties may also provide some insight into potential applications for these coatings. Therefore, in this chapter, the pull off strengths and electrical conductivities over the previously cold sprayed coatings were assessed.

This chapter has been submitted to the Journal of Thermal Spray Technology as :

Andre C. Liberati, Hanqing Che, Panteha Fallah, Phuong Vo, Stephen Yue, *"Pull-off Testing and Electrical Conductivity of Sn-based Metal Powder Mixtures Cold Sprayed on Carbon Fiber Reinforced Polymers"*, Journal of Thermal Spray Technology (2022) (Submitted)

6.2 Abstract

Tin was successfully cold sprayed onto carbon fiber reinforced polymers (CFRPs) in previous studies at McGill University and a "crack-filling" mechanism was described as the mechanism that allowed deposition of the metal onto the composite counterpart. By adding other metal powders (aluminum, copper, zinc), it was possible to improve the deposition efficiency (DE) of the tin on the CFRP, as well as improve the electrical conductivity of the coating (notably with copper). While the effect of mixing powders with tin, and more notably the effect of the secondary component (SC) properties on the deposition improvement, were more thoroughly addressed in

following studies, the question of the properties of these coatings remained. With the perspective of providing a metallic coating to a relatively poorly conductive composite substrate, this study aims to explore the electrical conductivity and the coating strength of cold sprayed tin with other SCs onto CFRPs. An extensive study fractured surfaces highlighted the importance of the CFRP surface finish, and it was observed that the coating strengths improved with decreasing DE of pure tin.

6.3 Introduction

"Metallizing", or applying metallic coatings onto polymeric substrates, has generated much interest in the past decades [1, 3], notably within the aerospace industry. Carbon fiber reinforced polymers (CFRPs) are a material of choice for their high strength-to-weight ratios, but on the downside, the carbons fibers and epoxy resins that compose this structure are respectively 1 000 and 1 000 000 more resistive than aluminum [56], thus limiting their use. As a result, there has been growing interest to develop metallized polymers and polymeric composites for structural applications [1, 5]. Different technologies have been explored, such as vacuum deposition techniques [8, 9], but these methods are limited by their inability to develop thick metal coatings (over 100 µm) [10]. Lay-up molding [147], wire-arc spray [11-13, 255], flame spray [15] or air plasma spray [17, 18] have also been considered, but these techniques require high levels of thermal energy that could lead to the accumulation of residual stresses [64], oxidation of the metallic powder as well as heat damage to the substrate [21].

Cold spraying is a solid state thermal spray process, where powder particles are accelerated by a supersonic gas jet and form a coating through plastic deformation upon impact with a substrate [19]. Since it uses relatively low temperatures (several hundred degrees versus several thousand degrees for other thermal spray techniques [20]), cold spray can avoid the typical issues brought by other thermal spray techniques, and positions itself as a legitimate metallization approach for polymeric substrates. While cold spraying metallic powders onto metallic substrates has been extensively explored and has provided promising results and applications [99, 117], cold spraying metallic powders onto polymeric substrates has provided more mixed results, mostly due to substrate erosion [25, 26, 28, 111]. In recent years, researchers have encountered some success in

metallizing polymeric substrates via cold spray with a variety of metals such as tin [28-31], iron [29], 316L stainless steel [32, 33], AlSi10Mg [33-35], copper [28, 29, 31, 36-38], aluminum [38] or titanium [233]. On the downside, generally reported issues included substrate damage [28, 31], relatively low deposition efficiencies (DEs) (i.e. the ratio of effectively deposited particles on the substrate versus the amount of sprayed particles) [29, 31, 32, 34], or delamination issues [36-38].

Several studies have tried to explain metal deposition mechanisms on polymeric substrates. In one of the earlier studies, Lupoi and O'Neill [31] noted a correlation between particle impact energy and deposition of metallic powders : elements such as copper would lead to erosion of the substrate due to high impact energies, while soft elements such as tin and lead could deposit with some success. Ganesan et al. [26] suggested that soft powders such as tin had the possibility to deform upon impact favoring mechanical anchoring, while harder particles such as copper could not. Che et al. [28] introduced a ''crack filling'' mechanism, where it was hypothesized that thermally softened or partially melted tin particles impact the substrate and, while the harder core of the particle generates microcracks in the surface epoxy, the molten part of the tin would be squeezed into these cracks and provide mechanical interlocking with the substrate. When describing the overall deposition process of metals onto polymeric substrates, they also advanced the importance of differentiating the process into two separate phases: the first-layer deposition phase (occurring between impinging metallic powders and the polymeric substrate) and the build-up phase (occurring between metallic powders and previously deposited metal powders) [29].

In the other cold spray work, several research groups studied enhancement effects relating to the mixing of ceramic powders with metal feedstock powders: these enhancements concerned improvements in the deposition process (increased DE, decreased porosity), but also improvement of coating properties (hardness, adhesion strength between the coating and the substrate) [39-41]. This led to establishing an in-situ shot peening cold spray deposition process, where the same improvements are obtained through the addition of large stainless steel particles (200-300 μm) [132, 217, 218]. Recently, Fernandez and Jodoin [42, 43] conducted an extensive study on potential mechanisms of improvement and explained that the coating deposition improvement is due to surface roughening by the secondary component (SC) through generation of asperities and

oxide removal, while the coating property improvements are related to generation of oxide clean surfaces and peening of the SC. When exploring the deposition of metals onto polymeric substrates with mixed metal powders, Che et al. [44] made similar observations relating to coating deposition improvement when spraying tin powders with SC such as zinc or copper, and this improvement was associated with the shot-peening effect of the SC on the relatively softer tin. Nevertheless, in recent work at McGill University [250], evidence appeared that the shot-peening effect may not be an effective mechanism when cold spraying tin mixed with metallic powders. In a follow-up study [256] the correlation between various SC properties was explored and the deposition improvement was associated with a suitable SC hardness range, as well as a suitable SC impact energy. Nevertheless, these studies [250, 256] were mainly focused on deposition mechanisms and only briefly touched on adhesion of the coatings with the substrates.

As a matter of fact, a review of literature for cold sprayed coatings on CFRP substrates reveals that few studies have considered adhesion strengths. This may principally be explained by the difficulty to obtained full coatings on CFRP [29, 31, 32, 34] and/or to delamination issues before being able to conduct adhesion tests [36-38], but it may also be explained by the relative novelty of using the cold spray process to metallize polymeric substrates with most studies being quite recent [6, 28-30, 32-34, 36-38, 44, 45, 147, 246, 250, 256, 257], thus confirming the research community is still in the early stages of understanding how this process can be carried out efficiently. From the few studies that did report results, adhesion strengths were generally quite low. Che et al. [28] reported adhesion strengths as high as 7.6 MPa for a tin coating cold sprayed on an epoxy CFRP. Other thermal spray results with other polymeric substrates can provide some reference as well. While cold spraying copper onto a polyvinyl chloride (PVC) substrate, Ganesan et al. [111] obtained shear adhesion strengths below 3 MPa, then in another study [27], they projected copper on CFRP with an atmospheric plasma spray system and recorded adhesion strengths of up to 5.4 MPa (with a tin interlayer). Małachowska et al. [232] observed similar adhesion strengths (3.6MPa) with a low pressure cold sprayed copper on polyamide 6 substrates, as well as Zhou et al. [113] with aluminum coatings cold sprayed onto a PEEK-CFRP. Rezzoug et al. [255] recorded some better results when adding various CFRP interlayers before depositing zinc via wire-arc spray (up to 7 MPa): the effect of the interlayer greatly affected the adhesion strength. More recently, Che et al. [257] obtained some of the highest recorded strengths with cold

sprayed SnBi on the thermoplastic acrylonitrile butadiene styrene (ABS) (14.5 MPa versus 6.8 MPa for pure tin).

With the perspective of developing suitable coatings for potential applications in the aerospace industry, or any other field that could require polymeric substrates with thick coatings (> 100 µm), it is essential to determine the properties of cold sprayed metallic coatings and understand inherent mechanisms that could lead towards developing a usable process. As the cold spraying of tin mixed with metallic SC powders allowed a further understanding of deposition of coatings on CFRP [250, 256], this study aims to assess the effects of these SC on some coating properties (pull off strength and electrical conductivity) and understand how the SC may impact the adhesion of a tin coating to the CFRP.

In this study, the properties of coatings from previous studies [250, 256] are investigated. These coatings were obtained by cold spraying tin mixed with various SCs on several CFRP substrates and mild steel substrates. The choice of SC was made to cover a wide range of SC properties (hardness, density, morphology, median particle size, and by extension impact energy), as described in [256]. In both studies [250, 256], tin and tin-SC mixed powders with 90:10 weight ratio are cold sprayed with a low-pressure cold spray system, onto thermosetting epoxy-CFRP substrates with varying surface finishes, a thermoplastic Polyether-Ether-Ketone (PEEK)-CFRP and mild steel substrates. In this way, variability in the properties originating from the powder mixture and/or from the substrate may be observed. Pull off strength and electrical conductivity were then evaluated, and relations between coating properties, SC and substrates was established.

6.4 Experimental Methods

6.4.1 Materials and cold spray conditions

The feedstock materials considered in this work were described and sprayed in previous studies [250, 256]: they are summarized in Table 6-1. These powders were chosen to cover a variety of material properties (namely density and hardness), with a variety of morphologies and

Table 6-1: *Properties of the feedstock powders considered in this work.*

Ref.	Powder	Morphology	Supplier	D_{50} (μm)	Hardness ($HV_{0.01}$)	Density ($g.cm^{-3}$)	Average kinetic energy (J) [256]
[250]	Sn	Spheroidal	CenterLine	12	7±1	7.29	$2.28.10^{-6}$
	Al	Spherical	Valimet	23	24±2	2.70	$2.09.10^{-6}$
	Al5083	Spherical	Valimet	17	66±11	2.66	$1.62.10^{-6}$
	Al6061	Spherical	Valimet	23	72±8	2.70	$2.62.10^{-6}$
	Al7075	Spherical	Valimet	20	118±23	2.81	$1.96.10^{-6}$
[256]	Sn	Spheroidal	CenterLine	13	8±1	7.29	$1.32.10^{-6}$
	Cu	Mixed	Giken	30	68±7	8.96	$5.19.10^{-6}$
	Cu-IR	Dendritic	CenterLine	33	32±4	8.96	$6.88.10^{-6}$
	Fe	Mixed/IR	Goodfellow	37	89±14	7.87	$7.30.10^{-6}$
	SS316L	Spherical	Sandvik	23	215±26	8.00	$2.84.10^{-6}$
	Ti-SP	Spherical	Raymor (AP&C)	20	196±22	4.50	$1.58.10^{-6}$
	Ti-AG	Angular	Cerac	30	178±34	4.50	$4.36.10^{-6}$
	Ti6Al4V	Spherical	Raymor (AP&C)	37	340±14	4.43	$4.56.10^{-6}$

particle sizes. Powders from several studies at McGill University [44, 123, 131, 221] were chosen to offer a meaningful spread for each property. As such, the selection was made from aluminium/aluminium alloy powders from the paper [250], copper powders from studies by Che et al. [28, 44], iron and stainless steel 316L powders from studies by Chu et al. [131, 219] and titanium/Ti6Al4V powders from studies by Wong et al. [123]. The properties were observed between 2.66 and 8.96 $g.cm^{-3}$ for density, 7 and 340 HV for hardness, 12 and 37 μm for median particle size (D_{50}); for the given process variables, the impact energy was between $1.32.10^{-6}$ J and $7.30.10^{-6}$ J. The characterization of the powder hardness, median particle size and average impact energy was described in [256].

The substrates used in this work were epoxy-CFRPs provided by Bombardier Aerospace (Montreal, Canada), Polyether-Ether-Ketone (PEEK)-CFRPs provided by TenCate (Netherlands) and 1020 mild steel plates. The steel substrates were used as a benchmark to compare the spraying

of powders on CFRPs to a typical metal–metal cold spraying situation and are not further studied here. Top surface images of the CFRP substrates were presented elsewhere (Fig. 2 [250]).

The epoxy-CFRPs (abbreviated as e-CFRP) used here consists of a thermosetting epoxy matrix with continuous carbon fiber reinforcements. The e-CFRP panels were made of four plies of epoxy/carbon fiber prepreg ($[0/90]_{2s}$) and have the following coating finishes used by the manufacturer: a bare finish, a putty finish, and a surface film. The bare finish e-CFRP is the as-manufactured material, the putty e-CFRP is a surface filled with a pinhole filler and surfacer to produce defect-free surfaces and the surface film e-CFRP includes a neat epoxy resin film with an embedded veil, normally a mat, at the top surface (to help handle the resin film). The cross-section of these substrates was observed using a Light Optical Microscope (LOM) and are presented in Fig. 6-1 a-c. The bare e-CFRP (Fig. 6-1 a) and putty e-CFRP (Fig. 6-1 b) appear similar in

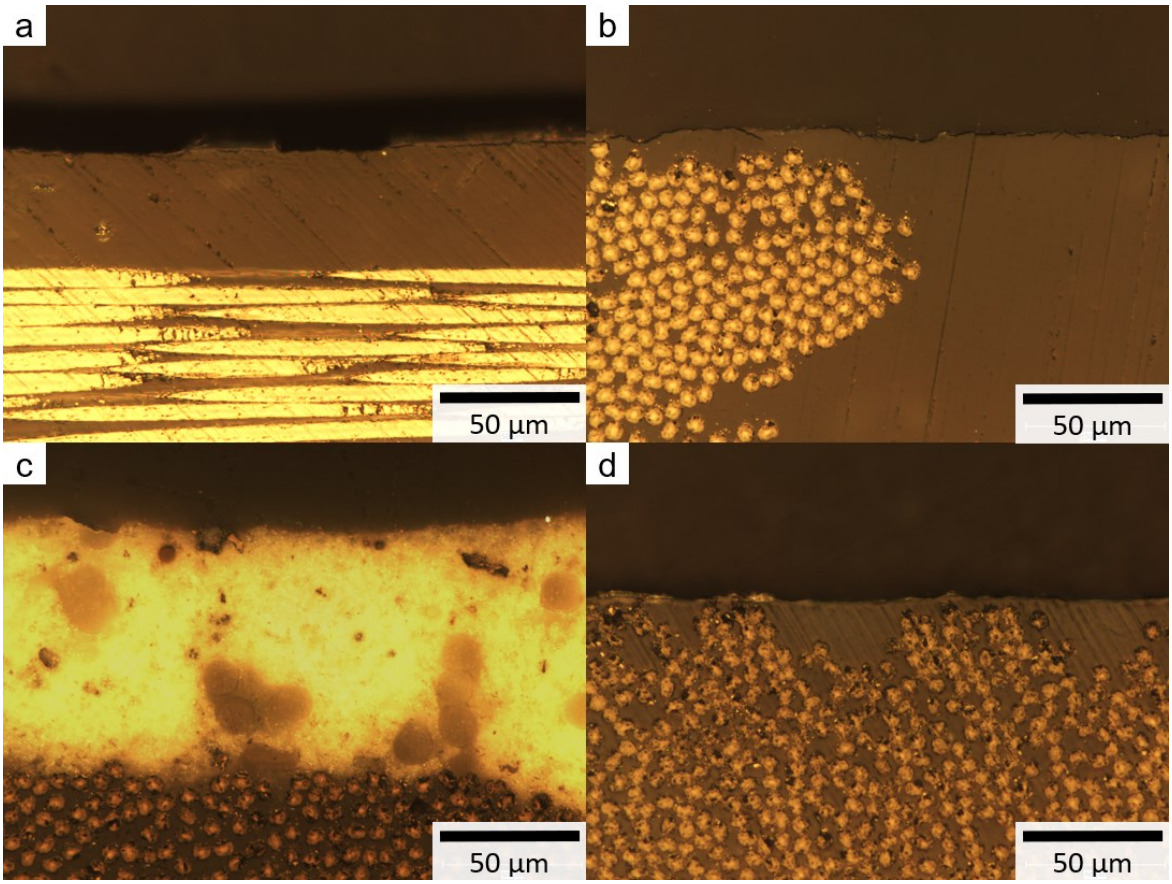

Fig. 6-1: *Optical images of the substrate cross-sections, near the top-surface: a) bare e-CFRP, b) putty e-CFRP, c) surface film e-CFRP, d) PEEK-CFRP.*

structure, with areas rich in carbon fibers close to the top surface, and others rich in polymer close to the surface: the thickness of the putty is unclear though. Profilometric data was acquired for the raw substrates on areas of 3mm x 3mm as shown in Fig. 6-2 (methodology presented in next section), and the bare e-CFRP surface presents a rough, ridged surface (Sa = 4.6µm, Fig. 6-2 a) while the putty e-CFRP presents a smoother surface with fine inter-crossing curves (Sa = 1.3µm, Fig. 6-2 b). The surface film e-CFRP (Fig. 6-1 c) presents a different cross-sectional profile with the top layer being notably different from the underlying CFRP material. While having a different top-surface appearance than the putty e-CFRP (Fig. 2 of [250]), these two substrates actual have similar surface textures and roughness values (Sa = 1.6 µm, Fig. 6-2 c): as both surface finishes are destined to provide a smooth surface, the structure of inter-crossing curves may be associated to the processing step that smooths the surface. The hardness of these substrates was measured, and the values were 39±8 $HV_{0.01}$ for the bare e-CFRP, 51±15 $HV_{0.01}$ for the putty e-CFRP and 40±13 $HV_{0.01}$ for the surface film e-CFRP.

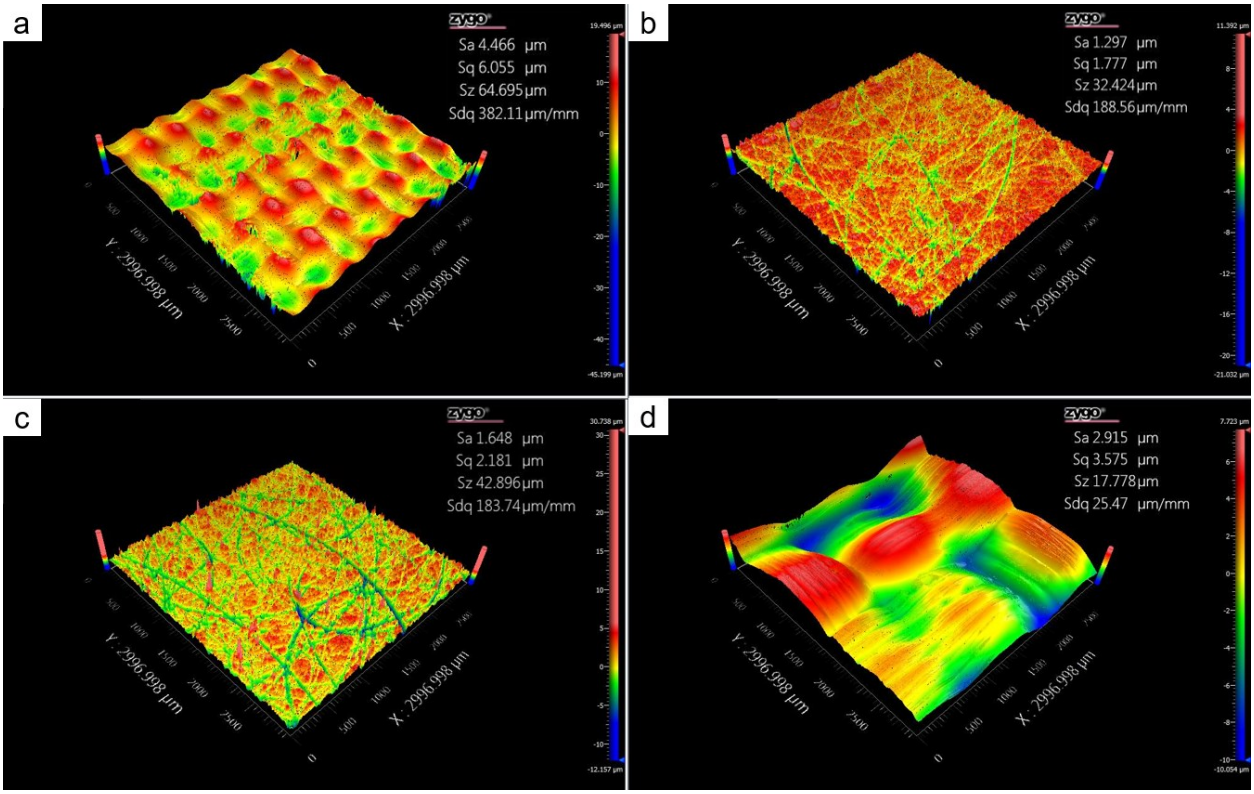

Fig. 6-2: *Height profiles of the as-received substrates at 2,75x: a) bare e-CFRP, b) putty e-CFRP, c) surface film e-CFRP, d) PEEK-CFRP.*

The PEEK-CFRP used here consists of a thermoplastic polyether-ether-ketone matrix with continuous carbon fiber reinforcements. These panels were made of five plies of PEEK/carbon fiber ($[(0,90)_2/(0,90)_{3R}]$). The cross-section of this substrate is presented in Fig. 6-1 d. Its structure is fairly similar to that of the bare e-CFRP (Fig. 6-1 a) in such that the substrate has an as-manufactured finish, with areas where the carbon fibers are close to the top surface, versus other areas were the polymer is close to the surface, as well as a ridged surface, presumably with intertwining carbon fiber structures, as seen in Fig. 6-2 d: the roughness of this substrate is measured at 2.9 µm). The hardness of this substrate was differentiated between areas showing superficially pure PEEK areas, and superficially predominant carbon fiber areas. The respective hardness values for each area are 26±3 $HV_{0.01}$ and 63±22 $HV_{0.01}$.

Sheet sections of dimensions 7 x 7 cm were used as substrates during the cold spray campaigns. The substrates were degreased with ethanol, and the mild steel plates were grit-blasted with 24 grit alumina before cold spraying. The CFRP substrates were not grit-blasted as it would result in the erosion of the substrate.

The cold spraying was performed at the McGill-NRC cold spray facility at National Research Council Canada in Boucherville and was also presented in previous studies [250, 256]. The cold spraying was performed at low pressure with a commercially available CenterLine SST SSM-P3300 system (Supersonic Spray Technologies, CenterLine Windsor Limited, Canada). Pure tin powder, or powder mixtures with 90% tin and 10% of each SC powder, were cold sprayed onto each substrate with gas conditions of 310°C and 60 psi (0.41 MPa). These parameters were chosen based on previously successful cold spray campaigns with tin [28, 30, 44, 246, 250, 256, 257]; at the selected conditions, melting was observed in previous work [28, 30, 44, 246, 257]. A comparison between cold spraying pure tin and the powder mixtures with SCs of varying properties was thus possible, on a variety of CFRP substrates. The carrier gas was nitrogen, the standoff distance was 18 mm, the step size was 1 mm with 38 steps, and the gun travel speed was 25 mm/s. The powder feeder rate was between 9.9 and 16.9 g/min, measured every three sprays to accurately assess the variation. The substrates were pre-heated by operating a single pass, without powder injection. Then, only one pass was sprayed for each set of conditions, so that the results

provided from spraying on a large area, together with a study focused more on the behavior of the process than the numerical results, would be meaningful. All the substrates were aligned and sprayed at the same time for one condition, so that any external variation (e.g. feeding, temperature effects) may be neglected.

6.4.2 Coating properties and characterization

The pull off strength was measured by means of pull-off tests performed on all tin and tin-SC coated CFRP samples. The testing was modified based on the ASTM C-633-01 standard and required cutting the cold sprayed samples (Delta Abrasimet, Buehler, Illinois, USA) into specimens measuring approximately 1.5 x 1.5 cm^2. This approach was chosen given the relative difficulty to produce circular CFRP substrates. The coating surfaces were slightly ground in order to remove loose particles from the cold spray process, and then these surfaces were glued to another Al6061 cylinder with a room temperature curing adhesive. The substrate surfaces were also glued to pre-ground Al6061 cylinders. The pull off tests were performed using an MTS hydraulic pressure machine at a constant crosshead speed of 1.0 mm/min. For each coating, three tests were performed, and the average strength was taken. The glue strength was determined as the average strength for which coatings would not peel from the substrate and breaking of the glue would occur: this value was found to be around 13MPa. This would also indicate that coatings with indicated strengths above 13 MPa may actually be higher due to the glue breaking.

The samples were then taken, and the fracture surfaces were characterized with a Keyence (Japan) digital microscope and a Hitachi (Japan) SU3500 scanning electron microscope. A 3D optical surface profiler (ZYGO, Connecticut, USA) was also used to measure the surface roughness and support large-scale microstructural observations. The lateral resolution of the objectives used is below 2 µm. The main measurements were taken around the roughness Sa, the peak-to-valley height Sz and the root mean square gradient of the surface Sdq as they provide insight into the topography of the surfaces regarding not only height but also gradient [243, 244]. More specifically, Sdq is affected both by texture amplitude and spacing; therefore, Sdq can provide information on the slopes which comprise the surface in the case of coatings with similar

values of Sa [243]. This metric was successfully used to correlate surface changes in another study [246].

The electrical conductivity measurements were conducted at École Polytechnique de Montréal (Montréal, Québec, Canada) by using the four-point resistivity/conductivity measurement method. Essentially, this method involves aligning four sharp probes on a flat surface of the material to be considered, and while current is passed through the two outer electrodes, the potential is measured across the inner pair of electrodes [258]. From there, resistivity/conductivity of the coatings can be calculated with correction factors taking into account sample geometry and probe distancing [258, 259]. Further detail regarding this testing method is given in [258] and [259]. Before the measurements, the as-sprayed top surfaces were slightly ground to remove loose particles and obtain flat surfaces for measurement. For each sample, the measurements were taken at three different locations, and the average value was taken. The linearity of the conductivity was verified by taking measurements at 100mA and 50mA.

6.5 Results

6.5.1 Pull off test results

The pull off strength of the various deposited coatings from [250] and [256] are presented in Fig. 6-3: the glue adhesion strength was determined to be 13 MPa and is indicated on each graph for reference. The results vary notably between both studies (cf. Sn [250] and Sn [256]) presumably due to powder differences (e.g. oxide content), so it is important to observe the effects of the SC as compared to their respective pure Sn coatings. During the pull-off test, the coatings mostly peeled at the interface and presented adhesive failure. In some instances, mixed cohesive/adhesive failure was observed and areas with Sn could be observed on the substrate surface.

On the bare e-CFRP, the pull-off tests either led to failure of the coating at the substrate interface (with SC Al/Al alloys, Cu, Cu-IR) or the glue failed before peeling of the coating occurred (with SC Fe, SS316L, Ti-SP, Ti-AG, Ti6Al4V) (Fig. 6-3 a). For the coatings deposited in the first study [250], the addition of Al or Al alloys to Sn led to a decrease of the coating pull off strength by 2 to 5 times that of single component Sn (from 7.9 MPa to 1.7-4.4MPa). For the

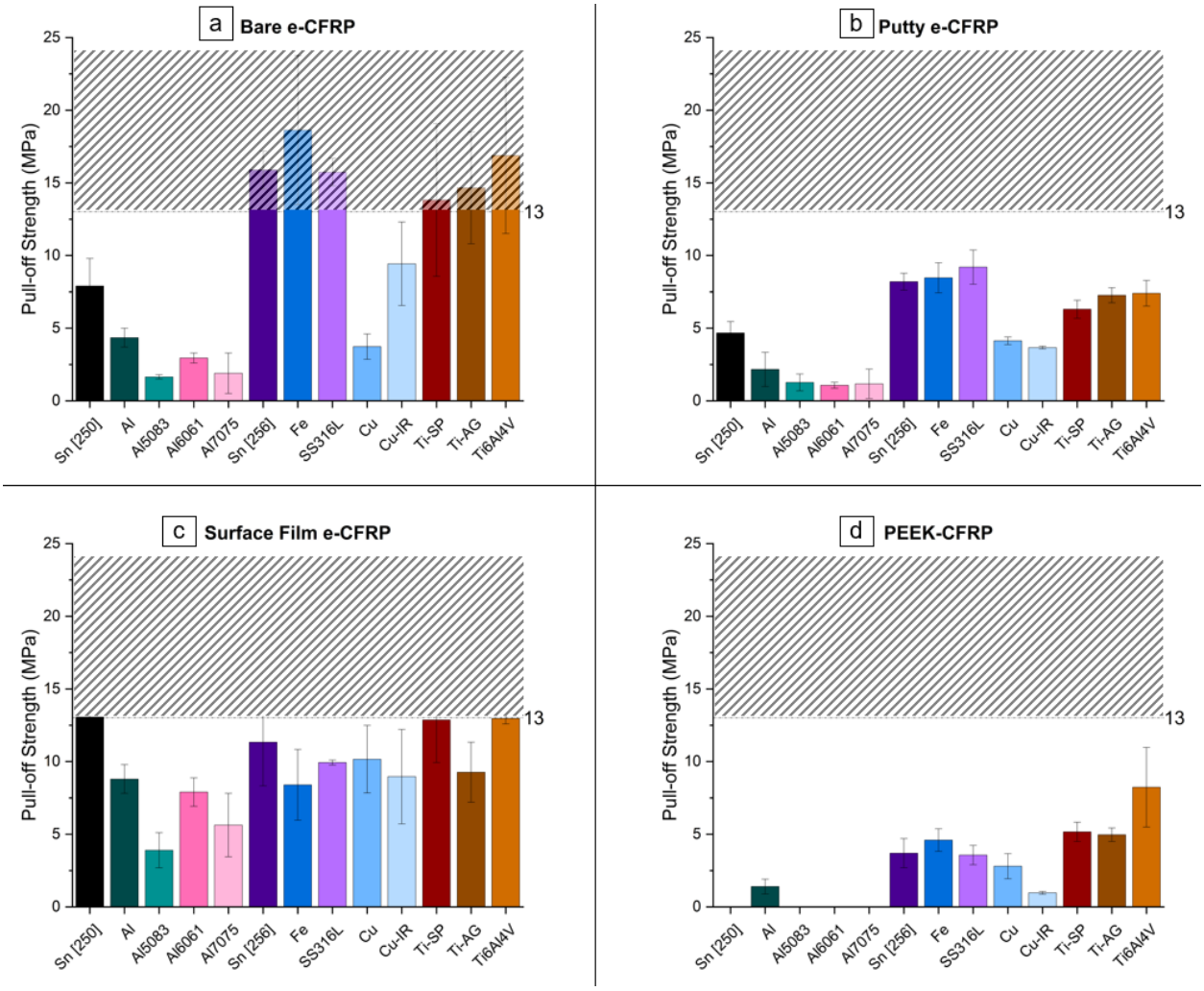

Fig. 6-3: *Pull-off strength of the Sn and Sn-SC powder mixtures on the various CFRP substrates: a) bare e-CFRP, b) putty e-CFRP, c) surface film e-CFRP, d) PEEK-CFRP. The values provided are the average of three measurements and values above 13 MPa are representative of the glue failure.*

Sn deposited on the bare e-CFRP in the second study [256], notably better strengths were obtained (coatings mostly did not peel). The addition of Fe, SS316L or any of the Ti/Ti6Al4V powders did not noticeably decrease the strength of the Sn on the bare e-CFRP, as all strengths remained above 13MPa: these results are actually higher than those reported in the literature for metallic coatings deposited onto polymeric substrates [27, 28, 111, 113, 232, 255, 257]. On the other hand, the addition of Cu, and, to a lesser extent, Cu-IR, led to lower strengths compared to the pure Sn coating that did not peel (respectively, 3.7MPa and 9.4MPa).

A similar graph profile may be observed between the bare e-CFRP and putty e-CFRP for the pull off strength of the cold sprayed coatings (Fig. 6-3 b). One notable difference is that strengths were generally lower for the putty e-CFRP and that glue failure never occurred (strengths < 10MPa). As with the bare e-CFRP, the addition of Al and Al alloys to Sn resulted in lower strengths as compared to the Sn coating sprayed in [250] (from 4.7MPa to 1.1-2.2MPa). The Sn coatings sprayed in the second study [256] showed an average strength of 8.2MPa on the putty e-CFRP. The addition of Fe/SS316L slightly increased that value (8.5MPa and 9.2MPa respectively), while the addition of Ti-SP, Ti-AG and Ti6Al4V led to slight decreases (6.3-7.4MPa). For this substrate, the addition of Cu and Cu-IR had the effect of reducing the strength by more than half (3.7-4.1MPa).

The pull-off strengths on the surface film e-CFRP (Fig. 6-3 c) showed a very different profile compared to the other e-CFRP substrates, as the coatings provided overall better strengths with an average of 9.5MPa across all the sprayed powders. The Sn coatings from the first study [250] had a strength of 13.1MPa and while the addition of Al/Al alloys again led to a decrease in pull off strength, this decrease was quite uneven with Al5083 providing the lowest strength (3.9MPa), while Al provided a strength of 8.8MPa. For coatings in the second study [256], strengths were above 8.4 MPa, with some notable variation (standard deviation above 2MPa for most powders). In this situation, and given the indicated errors, there does not seem to be noticeable variation of the pull off strength when adding the various SC, apart from Ti6Al4V that produces a coating with a high strength of 13.0MPa.

The pull off strength on the PEEK-CFRP provided the lowest strengths of this study (Fig. 6-3 d). When adding Al alloys to feedstock Sn powder [250], peeling was an issue during sample preparation, which made it impossible to measure an effective strength for these coatings (except for Al). For the coatings sprayed in the second study [256], there were no issues of peeling during sample preparation, and strengths were observed to be between 2.8MPa and 5.2MPa for most coatings. Two noticeable results appeared here with Cu-IR providing relatively lower strength (1.0MPa), while Ti6Al4V provided relatively higher strength (8.2MPa).

6.5.2 Characterization of fracture surfaces

6.5.2.1 Bare e-CFRP

Images of tested coatings on bare e-CFRP substrate are presented in Fig. 6-4. An example of the substrate side of the fracture is presented in Fig. 6-4. a, and several areas of interest can be noted. In the middle of the image, lines can be seen on the surface and are representative of carbon fibres near the surface. The epoxy appears to be roughened all over the surface. The light grey regions spread throughout the substrate are remnants of tin still bonded with the substrate after peeling of the coating. These tin remnants were generally more frequently found in areas with visible carbon fibers. When conducting SEM of the substrate side, exposure of the carbon fibers did not appear clearly but some carbon fibers were nevertheless observed, as shown by the linear

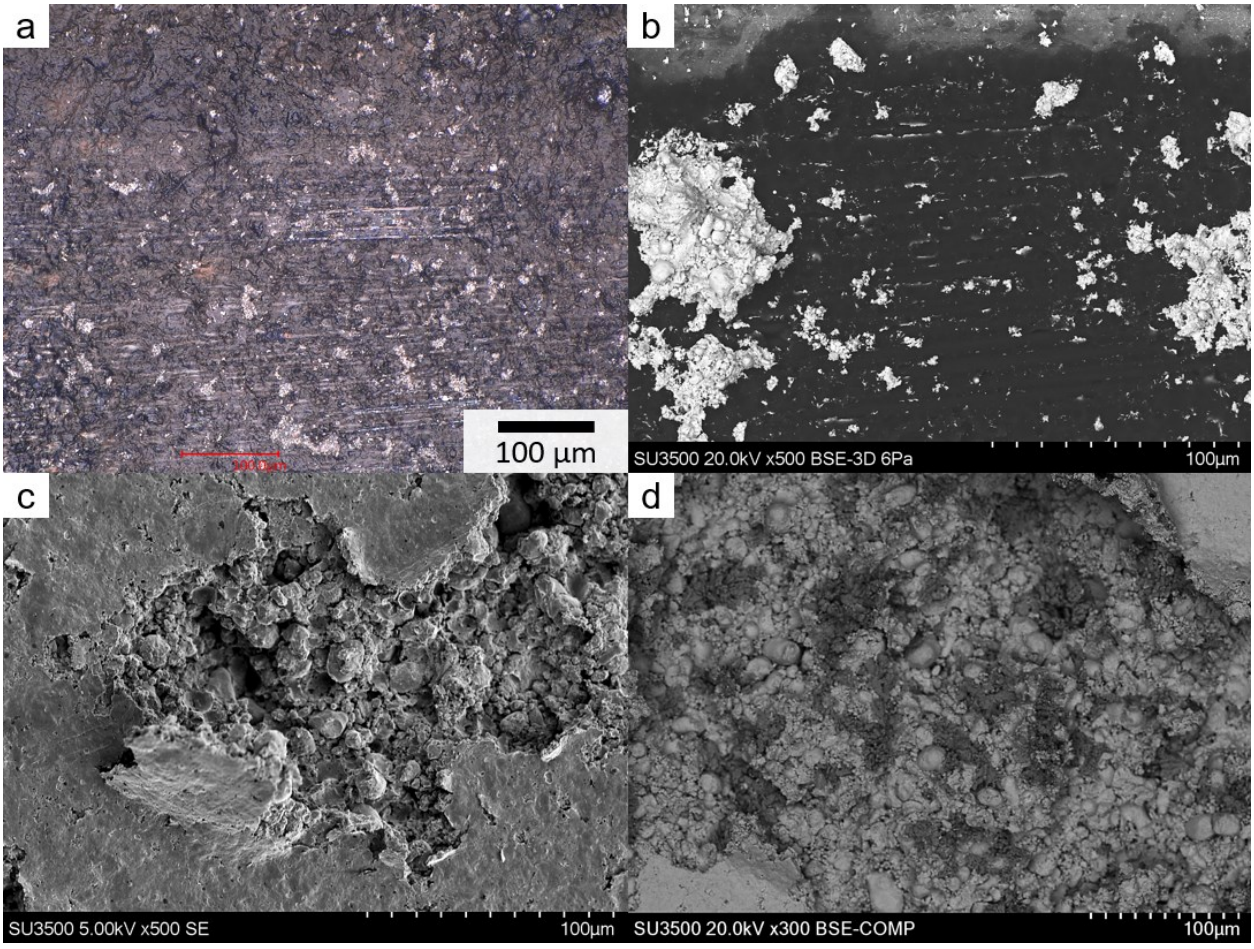

Fig. 6-4: *a) Keyence digital microscope image of the substrate side of a tested Sn-10Cu coating on bare e-CFRP. b) SEM image of the substrate side of a tested Sn-10Cu-IR coating on bare e-CFRP. c) SEM image of the coating side of a tested Sn-10Al5083 coating on bare e-CFRP, that showed mixed cohesive/adhesive failure. d) SEM BSE-COMP image of the coating side of a tested Sn-10Cu-IR coating on bare e-CFRP, that showed mostly cohesive failure: the darker contrast is Cu-IR.*

structures in the middle of Fig. 6-4 b. Around these areas, accumulations of tin powders were also noted: some powder-like shapes could be observed, but a general structure in these mounds was unclear. Furthermore, linear tin structures could be observed around the carbon fibers. When observing the coating side (Fig. 6-4 c), several other structures were observed: around the edge of the image, a flat tin surface corresponding to the interface of the coating/substrate was observed, while in the center of the image, the interior of the coating could be observed with apparent powder-like structures. When using SC Cu-IR, more mounds of tin were observed on the substrate, and larger areas of the interior of the coating could be observed. In BSE images of the coating side, a high proportion of darker contrast particles could be observed: these are Cu-IR particles as copper has a lower atomic number than tin and therefore generates darker contrasts (Fig. 6-4 d).

6.5.2.2 Putty e-CFRP

Images of tested coatings on putty e-CFRP substrate are presented in Fig. 6-5 and Fig. 6-6. An example of the substrate side of the fracture is presented in Fig. 6-5 a, and striated structures, attributed to the carbon fibers of the substrate, are visible. An example of coating cross-section before testing is presented in Fig. 6-5 b, and bonding of tin around the carbon fibers (circular structures of the lower half) can be noted before the test was conducted. In Fig. 6-6 a, the substrate side of the tested coating shows a homogeneous linear structure that is the carbon fibers of the substrate. The top and bottom edges of this image reveal a dark structure that covers the carbon fibers, and this is the epoxy polymer. Finally, bright linear areas seem to border the carbon fibers or some of the epoxy on the substrate. This would be tin from the peeled coating, but there is no specific morphology associated with it. In areas with mostly superficial polymer (Fig. 6-6 b), a very heterogeneous and roughened structure is observed. In this area, tin also seems to be present, with some local points of accumulation, but it is important to notice the scale of the image and that these points are quite small, and without any apparent structure. The coating side of an area matching the carbon fibers of the substrate is presented in Fig. 6-6 c. The structure of this coating seems complimentary to the carbon fibers of the substrate with long grooves, but these are discontinuous, and it seems that tin particles can be discerned within the grooves. On the coating side of an area matching the polymeric area (Fig. 6-6 d), a wave-like structure of tin particles can be observed, and this seems complimentary to the topography observed on the substrate side (Fig. 6-6 b).

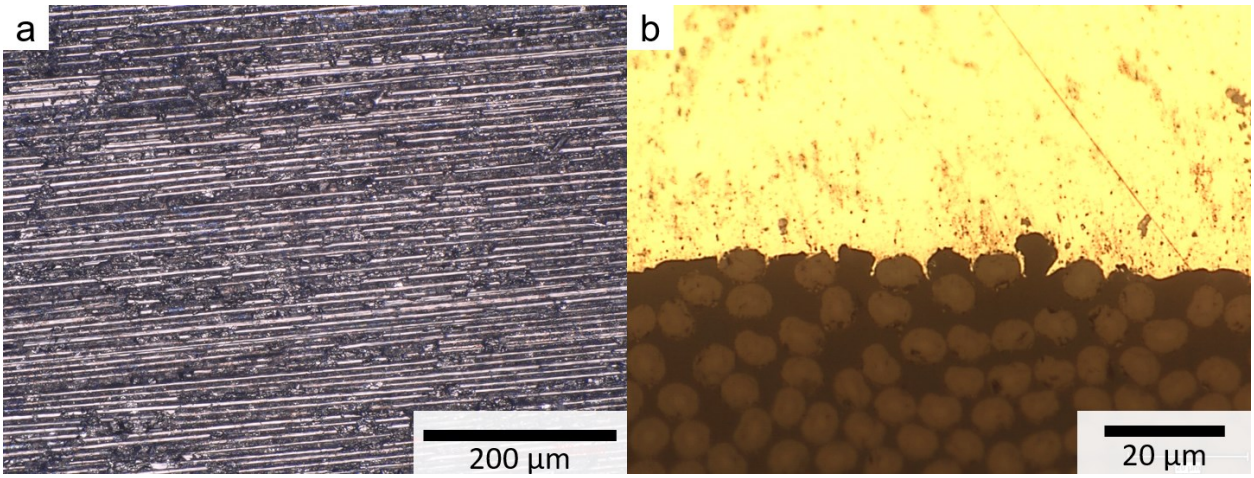

Fig. 6-5: *a) Keyence digital microscope image of the substrate side of a tested Sn-10Ti6Al4V coating on putty e-CFRP substrate. b) Optical image of the cross-section of a pure Sn [256] coating on the putty e-CFRP substrate, at the coating/substrate interface.*

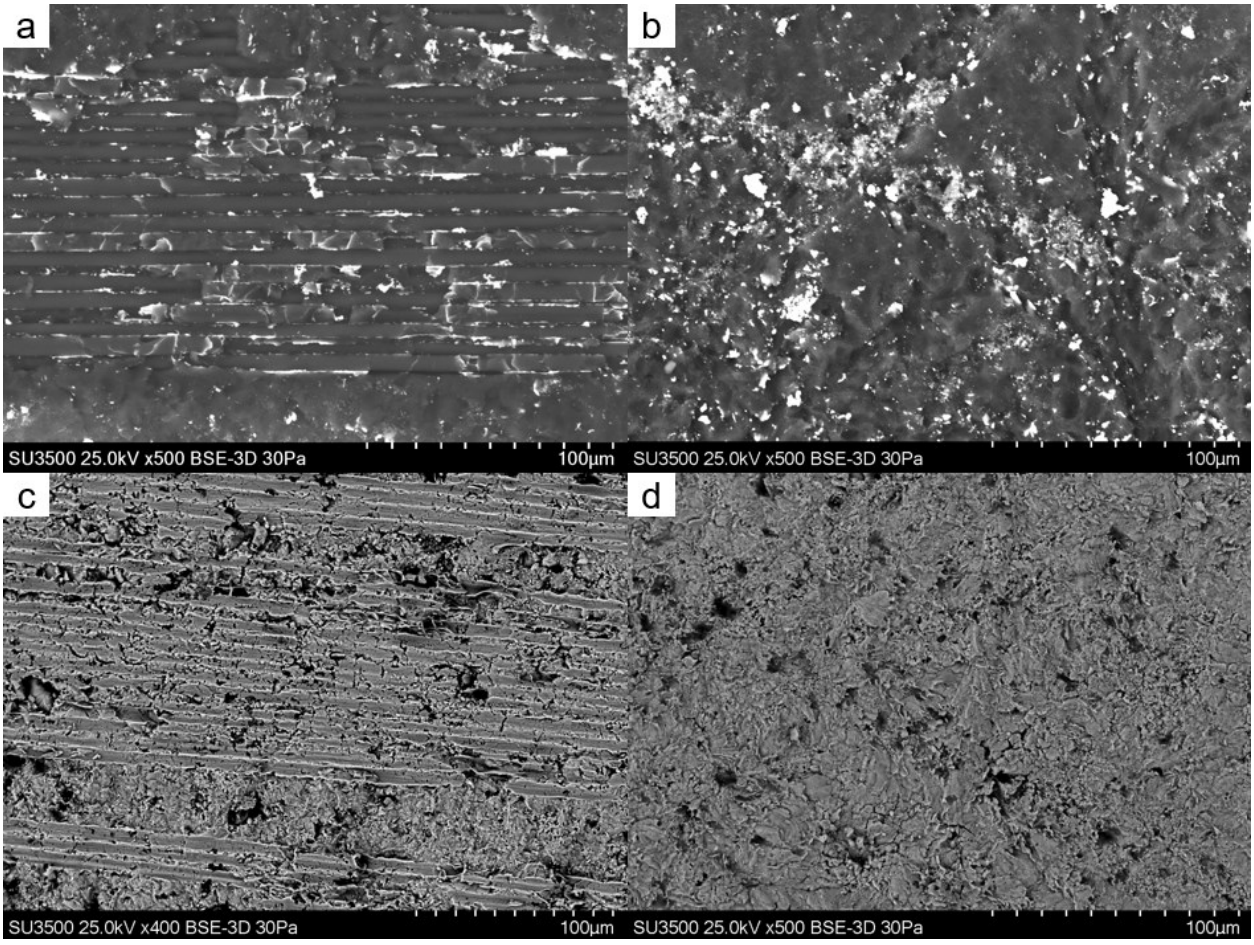

Fig. 6-6: *SEM images of tested coatings on putty e-CFRP: (a) substrate side of a tested Sn-10SS316L coating and (b) substrate side of a tested Sn-10Al coating. (c) and (d) are respectively the coating side of tested Sn-10Cu-IR and Sn-10Al coatings.*

6.5.2.3 Surface film e-CFRP

When characterizing the substrate surface, a heterogeneous fracture surface was obtained (Fig. 6-7 a): micron-sized spherical particles were observed to be embedded in the top surface of the substrate, with rings of highly contrasted elements (tin) surrounding them. Beside these particles, a roughened structure was present, similar to what observed on the polymer area of the putty e-CFRP (Fig. 6-6 b). Some large areas of tin were also observed on this coating (bright features of Fig. 6-7 b). Some greyish features, indicated by white arrows, can be observed in this area of bright contrast and they correspond to Cu-IR particles. The aforementioned spherical particles are also observed in the polymer, again, surrounded by rings of tin. On the coating side, spherical craters can be observed (Fig. 6-7 c) and they appear to be complimentary to the particles

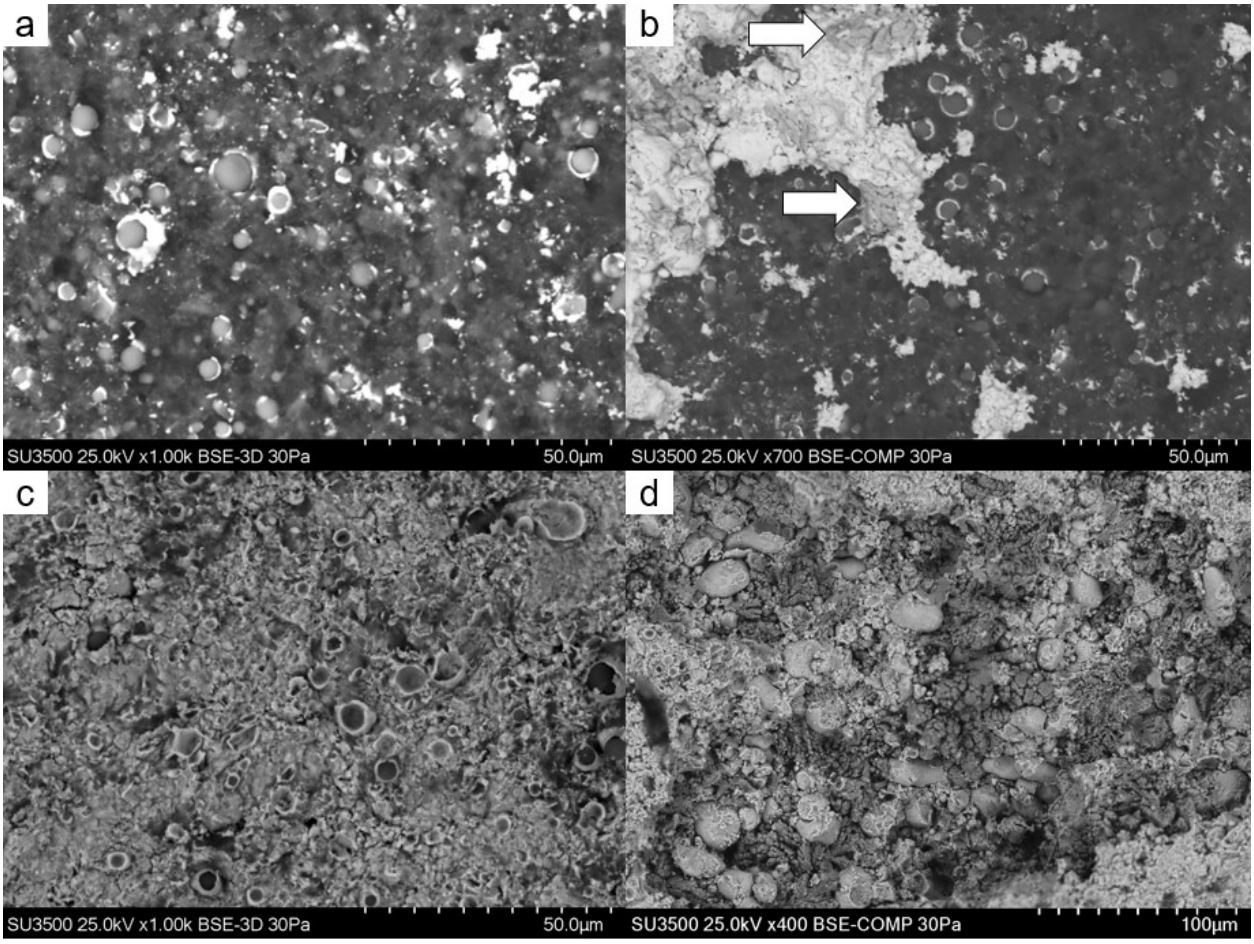

Fig. 6-7: *SEM images of tested coatings on surface film e-CFRP: (a) substrate side of a tested Sn-10Al coating and (b) substrate side of a tested Sn-10Cu-IR coating. (c) and (d) are respectively the coating side of tested Sn-10Al and Sn-10Cu-IR coatings. (b) and (d) are BSE-COMP images and the darker contrast of powder areas is Cu-IR.*

observed on the substrate surface. Around these craters, the structure of the tin particles seem to adopt a wave-like structure (Fig. 6-7 c), comparable to that of the putty e-CFRP (Fig. 6-6 d). Finally, with tin accumulations being present on the substrate for the SC Cu-IR coating (Fig. 6-7 b), it was possible to observe the interior of the peeled coating: tin particles (lighter contrast) were clearly visible, and a large number of Cu-IR particles were present.

6.5.2.4 PEEK-CFRP

Images of tested coatings on PEEK e-CFRP substrate are presented in Fig. 6-8 and Fig. 6-9. In Fig. 6-8, initially similar areas with superficial carbon fibers were considered: the light blue structure (edges of Fig. 6-8 a-b) are the PEEK polymer, and the linear structure of the center are the carbon fibers. A degree of discontinuity can be observed in the carbon fiber area with the tested pure Sn coating in Fig. 6-8 a, while the carbon fiber area seems larger and more damaged with the addition of SC Ti6Al4V in Fig. 6-8 b. No idea of roughness in the polymer is apparent here (as it was for the bare e-CFRP in Fig. 6-4 a), but this is due to the lower magnification. What is noticeable though, is the degree of roughening of the carbon fiber areas at this lower magnification. Some bright elements appear within the carbon fiber area, and these could be remnants of tin or reflections of light on damaged polymer/carbon fibers. Further characterization of these areas is conducted in Fig. 6-9. The carbon fiber area of a tested pure Sn coating is shown in Fig. 6-9 a, and several carbon fibers (vertical tubes) can be observed. These carbon fibers are partially covered by dark features that are the PEEK polymer. Furthermore, some highly contrasted linear features are present between the delimitations of the PEEK polymer and the carbon fibers, and this would be tin. Around the carbon fiber area, a slightly cratered polymer structure seems to appear. In Fig. 6-9 b, a similar substrate area of a tested Sn-10Ti6Al4V coating is presented: the image is slightly brighter, but the carbon fibers appear far more clearly. The area around these carbon fibers also appears more cratered. Further consideration is given to the area around the carbon fibers in Fig. 6-9 c, and a cratered structure is more obvious. Linear bright features seem to predominantly appear around the carbon fiber area, but not so much in the cratered area. Finally, the coating side of the tested Sn-10Ti6Al4V coating is observed in Fig. 6-9 d: the coating is complimentary to the carbon fibers of the substrate with long grooves, but these appear quite discontinuous, and tin particles can be made out within the grooves.

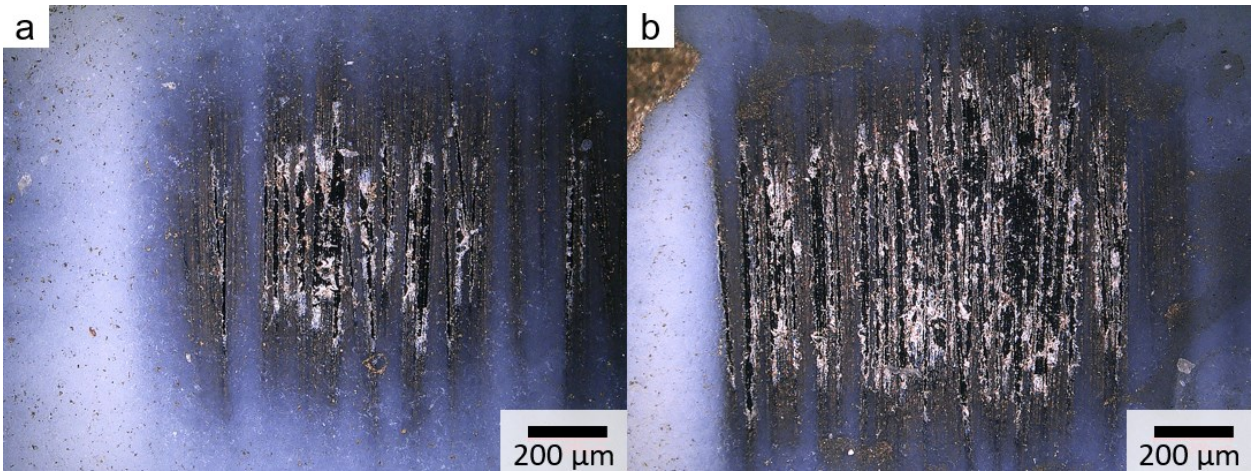

Fig. 6-8: *Keyence digital microscope image of the superficial carbon fiber area on the substrate side of tested coatings on PEEK-CFRP: (a) Sn [256], (b) Sn-10Ti6Al4V*

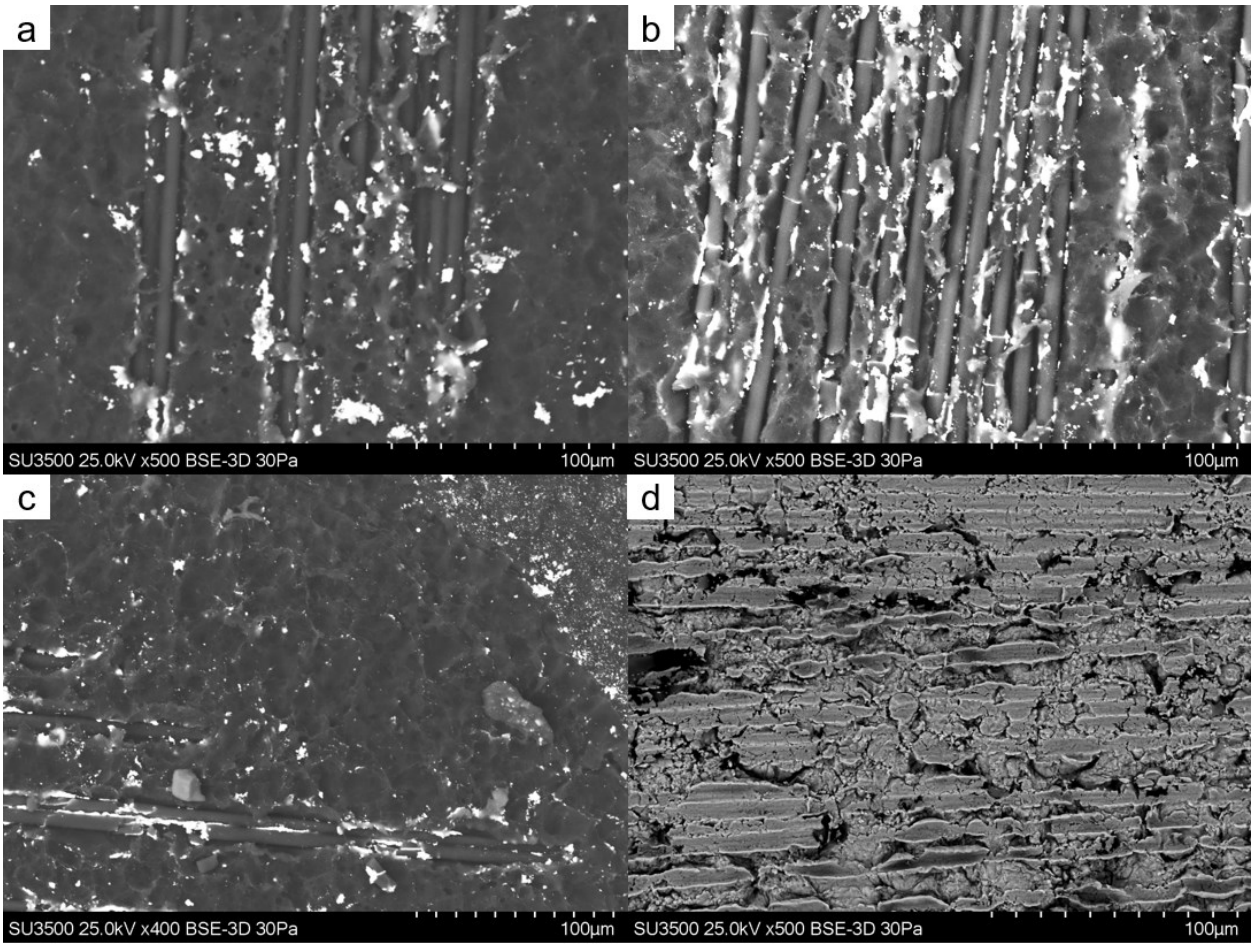

Fig. 6-9: *SEM images of tested coatings on PEEK-CFRP: (a) substrate side of a tested Sn [256] coating, (b, c) substrate side of a tested Sn-10Ti6Al4V substrate, (d) coating side of a tested Sn-10Ti6Al4V coating.*

6.5.3 Comparison of pull off strength and SC properties

While the previous section mostly focused on fracture surfaces for the various substrates, the SC may also play a role in the variation of coating strengths. In past studies, the importance of SC hardness [250, 256] and SC impact energy [256] appeared to be the key factors that affected DE, and will therefore be considered here. In the first section, it also appeared that the bare e-CFRP, putty e-CFRP and PEEK-CFRP provided similar trends with the Al and Cu powders providing coatings with lower strengths than pure Sn, and with the Fe and Ti-based powders providing similar or better strengths (Fig. 6-3). The putty e-CFRP and the PEEK-CFRP showed lower average strengths than the bare e-CFRP (Fig. 6-3), and the bare e-CFRP showed more contrast in the strength values then the other substrates. As a result, focus will be put on the relation between the SC properties and the pull off strengths on the bare e-CFRP in this section, but the trends that are described are similar for the putty e-CFRP and the PEEK-CFRP.

The pull-off strengths from the bare e-CFRP, as a function of SC impact energy and SC hardness, are presented in Fig. 6-10. It appears that SC with low hardness and any value of impact energy lead to pull off strengths lower than their tin counterpart: SC Al/Al alloy lead to strengths below 5 MPa, while Sn [250] has a strength above 5 MPa, and SC Cu/Cu-IR lead to strengths below 10 MPa, while the glue broke when testing Sn [256]. It should be noted that SC Cu-IR nevertheless led to a higher pull strength than the other SC Al and Cu powders, and Cu-IR had the highest average impact energy. For the SC with higher hardness, and any impact energy (Fe and Ti-based SC), the glue almost always broke during the testing which would indicate that they may provide pull off strengths on par or better than the Sn [256].

Height profiles of 827µm x 827µm areas were taken on the bare e-CFRP substrate for substrates that had peeled (Fig. 6-11) and roughness measurements were taken to study a potential relation between the substrate surface roughness and the pull off strengths of the coatings. The as-manufactured substrate (Fig. 6-11 a) naturally has lower roughness (Sa), peak-to-valley height (Sz) root mean square gradient (Sdq), than the substrates after removal of the coatings (Fig. 6-11 b-d). After removal of the pure tin coating, increases of each of these parameters are observed, with a

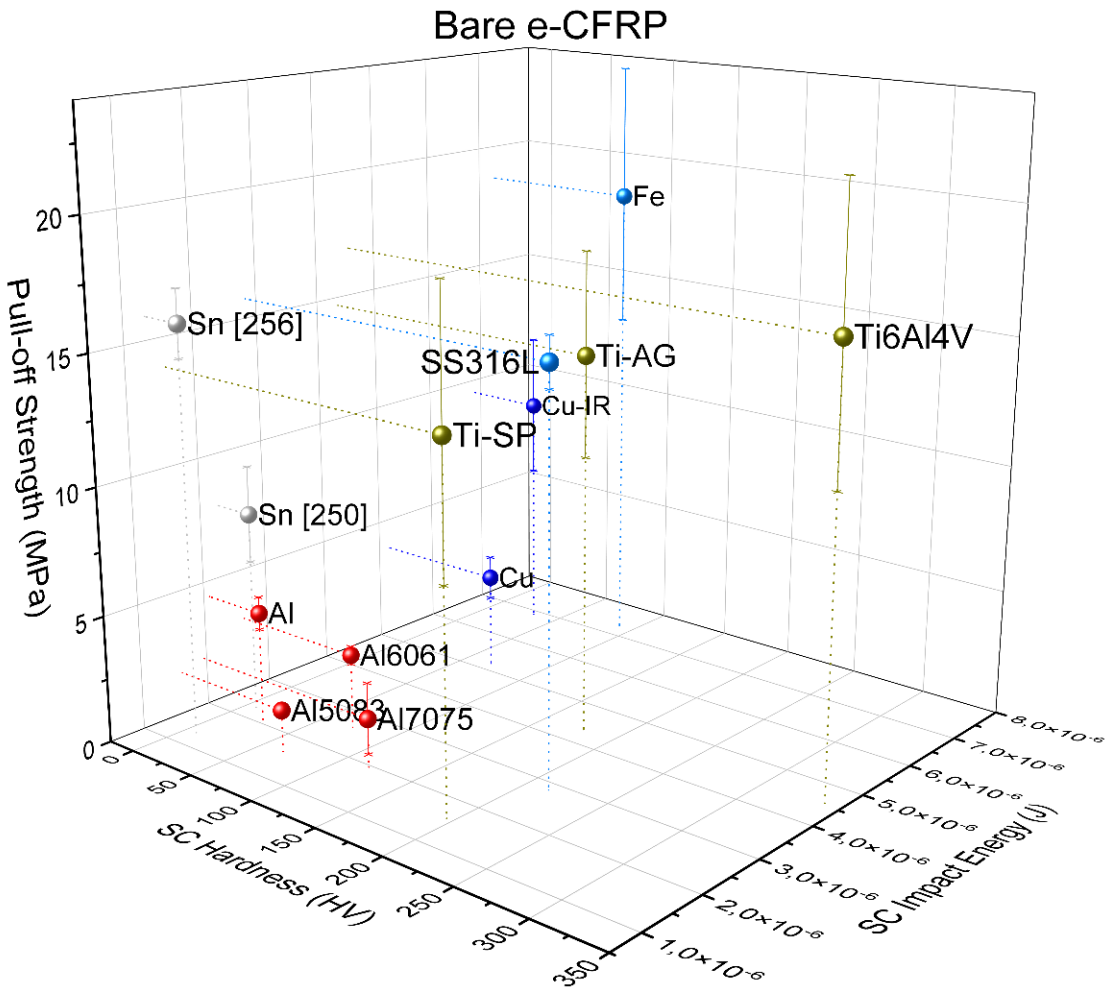

Fig. 6-10: *Pull-off strength on the bare e-CFRP for the various SCs, represented as a function of the SC hardness and impact energy.*

Near doubling of Sdq from 86µm/mm to 154µm/mm (Fig. 6-11 b). With the addition of SC to the powder mixture (Fig. 6-11 c-d), these increases were even higher with SC SS316L providing values of Sdq over 5 times that of the as-manufactured bare e-CFRP, and 3 times higher than the substrate surface after removal of the pure Sn coating.

6.5.4 Electrical conductivity

Electrical conductivity measurements were conducted on all substrates and are presented in Fig. 6-12. Generally, conductivities between 50% and 80% of the conductivity of pure Sn (9.10^6 S/m) are obtained. In some circumstances, the electrical conductivity was very low (Sn [250] on

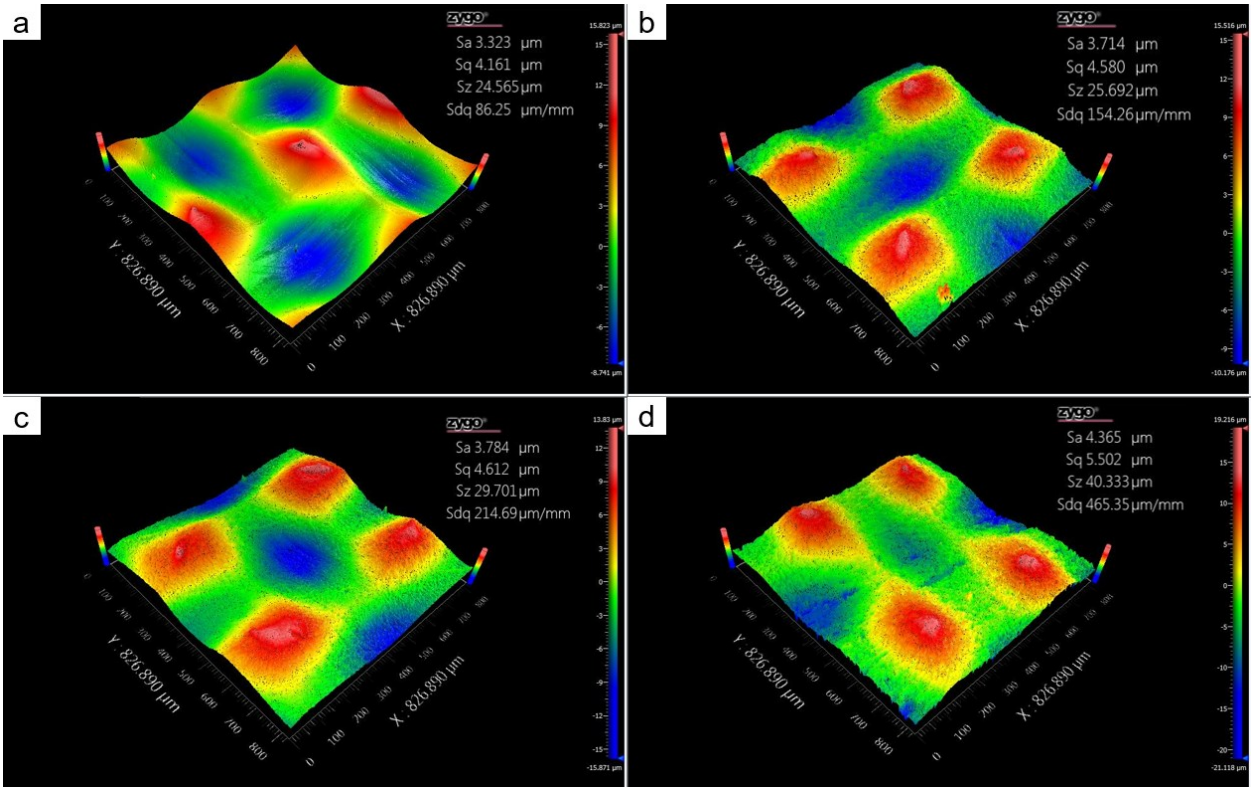

Fig. 6-11: *Height profiles of a bare e-CFRP substrate at 10x: a) as-received, b) after peeling of a Sn [250] coating, c) after peeling of a Sn-10Al5083 coating, d) after peeling of a Sn-10SS316L coating.*

the surface film e-CFRP or on the PEEK-CFRP, Sn-10Ti6Al4V on the PEEK-CFRP), but this could be associated with the "poor" or discontinuous aspect of these coatings [250, 256].

6.6 Discussion

6.6.1 Adhesion of coatings to CFRP

The main features observed in the characterization of the fracture surfaces were carbon fibers, polymer areas, and highly contrasted tin areas. These tin areas appeared under two forms: mounds of tin or linear structures. All these areas could vary in shape and size: typically, the carbon fibers would be more of less apparent, while the polymer area would appear more or less roughened. Finally, the tin mounds would be larger than the size of several particles (>10 µm), while the linear structures of tin would be smaller (<10 µm). The following section discusses a potential correlation between fracture surfaces and pull off strengths based on the observation of these features.

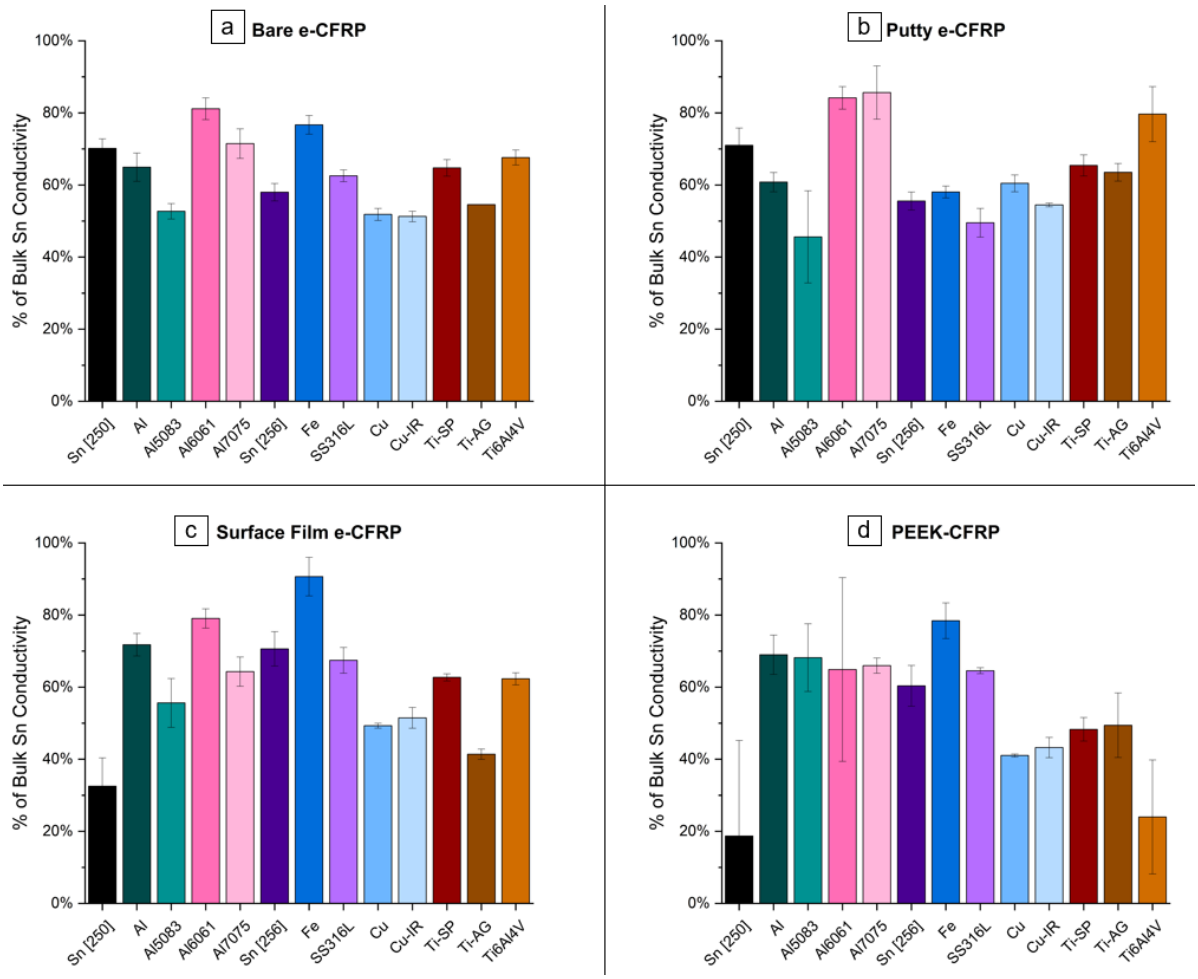

Fig. 6-12: *Electrical conductivity of the various Sn and Sn-SC powder mixtures, on the various CFRP substrates: a) bare e-CFRP, b) putty e-CFRP, c) surface film e-CFRP, d) PEEK-CFRP. The conductivity is expressed as a percentage of Bulk Sn conductivity (9.10^6 S/m).*

6.6.1.1 Bare e-CFRP

The presence of tin mounds at the surface of the bare e-CFRP substrate (Fig. 6-4 a-b) and the observation of the interior of the coating after the pull off test (Fig. 6-4 c-d) would indicate that the debonding is not purely adhesive, and that some cohesive component should be included. The epoxy is quite roughened on the substrate (Fig. 6-4 a) and could provide some retention, but the tin at the substrate/coating interface (Fig. 6-4 c) is highly deformed (flattened) so there seems to be little or no means of mechanical interlocking with the substrate in these areas. This would then suggest that the bonding of the coating with the substrate must occur in areas where the cohesive failure occurs. Furthermore, the small linear tin structures along the carbon fibers (Fig. 6-4 b) have

no specific structure and are very small in size: these may only be remnants from tin melting during the spraying process [28, 30, 44, 246, 257], and may not be elements of the coating. With tin being accumulated and quite deformed around the carbon fiber area (Fig. 6-4 b), it could then be suggested that the bonding of the coating intimately depends on the bonding with the carbon fiber area, and that more deformation (i.e. mechanical interlocking) can occur here. These results support conclusions of previous work [250, 256], where it was suggested that deposition would occur in the superficial carbon area, and that these areas would be prime for occurrence of the "crack-filling" mechanism. The areas of cohesive failure would then support the load applied during the pull off test. For the substrate side of the tested Sn-10Cu coating presented in Fig. 6-4 a, 3-4% of the surface is covered by tin mounds for a pull off strength of 3.7 MPa, which would correlate to tin in the coating fracturing at a strength of 93-123 MPa. With a bulk tensile strength of 220 MPa, this could be an additional indication of poor bonding in the cold sprayed coating. Therefore, even though these mounds of tin appear is remnants, their contribution to the coating adhesion may be significant, and further consideration should be given to assessing the proportion of areas of cohesive failure for these coatings.

The role of the SC is more difficult to explain: in some situations (with SC Fe, SS316L, Ti-SP, Ti-AG, Ti6Al4V), the coatings did not peel from the substrate, while other SC (Al/Al alloys, Cu/Cu-IR) led to relatively lower strengths than pure tin (Fig. 6-3). The SC is hypothesized to generate surface roughness (on the substrate or on the coating) and peening of the coating (during the build-up phase) [42, 43]. The SC are harder and generally have higher impact energies than the tin particles, so they should have higher potential for "crack-generation" at the substrate interface [250, 256], and therefore provide improved anchoring of tin to the substrate. More bonding of tin with the substrate would be expected and observed either through more areas of revealed carbon fibers (if adhesive strength is the limiting factor) or more areas of tin on the substrate side (if cohesive strength is the limiting factor). The tin particles within the observed coatings do not seem very deformed for SC Al5083 (Fig. 6-4 c) and SC Cu-IR (Fig. 6-4 d) as their morphology is comparable to the initial feedstock powder (Fig. 1a of [250] or Fig. 2a of [256]), so the involved SC may not provide notable peening, and bonding may be relatively poor when compared to the relatively higher bonding occurring at interfaces with carbon fibers. It is possible that these SC generate greater adhesive strength for the coating, but their presence in the coating

(albeit sometimes very low [256]) leads to more cohesive failure, and overall lower pull-off strengths than the pure Sn coatings. Typically, a large distribution of Cu-IR particles was observed in the back of the peeled coating (Fig. 6-4 d), and these particles were not as present in the areas of cohesive failure on the substrate side (Fig. 6-4 b): this could reinforce the idea that these SC bond poorly with Sn and weaken the pull off strength. As for the addition of other SC (Fe/SS316L, Ti/Ti6Al4V), peeling did not occur much like the Sn coating: it is possible that these SC helped with the crack filling mechanism and/or provided better cohesive bonding, potentially through improved peening of the coating.

6.6.1.2 Putty e-CFRP

On the putty e-CFRP substrate, no mounds of tin were observed and the coatings always peeled due to adhesive failure. Tin was present around the carbon fibers before testing (Fig. 6-5 b), the carbon fiber areas were well exposed after testing (Fig. 6-5 a, Fig. 6-6 a), and tin grooves on the coating side of tested coatings were observed, so it would seem that mechanical anchoring appears in the carbon fiber area. A contribution of anchoring from the deformed tin in roughened epoxy areas seems possible as well (Fig. 6-6 b, Fig. 6-6 d). Some linear tin structures were observed on the substrate side after fracture (Fig. 6-6 a-b), and probably do not have a role in coating adhesion. Nevertheless, while the bonding seems related to the carbon fiber area for this substrate, the strengths for all coatings are actually lower than on the bare e-CFRP (Fig. 6-3). Given the attribution of "good adhesion" to carbon fiber areas for the bare e-CFRP, the absence of tin mounds (cohesive failure) and the clear exposure of the carbon fiber areas should also be explained.

The nature of bonding with metal/polymer (or metal/composite) systems is still not entirely understood (with only the "crack-filling" as a point of reference [28]), but some observed elements may explain the differences with the bare e-CFRP. A first element of comparison would naturally be the surface finish of each substrate: with its as-manufactured finish, the bare e-CFRP is slightly rougher than the putty e-CFRP (Fig. 6-2 a, Fig. 6-2 b) which could be associated with better potential for mechanical interlocking. Furthermore, it is possible that some carbon fiber areas (those at the bottom of the valleys of Fig. 6-2 a) are covered by the pinhole filler in the putty finish

on the e-CFRP, therefore cutting in half the number of areas the coating could efficiently bond to. This pinhole filler would have a polymeric nature (i.e. little or no contribution to mechanical interlocking) and could also partially cover carbon fiber areas near the peaks of the holes, reducing the area that tin could bond to. Therefore, regardless the quality of bonding observed in the carbon fiber area, the overall load of the peel off test would be applied to a lower number of areas (i.e. higher local strain) and ultimately, the coating would show lower strength.

Another element to differentiate the widely varying pull off strengths between substrates could be the observation of tin particles on the backside of the coatings with cracks or voids between the particles (Fig. 6-6 c). This could indicate less uniformity and qualitatively less deformation of the tin impacting the substrate, when compared with tested coatings on the bare e-CFRP that had very uniform coating interfaces (Fig. 6-4 c): this could then lead to weaker bonding of the coating and, as a result, poorer mechanical interlocking with the substrate. Therefore, with seemingly less adhesive coatings in the carbon fiber areas and less areas to adhere to, the putty e-CFRPs would provide lower strengths than the bare e-CFRP. A direct consequence of weaker bonding would also be that the coating would present adhesive failure before any cohesive failure, which would explain the absence of tin mounds on this substrate, and any carbon fibers that would have been covered with tin mounds on the e-CFRP would be revealed due to the adhesive failure of the putty e-CFRP. Since the coatings with the highest strengths did not peel, it is nevertheless difficult to confirm if the bonding around the carbon fibers of the bare e-CFRP was on a large area (comparable to the putty e-CFRP).

6.6.1.3 Surface film e-CFRP

With an average pull off strength of 9.5 MPa, the strengths of coatings on the surface film e-CFRP compare as better than most reported results in the literature [27, 28, 111, 113, 232, 255, 257]. While carbon fiber structures were observed on tested coatings on bare e-CFRP and putty e-CFRP, the surface film e-CFRP coatings provided notably different observations: carbon fiber areas were never observed, and only micron-sized spherical particles with rings of tin appeared on the substrate side (Fig. 6-7 a, Fig. 6-7 b). These micron-sized particle seem to originate from the preparation of the substrate, as they could already be distinguished in the top layer of Fig. 6-1 c.

The rings of tin around these particles could be remnants of melted tin (Fig. 6-7 a-b) that appeared during the spray process, similar to the local tin tracks on the bare and putty e-CFRPs (Fig. 6-6 a-b): it is possible that their role for bonding is also negligible. Some coatings such as tin with SC Cu-IR left accumulations of tin at the surface (Fig. 6-7 b), indicating that debonding on this substrate was due to mixed adhesive/cohesive failure. Since it was quite unclear if the roughened structure of the putty e-CFRP (Fig. 6-6 b, Fig. 6-6 d) would portray mechanical interlocking of tin in the polymeric substrate area, it would seem that the bonding of the coatings to the surface film e-CFRP substrate is related to the bonding of the tin to the spherical particles at the top surface of the substrate. In the light of the high deformation of tin particles around these spherical elements (craters of Fig. 6-7 c) and the high average coating strength (Fig. 6-3 c), it could be suggested that this bonding is relatively strong. These spherical particles also seem heterogeneous in size and in distribution on the top surface of the substrate (Fig. 6-7 a-b) which could explain the strong variability observed for the bonding results (Fig. 6-3 c).

Finally, as with the bare e-CFRP, it seems Cu-IR led to some local cohesive failure with areas remaining bonded to the substrate (top left corner of Fig. 6-7 b): these areas are mostly tin with some Cu-IR particles. The coating side of the corresponding sample also presents tin particles with little deformation as compared to the initial feedstock powder, as well as a high proportion of Cu-IR (Fig. 6-7 d). A combination between a hypothesized local increase of spherical particles (that would increase adhesion due to strong bonding) and a cohesive failure due to poor bonding between the tin and Cu-IR could explain how these structures are obtained.

6.6.1.4 PEEK-CFRP

Pull off strengths for the PEEK-CFRP substrate presented a similar trend to those observed for the bare e-CFRP and the putty e-CFRP. As for the putty e-CFRP, no notable accumulation of tin was observed on the PEEK-CFRP substrate suggesting that all coatings on this substrate present adhesive failure. Through the observation of craters in the polymer area (Fig. 6-9 c), it could be suggested that peening of the PEEK polymer appears and little/no mechanical interlocking can occur here, as previously suggested [250]. This cratering appears in contrast to a roughened structure that was observed for the putty and surface film e-CFRPs (Fig. 6-6 d, Fig. 6-7 c). The

phenomenon could be related to the different polymeric nature of the substrate: PEEK being a thermoplastic material, it could be subjected to thermal softening and deformation, while the thermosetting epoxy in previous substrates would be directly subjected to cracking, fracture, and/or erosion.

Again, it would then seem that the bonding of the coatings is related to the mechanical interlocking of tin in the carbon fiber area of the substrate. Similar carbon fiber areas were observed for pure Sn (Fig. 6-8 a, Fig. 6-9 a) and for Sn-10Ti6Al4V (Fig. 6-8 b, Fig. 6-9 b), and it appeared that SC Ti6Al4V revealed the carbon fibers more, as the areas were larger, the fibers appeared more clearly and less polymer seemed present. The strength of this coating was also notably higher than the strength of the pure Sn coating (8.2 MPa compared to 3.7 MPa, Fig. 6-3 d). This information could prove to be quite valuable as previous studies suggested the SC could generate more surface roughening and catalyse the "crack-filling" mechanism on CFRP substrates [250, 256], but past observation never revealed notable difference between coatings that could support this theory, and the observation of the e-CFRPs did not provide results that could fully support this hypothesis. This would only explain the improvement of bonding between the pure Sn coating and the Sn-10Ti6Al4V though, and systematic analysis of the substrates after testing would need to be conducted to confirm if there is a relation between the area of revealed carbon fibers and the obtained strength.

Even though the structure of the PEEK-CFRP was close to that of the bare e-CFRP (as-manufactured finish), the PEEK-CFRP led to the lowest pull off strengths of this work. Where putty e-CFRP had a structural difference that could explain the decrease in pull off strengths (pinhole filler), the lower results with PEEK-CFRP seem related to the nature of the substrate. As previously mentioned, the thermoplastic polymer is subject to ductile deformations whereas thermosets are not, and so the bonding of the coating with the substrate may be worse, notably due to dissipation of the particle deformation energy in the substrate. This could be confirmed by the discontinuous grooves of Fig. 6-9 d where different particles are discernable, even more so than in the coating of the bare (Fig. 6-4 c) and putty e-CFRPs (Fig. 6-6 d). This lack of coating uniformity and lesser deformation of tin particles at the substrate interface seems more important than for the

putty e-CFRP and could therefore also explain why overall lower strengths are observed on the PEEK-CFRP, as compared to the bare and putty e-CFRPs.

6.6.1.5 Summary

Based on the results and observations for each substrate, the following points can be made:

- The bare e-CFRP provided some of the highest pull off strengths of this study with many coatings not peeling (Fig. 6-3 a). This would be related to high levels of deformation of the tin at the coating/substrate interface (Fig. 6-4 c), and good bonding in the carbon fiber area. Bonding was related to cohesive and adhesive elements, and the presence of some SC in the coating seemed to present a weakening effect on the coating strength.
- The putty e-CFRP pull off strengths showed a similar trend to the bare e-CFRP, albeit with lower values (Fig. 6-3 b). Bonding in the carbon fiber area was notably clearer (Fig. 6-5 a), but this seemed to be offset by the surface finish that removed half of the carbon fiber areas that the coating could bond to (areas that would be at the bottom of the filled pinholes, or the valleys of Fig. 6-2 a)
- The surface film e-CFRP provided overall good coating strengths (Fig. 6-3 c) and this was related with a different surface finish, comprised of micro-sized spherical particles embedded in the polymer at the surface of the substrate (Fig. 6-7 a-b). The tin seems to greatly deform around these particles, leading to good bonding, and their heterogeneous distribution would explain the variation in strength measurements.
- The PEEK-CFRP provided the weakest coatings of this work (Fig. 6-3 d), and this was mostly associated with the different substrate nature (thermoplastic versus thermoelastic, for epoxy). Of notable interest, it appeared that the presence of the SC generated increased presence of carbon fibers at the surface of the substrate, which could explain the increase between pure Sn and the coating with SC Ti6Al4V.

From the obtained results, it would then seem that better adhesion was obtained when 1) a high level of tin deformation was observed at the coating/substrate interface, and 2) tin had a feature that it could bond with (carbon fiber or spherical particles of the surface film e-CFRP). The

variety of obtained results highlights the importance of the surface finish, as Rezzoug et al. [255] had suggested in their study with wire-arc sprayed zinc on various interlayers on CFRP.

Some consideration should be given to the relevance of pull-off testing (ASTM C-633, EN -582) as this method presents some downsides that have already been mentioned for metallic coatings on metallic substrates [260]: beyond the apparent simplicity of the test and application of a uniaxial quasi-static tensile stress, the adhesion level of the test takes into account crack initiation and propagation energies. Furthermore, for heterogeneous interfaces, crack initiation is likely to occur at singularities where stresses are concentrated [260]. Uncertainty values are reported to be around 15% for this test [260]. For the CFRP substrates in this study, the heterogeneity of the surface structure and bonding locations between the coating and the substrate could lead to a degree of concentrated stresses. By choosing to adapt the ASTM C-633 standard and working with square specimens of approximately 1.5 x 1.5 cm^2 rather than circular specimens (more difficult to produce for CFRP substrates), an additional risk of stress concentration would also appear at the corners or edges of the samples. Therefore, the pull-off strengths obtained in this study may demonstrate a level of variability, and notably, they may be somewhat underestimated if concentration of stresses at sample edges generate premature peeling. Nevertheless, given the wide range of values obtained, the discussions on the obtained trends of this study seem to remain valid.

6.6.2 Influence of the SC on the pull off strength

By differentiating the SC properties, it appears more clearly that the decrease in strength related to the addition of Al/Al alloys to Sn in [250] would be related to SC with low hardness and low impact energy (Fig. 6-10). In [256], these SC provided the highest increases in pure Sn DE and this range of powder properties was described as ideal for powder deposition: in the light of these results, it would then seem that improved DE compares with a decrease in pull off strength, as can be seen in Fig. 6-13. The Al/Al alloy particles were described as having a hardness and an impact energy that would be sufficient to generate cracks that the tin could then fill [256], but as much as the deposition process may be catalyzed with these conditions, the bonding seems worse. Since Sn also has low hardness and similar impact energy, the difference could then be explained by the presence of Al/Al alloy in the coating, as explained for the bare e-CFRP. Given the chosen

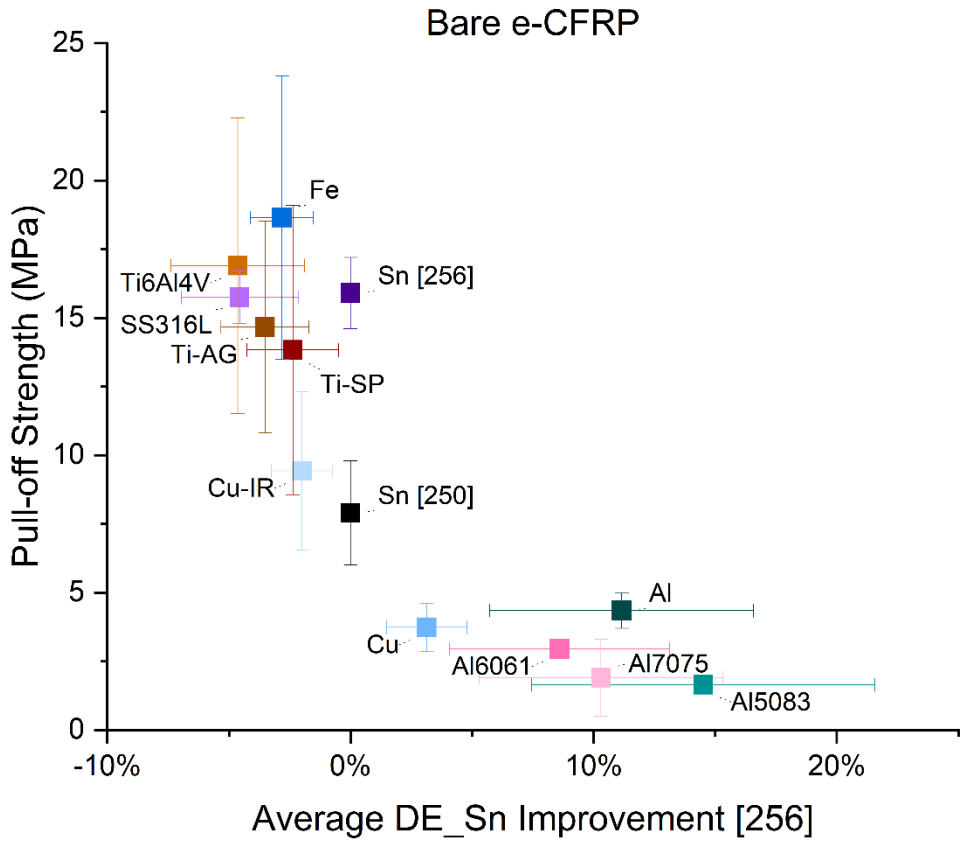

Fig. 6-13: *Pull-off strength as a function of the average pure Sn DE improvement [256] for the various SCs*

cold spray parameters (i.e. low velocities) and observations in another study [45], it is likely that Al is not bonding with the Sn in the coating and only being retained by mechanical interlocking: their retention rate was low (below 1% [250]) but if an analogy is taken with the coordination number of a close packed structure, one particle could affect a dozen neighboring particles (depending on size of the particles, etc.), so even a low percentage of retained Al/Al alloy particles in the coating could still act as a contaminant for the bonding of the coating.

Fe- and Ti-based SC led to decreases in the DE of pure Sn onto the CFRP and this was associated with higher impact energies and/or hardnesses that led to more erosion of the coating during the build-up phase [256]. From the perspective of strengths, these SC from [256] provided values on par, or slightly better, than the Sn powder they were sprayed with on the bare e-CFRP,

but also on the putty e-CFRP and on the PEEK-CFRP (Fig. 6-10). Their hardness is higher than the hardness of the substrates (above 180 $HV_{0.01}$, except for Fe), and their impact energy covers the range of energies considered for all powders. This supports the idea that the hardness of the SC is the key factor in maintaining or improving the pull off strength of the coatings. While SC Fe has a hardness of 89 $HV_{0.01}$ (lower than that of Al7075), it also has the highest average impact energy of this study ($7.3.10^{-6}$J). SC Cu and Cu-IR have low hardness values (on par with SC Al and Al alloys), but higher and increasing impact energy. Fig. 6-10 suggests that with increasing impact energy at lower hardness values, the pull off strength increases. This idea would then suggest that the SC impact energy has a second order effect behind SC hardness. Therefore, high hardness (and/or high impact energy) would be required to obtain good bonding on CFRP. This result is not entirely new as metallic surfaces are generally grit-blasted with hard particles (such as alumina) with the objective of enhancing adhesion strength [179], but from the perspective of composite materials where grit blasting leads to erosion of the substrate, this in-situ blasting by the SC on the CFRP could provide softer conditions that generate enhanced properties. Again, these trends are opposite to those observed for the DE of pure Sn, as high hardness (and/or high impact energies) would lead to lower pure Sn DE [256] (Fig. 6-13). On the other hand, the mechanism explaining the opposing trends would be the same as SC with high hardness and/or impact energy would have higher potential of roughening the surface and generating cracks that the tin could then fill to mechanically bond with the substrate, as seen for the PEEK-CFRP in Fig. 6-8. In conclusion, it would then seem that the pure Sn DE improvement mechanism discussed in previous studies [250, 256] would come at the expense of the pull off strength of the coating.

The role of the SC on the surface film e-CFRP had not yet been discussed, yet the trend seems more difficult to describe for this substrate. The bonding mechanism seems related to the presence of spherical particles at the top-surface of the substrate (Fig. 6-7 a-b) and high variability is observed for the strength of the various powder mixtures (Fig. 6-3), which could suggest that the effect of the SC for this coating is not as relevant as it may have been for the other CFRPs, where a strong component of the bonding mechanism came from crack-generation mainly around the carbon fiber area.

When looking at the roughness data of Fig. 6-11, the results seem to indicate that the addition of an SC leads to more surface roughening, which would support the idea that the SC could catalyse the deposition of tin onto CFRP (as discussed in [250, 256]). Nevertheless, correlations between the various roughness parameters, SC and coating strengths did not reveal clear trends that could explain the variations of strength. This assessment was also limited by the absence of peeling for the coatings that provided the highest strengths (with Fe- and Ti-based SC). More systematic analysis of the coatings would be required to determine the precise mechanisms at play (roughening of the surface by the SC or peening of the substrate/coating) to understand how the bonding occurs and what processing or powder factors may influence it.

6.6.3 Electrical conductivity

Differentiating the electrical conductivity results is a difficult task as there seems to be few common trends. From the perspective of the substrates, the average conductivities are not noticeably different, so the substrate does not appear to affect this property, as it may have affected the pull off strengths (Fig. 6-3). The SC do not seem to provide a trend either: although having similar hardness and impact energies, the addition of Al/Al alloy to pure Sn can have both positive effects (Al6061/Al7075) and negative effects (Al/Al5083) on the coating conductivity. The retention of Al in these coatings is always low (below 1%) [250] so retention of the SC should not noticeably affect the conductivity, while SC Fe, and to a lesser extent SS316L, provide better coating conductivity than pure Sn, regardless of higher retention rates (3-5% [256]) that could act as a contaminant.

While the variations may be difficult to understand, these conductivity results could be indicative of the bonding of the tin in the coating, as better bonding of the particles and less porosity (through increased plastic deformation) should lead to conductivities closer to those of the bulk material. However, plastic deformation would also lead to more dislocations in the particles, which could hinder electrical conductivity, and compete with the improvements provided by decreased porosity. Furthermore, the relation between conductivity and bonding quality could be supported by the cohesive failure that was observed for some coatings, such as Sn-10Al5083 on bare e-CFRP (Fig. 6-4 c), Sn-10Cu-IR on bare e-CFRP (Fig. 6-4 d) or Sn-10Cu-IR on surface

film e-CFRP (Fig. 6-7 d), as these coatings tend to present lower electrical conductivities than the other coatings (around 50%) (Fig. 6-12). As a result, while the mechanism is uncertain (competing effects), the SC would affect the coating conductivity via its impact on Sn in the coating, and not as much due to its own nature.

Few studies reported values of electrical conductivity for cold sprayed tin onto CFRP: Che et al. [6, 44] obtained conductivities around 50% bulk Sn conductivity without annealing in previous studies with Sn-10Cu or Sn-10Zn powder mixtures. In other instances of cold spray metallization of polymers, Małachowska et al. [261] reported electrical conductivities around 25% the conductivity of bulk tin when cold spraying on polycarbonates. Therefore, the measured electrical conductivities for the tin coatings in this work (Fig. 6-12) are higher than those reported in previous studies (50-80%). Post-processing treatments could be proposed to improve coating bonding, and therefore conductivity, as had observed Che et al. when annealing several Sn-Cu coatings (from 50% to 80% the bulk conductivity of tin) [44].

6.7 Conclusions

Coatings of tin mixed with various secondary components were cold sprayed with a CenterLine low-pressure cold spray system, onto thermosetting epoxy-CFRP substrates with varying surface finishes, a thermoplastic PEEK-CFRP and mild steel substrates. The pull off strength of these coatings was studied, and the fracture surfaces were characterized. The results indicate that the strength on the thermosetting CFRPs was better than the strength on the PEEK-CFRP. The mechanisms seem related to the degree of deformation/penetration of tin around the superficial carbon fiber areas for the bare e-CFRP, putty e-CFRP and PEEK-CFRP, while the surface film e-CFRP seems to react to a different mechanism (related to its surface finish). Correlation between the pull off strength and the SC properties was possible, and it seems that SC particles with higher hardness (and/or higher impact energies) led to improved strengths, while SC with low hardness led to lower strength than the pure Sn coating. These results are in opposition to the pure Sn DE improvement mechanism that relied on low hardness/low impact energy SC to catalyze Sn deposition. Attempts to characterize and correlate pull off strengths to surface roughness parameters were made on the bare e-CFRP substrates after peeling of the coatings, and

while preliminary results seemed promising (i.e. the addition of SC generated more surface roughening), there were no clear trends between the parameters and strength results. Finally, the electrical conductivity of each coated substrate was also measured, yet few trends appeared from the results: the conductivity results were generally better than those previously reported, and while they do not provide insight into the deposition/bonding mechanism, they could be an indication of the bonding of the tin in the coating.

6.8 Acknowledgments

The authors wish to acknowledge the financial support of the Natural Sciences and Engineering Research Council of Canada (NSERC) through the Green-SEAM strategic network and the McGill Engineering Doctoral Award (MEDA). The industrial partners, Bombardier Aerospace and Tencate (through Pratt and Whitney Canada) are gratefully acknowledged. Mr. Kévin Bricault from National Research Council Canada, Boucherville, is acknowledged for his contribution to the cold spray experiments. Mrs. Marie-Hélène Bernier from École Polytechnique de Montréal is acknowledged for her support in conducting the electrical conductivity measurements.

Chapter 7

Final conclusions and summary

7.1 Global Discussion

Previous results [44, 45, 240] suggested that SCs provided improvements to tin deposition, but with varying trends. Chapter 3 expanded on these results by mixing tin with aluminum and cold spraying the mixture on an epoxy CFRP at higher pressure ranges. The improvement mechanism of the SC was associated with shot-peening, or tamping, so the following chapters looked at assessing the contribution of the SC hardness (Chapter 4), as well as the contributions of the other SC properties (Chapter 5) when cold spraying on CFRPs of different nature. Finally, considerations on deposition are important, but to apply the coating in a real-life context, it is necessary to understand the properties of these coatings, and so the effect of SCs on coating pull off strength and electrical conductivity were studied in Chapter 6. Through the various studies, it was possible to gather information on the deposition mechanisms of tin on CFRP as well as better understand the influence of the SC.

In Chapter 3, cold spraying tin at higher pressures led to the development of protrusions on the substrate, and they were located around the last spray step. It was possible to establish an indirect deposition mechanism for these protrusions, built on rebounding or sweeping of some powders in the gas flow (Fig. 3-12). This reinforced the importance of differentiating the development of the first layer and build-up deposition phases in the case of cold spraying on composite materials (Fig. 3-13). In Chapter 4, tin coatings deposited preferentially in superficial carbon fiber areas and some of these coatings peeled revealing a dual-phase structure, with more deformed tin around carbon fiber areas than around pure polymer areas (Fig. 4-8 c). These observations were discussed in the light of the first layer and build-up deposition phases, and it appeared that first layer deposition of tin would seem to be preferential in the carbon fiber area, thus changing the perspective on how tin was depositing on CFRPs. By conducting pull-off tests in Chapter 6, it was possible to confirm that the deposition of tin and the bonding between the

coating and the substrate were related to a high degree of deformation of the tin around given features at the top surface of the substrates (carbon fibers generally, but also around spherical particles). To the best of our knowledge, this work is the first to describe the deposition mechanism of tin on the CFRP in such detail.

Based on these observations, the role of the SC could then influence the deposition of tin on the CFRP, as well as the adhesion of these coatings to the substrates. The focus of Chapter 4 was on the role of SC hardness. When choosing SCs with similar particle sizes, densities and morphologies, it appeared that the optimal deposition conditions were obtained when the SC hardness was on par with the hardness of the substrate. Based on the observations for the deposition mechanism of tin on CFRP, the role of the SC was then extended to the enhancement of the crack generation phenomenon, specifically around the carbon fiber area, which would then catalyze first layer tin deposition. Additional results in Chapter 4 also suggested that the SC would only play a limited role in the build-up deposition phase, which would mean that the shot-peening effect that was initially suspected of improving tin deposition may not be as relevant as the first layer catalysis. Chapter 5 built on these results and explored the effect of a larger variety of SC properties. Impact energy, a metric derived from the particle velocity, density, size (and, to some extent, morphology), was also considered. The results from this study confirmed the initial observations around the importance of SC hardness and also showed that the SC impact energy had an important role in influencing pure tin DE (Fig. 5-7). In retrospect, there did not seem to be any correlation between the results of Chapter 3 and the chosen SC (aluminum), but the latter may have participated in activating the CFRP surface for the indirect deposition of tin to occur.

Finally, Chapter 6 looked at the effect of the SC on the pull off strengths of various coatings on various substrates. The SCs showed effects on the pull off strength in opposition to their effect on the pure tin DE (as determined in Chapter 5) (Fig. 6-13). This was associated with the higher degree of roughening that a harder particle with higher impact energy could provide, so, as it may have been detrimental for deposition (erosive effect), it may have generated activated better anchoring sites for tin at the substrate surface and generated more bonding between the particles through peening of the coating. The improved bonding may have been expected to be seen in the

electrical conductivity results of these coatings, but no specific trend seemed to appear from these results in their as-sprayed state.

While this work was mainly focused on the cold spraying and the deposition of the metal particles, some importance was also given to the composite materials that were considered (e.g. thermosetting versus thermoplastic, various surface finishes). For the discussions on tin deposition (Chapter 4 and Chapter 5), the substrate did not seem to notably affect the deposition, beyond a variation in overall DEs. On the other hand, when studying the pull off strengths of the coatings (Chapter 6), the substrate seemed to play a greater role as the substrate finish would determine the roughness and the number of anchoring points of interest that the powder would be exposed to.

One final point of interest in our work was to correlate the observations on SCs with those of single component powders (section 5.6.3 and 5.7). By considering that single component powders could act as their own SCs, such as tin impacting itself during the cold spraying of tin on CFRP, the effects of SCs could be transferred to single component powders. It would then appear that deposition on CFRP would be possible with powders having a hardness close to the hardness of the CFRP (thus limiting material choice to metals such as Cu, Al, Sn, Zn or Sn), as well as an impact energy below ~2 μJ. This was extended to a limit on the particle diameter, based on the critical velocity of the associated powder material (Table 5-6), and results from the literature seemed in agreement with this limit. These criteria for single component deposition stem directly from observation of mixed powder mixtures and show the value to looking at more complex systems, to understand the relatively simpler systems of single component powders.

7.2 Conclusions

The objective of this work was to understand the role of the secondary component in the improvement mechanism associated with the deposition of tin on CFRP, and, ultimately to grasp a better understanding of the metallization of CFRP via cold spray. Based on these studies, the following conclusions can be drawn:

1) Differentiating the first layer and build-up deposition phases for the cold spraying of tin on CFRP is crucial to understanding the deposition mechanism of tin.

2) Tin preferentially deposits on substrate areas with greater potential for mechanical anchoring (superficial carbon fibers or other top surface features, depending on the surface finish). Improved adhesion strength is obtained when the tin is greatly deformed at the substrate/coating interface.

3) The secondary component would provide an ideal improvement in tin deposition efficiency when the secondary component hardness is on par with the substrate hardness, and when the impact energy of the secondary component is on part with that of the tin and below a specific criterion (~2 μJ).

4) The improvement mechanism of the secondary component is related to the enhancement it provides to crack generation during the first layer deposition phase of the coating, while shot peening may not be as relevant.

5) The effect of secondary component properties on coating pull off strengths are opposite to those on pure tin deposition efficiency.

6) The substrate nature (or finish) has a great effect on the pull off strengths of the various coatings, while it seems to have a limited effect on other metrics such as deposition efficiency and electrical conductivity.

7) The observations on secondary components can be translated to single component powders, and it can be suggested that cold sprayable powders on CFRP are powders with smaller particle sizes (<15-20 μm) and lower hardness values (<80 HV).

7.3 Contribution to Original Knowledge

The following contributions to original knowledge were made through the work conducted in this thesis:

1) The cold spraying of tin at higher pressures revealed the existence of an indirect deposition mechanism on CFRPs that was described and modeled for the first time.

2) An enhanced "crack-filling" mechanism was proposed where deposition of tin would occur preferentially in the superficial carbon fiber areas of the CFRP, due to crack generation (by the tin or by the secondary component) and subsequent filling by the tin particles.

3) A novel tin deposition efficiency improvement mechanism was proposed, in which the secondary component catalyzes the first layer deposition phase, while the previously suggested shot-peening mechanism does not seem to play a role in deposition efficiency enhancement.

4) The requirements for secondary component deposition efficiency enhancement were described and they were related to hardnesses similar to those of the substrate, as well as impact energies below a certain criterion (~2 μJ).

5) Enhancement criteria for secondary components were extended to single component powders (which can act as their own secondary components) and criteria on the powder hardness and particle size were suggested to obtain deposition on CFRP. Previous results from the literature confirmed the relevance of this contribution.

6) Fracture surfaces were generated by pull-off tests that were performed with pure Sn/Sn-based mixtures cold sprayed on various CFRP substrates (several thermosetting with different surface finishes and one thermoplastic). To the best of our knowledge, this is the first study to thoroughly study such fracture surfaces of cold sprayed metals on CFRP.

7) Enhanced pull-off strengths of tin on CFRP were associated with 1) tin having a feature that it could bond with (carbon fiber, spherical particle at the substrate interface) and 2) tin showing a high level of deformation around that feature.

8) The secondary component was shown to have opposing effects on tin deposition efficiency improvement and coating pull off strength: these could nevertheless be associated with the same roughening/crack generation mechanism.

7.4 Suggestions and Future Work

The following suggestions for future work could be made:

1) Cold spraying smaller metallic particles with hardnesses on par with the substrate would be useful to confirm the deposition requirements for CFRP metallization, as defined in sections 5.6.3 and 5.7. This could include the addition of secondary components to assist the deposition process.

2) Establishing a numerical physical interaction model to simulate the impact of a tin particle with a CFRP substrate, and comparing the obtained results with the impact of the same tin particle after impacting of other particles (i.e. secondary component), could help better describe how the secondary component assists the deposition of tin, and confirm the crack generation mechanism.

3) Additional characterization of the coating/substrate interface, notably for mechanically interlocked tin around carbon fibers, could help understand if the melting of tin as a role in the deposition mechanism, or if thermal softening alone is sufficient.

4) Warm spraying of copper or aluminum onto CFRP could be performed to induce a thermal softening effect in these powders that the low-pressure cold spray system could not provide.

5) Cold spraying tin onto other surface finishes, such as that of the surface film epoxy-CFRP, could be conducted to study the effect of a non-carbon fiber finish and understand the influence of the spherical particles on the coating adhesion (size of the particles, distribution on the substrate, etc.)

6) Annealing of the cold spray coated coatings could be conducted to study if the secondary components have an effect on the electrical conductivity of the coatings after heat treatments.

7) Refinement of the computation fluid dynamics (CFD) model discussed in Chapter 3 would be helpful for understanding thermal affects that may apply during the cold spraying of tin on the substrte.

8) Potentiometric measurements should be conducted around the coating/substrate interfaces as the coating adhesion mechanisms rely on tin mechanically interlocking in the carbon fiber area, which could lead to galvanic corrosion.

References

1. Gonzalez, R., H. Ashrafizadeh, A. Lopera, P. Mertiny, and A. McDonald, *A Review of Thermal Spray Metallization of Polymer-Based Structures.* Journal of Thermal Spray Technology, 2016. **25**(5): p. 897-919.

2. Mittal, K., *Metallized plastics 7 : fundamentals and applications*. 7 ed. 2001: VSP. 306.

3. Faupel, F., V. Zaporojtchenko, T. Strunskus, J. Erichsen, K. Dolgner, A. Thran, and M. Kiene. *Metallization of Polymers 2*. in *ACS Symposium Series (Kluwer Academic/Plenum, New York, 2002)*. 2002.

4. Rahimi, A., M. Hojjati, A. Dolatabadi, and C. Moreau, *Thermal Spray Coating on Polymeric Composite for De-Icing and Anti-Icing Applications.* Journal of Manufacturing Science and Engineering, 2021. **143**(10).

5. Black, S., *Lightning Strike Protection Strategies for Composite Aircraft*, in *High-Performace Composites*. 2013, Composites World. p. 52-61.

6. Che, H., M. Gagné, P.S.M. Rajesh, J.E. Klemberg-Sapieha, F. Sirois, D. Therriault, and S. Yue, *Metallization of Carbon Fiber Reinforced Polymers for Lightning Strike Protection.* Journal of Materials Engineering and Performance, 2018. **27**(10): p. 5205-5211.

7. Gagné, M. and D. Therriault, *Lightning strike protection of composites.* Progress in Aerospace Sciences, 2014. **64**: p. 1-16.

8. Siegel, J. and V. Kotál, *Preparation of thin metal layers on polymers.* Acta Polytechnica, 2007. **47**(1): p. 9-11.

9. Duguet, T., F. Senocq, L. Laffont, and C. Vahlas, *Metallization of polymer composites by metalorganic chemical vapor deposition of Cu: Surface functionalization driven films characteristics.* Surface and Coatings Technology, 2013. **230**: p. 254-259.

10. Kuroda, S., J. Kawakita, M. Watanabe, and H. Katanoda, *Warm spraying-a novel coating process based on high-velocity impact of solid particles.* Science and technology of advanced materials, 2008. **9**(3): p. 033002-033002.

11. Wang, R., D. Song, W. Liu, and X. He, *Effect of arc spraying power on the microstructure and mechanical properties of Zn–Al coating deposited onto carbon fiber reinforced epoxy composites.* Applied Surface Science, 2010. **257**(1): p. 203-209.

12. Feng, C., M. Gibbons, and S. Chandra, *Fabrication of Composite Heat Sinks Consisting of a Thin Metallic Skin and a Polymer Core Using Wire-Arc Spraying.* Journal of Thermal Spray Technology, 2019. **28**(5): p. 974-985.

13. Devaraj, S., B. Anand, M. Gibbons, A. McDonald, and S. Chandra, *Thermal spray deposition of aluminum and zinc coatings on thermoplastics.* Surface and Coatings Technology, 2020. **399**: p. 126114.

14. Bobzin, K., W. Wietheger, and M.A. Knoch, *Development of Thermal Spray Processes for Depositing Coatings on Thermoplastics.* Journal of Thermal Spray Technology, 2021. **30**(1-2): p. 157-167.

15. Gonzalez, R., A. McDonald, and P. Mertiny, *Effect of flame-sprayed Al–12Si coatings on the failure behaviour of pressurized fibre-reinforced composite tubes.* Polymer Testing, 2013. **32**(8): p. 1522-1528.

16. Wypych, A., P. Siwak, D. Andrzejewski, and J. Jakubowicz, *Titanium Plasma-Sprayed Coatings on Polymers for Hard Tissue Applications.* Materials, 2018. **11**(12): p. 2536.

17. Guanhong, S., H. Xiaodong, J. Jiuxing, and S. Yue, *Parametric study of Al and Al2O3 ceramic coatings deposited by air plasma spray onto polymer substrate.* Applied Surface Science, 2011. **257**(17): p. 7864-7870.

18. Huang, W., X. Fan, Y. Zhao, X. Zhou, X. Meng, Y. Wang, B. Zou, X. Cao, and Z. Wang, *Fabrication of thermal barrier coatings onto polyimide matrix composites via air plasma spray process.* Surface and Coatings Technology, 2012. **207**: p. 421-429.

19. Kosarev, V.F., S.V. Klinkov, A.P. Alkhimov, and A.N. Papyrin, *On some aspects of gas dynamics of the cold spray process.* Journal of Thermal Spray Technology, 2003. **12**(2): p. 265-281.

20. Kuroda, S., M. Watanabe, K. Kim, and H. Katanoda, *Current Status and Future Prospects of Warm Spray Technology.* Journal of Thermal Spray Technology, 2011. **20**(4): p. 653-676.

21. Affi, J., H. Okazaki, M. Yamada, and M. Fukumoto, *Fabrication of Aluminum Coating onto CFRP Substrate by Cold Spray.* Materials Transactions, 2011. **52**(9): p. 1759-1763.

22. Li, W., K. Yang, S. Yin, X. Yang, Y. Xu, and R. Lupoi, *Solid-state additive manufacturing and repairing by cold spraying: A review.* Journal of Materials Science & Technology, 2018. **34**(3): p. 440-457.

23. Rokni, M.R., S.R. Nutt, C.A. Widener, V.K. Champagne, and R.H. Hrabe, *Review of Relationship Between Particle Deformation, Coating Microstructure, and Properties in High-Pressure Cold Spray.* Journal of Thermal Spray Technology, 2017. **26**(6): p. 1308-1355.

24. Yin, S., M. Meyer, W. Li, H. Liao, and R. Lupoi, *Gas Flow, Particle Acceleration, and Heat Transfer in Cold Spray: A review.* Journal of Thermal Spray Technology, 2016. **25**(5): p. 874-896.

25. Zhang, D., P.H. Shipway, and D.G. McCartney, *Cold Gas Dynamic Spraying of Aluminum: The Role of Substrate Characteristics in Deposit Formation.* Journal of Thermal Spray Technology, 2005. **14**(1): p. 109-116.

26. Ganesan, A., M. Yamada, and M. Fukumoto, *Cold Spray Coating Deposition Mechanism on the Thermoplastic and Thermosetting Polymer Substrates.* Journal of Thermal Spray Technology, 2013. **22**(8): p. 1275-1282.

27. Ganesan, A., M. Yamada, and M. Fukumoto, *The Effect of CFRP Surface Treatment on the Splat Morphology and Coating Adhesion Strength.* Journal of Thermal Spray Technology, 2014. **23**(1-2): p. 236-244.

28. Che, H., P. Vo, and S. Yue, *Metallization of carbon fibre reinforced polymers by cold spray.* Surface and Coatings Technology, 2017. **313**: p. 236-247.

29. Che, H., X. Chu, P. Vo, and S. Yue, *Metallization of Various Polymers by Cold Spray.* Journal of Thermal Spray Technology, 2017. **27**(1-2): p. 169-178.

30. Sun, J., S. Zhou, K. Yamanaka, Y. Ichikawa, H. Saito, K. Ogawa, and A. Chiba, *Thermal Effects in Sn Coating on a Carbon Fiber Reinforced Plastic by Cold Spraying.* Journal of Thermal Spray Technology, 2021. **30**(5): p. 1254-1261.

31. Lupoi, R. and W. O'Neill, *Deposition of metallic coatings on polymer surfaces using cold spray.* Surface and Coatings Technology, 2010. **205**(7): p. 2167-2173.

32. Della Gatta, R., A. Viscusi, A.S. Perna, A. Caraviello, and A. Astarita, *Feasibility of steel powder deposition on composites through cold spray.* Materials and Manufacturing Processes, 2020. **36**(3): p. 281-291.

33. Perna, A.S., A. Astarita, P. Carlone, X. Guthmann, and A. Viscusi, *Characterization of cold-spray coatings on fiber-reinforced polymers through nanoindentation tests.* Metals, 2021. **11**(2): p. 1-16.

34. Della Gatta, R., A. Viscusi, A.S. Perna, A. Caraviello, and A. Astarita, *Cold spray process for the production of AlSi10Mg coatings on glass fibers reinforced polymers.* Materials and Manufacturing Processes, 2020. **36**(1): p. 106-121.

35. Viscusi, A., V. Antonucci, L. Carrino, R. Della Gatta, V. Lopresto, I. Papa, A.S. Perna, M.R. Ricciardi, and A. Astarita, *Manufacturing of an innovative composite structure: Design, manufacturing and impact behaviour.* Composite Structures, 2020. **250**: p. 112637.

36. Gillet, V., E. Aubignat, S. Costil, B. Courant, C. Langlade, P. Casari, W. Knapp, and M.P. Planche, *Development of low pressure cold sprayed copper coatings on carbon fiber reinforced polymer (CFRP).* Surface and Coatings Technology, 2019. **364**: p. 306-316.

37. Koithara, L.L., R.N. Raoelison, S. Costil, and X. Xie, *High deposition efficiency and delamination issues during high-pressure cold spraying metallization of PEEK using spherical copper powders.* International Journal of Advanced Manufacturing Technology, 2020. **107**(11-12): p. 4427-4436.

38. Lomonaco, P., S. Weiller, I. Feki, A. Debray, F. Delloro, M. Jeandin, B. Favini, and C. Rossignol, *Cold Spray Technology to Promote Conductivity of Short Carbon Fiber Reinforced Polyether-Ether-Ketone (PEEK).* Key Engineering Materials, 2019. **813**: p. 459-464.

39. Irissou, E., J.-G. Legoux, B. Arsenault, and C. Moreau, *Investigation of Al-Al2O3 Cold Spray Coating Formation and Properties.* Journal of Thermal Spray Technology, 2007. **16**(5-6): p. 661-668.

40. Koivuluoto, H. and P. Vuoristo, *Effect of Powder Type and Composition on Structure and Mechanical Properties of Cu + Al2O3 Coatings Prepared by using Low-Pressure Cold Spray Process.* Journal of Thermal Spray Technology, 2010. **19**(5): p. 1081-1092.

41. Lee, H.Y., Y.H. Yu, Y.C. Lee, Y.P. Hong, and K.H. Ko, *Cold Spray of SiC and Al2O3 With Soft Metal Incorporation: A Technical Contribution.* Journal of Thermal Spray Technology, 2004. **13**(2): p. 184-189.

42. Fernandez, R. and B. Jodoin, *Cold Spray Aluminum–Alumina Cermet Coatings: Effect of Alumina Content.* Journal of Thermal Spray Technology, 2018. **27**(4): p. 603-623.

43. Fernandez, R. and B. Jodoin, *Cold Spray Aluminum–Alumina Cermet Coatings: Effect of Alumina Morphology.* Journal of Thermal Spray Technology, 2019. **28**(4): p. 737-755.

44. Che, H., X. Chu, P. Vo, and S. Yue, *Cold spray of mixed metal powders on carbon fibre reinforced polymers.* Surface and Coatings Technology, 2017. **329**: p. 232-243.

45. Liberati, A., H. Che, P. Vo, and S. Yue, *Cold Spraying of Mixed Sn-Al Powders onto Carbon Fibre Reinforced Polymers*, in *Proceedings from the International Thermal Spray Conference*, K.B. F. Azarmi, T. Eden, T. Hussain, Y.-C. Lau, H. Li, K. Shinoda, Editor. 2018: Orlando, Florida, USA. p. 166-172.

46. Meng, F., D. Hu, Y. Gao, S. Yue, and J. Song, *Cold-spray bonding mechanisms and deposition efficiency prediction for particle/substrate with distinct deformability.* Materials & Design, 2016. **109**: p. 503-510.

47. Sova, A., R. Maestracci, M. Jeandin, P. Bertrand, and I. Smurov, *Kinetics of composite coating formation process in cold spray: Modelling and experimental validation.* Surface and Coatings Technology, 2017. **318**: p. 309-314.

48. Mittal, K., *Metallized Plastics 1 : Fundamental and Applied Aspects*. 1 ed. 1989: Springer US. 284.

49. Gibson, R.F., *Principles of Composite Material Mechanics*. 4 ed. 2016, Boca Raton: CRC Press. 700.

50. Skoczylas, J., S. Samborski, and M. Kłonica, *The application of composite materials in the aerospace industry.* Journal of Technology and Exploitation in Mechanical Engineering, 2019. **5**(1).

51. Rana, S. and R. Fangueiro, *1 - Advanced composites in aerospace engineering*, in *Advanced Composite Materials for Aerospace Engineering*, S. Rana and R. Fangueiro, Editors. 2016, Woodhead Publishing. p. 1-15.

52. Khalil, Y.F., *Eco-efficient lightweight carbon-fiber reinforced polymer for environmentally greener commercial aviation industry.* Sustainable Production and Consumption, 2017. **12**: p. 16-26.

53. Larsson, A., A. Delannoy, and P. Lalande, *Voltage drop along a lightning channel during strikes to aircraft.* Atmospheric Research, 2005. **76**(1-4): p. 377-385.

54. Chemartin, L., P. Lalande, B. Peyrou, A. Chazottes, P. Elias, C. Delalondre, B. Cheron, and F. Lago, *Direct effects of lightning on aircraft structure: analysis of the thermal, electrical and mechanical constraints.* AerospaceLab, 2012(5): p. p. 1-15.

55. Fisher, F., J.A. Plumer, and R.A. Perala, *Aircraft lightning protection handbook*. 1989, LIGHTNING TECHNOLOGIES INC PITTSFIELD MA.

56. US Department of Transportation, F.A.A., *Handbook-Airframe, Aviation Maintenance Technician* Vol. 1. 2018, Oklahoma City, OK.

57. Gardiner, G., *Lightning Strike Protection for Composite Structures*, in *High-Performance Composites*. 2006, Composites World. p. 44-50.

58. Fisher, F.A. and J.A. Plumer, *Lightning protection of aircraft.* 1977.

59. Feraboli, P. and H. Kawakami, *Damage of Carbon/Epoxy Composite Plates Subjected to Mechanical Impact and Simulated Lightning.* Journal of Aircraft, 2010. **47**(3): p. 999-1012.

60. Ebneth, H., L. Preis, H. Giesecke, and G.D. Wolf, *Metallized carbon fibres and composite materials containing these fibres*. 1984, Google Patents.

61. Rezzoug, A., S. Abdi, N. Bouhelal, and I. Daoud, *Metallic coating for carbon fiber reinforced polymer matrix composite substrate.* International Journal of Chemical, Molecular, 2016.

62. Liu, A., M. Guo, J. Gao, and M. Zhao, *Influence of bond coat on shear adhesion strength of erosion and thermal resistant coating for carbon fiber reinforced thermosetting polyimide.* Surface and Coatings Technology, 2006. **201**(6): p. 2696-2700.

63. Robitaille, F., M. Yandouzi, S. Hind, and B. Jodoin, *Metallic coating of aerospace carbon/epoxy composites by the pulsed gas dynamic spraying process.* Surface and Coatings Technology, 2009. **203**(19): p. 2954-2960.

64. Sturgeon, A., B. Dunn, S. Celotto, and B. O'Neill, *Cold Sprayed Coatings for Polymer Composite Substrate*, in *Proceedings of the 10th ISMSE, 8th ICPMSE*, B. Battrick, Editor. 2006: Collioure, France.

65. Cavaliere, P., L. Cavaliere, and Lekhwani, *Cold-Spray Coatings*. 2018: Springer.

66. James, A.W., G.P. Wagner, and B.B. Seth, *Cold spray repair process*. 2002, Google Patents.

67. Papyrin, A., V. Kosarev, S. Klinkov, A. Alkhimov, and V.M. Fomin, *Cold spray technology*. 2006: Elsevier.

68. Assadi, H., H. Kreye, F. Gärtner, and T. Klassen, *Cold spraying – A materials perspective.* Acta Materialia, 2016. **116**: p. 382-407.

69. Irissou, E., J.-G. Legoux, A.N. Ryabinin, B. Jodoin, and C. Moreau, *Review on cold spray process and technology: part I—intellectual property.* Journal of Thermal Spray Technology, 2008. **17**(4): p. 495-516.

70. Maev, R.G. and V. Leshchynsky, *Low-Pressure Cold Spray (LPCS)*, in *Cold-Spray Coatings: Recent Trends and Future perspectives*, P. Cavaliere, Editor. 2018, Springer International Publishing: Cham. p. 95-142.

71. Dykhuizen, R., M. Smith, D. Gilmore, R. Neiser, X. Jiang, and S. Sampath, *Impact of high velocity cold spray particles.* Journal of Thermal Spray Technology, 1999. **8**(4): p. 559-564.

72. Yin, S. and R. Lupoi, *Introduction to Cold Spray Additive Manufacturing*, in *Cold Spray Additive Manufacturing: From Fundamentals to Applications*. 2021, Springer International Publishing: Cham. p. 1-7.

73. Champagne, V.K., *Introduction*, in *Practical Cold Spray*, V.K. Champagne Jr, O.C. Ozdemir, and A. Nardi, Editors. 2021, Springer International Publishing: Cham. p. 1-25.

74. Assadi, H., T. Schmidt, H. Richter, J.O. Kliemann, K. Binder, F. Gärtner, T. Klassen, and H. Kreye, *On Parameter Selection in Cold Spraying.* Journal of Thermal Spray Technology, 2011. **20**(6): p. 1161-1176.

75. Villafuerte, J., *Current and future applications of cold spray technology.* Metal Finishing, 2010. **108**(1): p. 37-39.

76. Champagne, V.K., *The cold spray materials deposition process: fundamentals and applications*. 2007: Elsevier.

77. King, P., M. Yandouzi, and B. Jodoin, *The Physics of Cold Spray*, in *Modern Cold Spray: Materials, Process, and Applications*, J. Villafuerte, Editor. 2015, Springer International Publishing: Cham. p. 31-72.

78. Papyrin, A., V. Kosarev, S. Klinkov, A. Alkimov, and V. Fomin, *Chapter 1 - Discovery of the cold spray phenomenon and its basic features*, in *Cold Spray Technology*, A. Papyrin, et al., Editors. 2007, Elsevier: Oxford. p. 1-32.

79. Eden, T.J., O.C. Ozdemir, and V.K. Champagne, *Process Description*, in *Practical Cold Spray*, V.K. Champagne Jr, O.C. Ozdemir, and A. Nardi, Editors. 2021, Springer International Publishing: Cham. p. 27-51.

80. Hussain, T., *Cold Spraying of Titanium: A Review of Bonding Mechanisms, Microstructure and Properties.* Key Engineering Materials, 2013. **533**: p. 53-90.

81. Wong, W., E. Irissou, A.N. Ryabinin, J.-G. Legoux, and S. Yue, *Influence of Helium and Nitrogen Gases on the Properties of Cold Gas Dynamic Sprayed Pure Titanium Coatings.* Journal of Thermal Spray Technology, 2010. **20**(1-2): p. 213-226.

82. Davis, J.R., *Handbook of thermal spray technology*. 2004: ASM international.

83. Singh, H., T. Sidhu, and S. Kalsi, *Cold spray technology: future of coating deposition processes.* Frattura ed Integrità Strutturale, 2012. **6**(22): p. 69-84.

84. Borchers, C., F. Gärtner, T. Stoltenhoff, H. Assadi, and H. Kreye, *Microstructural and macroscopic properties of cold sprayed copper coatings.* Journal of applied physics, 2003. **93**(12): p. 10064-10070.

85. Balani, K., T. Laha, A. Agarwal, J. Karthikeyan, and N. Munroe, *Effect of carrier gases on microstructural and electrochemical behavior of cold-sprayed 1100 aluminum coating.* Surface and Coatings Technology, 2005. **195**(2-3): p. 272-279.

86. Koivuluoto, H., J. Näkki, and P. Vuoristo, *Corrosion properties of cold-sprayed tantalum coatings.* Journal of thermal spray technology, 2009. **18**(1): p. 75-82.

87. Champagne, V.K., A. Nardi, D. Helfritch, and M. Siopis, *Material Properties*, in *Practical Cold Spray*, V.K. Champagne Jr, O.C. Ozdemir, and A. Nardi, Editors. 2021, Springer International Publishing: Cham. p. 143-201.

88. Sansoucy, E., G.E. Kim, A.L. Moran, and B. Jodoin, *Mechanical Characteristics of Al-Co-Ce Coatings Produced by the Cold Spray Process.* Journal of Thermal Spray Technology, 2007. **16**(5): p. 651-660.

89. Villafuerte, J., *Modern Cold Spray*. 2015.

90. Grigoriev, S., A. Okunkova, A. Sova, P. Bertrand, and I. Smurov, *Cold spraying: From process fundamentals towards advanced applications.* Surface and Coatings Technology, 2015. **268**: p. 77-84.

91. Ghelichi, R. and M. Guagliano, *Coating by the Cold Spray Process: a state of the art.* Frattura ed Integrità Strutturale, 2009. **3**(8): p. 30-44.

92. Ernst, K.R., J. Braeutigam, F. Gaertner, and T. Klassen, *Effect of Substrate Temperature on Cold-Gas-Sprayed Coatings on Ceramic Substrates.* Journal of Thermal Spray Technology, 2013. **22**(2): p. 422-432.

93. Dietrich, D., B. Wielage, T. Lampke, T. Grund, and S. Kümmel, *Evolution of Microstructure of Cold-Spray Aluminum Coatings on Al2O3 Substrates.* Advanced Engineering Materials, 2012. **14**(4): p. 275-278.

94. Donner, K.-R., F. Gaertner, and T. Klassen, *Metallization of Thin Al2O3 Layers in Power Electronics Using Cold Gas Spraying.* Journal of Thermal Spray Technology, 2011. **20**(1): p. 299-306.

95. Drehmann, R., T. Grund, T. Lampke, B. Wielage, K. Manygoats, T. Schucknecht, and D. Rafaja, *Splat Formation and Adhesion Mechanisms of Cold Gas-Sprayed Al Coatings on Al2O3 Substrates.* Journal of Thermal Spray Technology, 2014. **23**(1): p. 68-75.

96. Drehmann, R., T. Grund, T. Lampke, B. Wielage, K. Manygoats, T. Schucknecht, and D. Rafaja, *Interface characterization and bonding mechanisms of cold gas-sprayed Al coatings on ceramic substrates.* Journal of Thermal Spray Technology, 2015. **24**(1): p. 92-99.

97. King, P.C., S. Zahiri, M. Jahedi, and J. Friend. *Cold spray electroding of piezoelectric ceramic*. in *Mater. Forum*. 2007. Citeseer.

98. King, P.C., S. Zahiri, M. Jahedi, and J. Friend, *Aluminium coating of lead zirconate titanate—A study of cold spray variables.* Surface and Coatings Technology, 2010. **205**(7): p. 2016-2022.

99. Moridi, A., S.M. Hassani-Gangaraj, M. Guagliano, and M. Dao, *Cold spray coating: review of material systems and future perspectives.* Surface Engineering, 2014. **30**(6): p. 369-395.

100. Champagne, V.K., P.K. Koh, T.J. Eden, D.E. Wolfe, J. Villafuerte, and D. Helfritch, *Applications*, in *Modern Cold Spray: Materials, Process, and Applications*, J. Villafuerte, Editor. 2015, Springer International Publishing: Cham. p. 341-376.

101. Chromik, R.R., S.A. Alidokht, J.M. Shockley, and Y. Zhang, *Tribological Coatings Prepared by Cold Spray*, in *Cold-Spray Coatings: Recent Trends and Future perspectives*, P. Cavaliere, Editor. 2018, Springer International Publishing: Cham. p. 321-348.

102. Eesley, G.L., A. Elmoursi, and N. Patel, *Thermal properties of kinetic spray Al–SiC metal-matrix composite.* Journal of Materials Research, 2003. **18**(4): p. 855-860.

103. Gyansah, L., N.H. Tariq, J.R. Tang, X. Qiu, B. Feng, J. Huang, H. Du, J.Q. Wang, and T.Y. Xiong, *Cold spraying SiC/Al metal matrix composites: effects of SiC contents and*

heat treatment on microstructure, thermophysical and flexural properties. Materials Research Express, 2018. **5**(2).

104. Jeandin, M., H. Koivuluoto, and S. Vezzu, *Coating Properties*, in *Modern Cold Spray: Materials, Process, and Applications*, J. Villafuerte, Editor. 2015, Springer International Publishing: Cham. p. 107-224.

105. Lima, R.S., J. Karthikeyan, C.M. Kay, J. Lindemann, and C.C. Berndt, *Microstructural characteristics of cold-sprayed nanostructured WC–Co coatings.* Thin Solid Films, 2002. **416**(1): p. 129-135.

106. Sansoucy, E., P. Marcoux, L. Ajdelsztajn, and B. Jodoin, *Properties of SiC-reinforced aluminum alloy coatings produced by the cold gas dynamic spraying process.* Surface and Coatings Technology, 2008. **202**(16): p. 3988-3996.

107. Sova, A., V.F. Kosarev, A. Papyrin, and I. Smurov, *Effect of Ceramic Particle Velocity on Cold Spray Deposition of Metal-Ceramic Coatings.* Journal of Thermal Spray Technology, 2011. **20**(1): p. 285-291.

108. Sova, A., A. Papyrin, and I. Smurov, *Influence of Ceramic Powder Size on Process of Cermet Coating Formation by Cold Spray.* Journal of Thermal Spray Technology, 2009. **18**: p. 633-641.

109. Spencer, K., D.M. Fabijanic, and M.X. Zhang, *The use of Al–Al2O3 cold spray coatings to improve the surface properties of magnesium alloys.* Surface and Coatings Technology, 2009. **204**(3): p. 336-344.

110. Fernandez, R. and B. Jodoin, *Effect of Particle Morphology on Cold Spray Deposition of Chromium Carbide-Nickel Chromium Cermet Powders.* Journal of Thermal Spray Technology, 2017. **26**(6): p. 1356-1380.

111. Ganesan, A., J. Affi, M. Yamada, and M. Fukumoto, *Bonding behavior studies of cold sprayed copper coating on the PVC polymer substrate.* Surface and Coatings Technology, 2012. **207**: p. 262-269.

112. King, P.C., A.J. Poole, S. Horne, R. de Nys, S. Gulizia, and M.Z. Jahedi, *Embedment of copper particles into polymers by cold spray.* Surface and Coatings Technology, 2013. **216**: p. 60-67.

113. Zhou, X.L., A.F. Chen, J.C. Liu, X.K. Wu, and J.S. Zhang, *Preparation of metallic coatings on polymer matrix composites by cold spray.* Surface and Coatings Technology, 2011. **206**(1): p. 132-136.

114. Gilmore, D.L., R.C. Dykhuizen, R.A. Neiser, M.F. Smith, and T.J. Roemer, *Particle velocity and deposition efficiency in the cold spray process.* Journal of Thermal Spray Technology, 1999. **8**(4): p. 576-582.

115. Goldbaum, D., J.M. Shockley, R.R. Chromik, A. Rezaeian, S. Yue, J.-G. Legoux, and E. Irissou, *The Effect of Deposition Conditions on Adhesion Strength of Ti and Ti6Al4V Cold Spray Splats.* Journal of Thermal Spray Technology, 2012. **21**(2): p. 288-303.

116. Li, C.-J., W.-Y. Li, and H. Liao, *Examination of the critical velocity for deposition of particles in cold spraying.* Journal of Thermal Spray Technology, 2006. **15**(2): p. 212-222.

117. Raoelison, R.N., Y. Xie, T. Sapanathan, M.P. Planche, R. Kromer, S. Costil, and C. Langlade, *Cold gas dynamic spray technology: A comprehensive review of processing conditions for various technological developments till to date.* Additive Manufacturing, 2018. **19**: p. 134-159.

118. Li, W.-Y., H. Liao, G. Douchy, and C. Coddet, *Optimal design of a cold spray nozzle by numerical analysis of particle velocity and experimental validation with 316L stainless steel powder.* Materials & Design, 2007. **28**(7): p. 2129-2137.

119. Lupoi, R. and W. O'Neill, *Powder stream characteristics in cold spray nozzles.* Surface and Coatings Technology, 2011. **206**(6): p. 1069-1076.

120. MacDonald, D., S. Leblanc-Robert, R. Fernández, A. Farjam, and B. Jodoin, *Effect of Nozzle Material on Downstream Lateral Injection Cold Spray Performance.* Journal of Thermal Spray Technology, 2016. **25**(6): p. 1149-1157.

121. Meyer, M. and R. Lupoi, *An analysis of the particulate flow in cold spray nozzles.* Mechanical Sciences, 2015. **6**(2): p. 127-136.

122. Jodoin, B., L. Ajdelsztajn, E. Sansoucy, A. Zúñiga, P. Richer, and E.J. Lavernia, *Effect of particle size, morphology, and hardness on cold gas dynamic sprayed aluminum alloy coatings.* Surface and Coatings Technology, 2006. **201**(6): p. 3422-3429.

123. Wong, W., P. Vo, E. Irissou, A.N. Ryabinin, J.G. Legoux, and S. Yue, *Effect of Particle Morphology and Size Distribution on Cold-Sprayed Pure Titanium Coatings.* Journal of Thermal Spray Technology, 2013. **22**(7): p. 1140-1153.

124. Mahdavi, A. and A. McDonald, *Effect of Substrate and Process Parameters on the Gas-Substrate Convective Heat Transfer Coefficient During Cold Spraying.* Journal of Thermal Spray Technology, 2017. **27**(3): p. 433-445.

125. Watanabe, Y., C. Yoshida, K. Atsumi, M. Yamada, and M. Fukumoto, *Influence of Substrate Temperature on Adhesion Strength of Cold-Sprayed Coatings.* Journal of Thermal Spray Technology, 2014.

126. Bae, G., K. Kang, H. Na, J.-J. Kim, and C. Lee, *Effect of particle size on the microstructure and properties of kinetic sprayed nickel coatings.* Surface and Coatings Technology, 2010. **204**(20): p. 3326-3335.

127. Tabbara, H., S. Gu, D.G. McCartney, T.S. Price, and P.H. Shipway, *Study on Process Optimization of Cold Gas Spraying.* Journal of Thermal Spray Technology, 2010. **20**(3): p. 608-620.

128. Pattison, J., S. Celotto, A. Khan, and W. O'Neill, *Standoff distance and bow shock phenomena in the Cold Spray process.* Surface and Coatings Technology, 2008. **202**(8): p. 1443-1454.

129. Helfritch, D. and V. Champagne, *A model study of powder particle size effects in cold spray deposition*. 2008, Army Research Lab Aberdeen Proving Ground MD.

130. Aydin, H., M. Alomair, W. Wong, P. Vo, and S. Yue, *Cold Sprayability of Mixed Commercial Purity Ti Plus Ti6Al4V Metal Powders.* Journal of Thermal Spray Technology, 2017. **26**(3): p. 360-370.

131. Chu, X., H. Che, P. Vo, R. Chakrabarty, B. Sun, J. Song, and S. Yue, *Understanding the cold spray deposition efficiencies of 316L/Fe mixed powders by performing splat tests onto as-polished coatings.* Surface and Coatings Technology, 2017. **324**: p. 353-360.

132. Wei, Y.-K., X.-T. Luo, C.-X. Li, and C.-J. Li, *Optimization of in-situ shot-peening-assisted cold spraying parameters for full corrosion protection of Mg alloy by fully dense Al-based alloy coating.* Journal of Thermal Spray Technology, 2017. **26**(1-2): p. 173-183.

133. Yue, S., W. Wong, H. Aydin, R. Mongrain, R. Barua, P. Vo, and R. Dolbec, *Improving cold sprayability: mixed metal powders.* Proceedings from the International Thermal Spray Conference, 2015: p. 473-478.

134. Dykhuizen, R. and M. Smith, *Gas dynamic principles of cold spray.* Journal of Thermal Spray Technology, 1998. **7**(2): p. 205-212.

135. Zhang, C., Q. Chen, J. Liu, W. Tang, K. Wang, and J. Song, *Numerical study on the effect of the cold powder carrier gas on powder stream characteristics in cold spray.* Surface and Coatings Technology, 2016. **294**: p. 177-185.

136. Ning, X.-J., J.-H. Jang, H.-J. Kim, C.-J. Li, and L. Changhee, *Cold spraying of Al–Sn binary alloy: Coating characteristics and particle bonding features.* Surface and Coatings Technology, 2008. **202**(9): p. 1681-1687.

137. Bae, G., S. Kumar, S. Yoon, K. Kang, H. Na, H.-J. Kim, and C. Lee, *Bonding features and associated mechanisms in kinetic sprayed titanium coatings.* Acta Materialia, 2009. **57**(19): p. 5654-5666.

138. Lee, K.-A., M.-J. Lee, J.-S. Yu, and H.-J. Kim, *Effect of powder preheating temperature on the properties of titanium coating layers manufactured by kinetic spraying.* Materials Transactions, 2014. **55**(3): p. 622-628.

139. Hussain, T., D.G. McCartney, P.H. Shipway, and D. Zhang, *Bonding Mechanisms in Cold Spraying: The Contributions of Metallurgical and Mechanical Components.* Journal of Thermal Spray Technology, 2009. **18**(3): p. 364-379.

140. Sharma, M.M., T.J. Eden, and B.T. Golesich, *Effect of Surface Preparation on the Microstructure, Adhesion, and Tensile Properties of Cold-Sprayed Aluminum Coatings on AA2024 Substrates.* Journal of Thermal Spray Technology, 2014. **24**(3): p. 410-422.

141. Assadi, H., F. Gärtner, T. Stoltenhoff, and H. Kreye, *Bonding mechanism in cold gas spraying.* Acta Materialia, 2003. **51**(15): p. 4379-4394.

142. Schmidt, T., H. Assadi, F. Gärtner, H. Richter, T. Stoltenhoff, H. Kreye, and T. Klassen, *From Particle Acceleration to Impact and Bonding in Cold Spraying.* Journal of Thermal Spray Technology, 2009. **18**(5-6): p. 794-808.

143. Xiong, Y., G. Bae, X. Xiong, and C. Lee, *The Effects of Successive Impacts and Cold Welds on the Deposition Onset of Cold Spray Coatings.* Journal of Thermal Spray Technology, 2010. **19**(3): p. 575-585.

144. Schmidt, T., F. Gärtner, H. Assadi, and H. Kreye, *Development of a generalized parameter window for cold spray deposition.* Acta Materialia, 2006. **54**(3): p. 729-742.

145. Zou, Y., W. Qin, E. Irissou, J.-G. Legoux, S. Yue, and J.A. Szpunar, *Dynamic recrystallization in the particle/particle interfacial region of cold-sprayed nickel coating: Electron backscatter diffraction characterization.* Scripta Materialia, 2009. **61**(9): p. 899-902.

146. Rahmati, S. and A. Ghaei, *The Use of Particle/Substrate Material Models in Simulation of Cold-Gas Dynamic-Spray Process.* Journal of Thermal Spray Technology, 2014. **23**(3): p. 530-540.

147. Archambault, G., B. Jodoin, S. Gaydos, and M. Yandouzi, *Metallization of carbon fiber reinforced polymer composite by cold spray and lay-up molding processes.* Surface and Coatings Technology, 2016. **300**: p. 78-86.

148. Samson, T., D. MacDonald, R. Fernández, and B. Jodoin, *Effect of Pulsed Waterjet Surface Preparation on the Adhesion Strength of Cold Gas Dynamic Sprayed Aluminum Coatings.* Journal of Thermal Spray Technology, 2015. **24**(6): p. 984-993.

149. Rahmati, S. and B. Jodoin, *Physically Based Finite Element Modeling Method to Predict Metallic Bonding in Cold Spray.* Journal of Thermal Spray Technology, 2020. **29**(4): p. 611-629.

150. Chu, X., *Cold spray characteristics of mixed 316L stainless steel and commercial purity Fe powders*, in *Mining and Materials Engineering*. 2020, McGill University: Montreal, Canada.

151. Champagne, V.K., D. Helfritch, P. Leyman, S. Grendahl, and B. Klotz, *Interface material mixing formed by the deposition of copper on aluminum by means of the cold spray process.* Journal of Thermal Spray Technology, 2005. **14**(3): p. 330-334.

152. Kim, K. and S. Kuroda, *Amorphous oxide film formed by dynamic oxidation during kinetic spraying of titanium at high temperature and its role in subsequent coating formation.* Scripta Materialia, 2010. **63**(2): p. 215-218.

153. Grujicic, M., C.L. Zhao, W.S. DeRosset, and D. Helfritch, *Adiabatic shear instability based mechanism for particles/substrate bonding in the cold-gas dynamic-spray process.* Materials & Design, 2004. **25**(8): p. 681-688.

154. Nardi, A., D. Cote, and V.K. Champagne, *Feedstock Powders*, in *Practical Cold Spray*, V.K. Champagne Jr, O.C. Ozdemir, and A. Nardi, Editors. 2021, Springer International Publishing: Cham. p. 101-142.

155. Khodabakhshi, F., B. Marzbanrad, H. Jahed, and A.P. Gerlich, *Interfacial bonding mechanisms between aluminum and titanium during cold gas spraying followed by friction-stir modification.* Applied Surface Science, 2018. **462**: p. 739-752.

156. Walker, M., *Microstructure and bonding mechanisms in cold spray coatings.* Materials Science and Technology, 2018. **34**(17): p. 2057-2077.

157. Zhu, L., T.-C. Jen, Y.-T. Pan, and H.-S. Chen, *Particle Bonding Mechanism in Cold Gas Dynamic Spray: A Three-Dimensional Approach.* Journal of Thermal Spray Technology, 2017. **26**(8): p. 1859-1873.

158. Barradas, S., V. Guipont, R. Molins, M. Jeandin, M. Arrigoni, M. Boustie, C. Bolis, L. Berthe, and M. Ducos, *Laser shock flier impact simulation of particle-substrate interactions in cold spray.* Journal of Thermal Spray Technology, 2007. **16**(4): p. 548-556.

159. Xie, Y., S. Yin, C. Chen, M.-P. Planche, H. Liao, and R. Lupoi, *New insights into the coating/substrate interfacial bonding mechanism in cold spray.* Scripta Materialia, 2016. **125**: p. 1-4.

160. Hassani-Gangaraj, M., D. Veysset, V.K. Champagne, K.A. Nelson, and C.A. Schuh, *Adiabatic shear instability is not necessary for adhesion in cold spray.* Acta Materialia, 2018. **158**: p. 430-439.

161. Assadi, H., F. Gärtner, T. Klassen, and H. Kreye, *Comment on 'Adiabatic shear instability is not necessary for adhesion in cold spray'.* Scripta Materialia, 2018.

162. Hassani-Gangaraj, M., D. Veysset, V.K. Champagne, K.A. Nelson, and C.A. Schuh, *Response to Comment on "Adiabatic shear instability is not necessary for adhesion in cold spray".* Scripta Materialia, 2018.

163. Hassani-Gangaraj, M., D. Veysset, K.A. Nelson, and C.A. Schuh, *In-situ observations of single micro-particle impact bonding.* Scripta Materialia, 2018. **145**: p. 9-13.

164. Ji, Y., G. Bae, K. Kang, and C. Lee, *Influence of the interface temperature and strain gradients on the impact energy model of a soft particle on a hard substrate during kinetic spraying.* Metals and Materials International, 2011. **17**(2): p. 335-340.

165. King, P.C., G. Bae, S.H. Zahiri, M. Jahedi, and C. Lee, *An Experimental and Finite Element Study of Cold Spray Copper Impact onto Two Aluminum Substrates.* Journal of Thermal Spray Technology, 2009. **19**(3): p. 620-634.

166. Wang, K., L. Kong, Y. Tao, T. Li, and T. Xiong, *Numerical Simulation of Minimal Average Bonding Strength to Suppress Rebounding in Cold Spraying Cu/Cu: A Preliminary Study.* Journal of Thermal Spray Technology, 2014.

167. Kang, K., S. Yoon, Y. Ji, and C. Lee, *Oxidation dependency of critical velocity for aluminum feedstock deposition in kinetic spraying process.* Materials Science and Engineering: A, 2008. **486**(1-2): p. 300-307.

168. Li, W.Y., C. Zhang, H.T. Wang, X.P. Guo, H.L. Liao, C.J. Li, and C. Coddet, *Significant influences of metal reactivity and oxide films at particle surfaces on coating microstructure in cold spraying.* Applied Surface Science, 2007. **253**(7): p. 3557-3562.

169. Wu, J., H. Fang, S. Yoon, H. Kim, and C. Lee, *The rebound phenomenon in kinetic spraying deposition.* Scripta Materialia, 2006. **54**(4): p. 665-669.

170. Li, W.-Y., C.-J. Li, and G.-J. Yang, *Effect of impact-induced melting on interface microstructure and bonding of cold-sprayed zinc coating.* Applied Surface Science, 2010. **257**(5): p. 1516-1523.

171. Stoltenhoff, T., H. Kreye, and H. Richter, *An analysis of the cold spray process and its coatings.* Journal of Thermal Spray Technology, 2002. **11**(4): p. 542-550.

172. Gärtner, F., T. Stoltenhoff, T. Schmidt, and H. Kreye, *The Cold Spray Process and Its Potential for Industrial Applications.* Journal of Thermal Spray Technology, 2006. **15**(2): p. 223-232.

173. Wang, F.F., W.Y. Li, M. Yu, and H.L. Liao, *Prediction of Critical Velocity During Cold Spraying Based on a Coupled Thermomechanical Eulerian Model.* Journal of Thermal Spray Technology, 2013. **23**(1-2): p. 60-67.

174. Li, W.Y., M. Yu, F.F. Wang, S. Yin, and H.L. Liao, *A Generalized Critical Velocity Window Based on Material Property for Cold Spraying by Eulerian Method.* Journal of Thermal Spray Technology, 2013. **23**(3): p. 557-566.

175. Pérez-Andrade, L.I., F. Gärtner, M. Villa-Vidaller, T. Klassen, J. Muñoz-Saldaña, and J.M. Alvarado-Orozco, *Optimization of Inconel 718 thick deposits by cold spray processing and annealing.* Surface and Coatings Technology, 2019. **378**: p. 124997.

176. Hassani, M., D. Veysset, Y. Sun, K.A. Nelson, and C.A. Schuh, *Microparticle impact-bonding modes for mismatched metals: From co-deformation to splatting and penetration.* Acta Materialia, 2020. **199**: p. 480-494.

177. Hassani-Gangaraj, M., D. Veysset, K.A. Nelson, and C.A. Schuh, *Impact-bonding with aluminum, silver, and gold microparticles: Toward understanding the role of native oxide layer.* Applied Surface Science, 2019. **476**: p. 528-532.

178. Van Steenkiste, T.H., J.R. Smith, and R.E. Teets, *Aluminum coatings via kinetic spray with relatively large powder particles.* Surface and Coatings Technology, 2002. **154**(2): p. 237-252.

179. Theimer, S., M. Graunitz, M. Schulze, F. Gaertner, and T. Klassen, *Optimization Adhesion in Cold Spraying onto Hard Substrates: A Case Study for Brass Coatings.* Journal of Thermal Spray Technology, 2019. **28**(1): p. 124-134.

180. Meng, F., S. Yue, and J. Song, *Quantitative prediction of critical velocity and deposition efficiency in cold-spray: A finite-element study.* Scripta Materialia, 2015. **107**: p. 83-87.

181. Che, H., P. Vo, and S. Yue, *Investigation of Cold Spray on Polymers by Single Particle Impact Experiments.* Journal of Thermal Spray Technology, 2019. **28**(1): p. 135-143.

182. Imbriglio, S.I., N. Brodusch, M. Aghasibeig, R. Gauvin, and R.R. Chromik, *Influence of Substrate Characteristics on Single Ti Splat Bonding to Ceramic Substrates by Cold Spray.* Journal of Thermal Spray Technology, 2018. **27**(6): p. 1011-1024.

183. Zhang, Y., N. Brodusch, S. Descartes, J.M. Shockley, R. Gauvin, and R.R. Chromik, *The Effect of Submicron Second-Phase Particles on the Rate of Grain Refinement in a Copper-Oxygen Alloy During Cold Spray.* Journal of Thermal Spray Technology, 2017. **26**(7): p. 1509-1516.

184. Tiamiyu, A.A. and C.A. Schuh, *Particle flattening during cold spray: Mechanistic regimes revealed by single particle impact tests.* Surface and Coatings Technology, 2020. **403**: p. 126386.

185. Fukumoto, M., M. Mashiko, M. Yamada, and E. Yamaguchi, *Deposition behavior of copper fine particles onto flat substrate surface in cold spraying.* Journal of thermal spray technology, 2010. **19**(1-2): p. 89-94.

186. Matějíček, J., B. Kolman, J. Dubský, K. Neufuss, N. Hopkins, and J. Zwick, *Alternative methods for determination of composition and porosity in abradable materials.* Materials Characterization, 2006. **57**(1): p. 17-29.

187. Kulkarni, A., J. Gutleber, S. Sampath, A. Goland, W.B. Lindquist, H. Herman, A.J. Allen, and B. Dowd, *Studies of the microstructure and properties of dense ceramic coatings produced by high-velocity oxygen-fuel combustion spraying.* Materials Science and Engineering: A, 2004. **369**(1): p. 124-137.

188. Rogé, B., A. Fahr, J.S.R. Giguère, and K.I. McRae, *Nondestructive measurement of porosity in thermal barrier coatings.* Journal of Thermal Spray Technology, 2003. **12**(4): p. 530-535.

189. Ang, A.S.M. and C.C. Berndt, *A review of testing methods for thermal spray coatings.* International Materials Reviews, 2014. **59**(4): p. 179-223.

190. Marrocco, T., D.G. McCartney, P.H. Shipway, and A.J. Sturgeon, *Production of Titanium Deposits by Cold-Gas Dynamic Spray: Numerical Modeling and Experimental Characterization.* Journal of Thermal Spray Technology, 2006. **15**(2): p. 263-272.

191. Lima, R., A. Kucuk, C. Berndt, J. Karthikeyan, C. Kay, and J. Lindemann, *Deposition efficiency, mechanical properties and coating roughness in cold-sprayed titanium.* Journal of Materials Science Letters, 2002. **21**(21): p. 1687-1689.

192. Song, X., K.L. Ng, J.M.-K. Chea, W. Sun, A.W.-Y. Tan, W. Zhai, F. Li, I. Marinescu, and E. Liu, *Coupled Eulerian-Lagrangian (CEL) simulation of multiple particle impact during Metal Cold Spray process for coating porosity prediction.* Surface and Coatings Technology, 2020. **385**: p. 125433.

193. Munagala, V.N.V., S. Bessette, R. Gauvin, and R.R. Chromik, *Sliding wear of cold sprayed Ti6Al4V coatings: Effect of porosity and normal load.* Wear, 2020. **450-451**: p. 203268.

194. Champagne, V.K. and D.J. Helfritch, *Mainstreaming cold spray – push for applications.* Surface Engineering, 2014. **30**(6): p. 396-403.

195. Jones, R., N. Matthews, C.A. Rodopoulos, K. Cairns, and S. Pitt, *On the use of supersonic particle deposition to restore the structural integrity of damaged aircraft structures.* International Journal of Fatigue, 2011. **33**(9): p. 1257-1267.

196. Rokni, M.R., C.A. Widener, G.A. Crawford, and M.K. West, *An investigation into microstructure and mechanical properties of cold sprayed 7075 Al deposition.* Materials Science and Engineering: A, 2015. **625**: p. 19-27.

197. Zahiri, S.H., C.I. Antonio, and M. Jahedi, *Elimination of porosity in directly fabricated titanium via cold gas dynamic spraying.* Journal of Materials Processing Technology, 2009. **209**(2): p. 922-929.

198. Cinca, N., M. Barbosa, S. Dosta, and J.M. Guilemany, *Study of Ti deposition onto Al alloy by cold gas spraying.* Surface and Coatings Technology, 2010. **205**(4): p. 1096-1102.

199. International, A., *ASTM C633-13, Standard Test Method for Adhesion or Cohesion Strength of Thermal Spray Coatings*. 2017: West Conshohocken, PA.

200. Koivuluoto, H., J. Lagerbom, M. Kylmälahti, and P. Vuoristo, *Microstructure and Mechanical Properties of Low-Pressure Cold-Sprayed (LPCS) Coatings.* Journal of Thermal Spray Technology, 2008. **17**(5): p. 721-727.

201. Huang, R. and H. Fukanuma, *Study of the Influence of Particle Velocity on Adhesive Strength of Cold Spray Deposits.* Journal of Thermal Spray Technology, 2012. **21**(3): p. 541-549.

202. Huang, R., W. Ma, and H. Fukanuma, *Development of ultra-strong adhesive strength coatings using cold spray.* Surface and Coatings Technology, 2014. **258**: p. 832-841.

203. Chromik, R.R., D. Goldbaum, J.M. Shockley, S. Yue, E. Irissou, J.-G. Legoux, and N.X. Randall, *Modified ball bond shear test for determination of adhesion strength of cold spray splats.* Surface and Coatings Technology, 2010. **205**(5): p. 1409-1414.

204. Binder, K., J. Gottschalk, M. Kollenda, F. Gärtner, and T. Klassen, *Influence of Impact Angle and Gas Temperature on Mechanical Properties of Titanium Cold Spray Deposits.* Journal of Thermal Spray Technology, 2011. **20**(1): p. 234-242.

205. Goldbaum, D., J. Ajaja, R.R. Chromik, W. Wong, S. Yue, E. Irissou, and J.-G. Legoux, *Mechanical behavior of Ti cold spray coatings determined by a multi-scale indentation method.* Materials Science and Engineering: A, 2011. **530**: p. 253-265.

206. Stoltenhoff, T., C. Borchers, F. Gärtner, and H. Kreye, *Microstructures and key properties of cold-sprayed and thermally sprayed copper coatings.* Surface and Coatings Technology, 2006. **200**(16): p. 4947-4960.

207. Sudharshan Phani, P., V. Vishnukanthan, and G. Sundararajan, *Effect of heat treatment on properties of cold sprayed nanocrystalline copper alumina coatings.* Acta Materialia, 2007. **55**(14): p. 4741-4751.

208. Sudharshan Phani, P., D. Srinivasa Rao, S.V. Joshi, and G. Sundararajan, *Effect of Process Parameters and Heat Treatments on Properties of Cold Sprayed Copper Coatings.* Journal of Thermal Spray Technology, 2007. **16**(3): p. 425-434.

209. Venkatesh, L., N.M. Chavan, and G. Sundararajan, *The Influence of Powder Particle Velocity and Microstructure on the Properties of Cold Sprayed Copper Coatings.* Journal of Thermal Spray Technology, 2011. **20**(5): p. 1009-1021.

210. Chavan, N.M., M. Ramakrishna, P.S. Phani, D.S. Rao, and G. Sundararajan, *The influence of process parameters and heat treatment on the properties of cold sprayed silver coatings.* Surface and Coatings Technology, 2011. **205**(20): p. 4798-4807.

211. Meng, X.-M., J.-B. Zhang, W. Han, J. Zhao, and Y.-L. Liang, *Influence of annealing treatment on the microstructure and mechanical performance of cold sprayed 304 stainless steel coating.* Applied Surface Science, 2011. **258**(2): p. 700-704.

212. Li, Z., X. Yang, J. Zhang, B. Zheng, Y. Zhou, A. Shan, and E.J. Lavernia, *Microstructure evolution and mechanical behavior of cold-sprayed, bulk nanostructured titanium.* Metallurgical and Materials Transactions A, 2014. **45**(11): p. 5017-5028.

213. Rokni, M.R., C.A. Widener, V.K. Champagne, G.A. Crawford, and S.R. Nutt, *The effects of heat treatment on 7075 Al cold spray deposits.* Surface and Coatings Technology, 2017. **310**: p. 278-285.

214. Shkodkin, A., A. Kashirin, O. Klyuev, and T. Buzdygar, *Metal particle deposition stimulation by surface abrasive treatment in gas dynamic spraying.* Journal of Thermal Spray Technology, 2006. **15**(3): p. 382-386.

215. Spencer, K. and M.X. Zhang, *Optimisation of stainless steel cold spray coatings using mixed particle size distributions.* Surface and Coatings Technology, 2011. **205**(21): p. 5135-5140.

216. Perry, J., P. Richer, B. Jodoin, and E. Matte, *Pin Fin Array Heat Sinks by Cold Spray Additive Manufacturing: Economics of Powder Recycling.* Journal of Thermal Spray Technology, 2019. **28**(1): p. 144-160.

217. Luo, X.-T., Y.-K. Wei, Y. Wang, and C.-J. Li, *Microstructure and mechanical property of Ti and Ti6Al4V prepared by an in-situ shot peening assisted cold spraying.* Materials & Design, 2015. **85**: p. 527-533.

218. Wei, Y.-K., Y.-J. Li, Y. Zhang, X.-T. Luo, and C.-J. Li, *Corrosion resistant nickel coating with strong adhesion on AZ31B magnesium alloy prepared by an in-situ shot-peening-assisted cold spray.* Corrosion Science, 2018. **138**: p. 105-115.

219. Chu, X., R. Chakrabarty, H. Che, L. Shang, P. Vo, J. Song, and S. Yue, *Investigation of the feedstock deposition behavior in a cold sprayed 316L/Fe composite coating.* Surface and Coatings Technology, 2018. **337**: p. 53-62.

220. Chu, X., H. Che, C. Teng, P. Vo, and S. Yue, *A multiple particle arrangement model to understand cold spray characteristics of bimodal size 316L/Fe powder mixtures.* Surface and Coatings Technology, 2020. **381**: p. 125137.

221. Chu, X., H. Che, and S. Yue, *Understanding the Cold Spray Deposition Characteristics of Mixed Metal Powders.* MRS Advances, 2019. **4**(55-56): p. 2989-2995.

222. Askeland, D.R., P.P. Phulé, W.J. Wright, and D. Bhattacharya, *The science and engineering of materials.* 2003.

223. Schultheiß, D., *Permeation barrier for lightweight liquid hydrogen tanks*, in *Faculty of Mathematics, Natural Sciences and Materials Engineering*. 2008, University of Augsburg: Augsburg.

224. Barkoula, N.-M. and J. Karger-Kocsis, *Review Processes and influencing parameters of the solid particle erosion of polymers and their composites.* Journal of Materials Science, 2002. **37**(18): p. 3807-3820.

225. Arjula, S. and A.P. Harsha, *Study of erosion efficiency of polymers and polymer composites.* Polymer Testing, 2006. **25**(2): p. 188-196.

226. Stachowiak, G. and A.W. Batchelor, *Abrasive, erosive and cavitation wear*, in *Engineering Tribology*. 1993. p. 557-612.

227. Friedrich, K., *Erosive wear of polymer surfaces by steel ball blasting.* Journal of Materials Science, 1986. **21**(9): p. 3317-3332.

228. Drensky, G., A. Hamed, W. Tabakoff, and J. Abot, *Experimental investigation of polymer matrix reinforced composite erosion characteristics.* Wear, 2011. **270**(3-4): p. 146-151.

229. Parmar, H., F. Tucci, P. Carlone, and T.S. Sudarshan, *Metallisation of polymers and polymer matrix composites by cold spray: state of the art and research perspectives.* International Materials Reviews, 2021: p. 1-25.

230. Chen, C., X. Xie, Y. Xie, X. Yan, C. Huang, S. Deng, Z. Ren, and H. Liao, *Metallization of polyether ether ketone (PEEK) by copper coating via cold spray.* Surface and Coatings Technology, 2018. **342**: p. 209-219.

231. Rokni, M.R., P. Feng, C.A. Widener, and S.R. Nutt, *Depositing Al-Based Metallic Coatings onto Polymer Substrates by Cold Spray.* Journal of Thermal Spray Technology, 2019. **28**(7): p. 1699-1708.

232. Małachowska, A., M. Winnicki, Ł. Konat, T. Piwowarczyk, L. Pawłowski, A. Ambroziak, and M. Stachowicz, *Possibility of spraying of copper coatings on polyamide 6 with low pressure cold spray method.* Surface and Coatings Technology, 2017. **318**: p. 82-89.

233. Gardon, M., A. Latorre, M. Torrell, S. Dosta, J. Fernández, and J.M. Guilemany, *Cold gas spray titanium coatings onto a biocompatible polymer.* Materials Letters, 2013. **106**: p. 97-99.

234. Vucko, M.J., P.C. King, A.J. Poole, C. Carl, M.Z. Jahedi, and R. de Nys, *Cold spray metal embedment: an innovative antifouling technology.* Biofouling, 2012. **28**(3): p. 239-248.

235. Papa, I., P. Russo, A. Astarita, A. Viscusi, A.S. Perna, L. Carrino, and V. Lopresto, *Impact behaviour of a novel composite structure made of a polymer reinforced composite with a 3D printed metallic coating.* Composite Structures, 2020. **245**: p. 112346.

236. Giraud, D., F. Borit, V. Guipont, M. Jeandin, and J. Malhaire. *Metallization of a polymer using cold spray: application to aluminum coating of polyamide 66*. in *Internation Thermal Spray Conference (ITSC)*. 2012. Houston, USA.

237. Ye, H. and J. Wang, *Preparation of aluminum coating on Lexan by cold spray.* Materials Letters, 2014. **137**: p. 21-24.

238. Kromer, R., Y. Danlos, E. Aubignat, C. Verdy, and S. Costil, *Coating deposition and adhesion enhancements by laser surface texturing—metallic particles on different classes of substrates in cold spraying process.* Materials and Manufacturing Processes, 2017. **32**(14): p. 1642-1652.

239. Fallah, P., S. Rajagopalan, A. McDonald, and S. Yue, *Development of hybrid metallic coatings on carbon fiber-reinforced polymers (CFRPs) by cold spray deposition of copper-assisted copper electroplating process.* Surface and Coatings Technology, 2020. **400**: p. 126231.

240. Che, H., A. Liberati, P. Vo, and S. Yue, *Cold Spray of Mixed Sn-Zn and Sn-Al Powders on Carbon Fiber Reinforced Polymers.* Materials Science Forum, 2018. **941**: p. 1892-1897.

241. Menningen, M. and H. Weiss, *Application of fracture mechanics to the adhesion of metal coatings on CFRP.* Surface and Coatings Technology, 1995. **76-77**: p. 835-840.

242. Samareh, B., O. Stier, V. Lüthen, and A. Dolatabadi, *Assessment of CFD Modeling via Flow Visualization in Cold Spray Process.* Journal of Thermal Spray Technology, 2009. **18**(5): p. 934.

243. Zygo, *Mx Surface Texture Parameters*. 2018.

244. Gomez, C., R. Su, A. Thompson, J. DiSciacca, S. Lawes, and R.K. Leach, *Optimization of surface measurement for metal additive manufacturing using coherence scanning interferometry.* Optical Engineering, 2017. **56**(11): p. 1-8, 8.

245. *Fluent 6.3 User's Guide*. 2006, Lebanon, NH, USA: Fluent Inc.

246. Liberati, A.C., H. Che, P. Vo, and S. Yue, *Observation of an Indirect Deposition Effect while Cold Spraying Sn-Al Mixed Powders onto Carbon Fiber Reinforced Polymers.* Journal of Thermal Spray Technology, 2020. **29**: p. 134-146.

247. Della Gatta, R., A. Viscusi, A.S. Perna, A. Caraviello, and A. Astarita, *Cold spray process for the production of AlSi10Mg coatings on glass fibers reinforced polymers.* Materials and Manufacturing Processes, 2020: p. 1-16.

248. Della Gatta, R., A. Viscusi, A.S. Perna, A. Caraviello, and A. Astarita, *Feasibility of steel powder deposition on composites through cold spray.* Materials and Manufacturing Processes, 2020: p. 1-11.

249. Miyazaki, N. and N. Takeda, *Solid particle erosion of fiber reinforced plastics.* Journal of Composite Materials, 1993. **27**(1): p. 21-31.

250. Liberati, A.C., H. Che, P. Vo, and S. Yue, *Influence of Secondary Component Hardness When Cold Spraying Mixed Metal Powders on Carbon Fiber Reinforced Polymers.* Journal of Thermal Spray Technology, 2021. **30**(5): p. 1239-1253.

251. Carlson, R. and J.E. Carlson, *1.11 - The Study of Experimental Factors*, in *Comprehensive Chemometrics*, S.D. Brown, R. Tauler, and B. Walczak, Editors. 2009, Elsevier: Oxford. p. 301-344.

252. Poirier, D., J.-G. Legoux, P. Vo, B. Blais, J.D. Giallonardo, and P.G. Keech, *Powder Development and Qualification for High-Performance Cold Spray Copper Coatings on Steel Substrates.* Journal of Thermal Spray Technology, 2019. **28**(3): p. 444-459.

253. Özdemir, O.Ç., J.M. Conahan, and S. Müftü, *Particle Velocimetry, CFD, and the Role of Particle Sphericity in Cold Spray.* Coatings, 2020. **10**(12): p. 1254.

254. Zeng, Z., N. Sakoda, T. Tajiri, and S. Kuroda, *Structure and corrosion behavior of 316L stainless steel coatings formed by HVAF spraying with and without sealing.* Surface and Coatings Technology, 2008. **203**(3): p. 284-290.

255. Rezzoug, A., S. Abdi, A. Kaci, and M. Yandouzi, *Thermal spray metallisation of carbon fibre reinforced polymer composites: Effect of top surface modification on coating adhesion and mechanical properties.* Surface and Coatings Technology, 2018. **333**: p. 13-23.

256. Liberati, A.C., H. Che, S. Yue, and P. Vo, *On the Importance of Secondary Component Properties for Cold Spray Metallization of Carbon Fiber Reinforced Polymers.* Journal of Thermal Spray Technology, 2021. **Invited Paper selected from presentations at the 2021 International Thermal Spray Conference, Submitted**.

257. Che, H., A.C. Liberati, X. Chu, M. Chen, A. Nobari, P. Vo, and S. Yue, *Metallization of polymers by cold spraying with low melting point powders.* Surface and Coatings Technology, 2021. **418**: p. 127229.

258. Valdes, L.B., *Resistivity measurements on germanium for transistors.* Proceedings of the IRE, 1954. **42**(2): p. 420-427.

259. Smits, F.M., *Measurement of sheet resistivities with the four-point probe.* The Bell System Technical Journal, 1958. **37**(3): p. 711-718.

260. Arrigoni, M., S. Barradas, M. Braccini, M. Dupeux, M. Jeandin, M. Boustie, C. Bolis, and L. Berthe, *A comparative study of three adhesion tests (EN 582, similar to ASTM C633, LASAT (LASer Adhesion Test), and bulge and blister test) performed on plasma sprayed copper deposited on aluminium 2017 substrates.* Journal of Adhesion Science and Technology, 2006. **20**(5): p. 471-487.

261. Małachowska, A., M. Winnicki, M. Stachowicz, and M. Korzeniowski, *Metallisation of polycarbonates using a low pressure cold spray method.* Surface Engineering, 2018. **34**(3): p. 251-258.